AD-A134 270 WAVE-PARTICLE INTERACTIONS ON RELATIVISTIC ELECTRON BEAMS(U) YALE UNIV NEW HAVEN CONN I B BERNSTEIN ET AL. 20 OCT 83 N00014-79-C-0588 1/2

UNCLASSIFIED F/G 20/5 NL

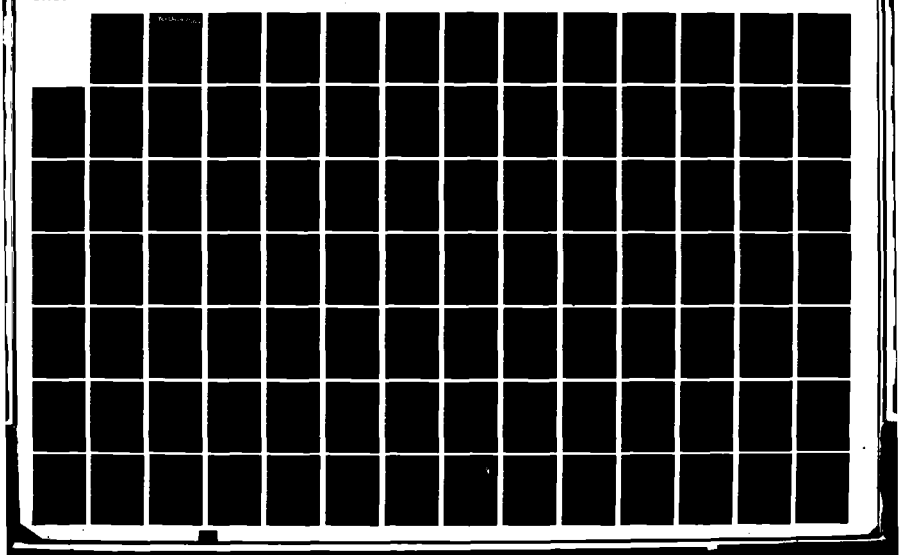

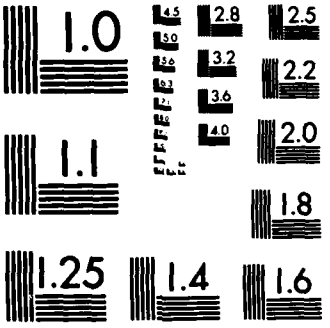

YALE UNIVERSITY

FINAL REPORT

To The Office of Naval Research

For Contract N00014-79-0-0588

by

Applied Physics Section

Yale University, New Haven, Connecticut 06520

WAVE-PARTICLE INTERACTIONS ON RELATIVISTIC ELECTRON BEAMS

Principal Investigators

J. L. Hirshfield
Ira B. Bernstein

October 20, 1983

UNCLASSIFIED

SECURITY CLASSIFICATION OF THIS PAGE (When Data Entered)

REPORT DOCUMENTATION PAGE	READ INSTRUCTIONS BEFORE COMPLETING FORM
1. REPORT NUMBER: 11	2. GOVT ACCESSION NO.: AD-A134270
3. RECIPIENT'S CATALOG NUMBER:	
4. TITLE (and Subtitle): Wave-Particle Interaction on Relativistic Electron Beams	5. TYPE OF REPORT & PERIOD COVERED: Final Technical Report
	6. PERFORMING ORG. REPORT NUMBER: 11
7. AUTHOR(s): Ira B. Bernstein and J. L. Hirshfield	8. CONTRACT OR GRANT NUMBER(s): N00014-79-0-0588
9. PERFORMING ORGANIZATION NAME AND ADDRESS: Yale University, Applied Physics Section, New Haven, CT 06520	10. PROGRAM ELEMENT, PROJECT, TASK AREA & WORK UNIT NUMBERS: NR 020-043
11. CONTROLLING OFFICE NAME AND ADDRESS: Office of Naval Research, Physics Progam Code 421, 800 N. Quincy Street, Arlington, VA 22217	12. REPORT DATE: October 20, 1983
	13. NUMBER OF PAGES: 103
14. MONITORING AGENCY NAME & ADDRESS(if different from Controlling Office)	15. SECURITY CLASS. (of this report): Unclassified
	15a. DECLASSIFICATION/DOWNGRADING SCHEDULE
16. DISTRIBUTION STATEMENT (of this Report): Approved for public release; distribution unlimited	
17. DISTRIBUTION STATEMENT (of the abstract entered in Block 20, if different from Report)	Accession For NTIS GRA&I [X] DTIC TAB [ ] Unannounced [ ] Justification By Distribution/ Availability Codes Dist | Avail and/or Special A/1
18. SUPPLEMENTARY NOTES	
19. KEY WORDS (Continue on reverse side if necessary and identify by block number): Free Electron Laser; Relativistic Beam Plasma Interaction	DTIC COPY INSPECTED

20. ABSTRACT (Continue on reverse side if necessary and identify by block number)

A summary of research performed under subject contract is given. The work is in the main concerned with the theory, both linear and non-linear, for the gain of a free electron laser (FEL) in a strong axial magnetic field. Both wiggler and wiggler-free configuration are considered. An experimental study is described of the transition from helical to non-helical orbits in a wiggler with a guide field. The exact magnetic field of a filimentary bifilar current-carrying helix is given. The degradation in gain of a FEL without axial guide guide field due to velocity spread is given. Twelve published papers are appended.

DD FORM 1 JAN 73 1473 EDITION OF 1 NOV 65 IS OBSOLETE

S/N 0102-LF-014-6601

UNCLASSIFIED

SECURITY CLASSIFICATION OF THIS PAGE (When Data Entered)

SUMMARY OF RESEARCH COMPLETED

Research on free electron lasers (FELs) carried out over a three-year period with support by the Office of Naval Research has resulted in a number of significant contributions. The emphasis throughout this work has been on FEL configurations which include a strong uniform axial guide magnetic field, since such a field is used in many experiments to guide the electron beam. Moreover, as we shall discuss presently, the axial magnetic field can introduce a number of physical features not present when this field is absent. Some of these features can be deletereous to FEL operation; others can be advantageous.

Copies of all major publications which resulted from this research program are appended to this report. A list of these papers follows:

PUBLICATION LIST

1. "Free-Electron Laser with a Strong Axial Magnetic Field," L. Friedland and J. L. Hirshfield, Phys. Rev. Lett. 44, 1456 (1980).

2. "Electron Beam Dynamics in Combined Guide and Pump Magnetic Fields for Free Electron Laser Applications," L. Friedland, Phys. Fluids 23, 2376 (1980).

3. "Orbit Stability in Free Electron Lasers," P. Avivi, F. Dothan, A. Fruchtman, A. Ljudmirsky, and J. L. Hirshfield, Int. J. Infrared and Millimeter Waves 2, 1071 (1981).

4. "Degradation in Gain for a Free Electron Laser Amplifier Due to Electron Momentum Spread," A. Fruchtman and J. L. Hirshfield, Int. J. Infrared and Millimeter Waves 2, 905 (1981).

5. "Theory of the Free-Electron Laser in Combined Helical Pump and Axial Guide Fields," Ira B. Bernstein and Lazar Friedland, Phys. Rev. A 23, 816 (1981).

6. "Exact Magnetic Field of a Helical Wiggler," S. Y. Park, J. M. Baird, R. A. Smith, and J. L. Hirshfield, J. Appl. Phys. 53, 1320 (1982).

7. "Free Electron Lasers in the Collective Regime," J. L. Hirshfield, Proc. Japan-U.S. Seminar on Theory and Application of Multiply-Ionized Plasmas Produced by Laser and Particle Beams, Nara, Japan (1982) pp. 515-525.

8. "Amplification of Frequency Upshifted Radiation by Cold Relativistic Guided Electron Beams," A. Fruchtman and L. Friedland, J. Appl. Phys. 53, 4011 (1982).

9. "Amplification on Relativistic Electron Beams in Combined Helical and Axial Magnetic Fields," L. Friedland and A. Fruchtman, Phys. Rev. A 25, 2693 (1982).

10. "Nonlinear Theory of the Free-Electron Laser with an Axial Magnetic Field," Lazar Friedland and Ira B. Bernstein, Phys. Rev. A 26, 2778 (1982).

11. "Wiggler-Free Free Electron Waveguide Laser in a Uniform Axial Magnetic Field: Single Particle Treatment," A. Fruchtman, J. Appl. Phys. 54, 4289 (1983).

12. "Theory of a Nonwiggler Collective Free Electron Laser in Uniform Magnetic Field," A. Fruchtman and L. Friedland, IEEE J. Quantum Electronics QE-19, 327 (1983).

Most of the published work is theoretical, although an important experimental confirmation (paper 3) of one aspect of the work was obtained by the Hebrew University group which has carried on a continuing collaboration with the Yale group.

The key work underlying much of what followed is paper #2 (which was actually submitted for publication prior to the letter #1). This work showed for the first time that electron orbits in a helical wiggler with a superimposed axial guide magnetic field were not necessarily helical. Helical orbits could be well approximated if the wiggler parameters and entrance conditions were carefully chosen. But for carelessly chosen parameters, the orbits would be strongly non-helical, thus rendering such a beam useless in a FEL. However it was shown possible that one could operate close to a point of transition where the equilibrium orbit would be nearly helical, but where small perturbations (say due to a co-propagating electromagnetic wave) would be strongly enhanced by coupling to a natural resonance of the orbit. In paper #1, a single-particle analysis showed that considerable small-signal FEL gain enhancement could be achieved, based on this phenomena, without increasing the electron's undulatory velocity. (An increase

in undulatory velocity gives rise to a decrease in the up-shifted frequency which can be amplified; thus a higher beam energy would be required if a given frequency were to be amplified; the aforementioned resonance with the orbit's natural response makes these adjustments unnecessary.)

The experiment reported in paper #3 explores the transition from helical to non-helical orbits, and the data show good agreement with theory for the parameter governing this transition, as predicted in paper #2. Since the work reported in paper #3, the Hebrew University group has continued its work on beam diagnostics for FEL applications, under support by the U.S.-Israel Binational Science Foundation.

Paper #4 shows the effect of a spread in axial electron momenta upon the gain of a FEL operating in the collective regime, without the axial magnetic field. Exact gain degradation results for a box-like axial momentum distribution are presented, as are some approximate scaling laws which can be useful for rough estimates.

Paper #5 is an extension into the collective regime of the calculation given in paper #1, using the fluid equations. This work applies either for a magnetostatic or for an electromagnetic pump.

Paper #6 is a derivation for the exact magnetic field of a current-carrying bifilar helix. The main point of this paper is to determine the range of validity for the approximate formula for the field of a wiggler commonly used in the literature [i.e. $\underline{B}(z) = B_o(\hat{e}_x \sin kz - \hat{e}_y \cos kz)$]. A secondary point was to be able to calculate the higher spatial harmonics of the field, so as to estimate their utility in a harmonic FEL.

Paper #7 reviews the theory of FELs in the collective regime with an axial guide field, and cites some of the important experiments. The paper also contains a proposal for a two-stage FEL to generate micron wavelength

radiation using an intense electromagnetic wave, generated in the first stage, as a pump in the second stage. Neither stage employs a magnetic wiggler. The theory underlying the first stage of this proposed device is given in detail in papers #8 and #12.

Paper #8 considers wave propogation along a cold electron beam with pre-imposed spatially coherent helical orbits. Radiation at the Doppler-shifted cyclotron frequency is amplified by such a system, but with higher gain than for the case of spatially incoherent helical orbits.

Paper #9 is an extension of the work reported in paper #5. The governing equations are reduced to a set of coupled first-order ordinary differential equations, with due attention to the problem of unstable equilibrium orbits. The actual spatial evolution of the field along the axis of an amplifying device is found.

Paper #10 gives a non-linear cold-fluid approximation for the theory of a FEL with an axial magnetic field. As in paper #9, a coupled set of non-linear first order ordinary differential equations is analyzed to give both the initial linear regime of spatial growth, as well as the non-linear saturation. Axial evolution is found.

Papers #11 and #12 treat a system of a beam of spatially coherent helical orbits in a uniform magnetic field, but with no wiggler. Paper #11 is a single-particle treatment but for bounded TE and TM waves, and the small-signal gain is shown to be larger than for the case with unbounded waves. A practical amplifier based on this principal is proposed. Paper #12 contains the collective theory for this interaction, and gain is compared for beams with helical, bi-helical, and randomly phased cold distributions. Orderly transverse phase distributions are shown to provide greater gain and bandwidth, than for the case of random phases.

In summary, the body of published research which resulted from Office of Naval Research support under this contract has extended knowledge and understanding for an important class of free electron lasers, namely those having an axial magnetic field. Other research groups have made contributions as well, but in many cases following the pace of the work presented here.

Free-Electron Laser with a Strong Axial Magnetic Field

L. Friedland and J. L. Hirshfield
Department of Engineering and Applied Science, Mason Laboratory, Yale University, New Haven, Connecticut 06520
(Received 27 February 1980)

A small-signal theory is given for gain in a free-electron laser comprising a cold relativistic electron beam in a helical periodic transverse, and a strong uniform axial, magnetic field. Exact finite-amplitude, steady-state helical orbits are included. If perturbed, these orbits oscillate about equilibrium, so that substantial gain enhancement can occur if the electromagnetic perturbations resonate with these oscillations. This gain enhancement need not be at the cost of frequency upshift.

PACS numbers: 42.55.-f, 41.70.+t, 41.80.Dd

Intensive activity is underway to exploit the gain properties of a relativistic electron beam undulating in a periodic transverse magnetic field. Such free-electron laser (FEL) configurations have provided oscillation at 3.4 (Ref. 1) and 400 μm,[2] and amplification at 10.6 μm.[3] Theory has advanced apace,[4] and elaborate schemes have been proposed for obtaining high FEL efficiency.[5] A factor which limits the practical application of this interaction at wavelengths shorter than perhaps a few microns is the rapid decrease in small-signal gain G_0 as the electron energy increases. This is shown explicitly in the well-known result[6] for G_0 in the single-particle limit (i.e., when collective effects are negligible)

$$G_0 = (\omega_p \xi/k_0 c)^2 (k_0 L/2\gamma)^3 F'(\theta). \quad (1)$$

Here ω_p and γ are the beam plasma frequency $Ne^2/m\epsilon_0$ and normalized energy W/mc^2, k_0 and ξ are the helical transverse magnetic field wave number $2\pi/l$ and normalized strength $eB_\perp/mck_0$, L is the interaction length, and $F'(\theta) = (d/d\theta)(\sin\theta/\theta)^2$ is the line-shape factor, with $\theta = [k_0 v_{30} - \omega(1 - v_{30}/c)](L/2c)$, where v_{30} is the unperturbed electron axial velocity. The peak gain occurs at $\theta = 1.3$, where $F'(\theta) = 0.54$. For example, with γ

$=10$, $l=1.05$ cm, $\omega_p=5\times10^7$ sec^{-1}, $\xi=1$ ($B_\perp=10.2$ kG), and $L=130$ cm, the peak gain is $G_{0p}=0.002\,47$ at a wavelength of 105 μm. For $\gamma=100$, $l=10.5$ cm, $\omega_p=2\times10^9$ sec^{-1}, $\xi=1$ ($B_\perp=1.02$ kG), and $L=260$ cm, the peak gain is $G_{0p}=0.003\,16$ at a wavelength of 10.5 μm. These gain values may be large enough to sustain oscillations if highly reflecting mirrors are judiciously added but the strong helical fields required (particularly the 10.2-kG case) may be beyond the capability of present superconducting coil technology.[7]

A suggestion has appeared for enhancing the small-signal gain above values given by Eq. (1) (or for achieving comparable gains with smaller $B_\perp$) by employing a strong axial magnetic field so as to exploit resonance between the cyclotron frequency and the undulatory frequency.[8] The present Letter presents a single-particle derivation for the small-signal gain of a FEL in a uniform axial magnetic field B_0. We shall demonstrate that careful adjustment of the system parameters will allow enhancement of the FEL small-signal gain by an order of magnitude or more (for the above examples) *without increasing the undulatory velocity*. This result goes beyond that predicted by Sprangle and Granatstein[6] who have suggested that the only effect of the axial magnetic field would be to add a multiplicative factor $(1-\Omega/k_0c\gamma)^{-2}$ to Eq. (1), due to the aforementioned resonance giving an enhanced undulatory velocity $v_\perp$, where $\Omega=eB_0/m$. This result is in fact predicted by our analysis as a limiting case. Of course, any mechanism which increases the undulatory velocity $v_\perp$ would increase the gain, but this would also reduce the relativistic frequency upshift, since

$$\omega\simeq k_0c(1-v_{30}/c)^{-1}=2\gamma^2k_0c(1+\gamma^2v_\perp^2/c^2)^{-1}.$$

If, for example, $\gamma v_\perp/c=1$ without the axial magnetic field, then a given gain enhancement η achieved through this resonance alone would result in a reduction in frequency upshift by a factor $(1+\eta)/2$. The process we describe in this Letter will be shown to permit significant gain enhancement without undue sacrifice in frequency upshift. The gain enhancement originates when the electromagnetic perturbations resonate with the natural frequency of oscillation of electrons on finite amplitude equilibrium helical orbits. Prior workers have not considered this effect.

A full derivation of our result will be presented elsewhere.[9] Exact unperturbed relativistic orbits are considered in the customary FEL model magnetic field

$$\vec{B}(\vec{r})=B_0\hat{e}_z+B_\perp(\hat{e}_x\cos k_0z+\hat{e}_y\sin k_0z). \tag{2}$$

These orbits, which have been the subject of recent study,[10] can possess more than one steady state, depending upon γ, B_0, $B_\perp$, and k_0. These steady states are characterized by the normalized velocity components (i.e., $u_i=v_i/c$)

$$u_{10}=0,\quad u_{20}=k_0\xi u_{30}/(k_0u_{30}\gamma-\Omega/c),$$
$$u_{30}=(1-u_{20}^2-\gamma^{-2})^{1/2}, \tag{3}$$

where the basis vectors $\hat{e}_1(z)=-\hat{e}_x\sin k_0z+\hat{e}_y\times\cos k_0z$, $\hat{e}_2(z)=-\hat{e}_x\cos k_0z-\hat{e}_y\sin k_0z$, and $\hat{e}_3(z)=\hat{e}_z$ have been introduced to track the symmetry of the transverse magnetic field. Figure 1 shows u_{30} vs Ω/c for $k_0=6.0$ cm^{-1}, $\xi=1.0$, and $\gamma=10$. For $\Omega>\Omega_{cr}\equiv k_0c[(\gamma^2-1)^{1/3}-\xi^{2/3}]^{3/2}$, it is seen that only one branch exists (branch C). But for $\Omega<\Omega_{cr}$ two additional branches (A and B) are allowed: Branch B has been shown to be unstable, in that the orbits exhibit nonhelical, highly anharmonic motions, while branches A and C have orderly helical orbits. Stability is insured if $\mu^2\equiv a^2-bd>0$, where $a=k_0cu_{30}\xi/\gamma u_{20}$, $b=\Omega u_{20}/\gamma u_{30}$, and $d=k_0c\xi/\gamma$. The quantity μ is the natural resonance frequency in response to small perturbations of the orbit: We shall show that strong resonance response of the electrons to electromagnetic perturbation can lead to enhanced FEL gain for small μ, i.e., for Ω close to Ω_{cr}.

The derivation of FEL gain proceeds by solving the single-particle equations of motion, subject to weak electromagnetic perturbing fields $\vec{E}=\hat{e}_xE_0\cos(kz-\omega t)$ and $\vec{B}=\hat{e}_y(kc/\omega)E_0\cos(kz-\omega t)$,

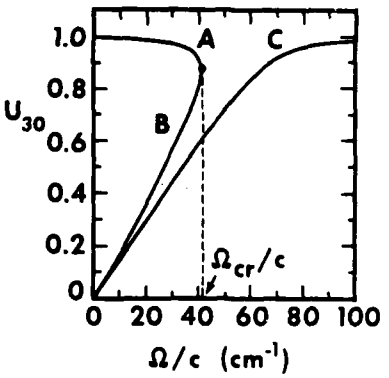

FIG. 1. Steady-state normalized axial velocity u_{30} as a function of normalized axial magnetic field Ω/c. For this example $k_0=6.0$ cm^{-1}, $\xi=1.0$, and $\gamma=10$. Gain enhancement discussed in this work is for orbits on either branch A or branch C.

about the equilibrium orbits on either branch A or C as discussed above. These equations are

$$\dot{u}_1 = (k_0 c u_3 - \Omega/\gamma)u_2 - (k_0 c \xi/\gamma)u_3 - (\dot{\gamma}/\gamma)u_1 + (eE_1/mc\gamma)(kcu_3/\omega - 1), \tag{4}$$

$$\dot{u}_2 = -(k_0 c u_3) - \Omega/\gamma)u_1 - (\dot{\gamma}/\gamma)u_2 + (eE_2/mc\gamma)(kcu_3/\omega - 1), \tag{5}$$

$$\dot{u}_3 = (k_0 c \xi/\gamma)u_1 + (kc/\omega - u_3)(\dot{\gamma}/\gamma), \tag{6}$$

where $\dot{\gamma} = -(e/mc)(u_1 E_1 + u_2 E_2)$ and

$$2(E_2 + iE_1) = -E_0 \exp\{i[(k_0 + k)u_3 ct - \omega t + \alpha]\}$$

with α the random initial electron phase. When time variations and electromagnetic fields are absent, Eqs. (4)–(6) lead to the exact steady states given by Eq. (3). To linearize Eqs. (4)–(6), we introduce the velocity perturbations $w_i = u_i - u_{i0} \ll u_{i0}$ and retain only the lowest-order quantities. This results in $\ddot{w}_1 + \mu^2 w_1 = AE_0 \cos(\beta t + \alpha)$, or

$$w_1 = \frac{AE_0}{\mu^2 - \beta^2}[\cos(\beta t + \alpha) - \cos\mu t \cos\alpha + (\beta/\mu)\sin\mu t \sin\alpha] + \mu^{-1}\dot{w}_1(0)\sin\mu t, \tag{7}$$

where

$$A = (a + \beta)(1 - u_{30}) + bu_{20}, \quad \beta = c(k + k_0)u_{30} - \omega, \quad \omega \simeq kc, \quad \dot{w}_1(0) = (eE_0/2\gamma mc)(1 - u_{30})\sin\alpha,$$

and $w_1(0) = 0$. The other components follow from

$$\dot{w}_2 = -aw_1 + (eE_0/2mc\gamma)(1 - u_{30} - u_{20}^2)\cos(\beta t + \alpha), \quad w_2(0) = 0; \tag{8}$$

and

$$\dot{w}_3 = dw_1 + (eE_0/2mc\gamma)u_{20}(1 - u_{30})\cos(\beta t + \alpha), \quad w_3(0) = 0. \tag{9}$$

Equation (7) for w_1 exhibits the aforementioned natural resonance at frequency μ, while the electromagnetic perturbation drives the transverse motion at frequency β. Gain enhancement can be expected when μ is close to β.

The energy gain for an electron is calculated from $(mc/e)d\gamma/dt \simeq -w_1 E_{10} - w_2 E_{20} - u_{20} E_{21}$. The first-order variation in electric field E_{21} originates from small phase variations as u_3 changes. Thus this becomes

$$(mc/e)d\gamma/dt = -w_1 E_{10} - w_2 E_{20} - \tfrac{1}{2}E_0(k + k_0)cu_{20}\sin(\beta t + \alpha)\int_0^t dt' w_3(t'). \tag{10}$$

The third term in Eq. (10) is much larger than the other two on account of the factor $k + k_0$. The dominant single-particle energy transfer in the FEL (even with an axial magnetic field) is seen to be by work $ecu_2 E_2$ done along the transverse undulatory motion, enhanced by the strong variation in E_2 as its phase varies through w_3. The energy variation [Eq. (10)] is averaged over random phase α to give $\langle d\gamma/dt\rangle$, which in turn leads to the gain through $G = 2(\epsilon_0 E_0^2)^{-1} Nmc^2 \int_0^T dt \langle d\gamma/dt\rangle$, where N is the beam electron density and $T = L/c$ is the total interaction time for the electrons in a system of length L.

The final result is

$$G = \frac{\omega_p^2 k_0 c}{16\gamma} u_{20}^2 T^3 \left\{\left[1 + \frac{a}{\mu_2}\left(a + \beta + \frac{u_{20}b}{1 - u_{30}}\right)\right]\left[F'(\theta) - \frac{F(\theta+\varphi) - F(\theta-\varphi)}{2\varphi}\right] + \frac{F(\theta+\varphi) - F(\theta-\varphi)}{2\varphi} - \frac{a}{\mu^2 T}\left[P'(\theta) - \frac{P(\theta+\varphi) - P(\theta-\varphi)}{2\varphi}\right]\right\}, \tag{11}$$

where $\theta = \beta T/2$, $\varphi = \mu T/2$, $F(x) = (\sin x/x)^2$, and $P(x) = xF(x)/2$; and where we have approximated $(k + k_0)(1 - u_{30}) \simeq k_0$. We shall examine Eq. (11) in several limits.

For $\mu \gg \beta$, only the terms involving $F'(\theta)$ and $P'(\theta)$ in Eq. (11) are significant, and on branch A the latter of these is smaller than the former by at least a factor 2φ. Thus to a good approximation we may write

$$G(\mu \gg \beta) = Z(\omega_p^2/16\gamma)k_0 c u_{20}^2 T^3 F'(\theta), \tag{12}$$

where $Z = 2 + \mu^{-2}[a\beta + bd(1 - u_{30})^{-1}]$. In the case where the axial magnetic field is absent, $\Omega = 0$, $\mu = a = k_0 c u_{30} \gg \beta$, and $u_{20} = \xi/\gamma$. Thus, $Z \simeq 2$ and Eq. (12) goes over to Eq. (1). When $\Omega \neq 0$ and μ

$\gg\beta$, gain enhancement can be achieved as claimed by the prior workers,[8] due to resonant enhancement of u_{20}, but not without sacrificing frequency upshift, as discussed above.

However a more attractive possibility exists when μ is small, and approaches β. Here one can approximate $Z \simeq \mu^{-2}bd(1-u_{30})^{-1} \gg 1$; this results from resonance between the electromagnetic perturbation which gives oscillatory motion to the electron at a frequency β, close to its natural oscillation frequency μ. Gain enhancement due to large Z is seen to be possible without simultaneously increasing u_{20}, so that the desirable frequency upshift property of the FEL need not be sacrificed.

We define a gain enhancement factor $\eta = G/G_0$ to compare two free-electron lasers, identical except that one has a strong axial magnetic field, while the second does not. In the first laser, the transverse magnetic field $B_\perp$ is reduced so that u_{20} is the same for both lasers. (This assures that both enjoy the same frequency upshift.) Then

$$\eta = Z\{1 - [F(\theta+\varphi) - F(\theta-\varphi)]/2\varphi F'(\theta)\}. \quad (13)$$

We have evaluated Eq. (13) for two examples with the parameters cited in the first paragraph of this Letter, holding $|\theta| = 1.3$ where $|F'(\theta)|$ has its maximum value. The results are shown in Fig. 2 for the $\gamma = 10$ example. In Fig. 2(a) we plot the gain enhancement factor η as a function of the transverse magnetic field normalized strength ξ for the FEL with the axial guide magnetic field. The solid curves are for steady-state orbits on branch C; the dashed curves for branch A. On branch A, gain occurs for $\theta > 0$, while on branch C gain occurs for $\theta < 0$. Two transverse magnetic fields for the FEL without axial field corresponding to $\xi_0 = 1$ and 0.5 are shown. Figure 2(b) shows the required values of axial guide field. One sees a gain enhancement of 31 (on branch C) at $\xi = 5 \times 10^{-3}$ for an axial guide field of 102 kG. The transverse magnetic field required is reduced to 51 G, and the gain is increased to 0.0766 at $\lambda = 105$ μm. Higher gain is predicted on branch A. For the $\gamma = 100$ example at $\lambda = 10.5$ μm, we find a gain enhancement of 16 (on branch A) at $\xi = 3 \times 10^{-2}$ for an axial guide field of 99.5 kG. The transverse magnetic field required is reduced to 30.6 G, and the gain is increased to 0.0506.

Of course when the predicted single-pass gain is large (say > 0.1) this theory must be modified. Furthermore, finite electron momentum spread (neglected here) will mitigate against gain, as for a FEL without a guide field. These effects deserve careful study. However, to the extent that these effects are negligible, our theory shows that provision of a strong uniform axial magnetic field can allow significant small-signal gain enhancement, and significant reduction in the required transverse magnetic field strength in a FEL, without undue compromise in operating frequency below that given by the idealized upshift value $2\gamma^2 k_0 c$.

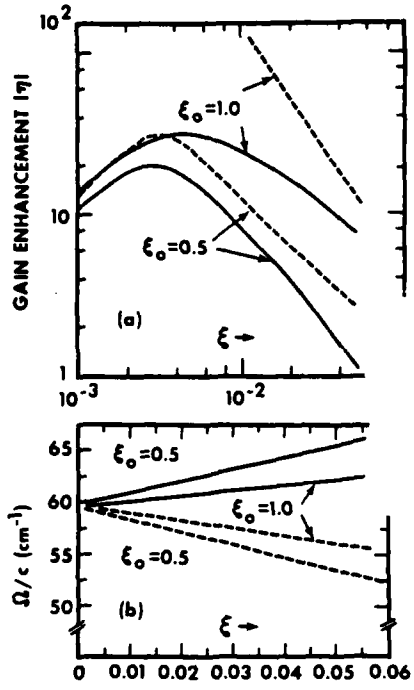

FIG. 2. (a) Gain enhancement $|\eta|$ and (b) corresponding normalized axial magnetic field Ω/c, vs transverse magnetic field parameter ξ. The values $\xi_0 = 0.5$ and 1.0 are for the FEL without axial field, and provide the same u_{20} as do the indicated (smaller) values of ξ for the FEL with the indicated axial field strength. Example is for $\gamma = 10$, $k_0 = 6.0$ cm^{-1}, and $L = 130$ cm. Solid curves, orbits on branch C; dashed curves, orbits on branch A. For high enhancement values, such as on the $\xi_0 = 1.0$ branch A example, the numerical precision required to compute accurate results suggests that the phenomenon is very sensitive to the system parameters.

This work was supported in part by the U. S. Office of Naval Research and in part by the U. S. Air Force Office of Scientific Research.

[1]L. R. Elias, W. M. Fairbank, J. M. J. Madey, H. A. Schwettman, and T. I. Smith, Phys. Rev. Lett. 36, 717 (1976).

[2]D. B. McDermott, T. C. Marshall, and S. P. Schlesinger, Phys. Rev. Lett. 41, 1368 (1978).
[3]D. A. G. Deacon, L. R. Elias, J. M. J. Madey, G. J. Ramian, H. A. Schwettman, and T. I. Smith, Phys. Rev. Lett. 38, 892 (1977).
[4]I. B. Bernstein and J. L. Hirshfield, Phys. Rev. Lett. 40, 761 (1978); T. Kwan and J. M. Dawson, Phys. Fluids 22, 1089 (1979); I. B. Bernstein and J. L. Hirshfield, Phys. Rev. A 20, 1661 (1979); P. Sprangle and R. A. Smith, Phys. Rev. A 21, 293 (1980).
[5]P. Sprangle, C.-M. Tang, and W. M. Manheimer, Phys. Rev. A 21, 302 (1980).
[6]W. B. Colson, *Physics of Quantum Electronics* (Addison-Wesley, Reading, Mass., 1977), Vol. 5.
[7]J. P. Blewett and R. Chasman, J. Appl. Phys. 48, 2692 (1977).
[8]P. Sprangle and V. L. Granatstein, Phys. Rev. A 17, 1792 (1978).
[9]L. Freidland and J. L. Hirshfield, to be published.
[10]L. Friedland, to be published.

Electron beam dynamics in combined guide and pump magnetic fields for free electron laser applications

L. Friedland

Department of Computer Science, Yale University, New Haven, Connecticut 06520
(Received 13 December 1979; accepted 21 August 1980)

The propagation of a cold relativistic electron beam in a free electron laser with an axial guide magnetic field is considered. The possibility of several steady-state helical trajectories for the electrons is shown, and the stability against perturbations and accessibility of such steady states is considered. Necessary and sufficient conditions for the stability are derived and indicate the importance of the transition region at the entrance of the laser. Possible modes of operation of the laser in different steady-state regimes are suggested and illustrated by numerical examples.

I. INTRODUCTION

The propagation of a relativistic electron beam in transverse periodic magnetic structures has been studied extensively in recent years. These studies were stimulated by the first experimentally successful free electron laser[1] which confirmed the theoretically predicted[2] possibility of using the energy stored in the relativistic beam as a source of short wavelength coherent radiation.

The most frequently used periodic magnetic pump field in a free electron laser is the transverse field produced on the axis of a double helical current winding with equal and opposite currents in each helix (a device usually referred to as a magnetic wiggler). The unperturbed motion of the electrons of the beam in the wiggler is quite simple. The reason for simplicity is that the magnetic field on the axis of a wiggler can be approximately described by a transverse vector potential $\mathbf{A}_\perp(z)$, depending only on the distance z along the axis. Therefore, the canonical transverse momentum $\mathbf{P}_\perp = \gamma m \mathbf{v}_\perp - (e/c)\mathbf{A}_\perp$ of an electron is a constant of motion,[3] which with the conservation of energy $\gamma = [1 - (v_\perp/c)^2 - (v_\parallel/c)^2]^{-1/2} = \text{const}$, uniquely defines the perpendicular and parallel components $\mathbf{v}_\perp$ and $\mathbf{v}_\parallel$ of the velocity of the electrons in the beam, for a given assignment of $\mathbf{A}_\perp(z)$. It can now be easily shown[4] that the electrons in a magnetic wiggler have helical trajectories with the same period as that of the wiggler. This simple model of the motion has been exploited in many theoretical studies, describing the operation and parametric behavior of the free electron laser.[5]

In all experiments, however, there is also an axial guide magnetic field.[1,6,7] This, of course, increases the number of parameters characterizing the free electron laser, but at the same time introduces greater complexity into the theory. The vector potential is now dependent on x and y and the perpendicular canonical momentum $\mathbf{P}_\perp$ is no longer a constant of motion; as a result, in general, no simple analytic solution for the electron trajectories can be found. Although so called "steady-state" helical trajectories with the same period as that of the wiggler and constant values of $|\mathbf{v}_\perp|$ and $|\mathbf{v}_\parallel|$ are allowed by the system, they cannot be obtained with arbitrary inlet conditions in the electron beam. Nevertheless, these are the trajectories usually used in the theory,[4,8] without studying the problem of how the steady-state situation can be achieved. An additional complication with the presence of an axial magnetic field is that, as will be shown in Sec. II of this paper, in general, there exist several possible steady-state trajectories for the same values of the axial field and wiggler parameters, and the question arises as to which of these states is accessible with given inlet conditions of the electron beam. Thus, in the presence of an axial guide field the initial conditions and the structure of the transition region at the entrance of the free electron laser may be of crucial importance in regard to the possible modes of operation of the device. These factors become even more important if the idea of recycling[9] is applied, and the electrons are forced to pass the transition region many times.

This paper presents a study of these important questions. In Sec. II, we derive the possible steady states in the homogeneous part of a free electron laser and study the stability of these states to perturbations of electron velocities. The transition region is included in the theory in Sec. III, where the possible ways of operating a free electron laser in different steady states are suggested and illustrated by numerical examples.

II. EQUATIONS OF MOTION AND STABILITY

Consider a cold relativistic electron beam moving in a magnetic field of the form

$$\mathbf{B} = \hat{B}(z)\mathbf{e}_z + \nabla \times \mathbf{A}, \tag{1}$$

where

$$\mathbf{A} = -\hat{A}(z)[\mathbf{e}_x \cos\phi(z) + \mathbf{e}_y \sin\phi(z)], \tag{2}$$

and

$$\phi = \int_0^z k_0(z')\,dz'. \tag{3}$$

For $\hat{A}$ and k_0 independent of z, the vector potential (2) describes the field on the axis of an infinite magnetic wiggler, where, as is well-known[10]

$$\hat{A} \propto I[\rho k_0 K_0(\rho k_0) + K_1(\rho k_0)], \tag{4}$$

where I is the current in the wiggler, ρ is its radius, $k_0 = 2\pi/\lambda_0$, λ_0 is the pitch of the winding of the wiggler, and $K_{0,1}$ are the modified Bessel functions of the second kind. By using the more general form (2) for the vector

 0031-9171/80/122376-07$00.90

potential, we have in mind primarily the possibility of slow variations of the wiggler parameters ρ and k_0 with z, and assume that in this case the magnitude $\hat{A}(z)$ in (2) can be approximated by expression (4), where ρ and k_0 correspond to the values of these parameters in the nonuniform wiggler at point z.

Although the magnetic field represented by the potential (2) does not satisfy $\nabla \times \mathbf{B} = 0$, it gives a good approximation of the exact curl-free field on an infinite wiggler at small distances r from its axis. Indeed, as was shown in Ref. 4, the relative deviation of the transverse component of the field from that described by (2) is of the order of $(k_0 r)^2$. Accordingly, if the beam radius l is such that $(k_0 l)^2 \ll 1$, the actual transverse field can be well represented by Eq. (2). The axial component of the field of a wiggler near the axis grows[4] as $k_0 r$; it can be neglected, however, in the presence of a strong axial guide field. We will also limit ourselves to low current beams so that the influence of the self-space charge on the beam can be neglected. We thus require that the transverse electrostatic field be much smaller than $v_\parallel B_\perp / c = v_\parallel k_0 \hat{A}/c$, or, assuming axial symmetry of the beam, $\omega_p^2 r \ll 2ek_0 \hat{A} v_\parallel / mc$, where ω_p is the plasma frequency. If, for example, $r = 0.3$ cm, $B = 500$ G, and $v_\parallel \simeq c$, the maximum current density allowed by the model will be approximately 250 A/cm^2. The small signal gain in a free electron laser at these conditions, however, may be substantial,[11] so that the results of the present work could be important in current experiments.

We now consider the momentum equation for the electrons of the beam

$$\frac{d}{dt}(\gamma \mathbf{v}) = -\frac{e}{mc}\mathbf{v} \times \mathbf{B}, \tag{5}$$

where

$$\gamma = [1 - (v^2/c^2)]^{-1/2}. \tag{6}$$

Let

$$\begin{aligned} \mathbf{e}_1(z) &= -\mathbf{e}_x \sin\phi + \mathbf{e}_y \cos\phi, \\ \mathbf{e}_2(z) &= -\mathbf{e}_x \cos\phi - \mathbf{e}_y \sin\phi, \\ \mathbf{e}_3(z) &= \mathbf{e}_z. \end{aligned} \tag{7}$$

Then, the cononical model vector potential is

$$\mathbf{A} = \hat{A}(z)\mathbf{e}_2, \tag{8}$$

and

$$\mathbf{B} = \hat{B}(z)\mathbf{e}_3 - \frac{d\hat{A}}{dz}\mathbf{e}_1 - k_0 \hat{A}\mathbf{e}_2. \tag{9}$$

On expressing the velocity $\mathbf{v}$ in terms of the orthogonal vectors $\mathbf{e}_1$, $\mathbf{e}_2$, and $\mathbf{e}_3$ and using

$$\frac{d\mathbf{e}_1}{dt} = k_0 v_3 \mathbf{e}_2; \quad \frac{d\mathbf{e}_2}{dt} = -k_0 v_3 \mathbf{e}_1, \tag{10}$$

one can rewrite (5) as

$$\begin{aligned} \gamma \frac{dv_1}{dt} &= \gamma k_0 v_2 v_3 - \frac{e}{mc}(v_2 \hat{B} + k_0 v_3 \hat{A}), \\ \gamma \frac{dv_2}{dt} &= -\gamma k_0 v_1 v_3 + \frac{e}{mc}\left(v_1 \hat{B} + v_3 \frac{d\hat{A}}{dz}\right), \\ \gamma \frac{dv_3}{dt} &= \frac{e}{mc}\left(k_0 v_1 \hat{A} - v_2 \frac{d\hat{A}}{dz}\right). \end{aligned} \tag{11}$$

On using normalized velocities $u_i = v_i/c$ and "time" $\tau = ct$ and defining $\xi(z) = e\hat{A}/mc^2$ and $\Omega = e\hat{B}/mc^2$, one can write (11) in the form

$$\dot{u}_1 = u_2\left(k_0 u_3 - \frac{\Omega}{\gamma}\right) - \frac{k_0 \xi}{\gamma} u_3, \tag{12}$$

$$\dot{u}_2 = \cdots \left(k_0 u_3 - \frac{\Omega}{\gamma}\right) + \frac{1}{\gamma}\frac{d\xi}{dz} u_3, \tag{13}$$

$$\dot{u}_3 = \frac{k_0 \xi}{\gamma} u_1 - \frac{1}{\gamma}\frac{d\xi}{dz} u_2. \tag{14}$$

First consider the homogeneous case, where $\Omega = \Omega_0 = \text{const}$, $k_0 = \text{const}$, and $\xi = \xi_0 = \text{const}$. In this case, Eqs. (12)–(14) have a particular solution

$$u_{10} = 0, \quad u_{30} = \text{const},$$

and

$$u_{20} = \frac{k_0 \xi_0 u_{30}/\gamma}{k_0 u_{30} - \Omega/\gamma}, \tag{15}$$

which with the conservation of energy

$$1/\gamma^2 = 1 - u_{20}^2 - u_{30}^2 \tag{16}$$

defines the values of u_{20} and u_{30}. The question arises as to how this steady-state solution can be achieved. One can answer this question only by considering the transition region of the wiggler, where ξ and k_0 may depend on z. Here, one would expect that for initial conditions in the beam $u_1 = u_2 = 0$, when the vector potential ξ grows slowly enough with z, the velocities u_2 and u_3 would gradually approach their steady-state values u_{20} and u_{30}, and at the same time u_1 remains zero. It can be shown, however, that, in general, this cannot be the case. In fact, one gets from (13) that if $u_1(z) \equiv 0$,

$$\dot{u}_2 - \frac{1}{\gamma}\frac{d\xi}{dz} u_3 = u_3 \frac{d}{dz}\left(u_2 - \frac{\xi}{\gamma}\right) = 0, \tag{17}$$

and therefore $u_2 = \xi/\gamma$, which, on using (12), requires that $\Omega(z) \equiv 0$. Thus, in the presence of an axial magnetic field and for the initial conditions on u considered here, u_1 cannot remain zero in the transition region. The maximum that can be expected is that the component u_1 in the transition region remains small in comparison with u_2 and u_3. When this is the case, and, in addition, u_1 remains small as the beam propagates in the homogeneous part of the wiggler we define the beam to be *stable* and now proceed to the study of this special kind of stability.

First, consider the homogeneous region of the device and in this region let

$$u_1(\tau) = w_1(\tau), \quad u_2(\tau) = u_{20} + w_2(\tau), \quad u_3(\tau) = u_{30} + w_3(\tau), \tag{18}$$

where u_{20} and u_{30} are given by (15) and (16), and $w_i(\tau)$ are small perturbations to the steady-state solution. Then, on linearizing Eqs. (12)–(14) one gets

$$\dot{w}_1 = a w_2 + b w_3, \tag{19}$$

$$\dot{w}_2 = -a w_1, \tag{20}$$

$$\dot{w}_3 = c w_1, \tag{21}$$

where

$$a = k_0 u_{30} - \frac{\Omega}{\gamma} = \frac{k_0 \xi_0}{\gamma} \frac{u_{20}}{u_{20}}, \tag{22}$$

$$b = k_0 u_{20} - \frac{k_0 \xi_0}{\gamma} = \frac{\Omega}{\gamma} \frac{u_{20}}{u_{30}}, \tag{23}$$

$$c = k_0 \xi_0 / \gamma . \tag{24}$$

Equation (19) then gives

$$\ddot{w}_1 = a\dot{w}_2 + b\dot{w}_3 = -(a^2 - bc) w_1 . \tag{25}$$

Thus, the necessary condition for the stability of the electron beam is

$$a^2 - bc > 0 , \tag{26}$$

or

$$\frac{\Omega}{k_0 \xi_0} \left(\frac{u_{20}}{u_{30}} \right)^3 < 1 . \tag{27}$$

Further study of the stability problem must involve a knowledge of u_{20} and u_{30}. Let us combine Eqs. (15) and (16); there results

$$1 - u_{30}^2 - \left(\frac{\xi}{\gamma} \right)^2 \frac{u_{30}^2}{(u_{30} - \Omega/\gamma k_0)^2} = \frac{1}{\gamma^2} . \tag{28}$$

This equation can be rewritten in the form

$$F = F_1 - F_2 = 0 , \tag{29}$$

where

$$F_1 = \frac{1 - 1/\gamma^2}{u_{30}^2} , \tag{30}$$

and

$$F_2 = 1 + \frac{(\xi_0/\gamma)^2}{(u_{30} - \Omega/k_0\gamma)^2} . \tag{31}$$

Assuming $(\xi_0/\gamma)^2 < 1 - 1/\gamma^2$ for γ large enough, the functions F_1 and F_2 have the general form shown in Fig. 1 for various values of Ω. It can be seen from Fig. 1(a) that for $\Omega = 0$, there are two solutions for u_{30}, corresponding to different directions of propagation of the electron beam. In the presence of a weak axial magnetic field, there exist two additional solutions for u_{30} adjacent to the resonance velocity $u_{3r} = \Omega/k_0\gamma$, as shown in Fig. 1(b). If one continues to increase Ω, a situation is reached, where again there remain only two real solutions for u_{30} [Figs. 1(c), (d)]. The diagram, where all possible real positive branches of u_{30} are presented as a function of Ω, is given in Fig. 2 for a sample case in which $\gamma = 1.587$, $k_0 = 1.5708\ \text{cm}^{-1}$, and $\xi_0 = 0.3873$.

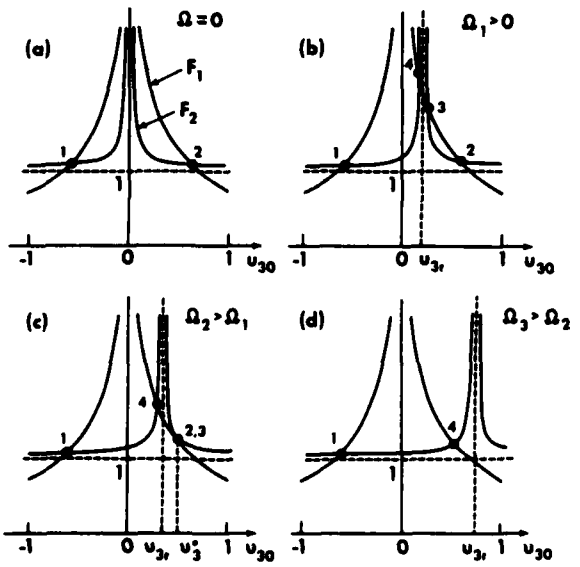

FIG. 1. Schematic of the functions F_1 and F_2, defining various possible steady-state solutions for u_{30}.

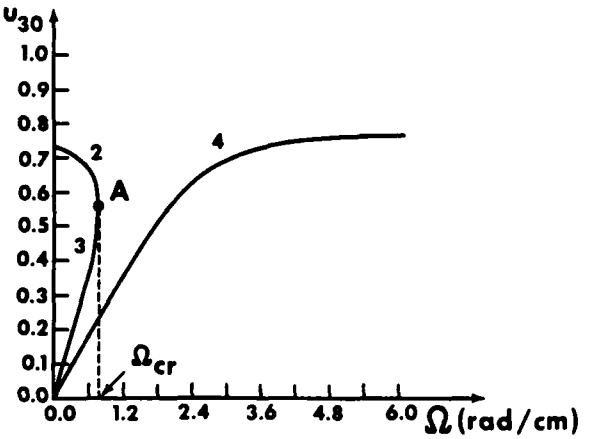

FIG. 2. The real positive branches of u_{30} vs the cyclotron frequency Ω, characterizing the guide magnetic field.

Let us now find the frequency Ω_{cr} at which the roots 2 and 3 on Fig. 2 become complex. This transition corresponds to the point A on the figure. One can find Ω_{cr} by observing that the function F in Eq. (29) has only one bounded maximum at the point u_3^*, such that $F'(u_3^*) = 0$, or

$$u_3^* = \frac{\Omega}{\alpha k_0 \gamma} , \tag{32}$$

where

$$\alpha = 1 - \left(\frac{(\xi_0/\gamma)^2}{1 - 1/\gamma^2} \right)^{1/3} . \tag{33}$$

It is now clear that when F has four real roots, they are contained in the following intervals: $[-1, 0]$, $[0, u_{3r}]$, $[u_{3r}, u_3^*]$, $[u_3^*, +1]$. On the ends of these intervals the function F changes its sign, which makes it easy to find the four roots numerically. It is also clear that the roots in the last two intervals become complex, when $F(u_3^*) = 0$. Simple algebra then leads to the following expression for Ω_{cr}:

$$\Omega_{cr} = k_0 \gamma \alpha^{3/2} \left(1 - \frac{1}{\gamma^2} \right)^{1/2} . \tag{34}$$

Considering our sample case shown in Fig. 2, Eq. (34) gives the value $\Omega_{cr} = 0.763$ rad/cm.

We now return to the question of stability. It is clear that inequality (27) (which is the necessary condition for the stability) is satisfied for branch 4 in Fig. 2, since, according to (15), u_{20} is negative on this branch. Simple analysis also shows that branch 2 is stable, since the left-hand side of (27) on this branch reaches its maximum value of 1 only at $\Omega = \Omega_{cr}$; branch 3, in contrast, is always unstable.

III. TRANSITION REGION

The inequality (27) is a necessary condition for stability of the electron beam in the homogeneous part of free electron laser. This condition becomes sufficient if the electron beam enters the homogeneous region with small enough component u_1 in its velocity. We now proceed to the study of the transition region, where as will be shown, special experimental steps must be taken in order to get a stable electron beam, corresponding to various branches on the diagram on Fig. 2. Let us assume that the vector potential ξ in the transition region is a slowly growing function of z. Experimentally, this would be the case, for example, if one gradually decreases the radius ρ of the wiggler, or increases the pitch length $\lambda_0 = 2\pi/k_0$ at the end of the device as can be seen from Eq. (4). Following the ideas used in the previous section, one can find approximate solutions of (12)–(14) by using expansions (18), where u_{20} and u_{30} are now functions of z and correspond to the components of the velocity in the homogeneous case with parameters such as those at the point z in the transition region. Then, similar to (19)–(21) one has

$$\dot{w}_1 = aw_2 + bw_3 , \tag{35}$$

$$\dot{w}_2 = -aw_1 + fu_{30} , \tag{36}$$

$$\dot{w}_3 = cw_1 - fu_{20} , \tag{37}$$

where a, b, and c are given by (22)–(24) and

$$f = \frac{1}{\gamma}\frac{d\xi}{dz} . \tag{38}$$

Taking the time derivative of Eq. (35) and assuming that the coefficients a and b are slowly varying functions of z, one gets the following equation

$$\ddot{w}_1 = a\dot{w}_2 + b\dot{w}_3 + \dot{a}w_2 + \dot{b}w_3 \simeq a\dot{w}_2 + b\dot{w}_3$$
$$= -(a^2 - bc)w_1 + f(au_{30} - bu_{20}) , \tag{39}$$

or, on using (22)–(24)

$$\ddot{w}_1 = -\mu^2 w_1 + g , \tag{40}$$

where

$$\mu^2 = a^2 - bc , \tag{41}$$

and

$$g = \mu^2 \frac{u_{20}\gamma}{k_0 \xi} f . \tag{42}$$

Assuming that μ is a slowly varying function of τ one can approximate the solution of the homogeneous equation

$$\ddot{w}_1 = -\mu^2 w_1 , \tag{43}$$

by the WKB solution

$$w_1(\tau) = \mu^{-1/2}[C_1 \cos\psi(\tau) + C_2 \sin\psi(\tau)] , \tag{44}$$

where

$$\psi = \int_0^\tau \mu(\tau')\, d\tau' . \tag{45}$$

Then, it can be easily shown, using the method of variation of constants in (44), that the solution of the inhomogeneous equation (40), with the initial conditions $w_1|_0 = \dot{w}_1|_0 = 0$, can be expressed as

$$w_1(\tau) = \frac{1}{\mu^{1/2}(\tau)} \int_0^\tau \frac{g(\tau')}{\mu^{1/2}(\tau')} \sin[\psi(\tau) - \psi(\tau')]\, d\tau' . \tag{46}$$

Thus, if the vector potential ξ grows slowly in the transition region (the function $f = 1/\gamma\, d\xi/dz$ is small enough), one expects the electron beam to enter the homogeneous part of the wiggler with a small magnitude of w_1, which is sufficient for the stability of the beam in this region if the inequality (27) is satisfied.

In such an adiabatic case, one can also find the trajectories of the electrons passing the transition region. Expressing the radius vector $\mathbf{r}$ of the electrons in the beam in terms of the unit vectors $\mathbf{e}_1$, $\mathbf{e}_2$, and $\mathbf{e}_3$ [see Eq. (7)], one has

$$\mathbf{r} = r_1\mathbf{e}_1 + r_2\mathbf{e}_2 + z\mathbf{e}_3 , \tag{47}$$

which on differentiation with respect to τ gives

$$\dot{\mathbf{r}} = (\dot{r}_1 - k_0 u_3 r_2)\mathbf{e}_1 + (\dot{r}_2 + k_0 u_3 r_1)\mathbf{e}_2 + \dot{z}\mathbf{e}_3 , \tag{48}$$

and therefore the trajectories are described by

$$\dot{r}_1 = u_1 + k_0 u_3 r_2 , \quad \dot{r}_2 = u_2 - k_0 u_3 r_1 . \tag{49}$$

This system of equations can be solved in the following way: Let

$$R = r_1 + ir_2 , \quad U = u_1 + iu_2 . \tag{50}$$

Then, on multiplying the second equation in (49) by i and adding it to the first equation, one gets

$$\dot{R} = U - ik_0 u_3 R . \tag{51}$$

If one splits R into two parts

$$R = R_0 + R_1 , \tag{52}$$

where

$$iR_0 = U/k_0 u_3 , \tag{53}$$

and R_1 is assumed to be small, then on linearization in Eq. (51),

$$\dot{R}_1 = -\dot{R}_0 - ik_0 u_3 R_1 . \tag{54}$$

The solution of this equation for R_1 is given by

$$R_1 = -\int_0^\tau \dot{R}_0(\tau') \exp(-i\{\phi[z(\tau)] - \phi[z(\tau')]\})\, d\tau' , \tag{55}$$

where ϕ is defined by (3). Thus, if the velocities u_1, u_2, and u_3 are slowly varying functions in the transition region, R_1 remains small along the trajectories and $R \simeq R_0$, or

$$r_1(z) \simeq \mathrm{Re}(R_0) \simeq \frac{u_{20}(z)}{k_0(z)u_{30}(z)} , \tag{56}$$

$$r_2(z) \simeq \mathrm{Im}(R_0) \simeq -\frac{u_{10}(z)}{k_0(z)u_{30}(z)} \ll r_1(z) , \tag{57}$$

and therefore the electrons in this case are moving on helical orbits with adiabatically changing radius r_1, and the pitch period as that of the wiggler.

Thus, we have shown that, in principle, one can obtain a stable electron beam in a free electron laser if the variations of the parameters of the wiggler in the transition region are slow enough. This conclusion,

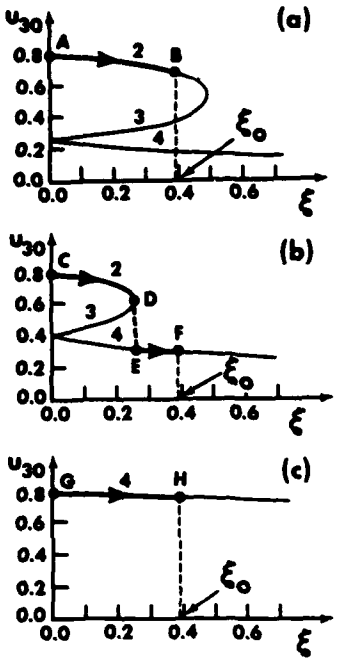

FIG. 3. The real positive branches of u_{30} vs ξ. (a) $\Omega = 0.6$ rad/cm; (b) $\Omega = 1.0$ rad/cm; (c) $\Omega = 4.0$ rad/cm.

however, is based on the approximate solution (46) for w_1 and one has to check whether all the assumptions, used in the derivation of this solution, are correct. One of these assumptions was the slowness of variation of the coefficients a and b in (35) as the beam propagates through the transition region. Let us show now that, in general, this is not guaranteed even if ξ varies slowly. The reason is that the real solutions for u_{20} and u_{30}, which are used in the definitions of a and b, do not always behave continuously. We demonstrate such a possibility in Fig. 3. In this figure, one can see the diagrams of the possible real positive solutions for u_{30}, obtained in a fashion similar to the diagram in Fig. 2, but for constant values of Ω and varying ξ. Our sample case parameters $\gamma = 1.587$ and $k_0 = 1.5708$ were again used in these graphs. As mentioned previously, the variation of ξ with constant value of k_0 can be experimentally obtained by varying the radius of the wiggler winding in the transition region, holding the pitch length $\lambda_0 = 2\pi/k_0$, constant. In Figs. 3(a,b), we show two cases with the values of Ω higher and lower than the critical value Ω_{cr} in the homogeneous region [Ω_{cr} is defined by Eq. (34), and in our sample case is equal to 0.763 rad/cm]. For $\Omega < \Omega_{cr}$, as ξ increases in the transition region, one follows the path AB in Fig. 3(a) and passes continuously to the homogeneous region corresponding to the point B on the diagram (at this point $\xi = \xi_0$). The beam is stable in this case. In contrast, if Ω is larger than Ω_{cr}, one arrives in the transition region at the point D [see Fig. 3(b)], where the branches 2 and 3 of u_{30} become complex and the homogeneous region can be only reached on the diagram by the discontinuous path DEF. The jump DE in u_{30} leads to the fast variation on the right-hand side of Eq. (12), which cannot remain small anymore, and u_1 grows in amplitude, leading to the instability of the beam. For sufficiently large values of Ω, one can again return to the stable regime. In fact, if $u_{3r} = \Omega/\gamma k_0 > 1$,

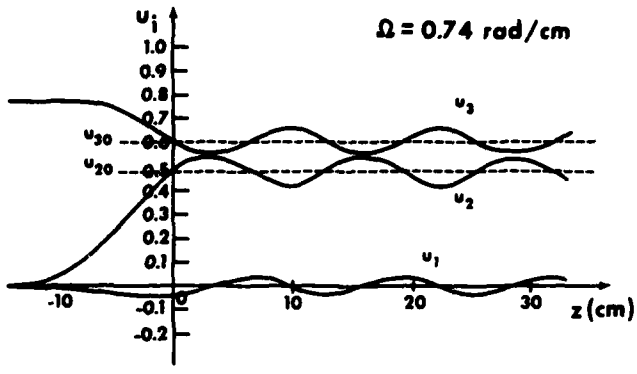

FIG. 4. The z dependence of various components of the electron velocities for $\Omega = 0.74$ rad/cm.

the only possible real branch of u_{30} is branch 4 (see Fig. 2). This situation is illustrated in Fig. 3(c). The beam follows a continuous path GH in the transition region in this case and remains stable.

In addition to these qualitative considerations, we illustrate the creation of the instability in the beam in Figs. 4 and 5, where the numerical solutions of Eqs. (12)–(14) for u_i are presented for our sample case for two values of $\Omega = 0.74$ and 0.77 rad/cm (recall that $\Omega_{cr} = 0.763$ rad/cm). We assumed in these calculations the following z dependence of the radius ρ of the wiggler winding in the transition region:

$$\rho = \begin{cases} \rho_0, & z \geq 0; \\ \rho_0 + (z/z_0)^2, & z < 0, \end{cases} \tag{58}$$

where $\rho_0 = 2.5$ cm and $z_0 = 8$ cm. The sudden transition to the unstable behavior when one goes from Fig. 4 to Fig. 5, where all the u_i's change rapidly (u_3 even becomes negative on the parts of the trajectory) is obvious.

Thus, in conclusion, if the vector potential ξ varies

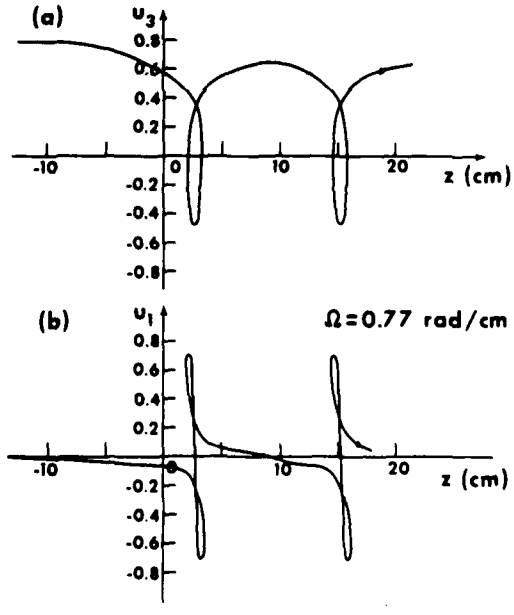

FIG. 5. The z dependence of u_1 and u_3 for $\Omega = 0.77$ rad/cm.

slowly in the transition region, one can get a stable electron beam for $\Omega < \Omega_{cr}$, and as the parameters of the wiggler vary adiabatically, the beam follows branch 2 of the possible solutions for u_{30} on Fig. 2. One can also have a stable situation for large axial magnetic fields, when branch 4 remains the only possible one for operation. One has to remember, however, that the necessary condition for the last possibility is that in the transition region $u_{3r} = \Omega/k_0\gamma > 1$. This condition can easily be satisfied when the growth of ξ in the transition region is due to the variation of the radius ρ of the wiggler, when $k_0 = \text{const}$. If in contrast, $\rho = \text{const}$ and k_0 is increasing as one approaches the end of the wiggler, larger values of the axial magnetic field are required in order to operate the device on branch 4.

Let us finally consider the question of whether it is possible with the initial conditions on the beam assumed here (namely, $u_1|_0 = u_2|_0 = 0$) to get a stable electron beam at a larger region of branch 4, especially for $u_{3r} \lesssim 1$. As mentioned before, the necessary condition (27) for stability is always satisfied on this branch, which makes it more attractive. The perpendicular component of the velocity on branch 4 can also become very large, which is again very important for possible electromagnetic wave amplification in the z direction.

The experimental scheme, which allows one to operate a free electron laser on branch 4 is shown in Fig. 6. We are exploiting the stability of the beam for large values of Ω [as demonstrated in Fig. 3(c)] and are applying a strong axial magnetic field in the transition region of the wiggler. Then, after passing this region the electrons will enter the homogeneous part of the wiggler, being on the upper part of branch 4 in Fig. 2. Now in the homogeneous region, where $\xi = \xi_0 = \text{const}$, one can gradually reduce the axial magnetic field. The beam will then follow the continuous branch 4 and one can easily reach region $\Omega \simeq \Omega_{cr}$, which was unstable with the constant axial magnetic field. We demonstrate this possibility in Fig. 7, where the solutions of Eqs. (12)–(14) are shown for exactly the same final Ω and ξ_0 as in the unstable case in Fig. 5. The same variation (58) for ρ was used in the computations. The cyclotron frequency was assumed to have the form

$$\Omega = \begin{cases} \Omega_1, & z \le 2L, \\ (\Omega_1 - \Omega_2)e^{-(z-2L)^2/L^2} + \Omega_2, & z > 2L, \end{cases} \tag{59}$$

where $\Omega_1 = 4$ rad/cm, $\Omega_2 = 0.77$ rad/cm, and $L = 4$ cm. It can be seen from Fig. 7 that the beam remains stable and corresponds to branch 4 with negative and larger values of u_{30} than in Fig. 4, which corresponds to branch 2.

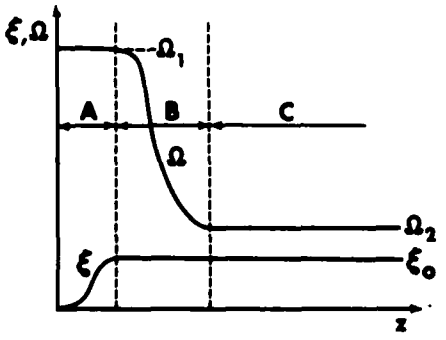

FIG. 6. Possible configuration of the pump and guide fields for operating on branch 4 of the steady-state regimes. A–transition region for ξ; B–transition region for Ω; C–homogenous part of the device.

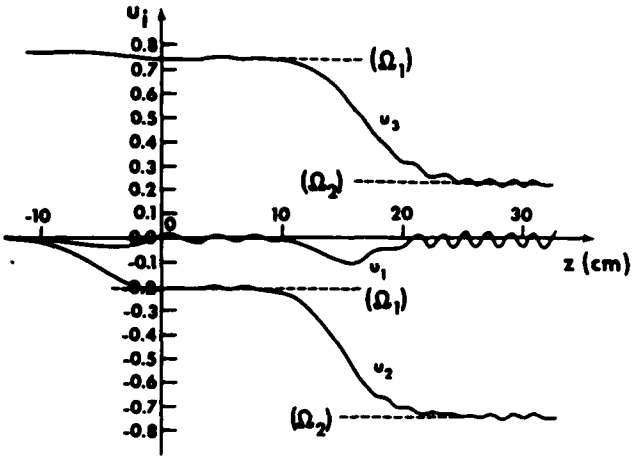

FIG. 7. The z dependence of the electron velocities in operating on branch 4 with varying guide magnetic field. Ω = 4 rad/cm, Ω = 0.77 rad/cm.

IV. CONCLUSIONS

(i) In operating a free electron laser with an axial magnetic field, different steady-state regimes of the helical motion of the electrons in the homogeneous part of the wiggler must be considered.

(ii) The necessary condition for the stability of these steady-state regimes is given by the inequality (27).

(iii) The transition region of a free electron laser plays an important role in determining the sufficient conditions for stability and in achieving the different modes of operation of a free electron laser for a given set of parameters of the homogeneous part of the device.

(iv) The following two models have been analyzed for operating a free electron laser in different steady-state regimes:

(a) The first is characterized by a constant axial magnetic field and gradual increase in the vector potential in the transition region. The stability of this scheme is limited by a critical value of the axial field given by Eq. (34). The value of the perpendicular component of the velocity is also limited in this steady-state regime.

(b) The second setup uses a strong axial magnetic field in the transition region. The field is then adiabatically decreased in the homogeneous part of the wiggler. This regime is always stable and can operate with any value of the axial magnetic field in the homogeneous region. The only limitation is imposed by the increasing radius of the helical trajectories of the electrons in the beam

as the perpendicular component of the velocities grows with a decrease in the axial guide field.

ACKNOWLEDGMENTS

The author wishes to express his appreciation to Professors I. B. Bernstein and J. L. Hirshfield for many useful discussions.

This work was supported in part by the Office of Naval Research and the Department of Energy.

[1]L. R. Elias, W. M. Fairbank, J. M. J. Madey, H. A. Schwettman, and T. I. Smith, Phys. Rev. Lett. 36, 717 (1976).
[2]H. Motz, J. Appl. Phys. 22, 527 (1951).
[3]I. B. Bernstein and J. L. Hirshfield, Phys. Rev. Lett. 40, 761 (1978).
[4]J. P. Blewett and R. Chasman, J. Appl. Phys. 48, 2692 (1977).
[5]Fo a review see P. Sprangle, R. A. Smith, and V. L. Granatstein, in *Infrared and Millimeter Waves*, edited by K. Button (Academic, New York, 1979), Chap. 7, p. 279.
[6]T. C. Marshall, S. Talmadge, and P. Efthimion, Appl. Phys. Lett. 31, 320 (1977).
[7]R. M. Gilgenbach, T. C. Marshall, and S. P. Schlesinger, Phys. Fluids 22, 1219 (1979).
[8]T. Kwan and J. M. Dawson, Phys. Fluids 22, 1089 (1979).
[9]L. R. Elias, Phys. Rev. Lett. 42, 977 (1979).
[10]W. R. Smythe, *Static and Dynamic Electricity* (McGraw-Hill, New York, 1950), p. 277.
[11]W. B. Colson, in *Physics of Quantum Electronics* (Addison-Wesley, New York, 1977), Vol. 5, p. 152.

International Journal of Infrared and Millimeter Waves, Vol. 2, No. 5, 1981

ORBIT STABILITY IN FREE ELECTRON LASERS*

P. Avivi, F. Dothan, A. F chtman, A. Ljudmirsky, and J. L. Hirshfield†

Center for Plasma Physics
Hebrew University
Jerusalem, Israel

Received June 2, 1981

Helical magnetic wigglers for free electron lasers can produce non-helical electron trajectories if a uniform axial guide magnetic field is imposed. Friedland's necessary criterion for the existence of helical orbits is reviewed and shown to apply for non-relativistic electron energies. An experiment designed to test this criterion is described and results are compared with theory.

Key words: free electron laser, magnetic wiggler, electron orbits.

Introduction

Considerable effort is currently underway in the analysis (1), design (2), and construction (3) of free electron lasers for amplification of infrared and far infrared radiation. A typical device comprises a good quality electron beam with energy of 10's of MeV which moves through a periodic static pump magnetic field, termed a magnetic wiggler. Radiation propagating along the electron beam has been shown experimentally (4) to be amplified, but the single-pass small-signal gain may be quite small (7% was reported for a 520 cm length at $\lambda = 10.6\mu$ in Ref. 4).

0195-9271/0900-1071$03.00/0

Suggestions for enhancing the small-signal gain by superposing a uniform axial magnetic upon the wiggler field have appeared, based upon both single-particle (5,6) and collective (7) models. The gain enhancement can result from either increased equilibrium undulatory momentum (5), or from dynamical resonance between induced electromagnetic perturbations and the natural oscillations of electrons on helical orbits (6,7). The increased undulatory momentum results in a decreased axial momentum, and thus a decreased Doppler up-shift, i.e. the laser output frequency is shifted to longer wavelength. Gain enhancement may still be achieved without this wavelength increase by operating the device with a reduced wiggler field.

A necessary condition for achievement of the gain enhancement is that the equilibrium electron orbits in the wiggler be nearly helical. Without the axial guide field a helical magnetic wiggler produces a helical orbit; this result follows from the constancy of canonical angular momentum. But when the axial guide field is present, the orbits are generally not helical (8). They can be arranged to be nearly helical if the entry conditions into the wiggler are suitably tailored, and if the wiggler and guide field parameters are in a regime of stability, determined from the orbit parameters (9).

In this paper, we shall review the basis underlying the criterion for orbit stability, and shall present results of an experiment designed to test this criterion quantitatively.

Orbit Stability

Here we summarize (8) some aspects of the dynamics of charged particles moving in a static magnetic field given by

$$\begin{aligned} \underline{B}(z) &= \hat{e}_z B_o + (\hat{e}_x \cos k_o z + \hat{e}_y \sin k_o z) B_\perp \\ &= \hat{e}_3 B_o - \hat{e}_2 B_\perp \quad . \end{aligned} \tag{1}$$

Here B_o is the magnitude of the uniform axial guide field, and $B_\perp$ is the magnitude of the transverse helical field with pitch $\ell_o = 2\pi/k_o$. It has been shown (1) that the

charged particle dynamics in this field are described compactly if a coordinate system with basis vectors ($\hat{e}_1$, $\hat{e}_2$, $\hat{e}_3$) is used, rather than the Cartesian system ($\hat{e}_x$, $\hat{e}_y$, $\hat{e}_z$). The coordinate transformations follow from the definitions of $\hat{e}_2$ and $\hat{e}_3$ given in Eq. (1), and by $\hat{e}_1 = \hat{e}_2 \times \hat{e}_3$.

Of course, the field given by Eq. (1) does not satisfy $\nabla \times \underline{B} = 0$; it is however a good approximation to the actual field near the axis of two identical interspersed helical conductors carrying currents in opposite directions. The exact field, and the precise nature of the approximations leading to Eq. (1) will be discussed in a forthcoming paper (10).

For a particle of charge e, rest mass m, and relativistic energy factor γ, the steady-state solutions of the equation of motion $md(\gamma\underline{v})/dt = -e\underline{v} \times \underline{B}$ [with $\underline{B}$ given by Eq. (1)] are

$$u_1 = 0$$

$$u_2 = \frac{k_o \xi u_3}{k_o u_3 \gamma - \Omega/c} \qquad (2)$$

$$u_3 = (1 - u_2^2 - \gamma^{-2})^{1/2}$$

where $\underline{u} = \underline{v}/c$, $\Omega = eB_o/m$, and $\xi = eB_\perp/k_o mc$. These components correspond to ideal helical trajectories, since u_2 and u_3 are constants. However, these steady-state values can only be approached asymptotically, for an actual wiggler, because of coupling between the components in the transition region at the entrance to the wiggler (8), and because the form given by Eq. (1) is only an approximation.

The solutions given by Eq. (2) are depicted (for γ = 10.0, k_o = 6.0 cm^{-1}, and ξ = 1.0) in Fig. 1. For $\Omega > \Omega_{cr}$ the equations are single-valued, whilst for $\Omega < \Omega_{cr}$ they are triple-valued. The critical axial guide field cyclotron frequency Ω_{cr} is given by

$$\Omega_{cr} = k_o c[(\gamma^2 - 1)^{1/3} - \xi^{2/3}]^{3/2} \quad . \qquad (3)$$

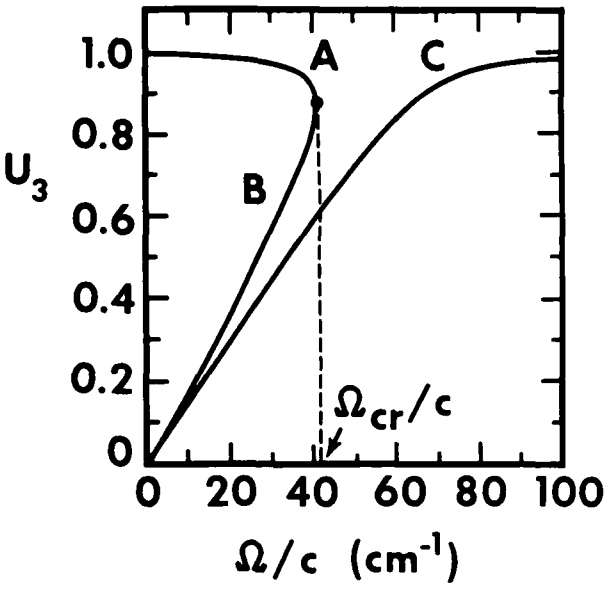

Figure 1. Solutions for steady-state axial momentum u_3, as a function of axial magnetic field, for $\gamma = 10$, $k_o = 6\ cm^{-1}$, and $\xi = 1$.

For smaller values of ξ than that chosen for Fig. 1, the curves hug more closely the asymptotes $u_3 = (1 - \gamma^{-2})^{1/2}$ and $u_3 = \Omega/k_o c\gamma$. Perturbation theory shows (8) that branches A and C in Fig. 1 are stable, whilst branch B is unstable. Thus, if a particle enters a wiggler along a gradually increasing guide field, it would move on a stable helical orbit along branch A, but at $\Omega = \Omega_{cr}$ the orbit would become unstable and thus severely non-helical. Examples of non-helical orbits are shown in Ref. 8. If Ω = const and the wiggler field increases gradually, a similar phenomenon occurs at ξ_{cr}, where

$$\xi_{cr} = [(\gamma^2 - 1)^{1/3} - (\Omega/k_o c)^{2/3}]^{3/2} , \qquad (4)$$

or $$(B_\perp/B_o)_{cr} = [(\gamma^2 - 1)^{1/3}(k_o c/\Omega)^{2/3} - 1]^{3/2} . \qquad (5)$$

Thus for a charged particle moving through a wiggler in a uniform axial guide field, the orbit can be nearly helical if $\xi < \xi_{cr}$ all along the wiggler but would depart significantly from helicity if $\xi > \xi_{cr}$.

Experiment

Although electron beams of interest for practical free electron lasers have relativistic energies, the phenomenon of helical orbit stability discussed above is not fundamentally a relativistic effect. Thus if the electron energy V is much less than 511 keV, so that we approximate $\gamma^2 - 1 \approx (2eV/mc^2)$, we can write Eq. (5) as

$$(B_\perp/B_o)_{cr} = [(8\pi^2 mV/eB_o^2 \ell_o^2)^{1/3} - 1]^{3/2}$$
$$= [(21.2V^{1/2}/B_o\ell_o)^{2/3} - 1]^{3/2} \quad (6)$$

where, in the final expression, V is in volts, B_o is in gauss, and ℓ_o is in cm.

In the experiments to be described, electron beams in the energy range 4-14 keV were employed; a simple dc low-current ($\sim$ 10's of μA) crt electron gun could then be used to provide the electron beam with a diameter of about 1 mm and energy resolution of better than 1%. The helical wiggler, to be described more fully below, had a period ℓ_o = 3.6 cm. Thus, from Eq. (6), one sees that the transition from stable to unstable orbits would occur for very small wiggler fields indeed if the axial magnetic field were adjusted to be slightly above $5.89V^{1/2}$ gauss, i.e. in the range between 350 and 700 gauss. The axial magnetic field was in fact adjusted to dc values between about 300 to 3000 gauss. For a given electron energy V and axial field B_o the wiggler field amplitude $B_\perp$ was varied continuously in time by triggering a spark gap to discharge a capacitor in series with the wiggler coil. The ensuing RC-decay could be calibrated to give $B_\perp$ values as a function of time during each discharge puise.

The wiggler coil itself was a bifilar periodic winding of 3 mm diam conductor would on a 53 mm diam cylinder with a uniform pitch of 36 mm. The uniform portion was 666 mm

long, i.e. 18.5 periods. At each end the wiggler diameter tapered outward to 100 mm over a 175 mm length. It was found that, in addition to provision of these tapered end portions, careful symmetrizing of the conductors at the end turns was essential for obtaining stable beam transmission through the wiggler. Furthermore, flux shunts at the ends were required to produce a smooth uniformly tapered transition into the wiggler. A plot of one component of the transverse field produced by this wiggler is shown in Fig. 2. (The uniform portion is not shown, as this portion is

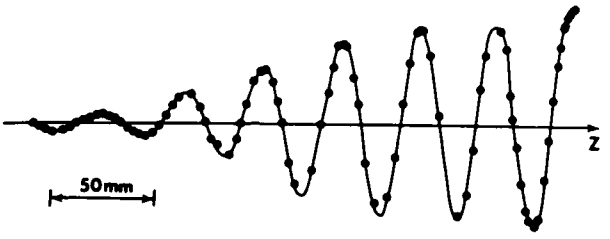

Figure 2. Measured transverse magnetic field at the entrance end of the wiggler.

relatively easy to produce.) This wiggler produced a field of about 20 gauss/kA, and fields up to 250 gauss have been routinely produced.

Several beam analyzers were constructed to examine the properties of the beam within the uniform portion of the wiggler. For the data to be presented in this paper, a movable analyzer was used consisting of two parallel plates spaced by 9 mm and positioned normal to the axial magnetic field. The first plate had a 3 mm hole in its center through which the beam would pass either in the absence of any wiggler field, or for wiggler field values below the critical value. In this case, paraxial helical orbits with diameter less than 3 mm were ascertained to be produced, so that the beam current was collected by the back plate. If the orbit were to involve excursions of more than 3 mm away from the axis, current would be collected by the front plate. When the beam was seen to migrate back and forth

between the two analyzer plates as the wiggler field decayed with time, this was taken as direct evidence for a strongly non-helical orbit. Two examples of this migration are shown in Fig. 3, which is traced from oscillograms of the

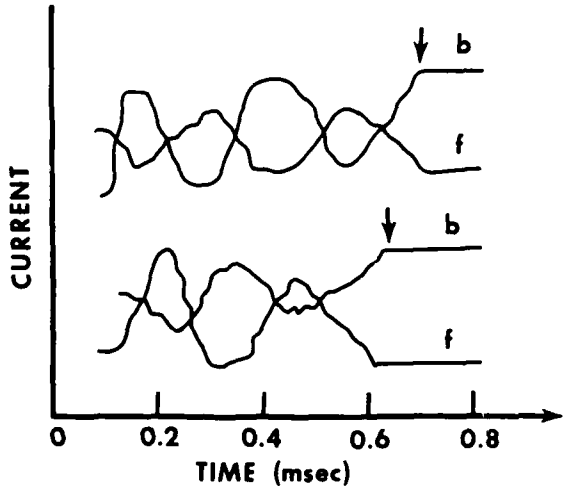

Figure 3. Measured currents to front (f) and back (b) plates of beam analyzer. Arrows indicate abrupt transitions from non-helical to helical orbits. Lower example is for a lower axial field value than upper example, so that transition occurs at higher value of wiggler field.

current waveforms to the analyzer plates as a function of time following firing of the wiggler field spark gap. The examples are for two different axial field values (lower for the bottom example than for the top). One sees the beam gyrate wildly back and forth between the two plates until a certain time, denoted by the arrows, when the wiggler field has decayed to a specific value. The transition to beam collection by the back plate alone (i.e. paraxial helical orbits) is seen to be abrupt. Values of wiggler field were noted at each transition point observed when axial field and beam energy were varied. These values are

plotted in Fig. 4 as a function of the independent variable

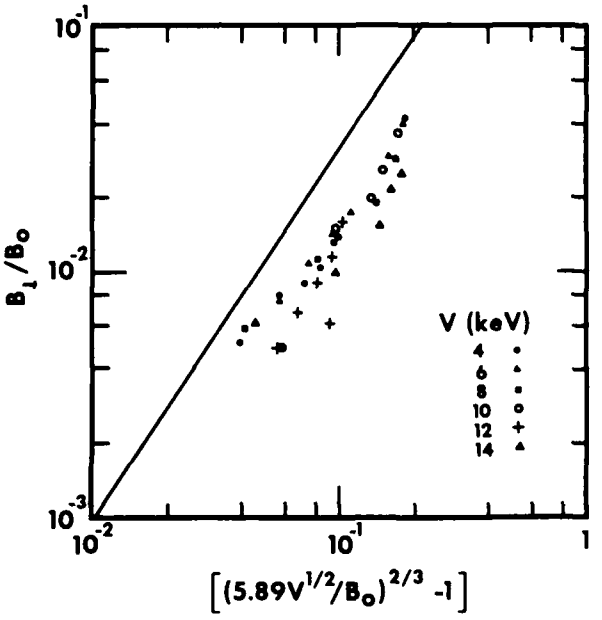

Figure 4. Measured values of $B_\perp/B_o$ at which transitions from stable to unstable orbits were observed, for electron energies between 4-14 keV. Solid line is theoretical prediction.

$(5.89V^{1/2}/B_o)^{2/3} - 1$, as suggested by Eq. (6) for ℓ_o = 3.6 cm. The straight line in Fig. 4 is this same variable raised to the three-halves power.

Transitions from unstable to stable orbits have been observed for wiggler fields as low as 2 gauss (lowest datum in Fig. 4).

Discussion

Magnetic wigglers for free electron laser applications produce helical electron orbits in the absence of an axial guide field, but may produce strongly non-helical orbits

if an axial field is present. One predicted (8) consequence of this phenomenon is an abrupt jump in the orbit from non-helical to helical once the magnetic wiggler field strength falls below a critical value, for fixed axial field and beam energy. This behavior has been observed experimentally over a wide range of (non-relativistic) beam energies and axial field strengths. The data follow an approximate three-halves power law in the variable $(8\pi^2 mV/eB_o^2 \ell_o^2)^{1/3} - 1$, as suggested by the theory. The data fall systematically about 10-20% higher in this variable than is predicted (corresponding to about a factor-of-two smaller value of $B_\perp/B_o$ than is predicted). An overestimate in measured electron beam energies could explain the discrepancy between theory and experiment, but measurement accuracies are believed sufficient to rule this out. Finite geometry effects, due either to off-axis departures of the wiggler field from Eq. (1), or from the finite spatial resolution of the analyzer, could also contribute to the apparent discrepancy.

However, the crucial points for users of magnetic wigglers in axial guide magnetic fields are (1), the care required in wiggler construction (especially at the "first" turn, and within a gradual transition region) in order to observe a paraxial helical orbit at all; and (2), the clear observation of an abrupt transition between stable and unstable orbits at (sometimes very low) critical wiggler fields, much as had been predicted by theory.

It may be that the non-helical orbits will be of utility, although it would be easy to despair in attempting to formulate a theory for free electron laser operation with such a complex equilibrium state. These orbits can possess large amplitude harmonic overtones (10) which should radiate incoherent radiation at wavelengths a few time shorter than $\ell_o/2\gamma^2$. It may even be possible to observe coherent amplification on such a spatial overtone of the fundamental wiggler period; but speculation carries risks....

Acknowledgments

The authors have benefited from instructive discussions with L. Friedland. A critical reading of the manuscript by S. Y. Park is appreciated.

References and Footnotes

* This research was sponsored by the U.S. Office of Naval Research, and by the U.S.-Israel Binational Science Foundation.

† Also at Mason Laboratory, Yale University, P.O. Box 2159 Yale Station, New Haven, Connecticut 06520.

1. I. B. Bernstein and J. L. Hirshfield, Phys. Rev. A 20, 1661 (1979).

2. See, for example, C. A. Brau, Laser Focus 17, 48 (1981).

3. See, for example, E. D. Shaw and C. K. N. Patel, Workshop on Free-Electron Generators of Coherent Radiation, Telluride, Colorado, Aug. 1979.

4. D. A. G. Deacon, L. R. Elias, J. M. J. Madey, G. J. Ramien, H. A. Schwettman, and T. I. Smith, Phys. Rev. Lett. 38, 892 (1977).

5. P. Sprangle and V. L. Granatstein, Phys. Rev. A 17, 1792 (1978).

6. L. Friedland and J. L. Hirshfield, Phys. Rev. Lett. 44, 1456 (1980).

7. I. B. Bernstein and L. Friedland, Phys. Rev. A 23, 816 (1981).

8. L. Friedland, Phys. Fluids 23, 2376 (1980).

9. Of course, these considerations also to apply to other applications for wigglers in axial fields, such as in tailoring solid electron beams for gyrotrons.

10. S. Y. Park, J. M. Baird, R. A. Smith, and J. L. Hirshfield, to be published.

International Journal of Infrared and Millimeter Waves, Vol. 2, No. 5, 1981

DEGRADATION IN GAIN FOR A FREE ELECTRON LASER AMPLIFIER DUE TO ELECTRON MOMENTUM SPREAD*

A. Fruchtman and J. L. Hirshfield†

Center for Plasma Physics
and Racah Institute of Physics
Hebrew University of Jerusalem, Israel

Received June 15, 1981

A finite spread in axial momentum for the electron beam in a free electron laser amplifier is shown to decrease the small-signal gain. For millimeter and sub-millimeter wave amplifiers, where exponential growth dominates the gain, it is shown that the gain is approximately 3 db below that for a cold beam if the relative momentum spread $(\Delta u/u)_{1/2} = (G_o/248)^{1/2}(\lambda_o/L)$, where $G_o >> 1$ is the gain in db for the cold-beam case, λ_o is the magnetic wiggler period, and L is the amplifier length. Exact numerical examples are given for representative FEL amplifiers at 35 and 550 GHz.

Key words: free electron laser, amplifier, electron momentum spread.

Most theoretical work concerning amplification of radiation in free electron lasers (FELs) deals of necessity with idealized models. One idealization widely employed involves the neglect of finite momentum spread of the electron beam. The underlying mechanism for small-signal amplification involves axial synchronization in propagation velocity between one of the allowed modes of radiation supported by the beam, and the beam itself. Thus when a spread in axial beam momentum is present, a mixing-in-phase can be expected to degrade the amplification which would otherwise be predicted for a cold beam. Prior workers (1,2) have taken note of this fact and have provided estimates of the

0195-9271/0900-0905$03.00/0

effect of momentum spread. This paper presents an exact analytical model to account for finite momentum spread for a particular distribution function. When exponential growth dominates the gain, a simple approximate formula is derived to estimate the loss in gain due to the momentum spread. Exact numerical examples are also given for representative FEL amplifiers at 35 and 550 GHz.

The basic FEL model adopted here is identical to that treated by Bernstein and Hirshfield (B-H) (3). That work gave an exact small-signal solution of the Vlasov-Maxwell equations for the steady-state evolution of the co-propagating disturbance which grows in space on a relativistic electron beam passing along the axis of a helical magnetic wiggler. The B-H theory was derived for a beam of arbitrary momentum distribution in a wiggler of arbitrary strength, but the solutions presented were for the case of a cold beam, viz.,

$$f_o(\alpha,\beta,u) = N_o\delta(\alpha)\delta(\beta)\delta(u-U) \ . \qquad (1)$$

Here α and β are the two transverse components of canonical angular momentum $U_x - eA_x/mc^2$ and $U_y - eA_y/mc^2$, A_x and A_y are the components of the wiggler's vector potential, U_x and U_y are the transverse components of translational momentum, and $U = (\gamma^2 - 1)^{1/2}$ is the total momentum as related to the relativistic energy factor . (All momenta are normalized to mc.) Eq. (1) thus describes a beam which, prior to entering the wiggler, contains electrons possessing both zero transverse momentum and unique axial momentum U.

As mentioned above, an important source of degraded amplification is the finite spread of axial momentum on the electron beam. In the work reported here, we choose the simplest distribution capable of describing such a spread, viz.,

$$f_o(\alpha,\beta,u) = N_o\delta(\alpha)\delta(\beta)\left[\frac{H(u-U_1) - H(u-U_2)}{\Delta U}\right] , \qquad (2)$$

where $H(x) = 1$ for $x > 0$, $H(x) = 0$ for $x < 0$, and $\Delta U = U_2 - U_1 > 0$. This distribution can of course not be realized in nature [in the same sense that the distribution given by Eq. (1) cannot]. It may, however, not be a bad approximation for certain accelerators (except for the

sharp edges); but its utility here is that it enables an analytic form to be derived for the governing dispersion relation.

The goal of the present work is identical to that in B-H, namely to calculate the power gain G (in db) for a single pass of electromagnetic radiation along a FEL amplifier of length L.

$$10^{G/10} = a_2(L)a_2^*(L) - 1 \tag{3}$$

Here $a_2(L)$ is the dimensionless wave electric field at the amplifier output, normalized to unity at the input. The subscript "2" labels one of the three polarizations permitted, namely that which twists in space a quarter-period behind the wiggler's vector potential. [Eqs. (35) and (37) in B-H give the other two polarizations.]

The wave amplitude $a_2(L)$ is a superposition of several co-propagating normal modes, each with its wavenumber k_j, viz.,

$$a_2(L) = \sum_j \frac{B(k_j)}{R'(k_j)} \exp(ik_jL) \tag{4}$$

The relative mode amplitudes $B(k_j)/R'(k_j)$ are prescribed once boundary conditions are set. $R(k_j) = 0$ is the dispersion relation for the system which determines the $k_j(\omega)$, assuming $R^{-1}(k)$ to have simple poles. For the cold beam case $R(k_j)$ is a sixth-order polynomial.

$$\begin{aligned} R(x) = {} & [(x-\mu)^2 - \delta^2(1+\xi^2)][(x+x_o)^2 - b^2][(x-x_o)^2 - b^2] \\ & + \xi^2\delta^2(x^2-b^2)(x^2+x_o^2-b^2) \ , \end{aligned} \tag{5}$$

where $x = kc/\omega$, $x_o = k_oc/\omega$; $\delta = (\omega_p/\omega)(U/\gamma U_z^3)^{1/2}$, $b = (1-U_z^2\delta^2)^{1/2}$, $\mu = \gamma/U_z$, $U_z = (U^2-\xi^2)^{1/2}$, and $\xi = -eB_o/mc^2k_o$. The wiggler field strength and wavenumber are B_o and k_o. This equation has been obtained as well by Sprangle (1), and related forms have been derived and discussed by Kroll and McMullin (2) and by Kwan, Dawson, and Lin (4). When $\delta << x_o << 1$, a reduced form of Eq. (5) is a good approximation, namely

$$R(x) \simeq [(x-\mu)^2 - \delta^2(1+\xi^2)][x - (b+x_o)] + \frac{1}{2}\xi^2\delta^2 x_o \quad . \quad (6)$$

For $k_o/k \lesssim (1+\xi^2)/2\gamma^2$ the maximum growth occurs near $b+x_o - \mu = (\delta^2\xi^2 x_o/2)^{1/2}$. To requisite accuracy the roots are

$$\begin{aligned} x_1 &= \mu + (\delta^2\xi^2 x_o/2)^{1/3}\exp(-\pi i/3) \\ x_2 &= x_1^* \\ x_3 &= \mu - (\delta^2\xi^2 x_o/2)^{1/3} \quad . \end{aligned} \quad (7)$$

These roots are of use in scaling estimates when exponential gain is dominant. Exact numerical evaluations given in B-H show, however, that Eq. (7) cannot be used to determine the entire gain spectrum.

When Eq. (2) is employed as the distribution function all the momentum-space integrals in the Vlasov formulation can be expressed analytically. We then find

$$\begin{aligned} R(x) = [(x-\mu_1)(x-\mu_2) - \delta'^2(1+\xi^2)][(x+x_o)^2 - b'^2] \\ \times [(x-x_o)^2 - b'^2] + \xi^2\delta'^2(x^2-d^2)(x^2+x_o^2-b'^2) \quad , \end{aligned} \quad (8)$$

where

$$\delta'^2 = -\frac{\omega_p^2}{\omega^2}\,\frac{1}{1+\xi^2}\,\frac{\Delta\mu}{\Delta U} \quad ;$$

$$b'^2 = 1 - \frac{\omega_p^2}{\omega^2}\,\frac{1}{\Delta U}\,\ell n\left(\frac{\gamma_2 + U_{z2}}{\gamma_1 + U_{z1}}\right) \quad ;$$

$$d^2 = 1 - \frac{1}{\Delta U}\,\frac{\omega_p^2}{\omega^2}\left[\Delta\mu - \frac{1+\xi^2}{\Delta\mu}\left(\frac{1}{U_{z1}} - \frac{1}{U_{z2}}\right)^2\right] \quad ;$$

$\Delta\mu = \mu_2 - \mu_1 < 0$, $\gamma_{1,2}^2 = 1 + U_{1,2}^2$, $U_{z1,2}^2 = U_{1,2}^2 - \xi^2$, and $\mu_{1,2} = \gamma_{1,2}/U_{z1,2}$.

When $\Delta U/U \ll 1$, $\Delta\mu \simeq -U\Delta U(1+\xi^2)\gamma U_z^3$, $\delta' \simeq \delta$, and $b' \simeq d \simeq b$. Thus the only effect of finite momentum spread in this limit is in the factor $(x-\mu_1)(x-\mu_2) = (x-\bar{\mu})^2 - (\Delta\mu/2)^2$ in the first bracket in Eq. (8), where $\bar{\mu} = (\mu_1+\mu_2)/2$. The close similarity between Eqs. (8) and (5), and the simplicity of the former, make determination of the roots k_j a routine matter. This simplicity is not enjoyed when the momentum spread is described by functions $f_o(\alpha,\beta,U)$ with non-zero values of $\partial f_o/\partial U$ in a finite interval, because of wave-particle resonance effects.

As for the cold-beam case, where $\delta' \ll x_o \ll 1$, Eq. (8) may be reduced to the approximate form

$$R(x) \simeq [(x-\bar{\mu})^2 - (\Delta\mu/2)^2][x-(b'+x_o)] + \xi^2\delta'^2 x_o/2 = 0. \quad (9)$$

If $(\Delta\mu/2)^2 \ll 3(\xi^2\delta'^2x_o/2)^{1/3}$, the roots of Eq. (9) near $b'+x_o-\bar{\mu} = (\xi^2\delta'^2x_o/2)^{1/2}$ are approximately

$$\begin{aligned} x_1 &= \bar{\mu} + (\xi^2\delta'^2x_o/2)^{1/3}\exp(i\pi/3) \\ &\qquad + \tfrac{1}{3}(\Delta\mu/2)^2(\xi^2\delta'^2x_o/2)^{-1/3}\exp(-i\pi/3) \\ x_2 &= x_1^* \\ x_3 &= \bar{\mu} - (\xi^2\delta'^2x_o/2)^{1/3} - \tfrac{1}{3}(\Delta\mu/2)^2(\xi^2\delta'^2x_o/2)^{-1/3}. \end{aligned} \quad (10)$$

Thus the spatial growth constant $\mathrm{Im}x_1$ is seen to decrease on account of momentum spread as

$$\mathrm{Im}x_1 \simeq \frac{\sqrt{3}}{2}\left(\xi^2\delta'^2x_o/2\right)^{1/3}\left[1-\frac{1}{3}\left(\frac{\Delta\mu}{2}\right)^2\left(\xi^2\delta'^2x_o/2\right)^{-2/3}\right]. \quad (11)$$

For pure exponential gain, i.e. excluding the 15.6 db input coupling loss (see B-H), one has

$$G = 54.58(L/\lambda)\mathrm{Im}x_1 \quad \text{db} \quad (12)$$

where λ is the radiation wavelength. From Eq. (11) we can write $G = G_o - G_1$, where G_o is the gain with no momentum spread, and G_1 is the small decrease due to the spread

$$G_o = 54.58(L/\lambda)\frac{\sqrt{3}}{2}(\xi^2\delta^2 x_o/2)^{1/3} \text{ db} . \quad (13)$$

For $\xi = 0.47$, $\lambda = 4.9$, $x_o = 2.73 \times 10^{-2}$, $\delta^2 = 3.80 \times 10^{-6}$, and $L/\lambda = 367$ (corresponding to a representative FEL amplifier to be discussed below), Eq. (13) gives $G_o = 39.1$ db. [If one subtracts the 15.6 db input coupling loss, the actual gain would be 23.5 db (at a wavelength of 560 μm).] Now

$$G_1 = \frac{54.58}{8\sqrt{3}} \frac{L}{\lambda} (\Delta\mu)^2 (\frac{1}{2}\xi^2\delta^2 x_o)^{-1/3} \text{ db} . \quad (14)$$

Substituting from Eq. (13) gives the value of $\Delta\mu$ which would bring about a gain loss G_1

$$(\Delta\mu)^2 = 5.37 \times 10^{-3} G_o G_1 (\lambda/L)^2 . \quad (15)$$

For the example cited above with $L/\lambda = 367$ we find $\Delta\mu = 2.16 \times 10^{-3}$ for $G_o = 39.1$ db and $G_1 = 3$ db, i.e. for a factor-of-two decrease in power amplification. This corresponds to a relative momentum spread $\Delta U/U = |\Delta\mu|[\gamma U_z^3/U^2(1 + \xi^2)]$ of 0.041.

Equation (10) also suggests that the frequency at which gain has its peak value will decrease as momentum spread increases.

Exact numerical evaluations for small-signal gain G have been carried out using the full dispersion relation [Eq. (8)], and with amplitudes [see Eq. (4)] appropriate to a perfectly matched amplifier output. One example is for a mm-wave amplifier employing an electron beam typical of that produced by a small Febetron accelerator, with $\gamma = 1.78$, $J = 100$ A/cm^2, $\lambda_o = 3.6$ cm, $\xi = 0.2$, and $L = 36$ cm. Gain curves are shown in Fig. 1 for zero momentum spread, and for finite momentum spreads between 5 and 20%. Gain is seen to fall by one-half for $\Delta U/U \simeq 0.15$, and the frequency for peak gain drops by about 6%. A second example is for a sub-mm wave amplifier employing a beam typical of the VEBA accelerator at Naval Research Laboratory, with $\gamma = 4.9$, $J = 6$ kA/cm^2, $\lambda_o = 2.0$ cm, $\xi = 0.47$, and $L = 20$ cm. For this case the computed gain curves are shown in Fig. 2, again for zero momentum spread and for spreads between 5 and 20%.

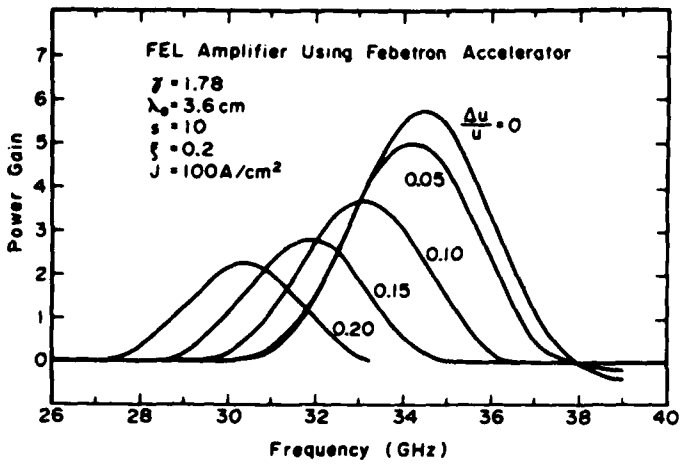

Figure 1. Gain curves for a FEL using a 400 kV electron beam, for electron momentum spread between 0 and 20%.

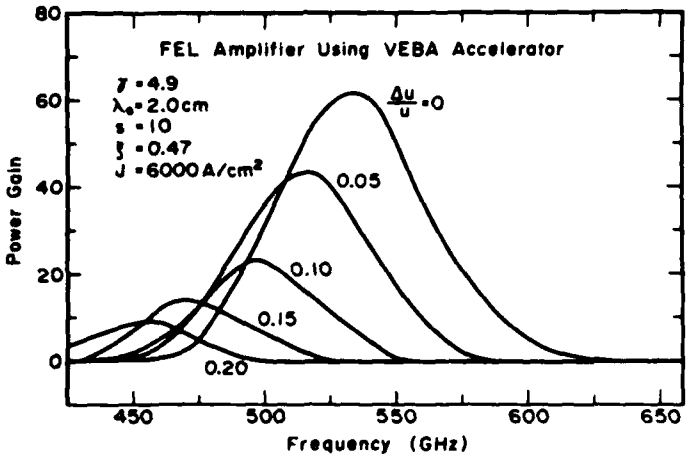

Figure 2. Gain curves for a FEL using a 2.0 MV electron beam, for electron momentum spread between 0 and 20%.

Comparisons between the exact results (Fig. 2) and the approximate predictions [Eqs. (12-15)] are instructive. The peak gain for the cold beam is 17.8 db (i.e. 60×) compared with the approximate value of 23.5 db. The gain drops by half to 14.8 db (i.e. 30×) for $\Delta U/U$ somewhat greater than 10%; our approximate result is 4.1%. These comparisons for the example presented in Fig. 1 are not meaningful since the peak gain G_o is less than 7.8 db (6×).

Finally, we point out the scaling laws suggested by Eqs. (12-15), valid for high gain devices where exponential growth dominates. For negligible momentum spread,

$$G_o \sim J^{1/3} L \xi^{2/3} \lambda^{-2/3} \lambda_o^{-1/3} \text{ db}$$

or equivalently (16)

$$G_o \sim J^{1/3} (L/\lambda_o) \xi^{2/3} \gamma^{4/3} \text{ db} \quad .$$

For the gain decrease $G_1 \ll G_o$ due to finite momentum spread we have

$$G_1 G_o \sim (\Delta U/U)^2 (L/\lambda_o)^2 \ (\text{db})^2 \quad . \qquad (17)$$

Eq. (17) indicates that high gain short amplifiers are less susceptible to gain degradation due to momentum spread, than are low gain long amplifiers. This scaling is independent of λ and γ provided G_o is high. For G_1 = 3 db, the numerical value for Eq. (17) gives $(\Delta U/U)_{1/2} = (G_o/248)^{1/2} (\lambda_o/L)$, where $(\Delta U/U)_{1/2}$ is the relative momentum spread for a factor-of-two decrease in gain. Gain degradation for long-wiggler FELs operating in the collective regime can be expected to be serious unless $\Delta U/U \ll 1$.

It should be added as a caveat however that momentum spread may not always degrade gain in a FEL. The geometrical optics theory for a FEL amplifier (5) shows that gain may arise from a wave-particle resonance, provided $f_o(\alpha,\beta,u)$ is not symmetric in u about its maximum, and provided $\partial f_o/\partial u$ has the requisite sign at the wave's phase velocity. It is expected that this mechanism would compete with that discussed in the present paper, and could in fact allow substantial gain in the presence of tailored momentum spread.

Acknowledgment

Appreciation is extended to Dr. S. Y. Park for a critical reading of the manuscript.

References

* This research was sponsored by the U.S. Office of Naval Research, and by the U.S.-Israel Binational Science Foundation.

† Also at Mason Laboratory, Yale University, P.O. Box 2159, Yale Station, New Haven, Connecticut 06520.

1. P. Sprangle and R. A. Smith, Phys. Rev. A 21, 293 (1980).

2. N. M. Kroll and W. A. McMullen, Phys. Rev. A 17, 300 (1978).

3. I. B. Bernstein and J. L. Hirshfield, Phys. Rev. A 20, 1661 (1979).

4. T. Kwan, J. M. Dawson, and A. T. Lin, Phys. Fluids 20, 581 (1977).

5. I. B. Bernstein and J. L. Hirshfield, Phys. Rev. Lett. 40, 761 (1978).

Theory of the free-electron laser in combined helical pump and axial guide fields

Ira B. Bernstein and Lazar Friedland
Department of Engineering and Applied Science, Yale University, New Haven, Connecticut 06520
(Received 7 July 1980)

The linearized theory of a free-electron-laser amplifier consisting of a relativistic electron beam transported along the axis of a helical wiggler in the presence of an axial guide field is solved exactly. With suitable re-identification of parameters, the theory also applies to the case where the wiggler is replaced by a circularly polarized subluminous radio-frequency pump. The dispersion relation is derived and numerical examples of solutions are presented. These indicate (a) that the use of an axial field permits operation of a laser of given high frequency and undulatory transverse velocity of the unperturbed electron beam at lower values of the pump field, (b) that the gain can be enhanced by approaching the condition of resonance between the effective frequency of the pump and the cyclotron frequency, and (c) that the breadth in frequency of the region corresponding to spatially exponentially growing operation can be much extended.

I. INTRODUCTION

The theory of a free-electron laser (FEL), consisting of a relativistic electron beam transported along the axis of a helical pump magnetic field, has been given by Bernstein and Hirshfield.[1] Their analysis was valid for arbitrary pump strength but weak rf fields, since it involved linearization in the amplitudes of the high-frequency quantities. Here we present the extension of that work to the case where, in addition, there is an axial magnetic field, conventionally present for beam collimation. It is also shown that with a suitable reinterpretation of parameters, the same theory applies when the magnetostatic pump is replaced by a circularly polarized subluminous rf pump. The axial field is shown to yield the additional benefits of permitting the use of weaker pumps, providing enhanced gain and yielding broader domains of spacial instability. This is discussed in detail in Sec. VI.

The work proceeds as follows. The general mathematical description is developed in Sec. II where the continuity and momentum equations describing the relativistic beam, and those governing the electromagnetic fields are presented. Section III describes the properties of a helical pump magnetostatic field, and Sec. IV those of a circularly polarized subluminous rf pump. The linearized equations governing the high-frequency fields are derived in Sec. V. Section VI is devoted to a brief discussion of the relation of this work to its predecessors, to a description of the numerical examples worked out, and conclusions concerning the effects of the axial field.

II. GENERAL MATHEMATICAL DESCRIPTION

Consider a cold relativistic electron beam described by the continuity equation

$$\frac{\partial N}{\partial t}+\nabla\cdot(N\vec{v})=0 \tag{1}$$

and the momentum equation

$$\left(\frac{\partial}{\partial t}+\vec{v}\cdot\nabla\right)(m\gamma\vec{v})=-e\left(\vec{E}+\vec{v}\times\frac{\vec{B}}{c}\right), \tag{2}$$

where m is the rest mass of the electron, and

$$\gamma=(1-v^2/c^2)^{-1/2} \tag{3}$$

If one forms the scalar product of (2) with $\gamma\vec{v}$ and uses (3) to express v in terms of γ, there results the energy equation

$$\left(\frac{\partial}{\partial t}+\vec{v}\cdot\nabla\right)mc^2\gamma=-e\vec{E}\cdot\vec{v}. \tag{4}$$

Let $\hat{B}$ be a constant. It is convenient to introduce the electromagnetic potential $\vec{A}$ and Φ via

$$\vec{B}=\hat{B}\vec{e}_z+\nabla\times\vec{A}, \tag{5}$$

$$\vec{E}=-\nabla\Phi-\frac{\partial}{\partial t}\left(\frac{\vec{A}}{c}\right). \tag{6}$$

Then with $\Omega=e\hat{B}/mc$ one can write (2) in the form

$$\begin{aligned}&\left(\frac{\partial}{\partial t}+\vec{v}\cdot\vec{\nabla}\right)(m\gamma\vec{v})\\&=-\left(\frac{e}{c}\right)\left(-c\nabla\Phi-\frac{\partial\vec{A}}{\partial t}+\vec{v}\times(\nabla\times\vec{A})+\hat{B}\vec{v}\times\vec{e}_z\right)\\&=m\Omega\vec{e}_z\times\vec{v}+\left(\frac{e}{c}\right)\left(c\nabla\Phi+\frac{\partial\vec{A}}{\partial t}+\vec{v}\cdot\nabla\vec{A}-(\vec{v}\vec{A})\cdot\vec{v}\right)\end{aligned} \tag{7}$$

or on rearranging terms

$$\begin{aligned}&\left(\frac{\partial}{\partial t}+\vec{v}\cdot\vec{\nabla}\right)\left(\gamma\vec{v}-\frac{e\vec{A}}{mc}\right)\\&=\Omega\vec{e}_z\times\vec{v}+\left(\frac{e}{mc}\right)[c\nabla\Phi-(\nabla\vec{A})\cdot\vec{v}].\end{aligned} \tag{8}$$

It follows from the Maxwell equations

$$c\nabla\times\vec{B}=4\pi\vec{J}+\frac{\partial\vec{E}}{\partial t}, \tag{9}$$

$$\nabla\cdot\vec{E}=4\pi\Sigma, \tag{10}$$

on employing (5) and (6), that

$$\nabla^2\vec{A}-c^{-2}\frac{\partial^2\vec{A}}{\partial t^2}+\left(\frac{4\pi}{c}\right)\vec{J}=\nabla\left(c^{-1}\frac{\partial\Phi}{\partial t}+\vec{\nabla}\cdot\vec{A}\right), \tag{11}$$

$$\nabla^2\Phi+4\pi\Sigma=-c^{-1}\nabla\cdot\frac{\partial\vec{A}}{\partial t}. \tag{12}$$

Thus if we adopt the canonical model of FEL theory, viz.

$$\vec{A}=A_x(z,t)\vec{e}_x+A_y(z,t)\vec{e}_y, \tag{13}$$

$$\Phi=\Phi(z,t) \tag{14}$$

(note that the vector potential is written in the Coulomb gauge) and assume that the only charged particles present are electrons, whence $\Sigma=-Ne$ and $\vec{J}=-Ne\vec{v}$, then (11) and (12) yield

$$\frac{\partial^2\vec{A}}{\partial z^2}-c^{-2}\frac{\partial^2\vec{A}}{\partial t^2}=\left(\frac{4\pi Ne}{c}\right)(\vec{v}-\vec{e}_z\vec{e}_z\cdot\vec{v}), \tag{15}$$

$$\frac{\partial^2\Phi}{\partial z^2}=4\pi Ne. \tag{16}$$

III. MAGNETOSTATIC PUMP

Consider the case of a free-electron laser in which the pump magnetostatic field is generated by helical windings and the self-fields of the electron beam are negligible. Then in cylindrical coordinates ρ,θ,z the vacuum magnetic scalar potential χ will be helically invariant, viz.

$$\chi=\chi(\rho,\theta-k_0z), \tag{17}$$

where $2\pi/k_0$ is the pitch, and will satisfy Laplace's equation

$$\nabla^2\chi=\frac{1}{\rho}\frac{\partial}{\partial\rho}\left(\rho\frac{\partial\chi}{\partial\rho}\right)+\left(k_0^2+\frac{1}{\rho^2}\right)\frac{\partial^2\chi}{\partial\theta^2}=0. \tag{18}$$

The general solution of (18), regular at $\rho=0$, on separation of variables is readily shown to be

$$\chi=-\hat{B}z+\sum_{m=1}^{\infty}\chi_m I_m(mk_0\rho)\cos[m(\theta-k_0z)+\lambda_m], \tag{19}$$

where the χ_m and λ_m are constants determined by the details of the helical windings. Recall that the Bessel function

$$I_m(\zeta)=\sum_{s=0}^{\infty}\frac{(\frac{1}{2}\zeta)^{m+2s}}{s!\,(m+s)!}. \tag{20}$$

Thus if a is the radius of the windings and $\rho\ll 2\pi/k_0$, the potential is well approximated by the term with $m=1$ alone, with I_1 approximated by the leading term in the series. The resulting expression for the associated magnetic field is, on choosing the coordinate system so that $\lambda_1=0$ and $\frac{1}{2}k_0\chi_1=-B_0$,

$$\vec{B}=-\nabla\chi\approx\hat{B}\vec{e}_z+B_0(\vec{e}_x\cos k_0z+\vec{e}_y\sin k_0z). \tag{21}$$

The nonconstant part of (21) can be written as the curl of the vector potential

$$\vec{A}=-(B_0/k_0)(\vec{e}_x\cos k_0z+\vec{e}_y\sin k_0z). \tag{22}$$

Expression (22), valid only near the axis, is the form conventionally taken for the magnetostatic pump field. A corresponding solution for the velocity and density can be obtained from (1) and (8) by introducing the basis vectors

$$\vec{e}_1=-\vec{e}_x\sin k_0z+\vec{e}_y\cos k_0z, \tag{23}$$

$$\vec{e}_2=-\vec{e}_x\cos k_0z-\vec{e}_y\sin k_0z, \tag{24}$$

$$\vec{e}_3=\vec{e}_z, \tag{25}$$

when on writing

$$A=A_1\vec{e}_1+A_2\vec{e}_2+A_3\vec{e}_3 \tag{26}$$

it follows that

$$\frac{\partial\vec{A}}{\partial z}=\left(\frac{\partial A_1}{\partial z}-k_0A_2\right)\vec{e}_1+\left(\frac{\partial A_2}{\partial z}+k_0A_1\right)\vec{e}_2+\frac{\partial A_3}{\partial z}\vec{e}_3. \tag{27}$$

Thus (1) and (8) imply

$$\left(\frac{\partial}{\partial t}+\frac{v_3\partial}{\partial z}\right)N=-\frac{N\partial v_3}{\partial z}, \tag{28}$$

$$\left(\frac{\partial}{\partial t}+\frac{v_3\partial}{\partial z}\right)\left(\gamma v-\frac{eA_1}{mc}\right)-k_0v_3\left(\gamma v_2-\frac{eA_2}{mc}\right)=-\Omega v_2, \tag{29}$$

$$\left(\frac{\partial}{\partial t}+\frac{v_3\partial}{\partial z}\right)\left(\gamma v_2-\frac{eA_2}{mc}\right)+k_0v_3\left(\gamma v_1-\frac{eA_1}{mc}\right)=\Omega v_1, \tag{30}$$

$$\left(\frac{\partial}{\partial t}+\frac{v_3\partial}{\partial z}\right)(\gamma v_3)=\left(\frac{e}{mc}\right)\left(c\frac{\partial\Phi}{\partial z}-v_1\frac{\partial A_1}{\partial z}-v_2\frac{\partial A_2}{\partial z}-k_0v_2A_1+k_0v_1A_2\right). \tag{31}$$

Now on combining (22) and (25) one can write

$$\vec{A}_0=(mc^2/e)\xi_0\vec{e}_2, \tag{32}$$

where ξ_0 is a dimensionless constant. It is then readily seen that if also $\Phi_0=0$, corresponding to $E_0=-\nabla\Phi_0=0$, then a solution is given by

$$\vec{v}_0=u\vec{e}_3+w\vec{e}_2, \tag{33}$$

$$N_0=\text{const}, \tag{34}$$

where $u=\text{const}$ and $w=\text{const}$, satisfy (27)–(30) provided that consequent to (29)

$$w=k_0cu\xi_0(k_0u\gamma_0-\Omega)^{-1}: \tag{35}$$

where

$$\gamma_0 = [1 - (u^2 + w^2)/c^2]^{-1/2} \tag{36}$$

This solution and its experimental accessibility has been analyzed in detail by Friedland.[2]

IV. RADIO-FREQUENCY PUMP

The solution given by (32), (33), and (34) with $\vec{E}_0 = 0$ can also be adapted to describe the case of a free-electron laser with an electromagnetic pump which in the laboratory frame has a phase velocity less than the speed of light. One then views the solution as given in the frame where the pump wave is at rest. Equation (15) then requires, on using (32) and (33), that

$$-k_0^2 c^2 \xi_0 = \omega_p^2 w/c\,, \tag{37}$$

which on using (35) can be written

$$-k_0 c = \omega_p^2 \mu (k_0 u \gamma_0 - \Omega)^{-1}\,, \tag{38}$$

where the plasma frequency, defined using the rest mass, is

$$\omega_p = (4\pi N_0 e^2/m)^{1/2}\,. \tag{39}$$

Let v_0 be the speed of the laboratory frame as seen from the wave frame. Distinguish quantities in the laboratory frame by a prime. Then on Lorentz transformation $z' = \hat{\gamma}(z - v_0 t)$, $t' = \hat{\gamma}(t - v_0 z/c^2)$, and

$$\omega' = -k_0 v_0 \hat{\gamma}\,, \tag{40}$$

$$k_0' = k_0 \hat{\gamma}\,, \tag{41}$$

where

$$\hat{\gamma} = (1 - v_0^2/c^2)^{-1/2}\,. \tag{42}$$

Clearly

$$v_0 = -\omega'/k_0'\,, \tag{43}$$

is the negative of the phase velocity of the wave. Moreover,

$$\vec{B}_0' = \hat{B}\vec{e}_3 + B_0'[\vec{e}_x \cos(k_0' z' - \omega' t') + \vec{e}_y \sin(k_0' z' - \omega' t')]\,, \tag{44}$$

where

$$B_0' = \hat{\gamma} B_0 \tag{45}$$

and

$$\vec{E}_0' = -(\omega'/k_0' c)\vec{e}_3 \times \vec{B}_0'\,. \tag{46}$$

Evidently the wave is transverse and circularly polarized. The associated potentials are

$$\Phi_0' = 0\,, \tag{47}$$

$$\vec{A}_0' = A_0'[\vec{e}_x \cos(k_0' z' - \omega' t') + \vec{e}_y \sin(k_0' z' - \omega' t')]\,, \tag{48}$$

where

$$A_0' = -\frac{B_0'}{k_0'} = -\frac{B_0}{k_0} = -\frac{mc^2}{e}\xi_0\,. \tag{49}$$

Clearly A_0' is a Lorentz invariant. Also

$$\gamma' = \gamma_0 \hat{\gamma}(1 - v_0 u/c^2)\,, \tag{50}$$

$$N' = N\hat{\gamma}(1 - v_0 u/c^2)\,, \tag{51}$$

$$u' = \frac{u - v_0}{1 - v_0 u/c^2}\,, \tag{52}$$

$$w' = \frac{w/\hat{\gamma}}{1 - v_0 u/c^2}\,. \tag{53}$$

The inverse transformations to (50)–(53) can be gotten by interchanging primed and unprimed variables and changing the sign of v_0.

The counterpart of (35) is now

$$w' = c\xi_0(k_0' u' - c_0')[\gamma_0'(k_0' u - \omega') - \Omega]^{-1}\,. \tag{54}$$

Equation (38) is carried into

$$(\omega'^2 - k_0'^2 c^2) = \omega_p'^2 (k_0' u' - \omega')[\gamma_0'(k_0' u' - \omega') - \Omega]^{-1}\,. \tag{55}$$

Equation (55) can be viewed as the dispersion relation for the pump electromagnetic field, but it is to be noted that the steady-state theory is not restricted to weak pump fields and a linearized theory.

V. STABILITY ANALYSIS

Let us work in the laboratory frame for the case of the magnetostatic pump and in the wave frame for the case of the radio-frequency pump. The stability analysis is then common. Let

$$\vec{A} = \vec{A}_0 - \mathrm{Re}\{(mc^2/e)[\xi_1(z)\vec{e}_1(z) + \xi_2(z)\vec{e}_2(z)]e^{-i\omega t}\}\,, \tag{56}$$

$$\vec{v} = \vec{v}_0 + \mathrm{Re}[\vec{V}(z)e^{-i\omega t}]\,, \tag{57}$$

$$\Phi = 0 + \mathrm{Re}[(mc^2/e)(\omega/kc)\xi_3 e^{-i\omega t}]\,, \tag{58}$$

$$\gamma = \gamma_0 + \mathrm{Re}(\Gamma e^{-i\omega t})\,, \tag{59}$$

$$N = N_0 + \mathrm{Re}(N_1 e^{-i\omega t})\,. \tag{60}$$

Then (29) and (30) yield on linearization

$$\left(-i\omega + u\frac{d}{dz}\right)(\gamma_0 V_1 + c\xi_1) - k_0\mu(\Gamma w + \gamma_0 V_2 + c\xi_2) - k_0 V_3(\gamma_0 w - c\xi_0) = -\Omega V_2 \tag{61}$$

$$\left(-i\omega + \frac{ud}{dz}\right)(\Gamma w + \gamma_0 V_2 + c\xi_2) + k_0\mu(\gamma_0 V_1 + c\xi_1) = \Omega V_1\,.$$

Rather than use (31) it is convenient to employ the linearized version of (4) which yields

$$\left(-i\omega + \frac{ud}{dz}\right)\Gamma = \left(\frac{\omega u}{kc}\right)\frac{d\xi_3}{dz} + \frac{i\omega w \xi_3}{c}\,. \tag{62}$$

Linearization of (1) gives

$$\left(-i\omega+\frac{ud}{dz}\right)N_1+\left(\frac{d}{dz}\right)(N_0V_3)=0\,, \tag{63}$$

while linearization of (3) implies

$$\Gamma/\gamma_0^3=(uV_3+wV_2)/c^2\,. \tag{64}$$

Equations (15) and (16) on using (27) yield

$$\frac{d^2\xi_1}{dz^2}-k_0^2\xi_1-2k_0\frac{d\xi_2}{dz}+\frac{\omega^2\xi_1}{c^2}=-\frac{\omega_p^2V_1}{c^3}\,, \tag{65}$$

$$\frac{d^2\xi_2}{dz^2}-k_0^2\xi_2+2k_0\frac{d\xi_1}{dz}+\frac{\omega^2\xi_2}{c^2}=-\left(\frac{\omega_p^2}{c^3}\right)\left(V_2+\frac{N_1w}{N_0}\right), \tag{66}$$

$$\frac{\omega}{kc}\frac{d^2\xi_3}{dz^2}=\frac{\omega_p^2}{c^2}\frac{N_1}{N_0}\,. \tag{67}$$

Note that Eqs. (60)–(67) are a system of eight linear ordinary differential equations with constant coefficients for the eight quantities V_1, V_2, V_3, Γ, N_1, ξ_1, ξ_2, and ξ_3. Thus we may seek solutions where all these scalars vary with z as e^{ikz}. If we write

$$\vec{E}=\mathrm{Re}[\vec{a}(z)e^{i\omega t}]\,, \tag{68}$$

then it follows from (6) that

$$\vec{a}=-i(mc\omega/e)\vec{\xi}\,. \tag{69}$$

Equations (60) through (67) then imply

$$i(ku-\omega)(\gamma_0V_1+c\xi_1)-(k_0u-\Omega/\gamma_0)(\gamma_0V_2+c\xi_2+\Gamma w)$$
$$=(\Omega/\gamma_0)c\xi_2+(\Omega/\gamma_0)\Gamma w+k_0V_3(\gamma_0w-c\xi_0)\,, \tag{70}$$

$$(k_0u-\Omega/\gamma_0)(\gamma_0V_1+c\xi_1)$$
$$+i(ku-\omega)(\gamma_0V_2+c\xi_2+\Gamma w)=-(\Omega/\gamma_0)c\xi_1\,, \tag{71}$$

$$\Gamma=\frac{\omega}{c}\,\frac{u\xi_3+w\xi_2}{ku-\omega}\,, \tag{72}$$

$$\frac{N_1}{N_0}=-\frac{kV_3}{ku-\omega}\,, \tag{73}$$

$$\Gamma=(\gamma_0^3/c^2)(uV_3+wV_2)\,, \tag{74}$$

$$[1-c^2(k_0^2+k^2)/\omega^2]\xi_1-(2ik_0kc^2/\omega^2)\xi_2$$
$$=-(\omega_p^2/\omega^2)(V_1/c)\,, \tag{75}$$

$$(2ik_0kc^2/\omega^2)\xi_1+[1-c^2(k_0^2+k^2)/\omega^2]\xi_2$$
$$=-(\omega_p^2/\omega^2)[(V_2/c)+(w/c)(N_1/N_0)\,, \tag{76}$$

$$N_1/N_0=-(kc\omega/\omega_p^2)\xi_3\,. \tag{77}$$

It is convenient to express Γ, N_1, V_1, V_2, and V_3 in terms of ξ_1, ξ_2, and ξ_3. The result can be represented in the form

$$\underline{\epsilon}\cdot\vec{\xi}=0\,, \tag{78}$$

where the dielectric tensor

$$\underline{\epsilon}=\underline{\theta}+(\omega_p^2\tau/\gamma_0\omega^2)\underline{\psi} \tag{79}$$

and

$$\tau=(\Omega/\gamma_0)[(ku-\omega)^2-(k_0u-\Omega/\gamma_0)^2]^{-1}\,. \tag{80}$$

The components of θ are

$$\begin{aligned}
\theta_{11}&=1-c^2(k_0^2+k^2)/\omega^2-\omega_p^2/\gamma_0\omega^2\,,\\
\theta_{13}&=\theta_{31}=0\,,\\
\theta_{12}&=-\theta_{21}=-2ic^2k_0k/\omega^2\,,\\
\theta_{22}&=1-c^2(k_0^2+k^2)/\omega^2\\
&\quad-(\omega_p^2/\gamma_0\omega^2)[1+(w^2/c^2)(k^2c^2-\omega^2)(ku-\omega)^{-2}]\,,\\
\theta_{23}&=\theta_{32}=-(\omega_p^2/\gamma_0)(ku-\omega)^{-2}(w/\omega)(k-\omega u/c^2)\,,\\
\theta_{33}&=1-(\omega_p^2/\gamma_0)(ku-\omega)^{-2}(1-u^2/c^2)\,.
\end{aligned} \tag{81}$$

The elements of $\underline{\psi}$ are

$$\psi_{11}=k_0u-\Omega/\gamma_0\,,$$

$$\psi_{12}=-i(ku-\omega)\left(1+\frac{w^2}{c^2}\,\frac{\omega}{ku-\omega}\right),$$

$$\psi_{13}=-i(ku-\omega)\left(\frac{uw}{c^2}\,\frac{\omega}{ku-\omega}+\frac{\xi_0k_0c\omega}{\omega_p^2}\,\frac{ku-\omega}{k_0u-\Omega/\gamma_0}\right),$$

$$\psi_{21}=i\left(\frac{k(u^2+w^2)}{u}-\omega\right), \tag{82}$$

$$\psi_{22}=\left(\frac{k(u^2+w^2)}{u}-\omega\right)\frac{k_0u-\Omega/\gamma_0}{ku-\omega}\left(1+\frac{w^2}{c^2}\,\frac{\omega}{ku-\omega}\right),$$

$$\zeta_{23}=\left(\frac{k(u^2+w^2)}{u}-\omega\right)\frac{k_0u-\Omega/\gamma_0}{ku-\omega}$$
$$\times\left(\frac{uw}{c^2}\,\frac{\omega}{ku-\omega}+\frac{\xi_0k_0c\omega}{\omega_p^2}\,\frac{ku-\omega}{k_0u-\Omega/\gamma_0}\right),$$

$$\psi_{31}=i\omega w/u\,,$$

$$\psi_{32}=\frac{\omega w}{u}\,\frac{k_0u-\Omega/\gamma_0}{ku-\omega}\left(1+\frac{w^2}{c^2}\,\frac{\omega}{ku-\omega}\right),$$

$$\psi_{33}=\frac{\omega w}{u}\,\frac{k_0u-\Omega/\gamma_0}{ku-\omega}\left(\frac{uw}{c^2}\,\frac{\omega}{ku-\omega}+\frac{\xi_0k_0c\omega}{\omega_p^2}\,\frac{ku-\omega}{k_0u-\Omega/\gamma_0}\right).$$

In the limit $\Omega\to0$, τ vanishes and $\underline{\epsilon}$ reduces to $\underline{\theta}$, which apart from notation is the form found by Bernstein and Hirshfield.[1]

VI. THE DISPERSION RELATION AND NUMERICAL EXAMPLES

In order that (78) have nontrivial solutions it is necessary that the determinant

$$D=\det\underline{\epsilon}=0\,. \tag{83}$$

This yields an eighth-order polynomial equation for k. In practice, for the cases of interest $\omega_p^2\ll\omega^2$ and $u\sim c$, and two of the roots are such that $\omega/k\approx-c$. That is, they propagate in the negative-z direction counter to the beam and are substantially unaffected by the tenuous beam. The remain-

ing six roots correspond to waves which propagate along the beam. When $\Omega \to 0$ the two of these which can be associated with cyclotron waves in the limit of no helical pump disappear, and one recovers the result of Bernstein and Hirshfield.[1] These features will be illustrated later when numerical examples are discussed.

Now Eqs. (61)–(67) comprise a tenth-order system of linear ordinary differential equations which require for a unique solution the stipulation of ten boundary conditions. Since usually there is negligible reflection of waves at the output end of an FEL amplifier of finite length, two conditions are the requirement that the amplitudes of the waves propagating counter to the beam be zero. This requirement can be most easily dealt with via solving the system of ordinary differential equations by means of a Laplace transform in z, as was done in Ref. 1, instead of the normal mode analysis. The dispersion relation, of course, determines the poles of the transform in terms of which the inversion can be readily accomplished. The resulting solution for $\tilde{\mathbf{a}}(z)$ can be written in terms $\tilde{\mathbf{a}}(0)$, assuming that all other first-order quantities are zero at $z=0$ and involve linear combinations of the six modes corresponding to the six roots with $\mathrm{Re}k>0$. Since in general these roots are nondegenerate, but differ by amounts of order Δk much less than ω/c, there will be interference amongst their contributions to $\tilde{\mathbf{a}}(z)$, which becomes evident after a distance of order $2\pi/\Delta k$. This feature has been examined in detail in Ref. 1. We will not pursue it further here, other than to note that the single particle theory in which one examines the second-order energy change in a distance z of an electron moving in the zero- and first-order electromagnetic field, and identifies this with the gain in energy of the high frequency field, is valid only for $z\Delta k<1$.

We now consider the dispersion relation (83) in an FEL with guide magnetic field. Because of the complexity of the dielectric tensor $\underline{\epsilon}$ [see Eq. (79)] it is convenient to study the dispersion relation by comparing two FEL's, identical except that one has an axial field while the second does not and thus is characterized by the dispersion relation $D_0=\det(\underline{\theta})=0$, the properties of which are well understood. We make the comparison between the two lasers by fixing the parameters of the FEL without the guide field and adjusting the value of the pump field parameter ξ_0 in the laser with the guide field so that the axial velocities u (and therefore also w) in both lasers are identical. This assures the same Doppler upshift of the frequencies in the lasers. A similar comparison has been made by Friedland and Hirshfield for the single particle model of FEL.[3]

Let ξ_0^0 be the pump field parameter in the FEL without the guide field. The unperturbed electron velocity components are then given by $w/c=\xi_0^0/\gamma_0$ and $u/c=[1-(1+\xi_0^0)/\gamma_0^2]^{1/2}$. Therefore, following Eq. (35), with the guide field

$$\xi_0=\xi_0^0\left(1-\frac{\Omega}{\gamma_0 k_0 u}\right). \tag{84}$$

This equation demonstrates the intriguing possibility of reduction of the pump field in an FEL as one approaches the cyclotron resonance condition $\Omega/\gamma_0 \to k_0 u$. Accessibility of the resonance, however, is not guaranteed, as was shown in the recent study[2] of the unperturbed electron beam orbits in an FEL with the guide field. It was demonstrated that for given values of γ_0, k_0, ξ_0, and Ω the electrons can possess more than one steady state. For example, Fig. 1 shows u/c versus Ω/c for $k_0=6\ \mathrm{cm}^{-1}$, $\gamma_0=3$, and $\xi_0=0.5$. For $\Omega>\Omega_{cr}$ it is seen that only one branch exists (branch C). But when $\Omega<\Omega_{cr}$ two additional branches (A and B) are allowed. It was also shown that the necessary condition for orbital stability of the steady-state solutions against small perturbations is given by the inequality

$$\frac{\Omega}{ck_0\xi_0}\left(\frac{w}{u}\right)^3<1. \tag{85}$$

Branch C is always stable, since $w<0$ on this branch. On branches A and B, $w>0$, but, as was shown, only branch A satisfied (85) and thus may be used in applications. Since the ratio w/u is kept constant in our comparative study, one can substitute the expression for ξ_0 found from (35) into (85) and write the stability condition in the following form:

$$\Omega<\Omega_{cr}=\frac{\gamma_0 k_0 u}{1+(w/u)^2}, \tag{86}$$

valid for branches A and B. In our sample case ($\gamma_0=3$, $k_0=6\ \mathrm{cm}^{-1}$, and $\xi_0^0=0.5$) one has $\Omega_{cr}/c=16.18\ \mathrm{cm}^{-1}$, and, therefore, according to (84),

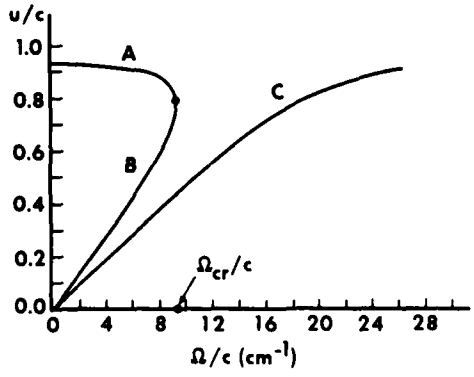

FIG. 1. Steady-state normalized axial velocity u/c as a function of normalized axial magnetic field Ω/c.

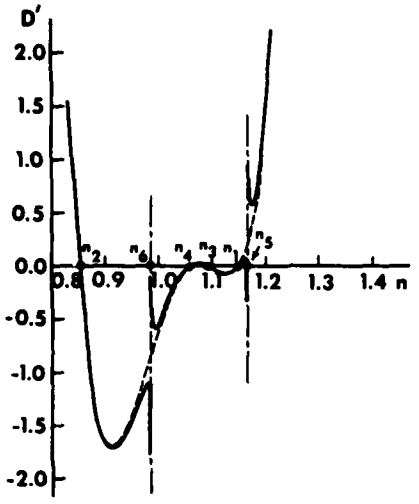

FIG. 2. Dispersion function D' on branch A for the case $\gamma_0=3$, $k_0=6\ \mathrm{cm}^{-1}$, and $\omega/c=40\ \mathrm{cm}^{-1}$. The dashed curve represents the FEL without the guide magnetic field and $\xi_0^0=0.5$. The solid curve is for the FEL with the guide field ($\Omega/c=6.5\ \mathrm{cm}^{-1}$), where smaller values of ξ_0^0 are used so as to provide the same values of u and w as for the dashed curve.

ξ_0 on branch A cannot become less than $\xi_{cr}=1.562\times10^{-2}$.

We return now to the study of the dispersion relation (83). The form of the dielectric tensor $\underline{\epsilon}$ [Eq. (79)] suggests that for values of ω_p small enough, the function D will differ significantly from D_0 only in the regions where $(ku-\omega)^2-(k_0u-\Omega/\gamma_0)^2\simeq 0$, as a result of the resonance in the denominator in τ [see Eq. (80)]. We demonstrate a typical effect of the axial guide field on the dispersion function D in Fig. 2, where the function $D'=D[ku-\omega)/\omega_p(1-u^2/c^2)]^2/\gamma_0$ (the full line) is shown versus $n=ck/\omega$ for branch A in the sample case when $\omega/c=40\ \mathrm{cm}^{-1}$, $\omega_p^2/c^2=0.5\ \mathrm{cm}^{-2}$, and $\Omega/c=6.5\ \mathrm{cm}^{-1}$. In the same figure the dashed line represents the case with no guide field.

It is well known[1] that the unstable regime in an FEL without the guide field can be described as a coupling between the transverse electromagnetic modes with the dispersion relation $n_{1,2}=1\pm ck_0/\omega$ and the electrostatic beam modes characterized by $n_{3,4}=c/u\pm c\omega_p/\gamma_0\omega u$. One can see from Fig. 2 that these four roots are only slightly perturbed by the presence of the axial field. There exist, however, two additional roots in the neighborhood of the resonance points $n_{5,6}=c/u\pm(ck_0/\omega-\Omega c/\gamma u\omega)$. If the resonances are widely separated as in the case of Fig. 2, the onset of the unstable mode is roughly the same as without the guide field, namely, as the frequency ω increases, the root n_1 moves to 1, passing the region $n_4<n<n_3$ (since $n_{3,4}=c/u$). The modes couple in this region,

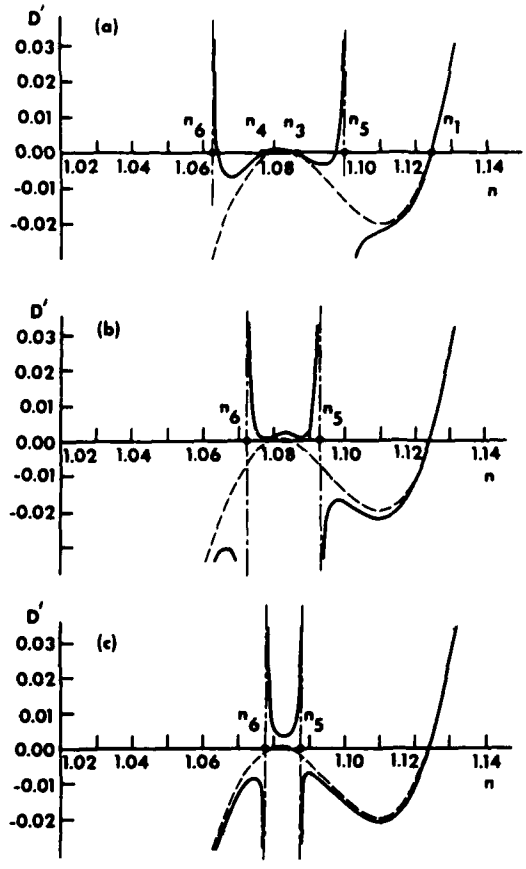

FIG. 3. Graphical representation of the dispersion function on branch A for the case $\gamma_0=3$, $k_0=6\ \mathrm{cm}^{-1}$, $\xi_0^0=0.5$, $\omega/c=50\ \mathrm{cm}^{-1}$, and increasing values of the guide field (the solid curves): (a) $\Omega/c=14\ \mathrm{cm}^{-1}$, (b) $\Omega/c=15\ \mathrm{cm}^{-1}$, (c) $\Omega/c=16\ \mathrm{cm}^{-1}$. The dashed curves correspond to the FEL without the guide field. Two pairs of roots of the dispersion relation become complex as the real roots n_3 and n_4 are squeezed by the resonances at n_5 and n_6.

and the roots of the dispersion relation are complex. When ω continues to increase, n_1 becomes less than n_4, the coupling diminishes, and one again has a stable regime.

New effects may occur when the resonances $n_{5,6}$ approach each other. This situation is shown in Fig. 3, where the full line represents the dispersion function on branch A for increasing values of Ω. One can see in this example that even for $\omega/c=50\ \mathrm{cm}^{-1}$ in our sample case (all the modes are stable in this case if $\Omega=0$) it is possible just by changing Ω to squeeze the roots $n_{3,4}$ by the resonances $n_{5,6}$ so that two pairs of the roots become complex. For higher frequencies, when again the FEL without the guide field is stable ($n_1<n_4$) one can also get an unstable regime as is demonstrated in Fig. 4 for $\omega/c=100\ \mathrm{cm}^{-1}$. Our numerical study

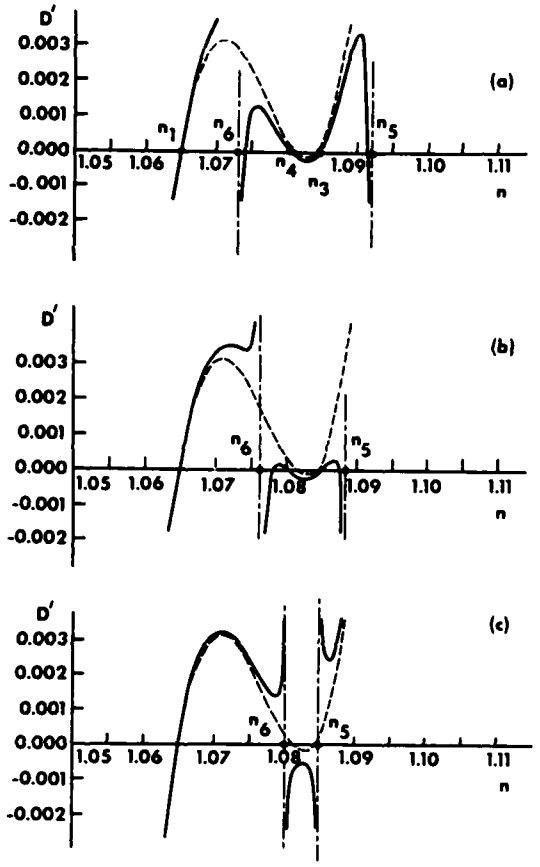

FIG. 4. Graphical representation of the dispersion function on branch A for the case $\gamma_0=3$, $k_0=6$ cm^{-1}, $\xi_0^0=0.5$, $\omega/c=100$ cm^{-1}. The solid curves: (a) $\Omega/c=14$ cm^{-1}; (b) $\Omega/c=15$ cm^{-1}; (c) $\Omega/c=16$ cm^{-1}. The dashed curves correspond to the FEL without the guide field.

shows that similar behavior is also characteristic for branch C with the only difference that there is only one pair of unstable modes in the low and the high frequency ranges, respectively.

We finally summarize our comparison of the FEL's with and without the guide field in Figs. 5 and 6, where the imaginary part of k is shown as a function of ω/c for various values of the axial field in our sample case ($\gamma_0=3$, $k_0=6$ cm^{-1}, $\xi_0^0=0.5$, $\omega_p^2/c^2=0.5$ cm^2). Figure 5 is for $0<\Omega/c<14.5$ cm^{-1} on branch A (the full lines) and $21<\Omega/c<28$ cm^{-1} on branch C (the dashed lines). The resonances $n_{5,6}$ are relatively wide apart from each other and formally the instability in this range of Ω occurs similarly to the case of the laser without the guide field. Nevertheless, the presence of the guide field increases the instability on branch A and tends to decrease it on branch C. In addition, the linewidth of the unstable regime is seen to be significantly increased at lower frequencies on branch A. Together with this, *no* instability exists at frequencies higher than those

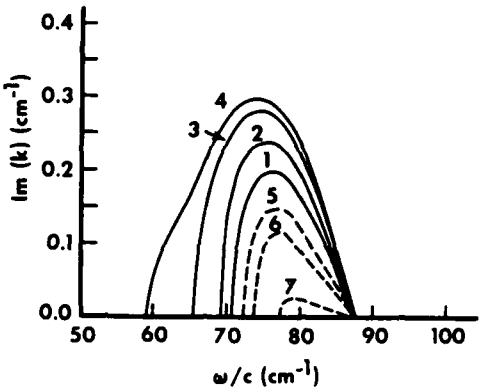

FIG. 5. Spacial growth rates Im(k) versus ω/c on branch A (solid curves) and C (dashed curves) for various values of Ω/c: (1) $\Omega/c=0$, (2) $\Omega/c=12$ cm^{-1}, (3) $\Omega/c=14$ cm^{-1}, (4) $\Omega/c=14.5$ cm^{-1}, (5) $\Omega/c=28$ cm^{-1}, (6) $\Omega/c=23$ cm^{-1}, (7) $\Omega/c=21$ cm^{-1}. For all the cases $\gamma_0=3$, $k_0=6$ cm^{-1}, and $\xi_0^0=0.5$.

characteristic of the FEL without the guide field. As one approaches the resonance condition $\Omega=\gamma_0 u k_0$ (further increasing Ω on branch A or decreasing it on branch C) a completely different type of behavior is observed as is shown in Fig. 6 for $\Omega/c=15.25$ cm^{-1} on branch A (the full line) and $\Omega/c=18$ cm^{-1} on branch C (the dashed line). The unstable region extends over the entire low-frequency range and there are two different unstable modes on branch A, as was mentioned previously. In addition there exist unstable modes in the high-frequency region, which was totally stable before. Note that the values of Imk in this high-frequency regime are only weakly dependent on the frequency itself.

Thus, in conclusion, we have demonstrated in

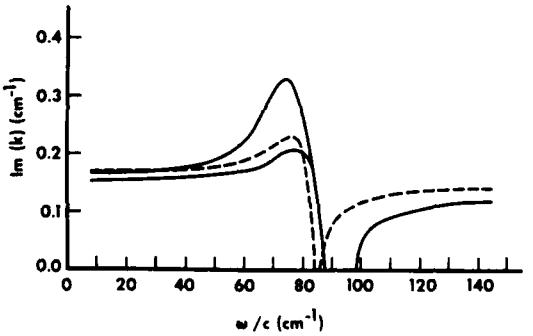

FIG. 6. Spatial growth rates Im(k) in the sample case ($\gamma_0=3$, $k_0=6$ cm^{-1}, $\xi_0^0=0.5$) versus ω/c in the regime, where the cyclotron modes couple to the beam modes (see Figs. 3,4). Branch A (solid curves): $\Omega/c=15.25$ cm^{-1}. Branch C (dashed curves): $\Omega/c=18$ cm^{-1}. The unstable modes are extended over the low- and high-frequency regions. There exist two different growth constants in this regime on branch A.

our numerical examples that the presence of the guide field in an FEL introduces the following desirable features:

(i) One can operate the laser with much lower magnitudes of the pump field without sacrificing the undulatory velocity of the electrons. This allows one to use shorter periods of the wiggler with the same currents.

(ii) The laser can be operated in higher gain regime by approaching the resonance condition $\Omega = k_0 \mu c \gamma_0$.

(iii) The linewidth of the unstable modes can be widely extended to both low- and high-frequency ranges.

ACKNOWLEDGMENT

This work was supported by the Office of Naval Research and by the National Science Foundation.

[1]I. B. Bernstein and J. L. Hirshfield, Phys. Rev. A 20, 1661 (1979).
[2]L. Friedland, Phys. Fluids 23, 2376 (1980).
[3]L. Friedland and J. L. Hirshfield, Phys. Rev. Lett. 44, 1456 (1980).

Exact magnetic field of a helical wiggler

S. Y. Park and J. M. Baird
B-K Dynamics, Rockville, Maryland 20850

R. A. Smith and J. L. Hirshfield
Mason Laboratory, Yale University, New Haven, Connecticut 06520

(Received 25 September 1981; accepted for publication 3 November 1981)

Exact solutions are presented for the magnetic field of single and double current-carrying helical windings. The latter is a configuration used widely in free electron lasers. Differences are shown between the exact field and the simple form commonly assumed in analyzing free electron laser interactions.

PACS numbers: 41.10.Dq, 42.60.By, 85.70.Nk

I. INTRODUCTION

A spatially-periodic static magnetic field is a central part of most free electron lasers. While a linearly polarized magnetic field is used in some devices,[1] most employ a circularily polarized field.[2] Theoretical analyses[3] commonly assume that this wiggler field can be represented, to a good approximation, by

$$\mathbf{B}(z) = B_\perp(0)(\hat{e}_x \sin kz - \hat{e}_y \cos kz), \tag{1}$$

where $B_\perp(0)$ is the constant magnitude of the field, $p = 2\pi/k$ is the period of the wiggler, and z is the symmetry axis.

Smythe[4] has derived a formula for the transverse magnetic field on the axis of a single filamentary helical winding of radius a and period p. For the wiggler configuration usually considered, two such windings are taken to be symmetrically interspersed, with currents flowing in opposite direction in each winding. For this configuration the magnitude of the transverse field on axis is twice Smythe's result, or

$$B_\perp(0) = (2\mu_0 I/p)(ka)K_1'(ka), \tag{2}$$

where I is the current in each winding and $K_1(t)$ is the Bessel function of imaginary argument. For most wigglers of practical interest the asymptotic representation for the Bessel function is a good approximation, i.e.,

$$K_1'(t) \sim -(\pi/2t)^{1/2} e^{-t}\left[1 + \frac{7}{8t} + \frac{57}{128t^2} + \ldots\right],$$

so that a handy result is

$$\frac{pB_\perp(0)}{I} \simeq -\frac{4\pi^2}{5}(a/p)^{1/2} e^{-2\pi a/p}, \tag{2a}$$

where p is in cm, $B_\perp(0)$ in gauss, and I in amperes.

Blewett and Chasman[5] have presented a derivation of the magnetic field within a cylindrical current sheet of radius a with a sinusoidal helical distribution, i.e.,

$$\mathbf{J} = \frac{I}{a}(\hat{e}_z + ka\hat{e}_\phi)\delta(r - a)\cos(\phi - kz).$$

However, this current distribution is a rather imperfect approximation to an actual helical winding; thus it is bound to give rise to a different radial dependence than that produced by a bifilar helix. In addition the ubiquitous spectrum of higher Fourier spatial harmonics produced by an actual winding is totally suppressed if one chooses the above idealized current distribution.

In view of the widespread use of bifilar helical wigglers, it is of interest to have an exact result for the magnetic field. Then the accuracy of an approximation, such as Eq. (1), can be judged carefully for a given coil design. This is especially critical when annular electron beams are used, and where the radial departure of the field from its value on axis can be

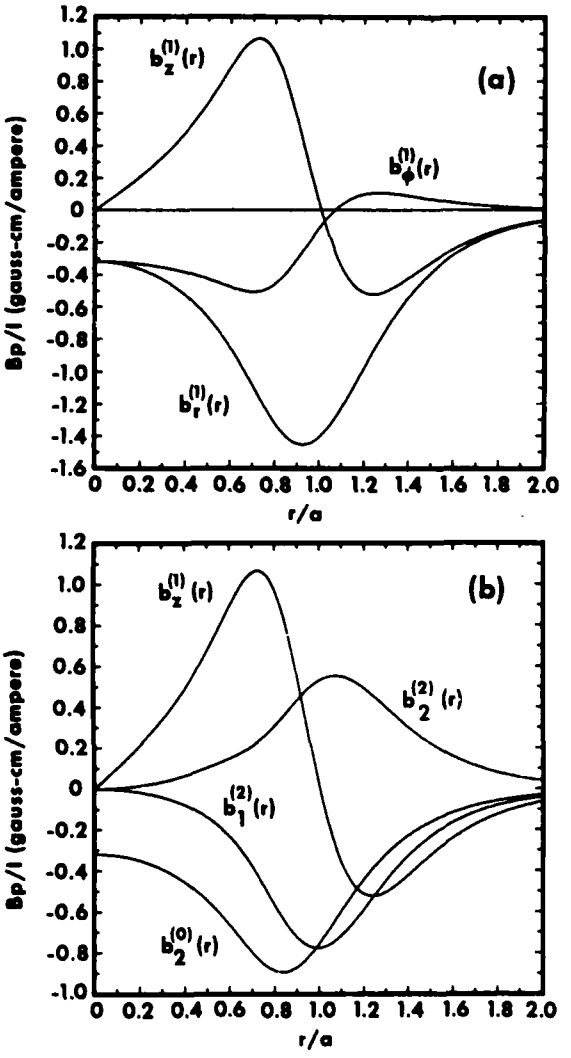

FIG. 1. Magnetic field amplitudes in (a) cylindrical and (b) helical coordinates, for $p/a = 2$. These amplitudes only give that portion of the field with fundamental periodicity.

 0021-8979/82/031320-06$02.40

large. Furthermore, it is conceivable that a free electron laser could be operated on one of the higher spatial harmonics, so as to produce radiation at a correspondingly shorter wavelength. In this case, an accurate theory for the harmonic field strengths would be indispensable.

The present paper presents an exact result for the magnetic field both in the interior and exterior of a single filamentary helix, i.e., a winding with a wire of negligible thickness. Superposition of the fields of two such helices, with oppositely directed currents, gives the results we seek. In addition to the mathematical results, we present graphs of the radial dependences for the fundamental and the first few spatial harmonic components of the field for several values of the radius-to-pitch ratio.

II. FIELD OF A SINGLE HELIX

We take the current I to flow along a filamentary helix of radius a and period $p = 2\pi/k$. The curent density is then

$$\mathbf{J} = \frac{I}{ka}(\hat{e}_z + ka\hat{e}_\phi)\delta(r-a)\delta\left(z - \frac{\phi}{k}\right), \tag{3}$$

where $\hat{e}_z$ and $\hat{e}_\phi$ are unit vectors along the axis and azimuth.

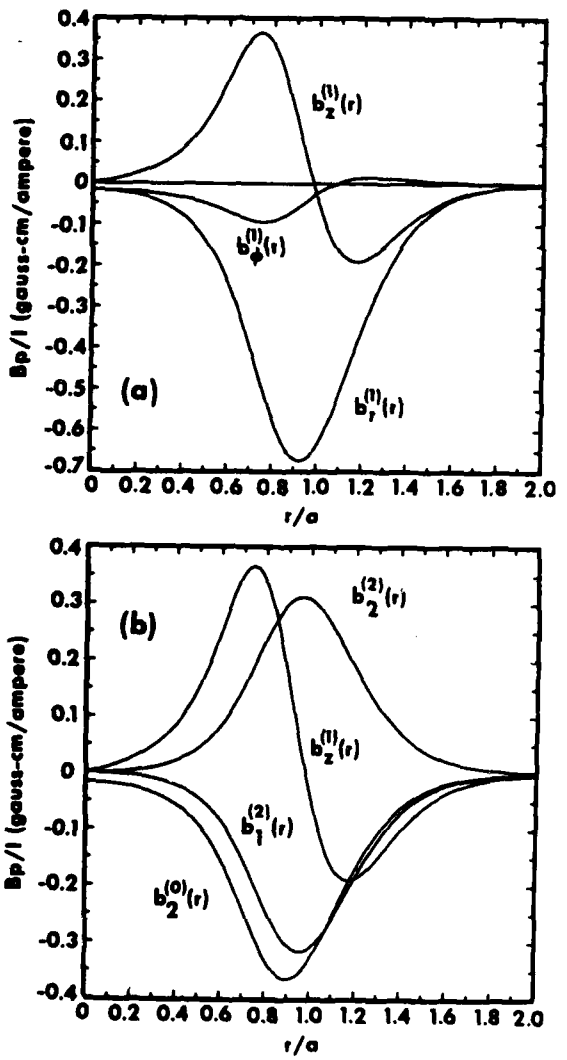

FIG. 2. Magnetic field amplitudes in (a) cylindrical and (b) helical coordinates, for $p/a = 1$.

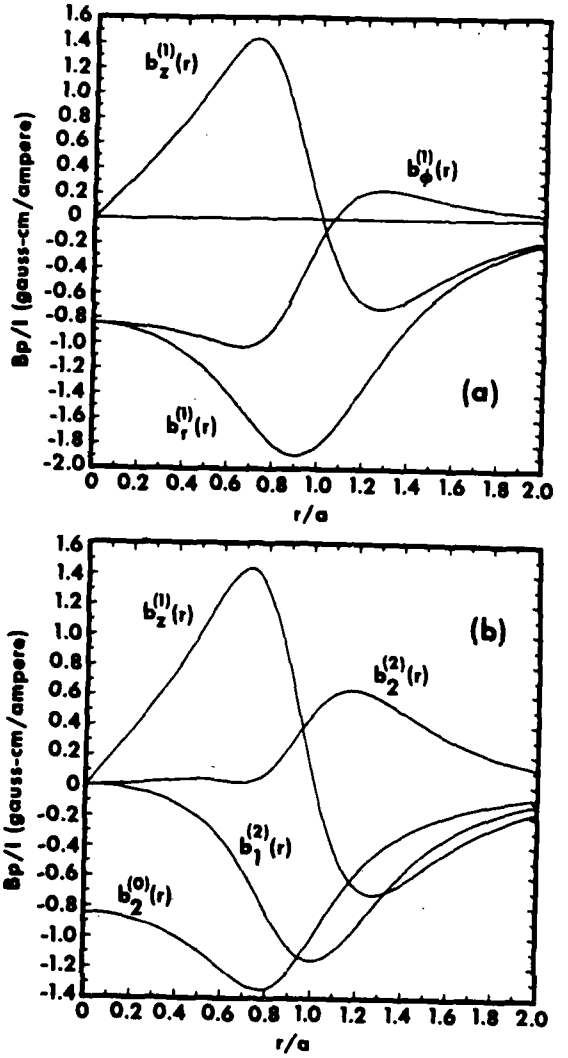

FIG. 3. Magnetic field amplitudes in (a) cylindrical and (b) helical coordinates for $p/a = 3$.

We first seek the vector potential

$$\mathbf{A}(\mathbf{r}) = \frac{\mu_0}{4\pi}\int d^3\mathbf{r}'\,\frac{\mathbf{J}(\mathbf{r}')}{|\mathbf{r}-\mathbf{r}'|}. \tag{4}$$

Now, $\mathbf{r} = \hat{e}_r r\cos\phi + \hat{e}_\phi r\sin\phi + \hat{e}_z z$, so that $|\mathbf{r}-\mathbf{r}'| = [r^2 + r'^2 + (z-z')^2 - 2rr'\cos(\phi-\phi')]^{1/2}$. After carrying out the r and z integrations, Eq. (4) becomes

$$\mathbf{A}(\mathbf{r}) = \frac{\mu_0 I}{4\pi}\int_{-\infty}^{\infty} d\phi'\,R^{-1}(\phi')(\hat{e}_z + \bar{a}\hat{e}_\phi\cdot), \tag{5}$$

where

$$R^2(\phi') = \bar{a}^2 = \bar{r}^2 + (\phi' - \bar{z})^2 - 2\bar{a}\bar{r}\cos(\phi' - \phi),$$

with $\bar{a} = ka$, $\bar{r} = kr$, and $\bar{z} = kz$. We introduce the helical variable $\psi = \phi - \bar{z}$ and use the binomial series for $R^{-1}(\phi')$, i.e.,

$$R^{-1}(\phi') = (\bar{\rho}^2 + \psi'^2)^{-1/2}\left[1 + \sum_{n=1}^{\infty}\binom{2n}{n}\left(\frac{\bar{a}\bar{r}}{2}\right)^n \times\frac{\cos^n(\psi'-\psi)}{(\bar{\rho}^2+\psi'^2)^n}\right],$$

where $\bar{\rho}^2 = \bar{a}^2 + \bar{r}^2$, and

$$\binom{l}{m} = \frac{l!}{m!(l-m)!}.$$

Then Eq. (5) becomes

$$\mathbf{A}(\mathbf{r}) = \frac{\mu_0 I}{4\pi}\int_{-\infty}^{\infty} d\psi'(\bar{\rho}^2+\psi'^2)^{-1/2}(\hat{e}_z - \hat{e}_1\bar{a}\sin\psi' + \hat{e}_2\bar{a}\cos\psi')\times\left[1+\sum_{n=1}^{\infty}\binom{2n}{n}\left(\frac{\bar{a}\bar{r}}{2}\right)^n\frac{\cos^n(\psi'-\psi)}{(\bar{\rho}^2+\psi'^2)^n}\right], \quad (6)$$

where we have introduced the unit vectors $\hat{e}_1 = \hat{e}_x\cos\bar{z} + \hat{e}_y\sin\bar{z}$, and $\hat{e}_2 = -\hat{e}_x\sin\bar{z} + \hat{e}_y\cos\bar{z}$, so that $\hat{e}_{\phi'} = -\hat{e}_1\sin\psi' + \hat{e}_2\cos\psi'$. It is convenient to separate the summation over n into even and odd sums, and to use

$$\cos^{2n}\theta = 2^{-2n}\left[\binom{2n}{n} + 2\sum_{m=1}^{n}\binom{2n}{n-m}\cos 2m\theta\right]$$

and

$$\cos^{2n-1}\theta = 2^{-2n+2}\sum_{m=1}^{n}\binom{2n-1}{n-m}\cos(2m-1)\theta.$$

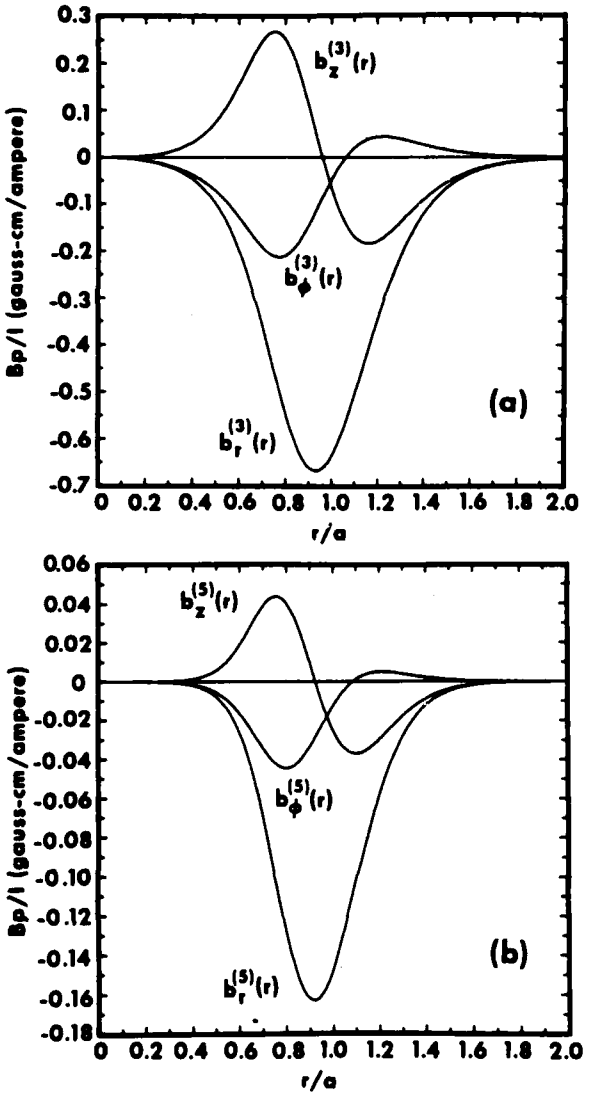

FIG. 4. Magnetic field amplitudes in cylindrical coordinates for the (a) third and (b) fifth axial harmonics, for $p/a = 3$.

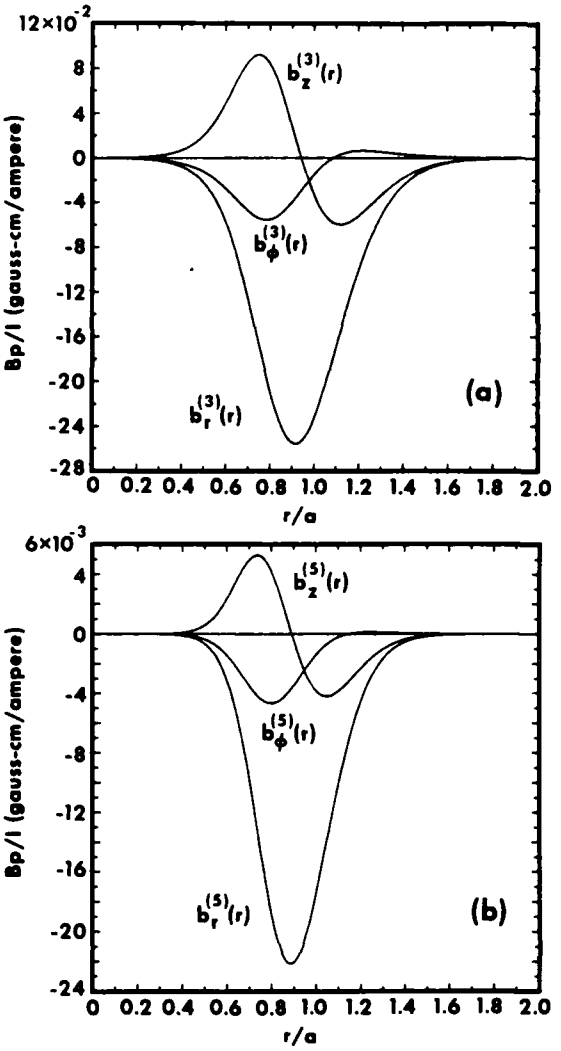

FIG. 5. Magnetic field amplitudes in cylindrical coordinates for the (a) third and (b) fifth axial harmonics, for $p/a = 2$.

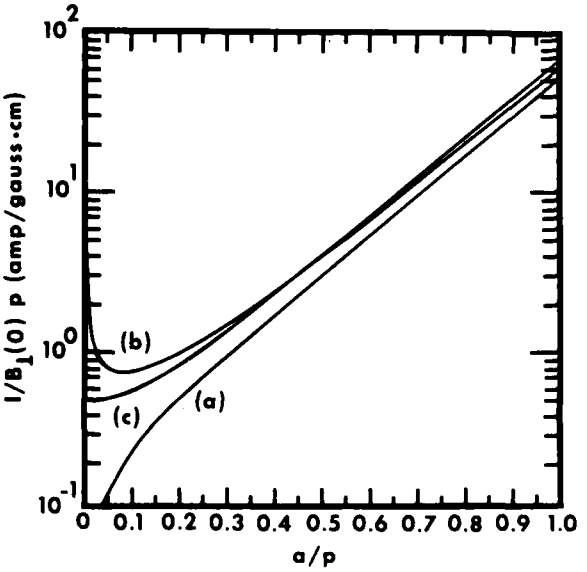

FIG. 6. Magnetic field amplitude on wiggler axis ($r = 0$) as a function of a/p. (a) Exact result (this paper) for a filamentary bifilar conductor; (b) asymptotic approximation (Eq. 2a); (c) result for a sinusoidal distributed current sheet (see Ref. 5).

Only terms in the integrand even in ψ' will survive the integration over ψ'. After some rearrangement, the result follows as

$$\mathbf{A}(\mathbf{r}) = \frac{\mu_0 I}{2\pi}\bar{a}\Bigg\{\frac{\hat{e}_z}{\bar{a}}\sum_{n=0}^{\infty}\frac{G_{2n}^{0}}{(n!)^2} + \hat{e}_2\sum_{n=0}^{\infty}\frac{G_{2n}^{1}}{(n!)^2} + \sum_{n=1}^{\infty}\sum_{m=1}^{n}\frac{1}{(n+m)!(n-m)!}$$
$$\times\Bigg[\frac{\hat{e}_z}{\bar{a}}2G_{2n}^{2m}\cos 2m\psi + (-\hat{e}_1\sin 2m\psi + \hat{e}_2\cos 2m\psi)G_{2n}^{2m-1}$$
$$+ (\hat{e}_1\sin 2m\psi + \hat{e}_2\cos 2m\psi)G_{2n}^{2m+1}\Bigg] + \sum_{n=1}^{\infty}\sum_{m=1}^{n}\frac{1}{(n+m-1)!(n-m)!}$$
$$\times\Bigg[\frac{\hat{e}_z}{\bar{a}}2G_{2n-1}^{2m-1}\cos(2m-1)\psi + (-\hat{e}_1\sin(2m-1)\psi + \hat{e}_2\cos(2m-1)\psi)$$
$$\times G_{2n-1}^{2m-2} + (\hat{e}_1\sin(2m-1)\psi + \hat{e}_2\cos(2m-1)\psi)G_{2n-1}^{2m}\Bigg]\Bigg\}, \tag{7}$$

where

$$G_l^m = \frac{(2l)!}{l!}\left(\frac{\bar{a}\bar{r}}{4}\right)^l\int_0^{\infty}d\psi'(\bar{\rho}^2+\psi'^2)^{-l-1/2}\cos m\psi'$$
$$= \left(\frac{\bar{a}\bar{r}}{2}\right)^l(m/\bar{\rho})^l K_l(m\bar{\rho}),\ m>0,$$
$$= \frac{(l-1)!}{2}\left(\frac{\bar{a}\bar{r}}{\bar{\rho}^2}\right)^l,\ m=0,\ l\neq 0,$$
$$= \ln\infty - \ln\bar{\rho},\ m=0,\ l=0,$$

where $\bar{\rho}^2 = \bar{a}^2+\bar{r}^2$, and $K_l(m\bar{\rho})$ is the Bessel function of imaginary argument. One can show that

$$(G_l^m)' \equiv \frac{d}{d\bar{r}}G_l^m = \frac{l}{\bar{r}}G_l^m - \frac{2}{\bar{a}}G_{l+1}^m.$$

The components of A(r) in cylindrical coordinates are found, again after rearrangement of terms using

$$\sum_{n=1}^{\infty}\sum_{m=1}^{n}f_n^m = \sum_{m=1}^{\infty}\sum_{n=1}^{\infty}f_{n+m-1}^m,$$

to be

$$A_z(\mathbf{r}) = \frac{\mu_0 I}{2\pi}\sum_{n=0}^{\infty}\frac{1}{n!}\left[\frac{C_{2n}^0}{n!} + 2\sum_{m=1}^{\infty}\frac{C_{2n+2m}^{2m}}{(n+2m)!} + 2\sum_{m=0}^{\infty}\frac{C_{2n+2m+1}^{2m+1}}{(n+2m+1)!}\right],$$
$$A_r(\mathbf{r}) = \frac{\mu_0 I}{2\pi}\bar{a}\sum_{n=0}^{\infty}\frac{1}{n!}\left[\sum_{m=1}^{\infty}\frac{2mS_{2n+2m-1}^{2m}}{(n+2m)!} + \sum_{m=0}^{\infty}\frac{(2m+1)S_{2n+2m}^{2m+1}}{(n+2m+1)!}\right],$$
and
$$A_\phi(\mathbf{r}) = \frac{\mu_0 I}{2\pi}a\sum_{n=0}^{\infty}\frac{1}{n!}\left[\frac{C_{2n+1}^0}{(n+1)!} + \sum_{m=1}^{\infty}\frac{(2m+2n)C_{2n+2m-1}^{2m}}{(n+2m)!} + \sum_{m=0}^{\infty}\frac{(2n+2m+1)C_{2n+2m}^{2m+1}}{(n+2m+1)!}\right], \tag{8}$$

where $C_l^m \equiv G_l^m\cos m\psi$ and $S_l^m \equiv G_l^m\sin m\psi$.

The associated magnetic field intensity follows from $\mathbf{B} = \nabla\times\mathbf{A}$, or

$$\mathbf{B} = k\{\hat{e}_r(\bar{r}^{-1}\dot{A}_z + \dot{A}_\phi) - \hat{e}_\phi(\dot{A}_r + A_z') + \hat{e}_z[A_\phi' + \bar{r}^{-1}(A_\phi - \dot{A}_r)]\},$$

where $\dot{A} \equiv \partial A/\partial\psi$ and $A' \equiv \partial A/\partial\bar{r}$. The components of B are

$$B_r(r,\psi) = \sum_{m=0}^{\infty}B_r^{(m)}(r,\psi),\ B_r^{(m)}(r,\psi) \equiv b_r^{(m)}(r)\sin m\psi,$$
$$B_\phi(r,\psi) = \sum_{m=0}^{\infty}B_\phi^{(m)}(r,\psi),\ B_\phi^{(m)}(r,\psi) \equiv b_\phi^{(m)}(r)\cos m\psi, \tag{9}$$
$$B_z(r,\psi) = \sum_{m=0}^{\infty}B_z^{(m)}(r,\psi),\ B_z^{(m)}(r,\psi) \equiv b_z^{(m)}(r)\cos m\psi,$$

where for, $m\neq 0$,

$$b_r^{(m)}(r) \equiv -\frac{\mu_0 I}{2\pi}k\bar{a}m\sum_{n=0}^{\infty}\frac{(2n+m)G_{2n+m-1}^m + 2(\bar{a}\bar{r})^{-1}G_{2n+m}^m}{n!(n+m)!},$$
$$b_\phi^{(m)}(r) \equiv -\frac{\mu_0 I}{2\pi}k\bar{a}\sum_{n=0}^{\infty}\frac{m^2G_{2n+m-1}^m + 2(n+m)(\bar{a}\bar{r})^{-1}G_{2n+m}^m - 4(\bar{a})^{-2}G_{2n+m+1}^m}{n!(n+m)!},$$
$$b_z^{(m)}(r) \equiv \frac{\mu_0 I}{\pi}k\bar{a}^2\sum_{n=0}^{\infty}\frac{2n(n+m)(\bar{a}\bar{r})^{-1}G_{2n+m-1}^m - (2n+m)(\bar{a})^{-2}G_{2n+m}^m}{n!(n+m)!},$$

and, for $m = 0$,

$$b_r^{(0)}(r) = 0,$$

$$b_\phi^{(0)}(r) = -\frac{\mu_0 I}{\pi} k\bar{a} \sum_{n=0}^{\infty} \frac{n(\bar{a}\bar{r})^{-1} G_{2n}^0 - (\bar{a})^{-2} G_{2n+1}^0}{n!n!},$$

$$b_z^{(0)}(r) = \frac{\mu_0 I}{\pi} k\bar{a}^2 \sum_{n=0}^{\infty} \frac{(n+1)(\bar{a}\bar{r})^{-1} G_{2n+1}^0 - (\bar{a})^{-2} G_{2n+2}^0}{n!(n+1)!}.$$

Alternatively, in the helical coordinates,

$$\begin{aligned} B_1(r,\psi) &\equiv B_r(r,\psi)\cos\psi - B_\phi(r,\psi)\sin\psi \\ &= \Big[-b_\phi^{(0)}(r)\sin\psi + \sum_{m=1}^{\infty} b_+^{(m)}(r)\sin(m-1)\psi \\ &\quad + b_-^{(m)}(r)\sin(m+1)\psi \Big], \end{aligned} \tag{10}$$

$$\begin{aligned} B_2(r,\psi) &\equiv B_r(r,\psi)\sin\psi + B_\phi(r,\psi)\cos\psi \\ &= \Big[b_\phi^{(0)}(r)\cos\psi + \sum_{m=1}^{\infty} (b_+^{(m)}(r)\cos(m-1)\psi \\ &\quad - b_-^{(m)}(r)\cos(m+1)\psi) \Big], \end{aligned}$$

with here

$$b_\pm^{(m)}(r) \equiv \tfrac{1}{2}[b_r^{(m)}(r) \pm b_\phi^{(m)}(r)].$$

That is, to our knowledge, the first exact result for the magnetic field generated by a current flowing along a helix. On the axis ($r = 0$), the fields given by Eq. (10) reduce to

$$B_1 = 0,$$

$$B_2 = -\frac{\mu_0 I}{2\pi} k\bar{a}[\bar{a}K_0(\bar{a}) + K_1(\bar{a})],$$

which agrees with Smythe's result,[4] and is equivalent to one half of Eq. (2) since $\bar{a}K_0(\bar{a}) + K_1(\bar{a}) = -\bar{a}K_1'(\bar{a})$.

III. FIELD OF A DOUBLE HELIX

For an arrangement of two symmetrically interspersed helices carrying identical currents in opposite directions the current density is

$$\mathbf{J} = \frac{I}{ka}(\hat{e}_z + ka\hat{e}_\phi)\delta(r-a)\left[\delta\left(z - \frac{\phi}{k}\right) - \delta\left(z - \frac{\phi+\pi}{k}\right)\right]. \tag{11}$$

The magnetic field may then be obtained directly from Eq. (9) by forming $\mathbf{B}(r,\psi) - \mathbf{B}(r,\psi+\pi)$. Terms even in ψ cancel, and the results are simply twice the odd parts of Eq. (9).

The fields of the double helix in cylindrical coordinates are thus

$$\begin{aligned} B_r(r,\psi) &= \sum_{m=0}^{\infty} B_r^{(2m+1)}(r,\psi), \\ B_\phi(r,\psi) &= \sum_{m=0}^{\infty} B_\phi^{(2m+1)}(r,\psi), \\ B_z(r,\psi) &= \sum_{m=0}^{\infty} B_z^{(2m+1)}(r,\psi), \end{aligned} \tag{12}$$

from which the cartesian components of fields are readily calculated by

$$B_x(r,\phi,z) = B_r(r,\psi)\cos\phi - B_\phi(r,\psi)\sin\phi,$$

$$B_y(r,\phi,z) = B_r(r,\psi)\sin\phi + B_r(r,\psi)\cos\phi.$$

Also, the fields in helical coordinates are

$$\begin{aligned} B_1(r,\psi) &\equiv B_r(r,\psi)\cos\psi - B_\phi(r,\psi)\sin\psi \\ &= \sum_{m=1}^{\infty} b_1^{(2m)}(r)\sin 2m\psi, \end{aligned} \tag{13}$$

$$\begin{aligned} B_2(r,\psi) &\equiv B_r(r,\psi)\sin\psi + B_\phi(r,\psi)\cos\psi \\ &= \Big[b_2^{(0)}(r) + \sum_{m=1}^{\infty} b_2^{(2m)}(r)\cos 2m\psi \Big], \end{aligned}$$

where

$$\begin{aligned} b_1^{(2m)}(r) &\equiv \tfrac{1}{2}[b_r^{(2m+1)}(r) + b_r^{(2m-1)}(r)] \\ &\quad + \tfrac{1}{2}[b_\phi^{(2m+1)}(r) - b_\phi^{(2m-1)}(r)], \\ b_r^{(2m)}(r) &\equiv \tfrac{1}{2}[b_r^{(2m+1)}(r) - b_r^{(2m-1)}(r)] \\ &\quad + \tfrac{1}{2}[b_\phi^{(2m+1)}(r) + b_\phi^{(2m-1)}(r)], \end{aligned} \tag{14}$$

and

$$b_2^{(0)}(r) \equiv \tfrac{1}{2}[b_r^{(1)}(r) + b_\phi^{(1)}(r)].$$

Near the axis the fields, up to quadratic power in r, are

$$\begin{aligned} B_1(r,\psi) &= b_1^{(2)}(r)\sin 2\psi, \\ B_2(r,\psi) &= [b_2^{(0)}(r) + b_r^{(2)}(r)\cos 2\psi], \\ B_z(r,\psi) &= b_z^{(1)}(r)\cos\psi, \end{aligned} \tag{15}$$

where

$$\begin{aligned} b_2^{(0)}(r) &= -\frac{\mu_0 I}{\pi} k\bar{a}\left\{ -K_1'(\bar{a}) + \frac{\bar{r}^2}{4}\left[-\frac{2}{\bar{a}}K_1(\bar{a}) + \left(1 - \frac{4}{\bar{a}^2}\right)K_2(\bar{a}) + \frac{1}{\bar{a}}K_3(\bar{a})\right]\right\} \\ &\simeq -\frac{\mu_0 I}{\pi} k\bar{a}\left(\frac{\pi}{2\bar{a}}\right)^{1/2} e^{-\bar{a}}\left(1 + \frac{7}{8\bar{a}}\right)\left(1 + \frac{\bar{r}^2}{4}\right), \\ b_1^{(2)}(r) &= -\frac{\mu_0 I}{\pi} k\bar{a}\frac{\bar{r}^2}{8}\left\{\left[\left(1 + \frac{4}{\bar{a}^2}\right)K_2(\bar{a}) - \frac{1}{\bar{a}}K_3(\bar{a})\right] + 9\left[K_2(3\bar{a}) + \frac{3}{\bar{a}}K_3(3\bar{a})\right]\right\} \\ &\simeq -\frac{\mu_0 I}{\pi} k\bar{a}\left[\left(\frac{\pi}{2\bar{a}}\right)^{1/2} e^{-\bar{a}}\left(1 + \frac{7}{8\bar{a}}\right) + \left(\frac{\pi}{6\bar{a}}\right)^{1/2} e^{-3\bar{a}9}\left(1 + \frac{29}{8\bar{a}}\right)\right]\frac{\bar{r}^2}{8}, \end{aligned} \tag{16}$$

$$b_2^{(2)}(r) = -\frac{\mu_0 I}{\pi} k\bar{a}\frac{\bar{r}^2}{8}\left\{-\left[\left(1+\frac{4}{\bar{a}^2}\right)K_2(\bar{a}) - \frac{1}{\bar{a}}K_3(\bar{a})\right] + 9\left[K_2(3\bar{a}) + \frac{3}{\bar{a}}K_3(3\bar{a})\right]\right\}$$

$$\simeq -\frac{\mu_0 I}{\pi} k\bar{a}\left[-\left(\frac{\pi}{2\bar{a}}\right)^{1/2} e^{-\bar{a}}\left(1+\frac{7}{8\bar{a}}\right) + \left(\frac{\pi}{6\bar{a}}\right)^{1/2} e^{-3\bar{a}9}\left(1+\frac{29}{8\bar{a}}\right)\right]\frac{\bar{r}^2}{8},$$

$$b_z^{(1)}(r) = -\frac{2\mu_0 I}{\pi} k\bar{a}^2 \bar{r} K_1'(\bar{a})$$

$$\simeq \frac{2\mu_0 I}{\pi} k\bar{a}^2\left(\frac{\pi}{2\bar{a}}\right)^{1/2} e^{-\bar{a}}\left(1+\frac{7}{8\bar{a}}\right)\bar{r}.$$

Again, in the limit $r \to 0$, these reduce to the canonical fields,

$$B_1 = B_z = 0,$$

$$B_2 = \frac{\mu_0 I}{\pi} k\bar{a}K_1'(\bar{a}). \tag{17}$$

IV. RESULTS

In this section we present representative numerical results obtained from evaluating the first several terms in the series expressions derived in the previous section. As stated in the Introduction, our objective is to illustrate limitations to the use of the canonical form for the helical wiggler field as given by Eq. 1.

Results are shown for double-helix windings of three different pitch-to-radius ratios $p/a = 1,2$, and 3. For smaller values of p/a the current required to achieve a wiggler field B (gauss) will exceed 100 Bp amperes; such currents pose serious practical design problems. For larger values of p/a higher spatial overtones become significant for off-axis locations.

Figure 1 shows the radial variation of the field for $p/a = 2$. Figure 1(a) shows the components in cylindrical coordinates, while Fig. 1(b) shows the components in the helical representation. Specifically, Fig. 1(a) shows $b_r^{(1)}(r)$, $b_\phi^{(1)}(r)$, and $b_z^{(1)}(r)$, that is the amplitudes for components of the field with the fundamental periodicity. Figure 1(b) shows $b_2^{(0)}(r)$, $b_1^{(2)}(r)$, $b_z^{(1)}(r)$, and $b_2^{(2)}(r)$. These are the components which, to lowest order, contribute to the field with fundamental periodicity. The canonical field is $b_2^{(0)}(0)$, so that the respresentation of Fig. 1(b) is convenient for determining the magnitude of departures from the approximation $\mathbf{B}(r,\phi,z) = \hat{e}_2 b_2^{(0)}(0)$. For example, at $r/a = 0.3$ one sees that $b_2^{(0)}(r)$ has increased by about 25% over $b_2^{(0)}(0)$, while $b_z^{(1)}(r)$ has become nearly equal to $b_2^{(0)}(r)$. The orthogonal helical component $b_1^{(2)}(r)$ has risen to about 25% of $b_2^{(0)}(0)$ at $r/a = 0.3$.

Figure 2 shows the field components for $p/a = 1$, with the cylindrical coordinate case in Fig. 2(a) and the helical coordinate case in Fig. 2(b). Here one sees that the current required for a given on-axis field is about 16 times *greater* than for $p/a = 2$ for the same pitch p. Deviations from the canonical value $b_2^{(0)}(0)$ for finite r are more severe than for $p/a = 2$.

Figure 3 shows the field componehts for $p/a = 3$. Here the current required to achieve a given field, at fixed pitch, is 2.5 times *less* than for $p/a = 2$. Furthermore the off-axis deviations of the field from its value on axis are smaller than for $p/a = 2$.

However, the apparent attractiveness of the $p/a = 3$ case over that for $p/a = 2$ is partially mitigated by higher space-harmonic components. This is shown in Fig. 4 for $p/a = 3$, where the field components, in cylindrical coordinates, are shown for the third [Fig. 4(a)] and fifth [Fig. 4(b)] spatial harmonics of the field. (Even space harmonics have zero amplitude due to the symmetry of the windings.) The harmonic amplitudes are not insignificant for $r/a > 0.4$. For comparison, Fig. 5 shows the same components for $p/a = 2$. Here the harmonic amplitudes are seen to be less significant.

Finally we show, in Fig. 6, a comparison with Fig. 1 of Ref. 5. This is a plot of $I/pB_\perp(0)$ vs a/p. Shown are three curves: (a) the result of this work, (b) the asymptotic form [Eq. (2a)], and (c) the result shown in Ref. 5. The latter (as well as the asymptotic form) fails at low values of a/p. This point is discussed in Ref. 1, but somehow never corrected. The difference between our curve and that of Ref. 5 at large a/p is due to the different current distributions in each model. The asymptotic form is reasonably accurate for $a/p > 0.5$.

V. CONCLUSIONS

An exact result has been presented for the magnetic field inside and outside a single and double helix winding. The results are expressed in both cylindrical and helix-like coordinates, as space-harmonic series in $(\phi - kz)$. The radial dependences are given in terms of Bessel functions $K_l(m\rho)$, where $\rho^2 = k^2(r^2 + a^2)$. This representation is valid both inside and outside the helix. It has the advantage of faster convergence over the more common piecewise solutions in terms of $I_n(mkr)$ (inside) and $K_n(mkr)$ (outside).

The results show that, depending upon the helix pitch-to-radius ratio p/a, both the magnitude and form of the field may differ considerably from the canonical form (Eq. 1). The first competing term is $B_z(r)$, which increases proportially with r for small r. For larger radii, as may be encountered in free electron lasers using annular electron beams, strong radial gradients and higher spatial harmonics are prevalent.

ACKNOWLEDGMENTS

S. Y. Park and J. M. Baird would like to acknowledge support in part by the Naval Research Laboratory. R. A. Smith and J. L. Hirshfield acknowledge support in part by the Office of Naval Research.

[1] A. N. Didenko, A. V. Kozhevnikov, A. F. Medvedyev, N. M. Nikitin, and V. Ya. Epp, Sov. Phys. JETP **49**, 973 (1979).

[2] D. A. G. Deacon, L. R. Elias, W. M. Fairbank, J. M. J. Madey, H. A. Schwettman, and T. I. Smith, Phys. Rev. Lett. **38**, 892 (1977).

[3] I. B. Bernstein and J. L. Hirshfield, Phys. Rev. A **20**, 1661 (1979).

[4] William R. Smythe, *Static and Dynamic Electricity* (McGraw-Hill, New York, 1950), pp. 276–279.

[5] J. P. Blewett and R. Chasman, J. Appl. Phys. **48**, 2692 (1977).

Japan-U.S. Seminar on Theory and Application of Multiply-Ionized Plasmas
Produced by Laser and Particle Beams, Nara, Japan, May 3-7, 1982

Free Electron Lasers in the Collective Regime

J. L. Hirshfield
Applied Physics, Yale University
P.O. Box 2159, New Haven, Connecticut 06520

Abstract

Free electron lasers operating in the collective regime are reviewed, with emphasis on effects associated with a strong axial magnetic field. One example of such a device is discussed, which operates without a periodic static pump magnetic field. This device, if operated at a wavelength of about one-half millimeter with a power output of about 600 MW, could act as the pump for a second one micron laser with an output of over 1 GW.

I. INTRODUCTION

The purpose of this paper is to review certain recent accomplishments in theory and experiment on free electron laser (FEL) interactions in the regime where collective effects play an important role. For such an interaction, oftimes termed "stimulated Raman scattering," the beam electrons move in electromagnetic fields which are themselves governed in both space and time by the selfsame electron motions. The established theoretical apparatus of plasma physics is well-suited to this regime; whereas in the opposite single-particle, or "stimulated Compton scattering," regime one needs deal basically with one-body equations-of-motion in assigned electromagnetic fields.

The general theme of this Seminar stresses plasma interactions in the optical portion of the spectrum, so that presumably the design of FEL's at wavelengths below 10 μm would be of great interest to this audience. A FEL operating fully in the collective regime would probably not operate at a wavelength shorter than about 100 μm. Thus the present paper attemps to motivate interest in collective-regime FELs by re-introducing their possible role as drivers in two-stage FEL systems yielding high-power tunable optical power. One example of a model two-stage system is given in Section II of this paper, and its features are contrasted with those customary single-stage approach. Section III reviews the rapidly growing body of experimental and theoretical work on collective-regime FELs, placing emphasis on effects of the ubiquitous uniform guide magnetic field.

Section IV discusses a new collective FEL concept originated by Fruchtman and Friedland [1], wherein no spatially periodic pump magnetic field is required, and illustrates how this device is ideally suited as the driver in a two-stage FEL.

II. TWO-STAGE FELs RE-EXAMINED

In 1979, Elias [2] proposed a two-stage FEL to produce kw-level tunable radiation in the 0.4 μm wavelength range. His device was to utilize two dc electrostatic accelerators at 2.13 and 9.38 MeV. A static magnetic pump wiggler in the first stage with a 3.2 cm period allowed generation of 0.6 mm radiation, which in turn was to be upshifted to 0.4 μm in a 2.4 m long second stage.

The device we describe here is conceptually similar to Elias', except that in place of dc electrostatic accelerators - which are limited to currents of tens of amperes - we envision two induction linear accelerators, at 2 and 5 MV - each capable of kiloampere level currents, and correspondingly higher peak powers [3].

In Section IV we shall describe a collective-regime FEL which is capable of producing significant power at sub-mm wavelengths; we pick 532 μm as the design wavelength for the first stage output. So as not to place undue requirements on the quality of the second-stage electron beam, we choose a system length of 474 pump periods (or 0.252 meter) - identical in number of pump periods to that put forward in a design example by Kroll, Morton, and Rosenbluth [4]. (For a tapered 2.3 cm period magnetic wiggler, these authors placed an upper limit on beam energy spread $(\Delta\gamma/\gamma)_{max} \leq 0.014$; we shall adopt the same limit.) The wavelength ratio $(\lambda_{pump}/\lambda_{optical}) \simeq 532 = 4\gamma_{\perp}^2$ for an electromagnetic pump; with $\gamma_{\perp}^2 \simeq \gamma^2$ this gives a beam energy of 5.2 MV. The Colson single-particle one-pass gain formula [5] can be written

$$G_o = (I/4270)\xi^2(\pi N/\gamma)^3(r_e k_p)^{-2}F'(\theta) \qquad (1)$$

where $F'(\theta)$ is the line-shape function (it's peak value is 0.54), I is the beam current in amperes, ξ is the dimensionless pump parameter eA/mc, with A the magnitude of the transverse component of the pump wave's vector potential, r_e is the electron beam radius, and $k_p = 2\pi/\lambda_p$ is the pump wavenumber. The high-efficiency design in Ref. [4] required a single-pass gain of 3.5. For the same gain value, and with $r_e = 0.125$ cm,

Eq. 1 requires $\xi^2 I = 2.78$ amperes. The saturation-level output from the first-stage collective FEL corresponds to $\xi_o = eE_{wave}/mc^2 k_p \simeq 0.01$; if this $\lambda = .5$ mm beam has a 1.25 cm diameter, we take a five-fold pump beam diameter compression to give $\xi = 0.05$. (The pump fields can be supported by a parallel-plane waveguide, with gradually increasing spacing to provide pump amplitude taper.) Thus the required beam current is 1.11 kA, and beam power is 5.78 GW. For 20% efficiency (see Ref. [4]) the peak laser output power at $\lambda_{optical} = 1$ μm would be 1.16 GW.

We now turn to the requirements this second-stage design would place on the first stage. In terms of the normalized pump parameter ξ the pump power is

$$P_{pump} = \frac{1}{8} (4\pi\varepsilon_o m^2 c^5/e^2)(k_p r_e)^2 \xi^2 \qquad (2)$$

where $(4\pi\varepsilon_o m^2 c^5/e^2) = 8.73$ GW. The values $\xi = 5 \times 10^{-2}$, $r_e = 0.125$ cm, and $2\pi/k_p = 0.0532$ cm give $P_{pump} = 594$ MW. A 2.04 MV, 3.34 kA electron beam in the first stage would furnish this power level if the collective FEL achieved an efficiency of 8.7%, which is well within predicted limits. The wiggler-free collective FEL will require a strong uniform axial magnetic field; for the example discussed here its strength is 20.1 kG, well within available superconducting magnet technology. The required interaction length is under 1 m.

A summary of the parameters of the proposed two-stage device is given in Table I, together with the parameters given for the illustrative device in Ref. [4].

III. REVIEW OF PRIOR WORK

Activity on FELs in the collective regime has intensified of late. Work prior to 1980 is well summarized in review articles prepared by Sprangle, Smith, and Granatstein [6], and by Marshall, Schlesinger, and McDermott [7]. Meanwhile, attention has focussed on the influence of an axial guide magnetic field on the FEL interaction, since virtually all collective-regime FEL experiments include such a field.

A major discovery in this area whose impact is still being appreciated concerns the equilibrium orbits in a FEL helical magnetic wiggler when a uniform axial magnetic field is imposed. Without the axial field, the allowed orbits are of course helical, but as was dramatically shown by Friedland [8], this is only an approximate result when the axial field

Stage I	Stage II	Single-Stage [4]
E_e = 2.04 MV	E_e = 5.2 MV	E_e = 111 MV
I_e = 3.34 kA	I_e = 1.1 kA	I_e = 11 A
γ = 5.0	γ = 11.5	γ = 218
$v_\perp$ = 0.1 c	$\Delta\gamma/\gamma$ = 0.014	N = 474
$v_\perp/v_\parallel$ = 0.103	N = 474	λ_p = 2.3 cm
k_o = 3 cm^{-1}	L = 25.2 cm	L = 10.9 m
Imk = 0.10 cm^{-1}	r_e = 0.125 cm	Q = 100
B_z = 20.11 kG	ξ = 0.05	r_e = 0.125 cm
η_e = 8.7%	G_o = 3.5	ξ = 1.75-1.18 z/L
P = 594 MW	η_e = 20%	B_W = 4.56-3.07 z/L kG
λ = 532 μm	P = 1.16 GW	η_e = 18%
	λ = 1.0 μm	P = 0.22 GW
		λ = 1.0 μm

Table I. Examples of parameters of a two-stage FEL (columns 1 and 2), compared with parameters of a single-stage device (column 3) [4].

is present, and depends critically upon the wiggler parameters and the entry conditions; orbits over most of the parameter range are strongly non-helical. Stability analysis showed that electrons on a nearly helical orbit have a natural resonance frequency for small oscillations about equilibrium. Experiments performed by Avivi et al. [9] have confirmed the predicted [8] threshold for orbit stability. Fig. 1 shows the data from this experiment, performed with a low-voltage, low current dc electron beam (the stability properties are not a relativistic effect); the threshold for orbit instability in this experiment was observed for wiggler field amplitudes as low as 2 gauss.

Analytic solutions to the exact non-linear orbit equations in a "canonical" helical wiggler field have been given by Smith et al. [10], and by Freund and Drobot [11]. (The "canonical" approximation neglects the off-axis gradients in the field of the bi-filer helix winding used to generate the field.) These analytic solutions bear out the properties discussed and shown in numerical solution by Friedland [8]. Exact analytic solutions for the magnetic field of a bi-filar helical winding have been recently obtained by Park, Baird, Smith, and Hirshfield [12]. These solutions show that, for annular beams, the canonical assumption may be strongly violated. In addition higher space harmonics may be significant.

Diament has studied particle orbits in a more realistic wiggler field [13].

The influence of the axial guide field upon FEL gain was first shown theoretically by Friedland and Hirshfield [14] using a single particle model. Gain enhancement of more than a factor of 10 was shown, above that for an otherwise identical FEL without the axial guide field, as shown in Fig. 2. This interaction was developed in a fully collective model by Bernstein and Friedland [15], Freund, et al. [16], and Freidland and Fruchtman [17]. Non-linear results have also been obtained by Friedland and Bernstein [18], including effects connected with non-helical orbits and saturation; the saturation levels are shown to be greatly influenced by large radial excursion of the orbits. Further detailed linear analysis has recently been performed by Freund, Sprangle, Dillenburg, da Jornada, Schneider, and Liberman [19].

The first experiment to show clear effects of the guide magnetic field upon a collective FEL interaction was reported by Birkett and Marshall [20]. Enhanced radiation was observed as a $\gamma = 2$ electron beam passed along a helical wiggler with 18 mm pitch and 40 cm length. When the guide field gyrofrequency and magnitude matched the sense and frequency of the helically driven undulation, enhanced radiation resulted; for reversed direction guide field the enhancement was absent. The authors explain the observed double resonance as a matching between either the pump or scattered signal to the electron gyrofrequency. An alternative explanation could lie in the strongly non-helical orbit which could have been present near the resonance between the gyro-and wiggler-frequencies; slight retuning on either side of the resonance could have restored the nearly helical orbit and thus provided the enhancement.

Using a similar electron beam generator the Ecole Polytechnique group [21] observed orders-of magnitude enhancement in mm-wave radiation as the guide field was adjusted near the aforementioned resonance, as shown in Fig. 3. However the authors point out that non-adiabatic conditions as the beam enters the wiggler could lead to poor beam quality, thus making imprecise the occurance of such a resonance in the orbits, especially in avoiding strongly non-helical orbits.

The precise origin of these observed enhancements has been called into question by Shefer and Bekefi [22]. These authors measured emission from a $\sim$ 1 MV, $\sim$ 5 kA electron beam in both a uniform magnetic field, and

in a uniform magnetic field superposed on a rippled magnetic field produced by a diffusive wiggler [23]. With the uniform field alone intense microwave resonance emission is observed between 8 and 140 GHz. It was shown that the conditions under which intense radiation is observed coincided with a matching between the electron cyclotron frequency, or one of its harmonics, and the cut-off frequency of one of five waveguide modes supported by the 2 cm diameter stainless steel drift tube surrounding the beam. The authors interpret this emission as being due to the cyclotron maser instability [24]. Imposition of the wiggler field did enhance the aforementioned resonances, but did not lead to additional radiation at the resonance between the gyro- and wiggler frequencies. The authors suggest that their wiggler increased the perpendicular energy, and thus the growth of the cyclotron maser instability, but did little else. No theory for the collective FEL with an axial guide field in a waveguide has yet appeared. It may be that the waveguide dispersive effects alter sufficiently the conditions under which guide-field enhancement of FEL radiation is expected. Be this as it may, some controversy does remain.

One further experiment deserves mention in this brief review: that reported by the Naval Research Laboratory group in 1982 [25]. These authors made a major advance in the art of generating intense MV electron beams by carefully designing the field-emission foil-less diode geometry to produce kiloampere beams whose axial velocity spread is claimed to be less than 0.1%. This is a requirement in the experiment reported, since the wiggler employed had $p = 21$ periods. Unless $\Delta u/u << p^{-1}$, one would expect phase mixing to wash out clear collective interaction between the beam and the wiggler. A significant observation in this experiment is the presence of two bands of mm-wave emission ($\lambda < 5$ mm) on either side of the resonance between gyro- and wiggler frequency, as shown in Fig. 4. The orbit stability studies [8] show that helical orbits are not possible close to this resonance, and the NRL group has found good agreement between their observation and prediction of theory.

IV. FEL WITHOUT A WIGGLER

In 1979, Ride and Colson [26] published a single-electron calculation of the stimulated emission from individual electrons on helical orbits in a uniform magnetic field. Careful study of the orbit perturbations arising from a copropagating electromagnetic wave revealed that axial velocity perturbations are present, in addition to the customary azimuthal velocity

perturbations. For an ensemble of such electrons with randomly-phased equilibrium helical orbits, the axial velocity modulation can give rise to wave amplification for slow electromagnetic waves, whilst relativistic energy changes give rise to amplification for fast electromagnetic waves [27]; the effects compete for traveling waves, but not for standing waves [28]. This class of interaction is widely exploited in gyrotron devices [24].

But, when an ensemble of electrons have phase coherence in their helical orbits, the system has much in common with a FEL in a helical magnetic wiggler. For the latter the equilibrium orbits are coherent helices with axial period ℓ equal to that of the static magnetic pump; for the former the equilibrium orbits may be coherent helices with axial period $\ell_o = 2\pi\gamma u/\Omega$, where u is the axial velocity and $\Omega = eB_o/m$ is the rest electron gyrofrequency. While the equilibria may be identical in the two configurations, perturbations (i.e. stimulated emission) will differ, since the pump magnetic field in the conventional FEL clearly influences the subsequent motion. A principal difference between FELs with and without a periodic magnetic pump is that the output wavelength for the former would be $\lambda \simeq \ell/2\gamma^2$, whereas for the latter it would be $\lambda \simeq \ell_o/2\gamma^2 = \pi u/\Omega\gamma$. The use of a uniform magnetic field FEL will not permit operation at wavelengths below about γ^{-1} mm, for magnetic field strengths below 100 kG.

The Ride-Colson analysis [26], and subsequent large-signal extensions thereto [29] do not of course apply in the collective regime. However electron beams in most experimental devices which operate in the mm or sub-mm wavelength range are intense enough (kA currents) to require a collective description. A collective theory has recently been developed by Fruchtman and Friedland [1], who have shown that spatial amplification rates for waves on a cold, spatially coherent beam of helically orbiting electrons in a uniform magnetic field are comparable to those predicted for conventional collective FELs in the same parameter regimes [16]. Here we present a highly condensed version of the Fruchtman-Friedland analysis.

The authors consider wave propagation down a uniform magnetic field $\underline{B} = \hat{e}_z B_o$, along which an unbounded electron beam flows. The electron beam is characterized by the cold velocity-distribution $f(\underline{v},z) = N\delta[\underline{v} - \underline{V}(z)]$, where $\underline{V}(z) = -w[\hat{e}_x \cos(k_o z + \phi) + \hat{e}_y \sin(k_o z + \phi)] + u\hat{e}_z = -w\hat{e}_2 + u\hat{e}_3$, and N is the beam density. The perpendicular and parallel speeds are w and u,

ϕ is a constant phase which assigns $\underline{V}(0)$, $k_o = eB_o/m\gamma u$, and $(\hat{e}_1,\hat{e}_2,\hat{e}_3)$ is the set of basis vectors which track the orbit helix [29]. Maxwell's equations for the fields, and momentum and energy conservation equations for the particles are linearized, for the steady-state spatial evolution of the perturbed quantities i.e., for the amplifier problem. In the helical coordinate system these equations reduce to a set of eight first-order, linear, ordinary differential equations, with constant coefficients - as long as spatial evolution rates are on a scale much longer than c/ω. Subject to assigned boundary values, say at $z = 0$, one can then determine the spatial evolution of the system in the form $\psi(z) = \psi_k \exp(ikz)$. Coupled algebraic equations result for the three components of the velocity perturbation, for the three components of the electric field of the wave, and for the perturbed beam density and electron energy. The equations may be rearranged to appear in the form $\varepsilon_{11}E_{1k} + \varepsilon_{12}E_{2k} = 0$ and $\varepsilon_{21}E_{1k} + \varepsilon_{22}E_{2k} = 0$, where E_{1k} and E_{2k} are electric field amplitudes in the directions of $\hat{e}_1$ and $\hat{e}_2$, and where the ε_{ij} are elements of a dispersion tensor. The dispersion relation $\varepsilon_{11}\varepsilon_{22} - \varepsilon_{12}\varepsilon_{21} = 0$ yields the allowed (possibly complex) values of k for assigned values of ω and the other parameters; this dispersion relation is of eighth algebriac order in k. However, for k near k_o considerable simplification results, and the dispersion relation has the approximate form

$$(\Delta - \beta)(\Delta^2 - \zeta^2) - \xi^2\zeta^2\mu/4 = 0 \qquad (3)$$

where $\Delta = ku/c - \omega(1 - u/c)/c$, $\beta = k_o u/c - \omega(1 - u/c)/c$, $\zeta^2 = \omega_p^2/\gamma^3 c^2$, $\xi^2 = \gamma^2 w^2/c^2$, and $\mu = k_o(1 - \zeta^2/\Delta^2) - \omega(1 - u/c)/c$. This dispersion relation superficially resembles that for a conventional FEL [30], wherein coupling between electromagnetic ($\Delta \approx \beta$) and beam ($\Delta \approx \pm\zeta$) modes leads to wave growth where $\xi^2\zeta^2$ is the (small) coupling constant. [If μ were to be replaced by $-2k_o$, Eq. (3) would be the reduced FEL equation.] But since μ in Eq. (3) is a function of Δ, the equation is of higher order (fifth) and the solutions are more complex. In fact, two modes may be simultaneously unstable.

Numerical results are shown in Fig. 5, where the spatial growth rates for the two unstable modes are shown as functions of frequency. Two different combinations of axial magnetic field strength and beam energy are given, but the product $k_o\gamma^2$ is taken as 75 for both examples, so that peak gain occurs for both examples at the same frequency (i.e. near $\omega/c = 118$ cm^{-1} or $\lambda = 2\pi/118 = 0.0532$ cm). The solid curves are for $\gamma = 5$,

$k_o = 3\ cm^{-1}$; the dashed curves are for $\gamma = 2$, $k_o = 18.75\ cm^{-1}$; both curves are for $(\omega_p/c)^2 = 2\ cm^{-1}$, corresponding to a current density of 2658 A/cm^2. It is important to note the wide band width for the lower solid curve, indicating the potential for generating intense wide-band power in the sub-mm range using this interaction. The growth rate of 0.10 cm^{-1} at the peak of the upper solid curve in Fig. 4 suggests that the length of the first stage can be less than 1 m if an 80-90% reflection output coupler is used. Preliminary non-linear studies [31] indicate that this interaction will begin to saturate when $e|E|/mc^2 \approx 0.6\ cm^{-1}$, or when $\xi_o = e|E|/mc^2k_p \approx 5 \times 10^{-3}$; we have adopted a fully saturated level $\xi_o = 10^{-2}$ in our considerations in Section II.

V. ACKNOWLEDGEMENTS

Appreciation is extended to the many members of the "FEL Collective" who kindly furnished the author with their recent research results, including much unpublished work. Responsibility for misrepresentation is soley that of this author. Space limitations prevented review and mention of all the relevant work, so that certain subjective choices were made; no judgement on much of the fine recent work not discussed here is intended. This work was sponsored in part by the U.S. Office of Naval Research.

REFERENCES

1. A. Fruchtman and L. Friedland, J. Appl. Phys. 53, May (1982).
2. L. R. Elias, Phys. Rev. Lett. 42, 977 (1979).
3. D. Prosnitz, Energy and Technology Review, Lawrence Livermore Laboratory, January, 1982, pp. 19-29; Physics Today 35, 20 (1982).
4. N. M. Kroll, P. L. Morton, and M. N. Rosenbluth, IEEE J. Quantum Electronics QE-17, 1436 (1981).
5. W. B. Colson, Physics of Quantum Electronics 5, Addison-Wesley, Reading, MA, 1977.
6. P. Sprangle, R. A. Smith, and V. L. Granatstein, Infrared and Millimeter Waves V. 1, K. J. Button, Ed., Academic Press, New York, 1979.
7. T. C. Marshall, S. P. Schlesinger, and D. B. McDermott, Adv. Electronics and Electron Physics 53, Academic Press, New York, 1980; T. C. Marshall, Proc. Intl. School Quantum Electronics, Erice, Sicily, August 1980, Plenum Press.
8. L. Freidland, Phys. Fluids 23, 2376 (1980).
9. P. Avivi, F. Dothan, A. Fruchtman, A Ljudmirsky, and J. L. Hirshfield, Intl. J. Infrared and Millimeter Waves 2, 1071 (1981).
10. R. A. Smith, J. L. Hirshfield, S. Y. Park, and J. M. Baird, Bull. APS 25, 919 (1980).
11. H. P. Freund and A. T. Drobot, Phys. Fluids 27, (1982).

12. S. Y. Park, J. M. Baird, R. A. Smith, and J. L. Hirshfield, J. Appl. Phys. 53, Mar. (1982).

13. P. Diament, Phys. Rev. A 23, 2537 (1981).

14. L. Friedland and J. L. Hirshfield, Phys. Rev. Lett. 44, 1456 (1980).

15. I. B. Bernstein and L. Freidland, Phys. Rev. A 23, 816 (1981).

16. H. P. Freund, P. Sprangle, D. Dillenburg, E. H. da Jornada, B. Liberman, and R. S. Schneider, Phys. Rev. A 24, 1965 (1981).

17. L. Friedland and A. Fruchtman, Phys. Rev. A (to be published).

18. L. Friedland and I. B. Bernstein, Phys. Fluids (to be published).

19. H. P. Freund, P. Sprangle, D. Dillenburg, E. H. da Jornada, R. S. Schneider, and B. Liberman, NRL Memo Rpt. 4763, Feb. 19, 1982 (submitted for publication).

20. D. S. Birkett and T. C. Marshall, Phys. Fluids 24, 178 (1981).

21. K. L. Felch, L. Vallier, J. M. Buzzi, P. Drossart, H. Boehmer, H. J. Doucet, B. Etlicher, H. Lamain, and C. Rouillé, IEEE J. Quantum Electronics QE-17, 1354 (1981).

22. R. E. Shefer and G. Bekefi, Int. J. Electronics 51, 569 (1981).

23. K. D. Jacobs, R. E. Shefer, and G. Bekefi, Appl. Phys. Lett. 37, 583 (1980).

24. J. L. Hirshfield, Infrared and Millimeter Waves V. 1, K. J. Button, Ed., Academic Press, New York, 1979.

25. R. K. Parker, R. H. Jackson, S. H. Gold, H. P. Freund, V. L. Granatstein, P. C. Efthimion, M. Herndon, and A. K. Kinkead, Phys. Rev. Lett. 48, 238 (1982).

26. S. K. Ride and W. B. Colson, Appl. Phys. 20, 41 (1979).

27. K. R. Chu and J. L. Hirshfield, Phys. Fluids 21, 461 (1978).

28. J. L. Hirshfield, I. B. Bernstein, and J. M. Wachtel, IEEE J. Quantum Electronics QE-1, 237 (1965).

29. Y. Gell, J. R. Torstensson, H. Wilhelmsson, and B. Levush, Appl. Phys. B27, 15 (1982).

30. I. B. Bernstein and J. L. Hirshfield, Phys. Rev. A 20, 1661 (1979).

31. L. Friedland, private communication.

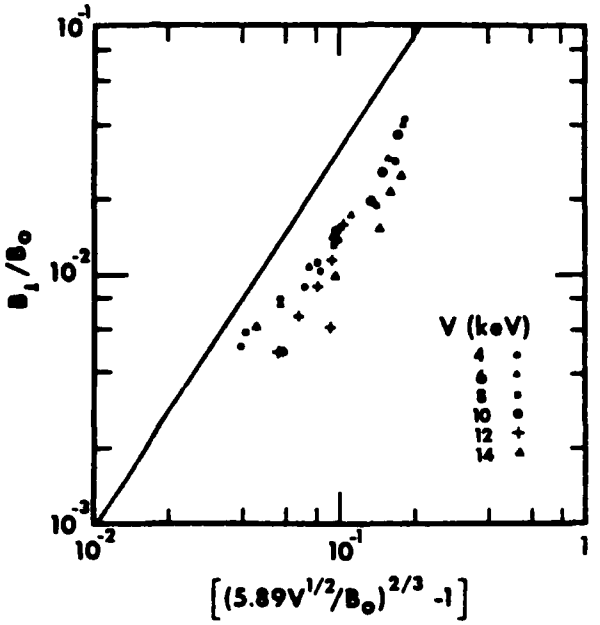

Figure 1. Measured values of $B_\perp/B_0$ at which transitions from stable to unstable orbits were observed, for electron energies between 4-14 keV. Solid line is theoretical prediction. [9]

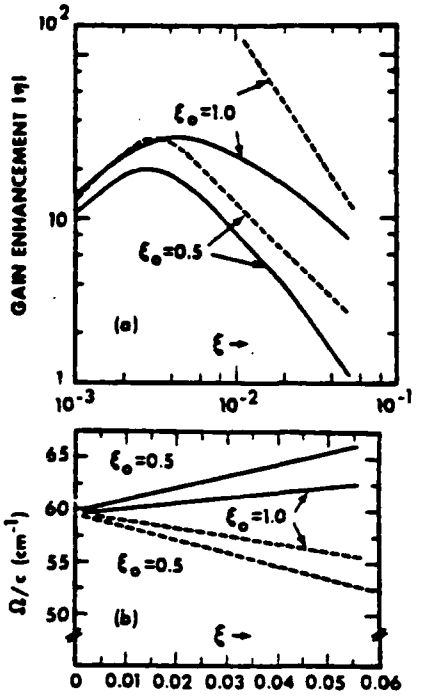

FIG. 2. (a) Gain enhancement $|\eta|$ and (b) corresponding normalized axial magnetic field Ω/c, vs transverse magnetic field parameter ξ. The values $\xi_0 = 0.5$ and 1.0 are for the FEL without axial field, and provide the same $\omega_{\gamma 0}$ as do the indicated (smaller) values of ξ for the FEL with the indicated axial field strength. Example is for $\gamma = 10$, $k_0 = 6.0$ cm^{-1}, and $L = 130$ cm. Solid curves, orbits on branch C; dashed curves, orbits on branch A. For high enhancement values, such as on the $\xi_0 = 1.0$ branch A example, the numerical precision required to compute accurate results suggests that the phenomenon is very sensitive to the system parameters. [14]

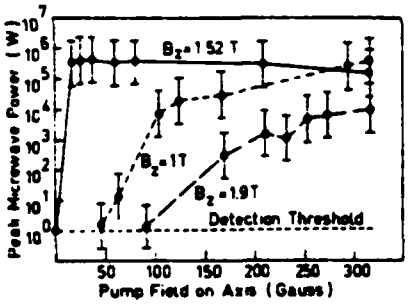

Fig. 3. Microwave power as a function of the pump field strength for frequencies greater than 100 GHz and three values of the longitudinal magnetic field B_z. [21]

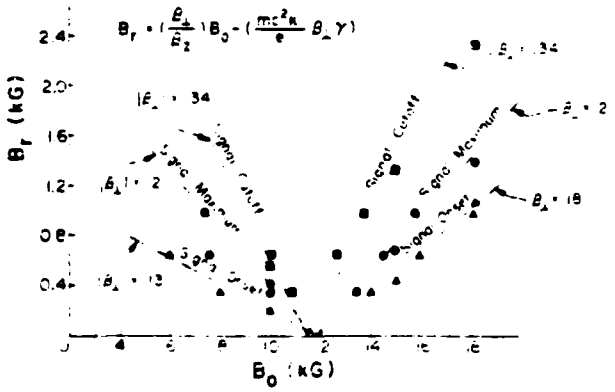

FIG. 4. Signal variation with pump and guide magnetic fields. Signal onset, maximum, and cutoff are plotted as triangles, circles, and squares. The lines correspond to constant values of $B_\perp$. [25]

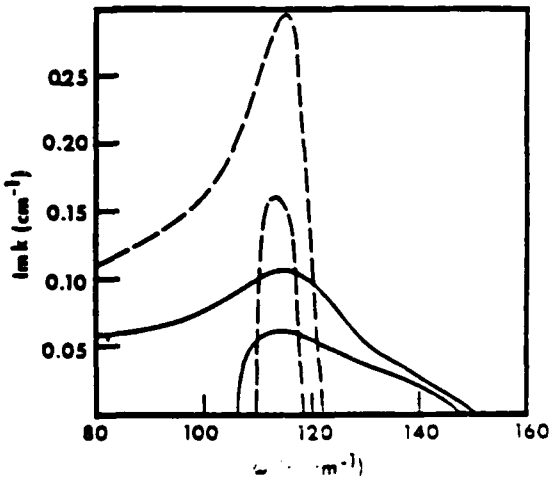

FIG. 5. Spatial growth rates versus frequency for the FEL without a wiggler. [1] See text for parameters.

Amplification of frequency upshifted radiation by cold relativistic guided electron beams

A. Fruchtman
Center for Plasma Physics, Racah Institute of Physics, Hebrew University of Jerusalem, Jerusalem, Israel

L. Friedland
Center for Plasma Physics, Racah Institute of Physics, Hebrew University of Jerusalem, Jerusalem, Israel and Applied Physics, Yale University, New Haven, Connecticut 06520

(Received 21 December 1981; accepted for publication 3 February 1982)

An amplifier on cold, relativistic, guided electron beams is considered. The problem is reduced to a set of first-order, linear, ordinary differential equations. The dispersion relation governing the stability of the system is derived and its solutions are studied numerically. The results of the calculations show that in the submillimeter regime, the spatial growth rates in the system may be comparable to those predicted for Raman-free electron lasers.

PACS numbers: 42.55.Bi, 41.70. + t, 41.80.Dd

I. INTRODUCTION

A great experimental and theoretical effort has been made in recent years in developing powerful sources of coherent radiation, using relativistic electron beams. In free electron lasers, for example, the beams are scattered on periodic magnetostatic structures and amplify electromagnetic signals at a wavelength $\lambda \simeq \lambda_0/2\gamma^2$, where λ_0 is the spatial period of the scattering magnetic field and $\gamma = [1-(v/c)^2]^{-1/2}$ is the relativistic factor, v being the velocity of the beam.[1] These devices have shown a capability for operation in a wide frequency range from millimeter waves to infrared. This broad spectrum of operation is obtained by changing the energy of the electron beam, thus varying the amount of the Doppler upshift in frequency, which is proportional to γ^2.

A different mechanism of amplification of a high-frequency radiation was suggested by Hirshfield *et al.*,[2] who demonstrated the possibility of exploiting the cyclotron maser type instability at Doppler upshifted frequencies. In contrast to free electron lasers, the mechanism discussed[2] does not need to have magnetostatic scattering and relies on the electron beam gyrating in a strong uniform magnetic field. The amplification of an electromagnetic signal is expected at frequencies $\omega \simeq 2\gamma^2\Omega$, where $\Omega = eB/mc\gamma$ is the relativistic electron cyclotron frequency. As is common to many studies of cyclotron masers, the electron beam[2] was assumed to have the following velocity distribution function

$$f(v_x,v_y,v_z) = f(|\mathbf{v}_\perp|,v_z)\,, \tag{1}$$

where $\mathbf{v}_\perp$ is the velocity perpendicular to the magnetic field. Thus the direction of $\mathbf{v}_\perp$ was assumed to be distributed uniformly. In this case the transverse and longitudinal electromagnetic modes in the system are decoupled and, as was shown,[2] one of the transverse modes is spatially unstable.

In the present paper we are also exploiting the idea of using relativistic electron beams in strong uniform magnetic fields. In contrast to Ref. 2, however, we consider a different velocity distribution function. We assume that initially, at the entrance into the interaction region, the distribution function is

$$f(v_x,v_y,v_z)|_{z=0} = A\delta(v_x - v_{x0})\delta(v_y - v_{y0}) \times \delta(v_z - v_{z0})\,, \tag{2}$$

where δ is the Dirac function. The interaction of such a beam with radiation in a uniform axial magnetic field can be described by the cold fluid model, as opposed to case (1), where the study of the interaction of the beam with radiation requires the Vlasov description.[2] In Sec. II we will derive a simple set of equations describing the evolution of the electromagnetic field along the device, by using a method similar to that applied recently to free electron lasers.[3] In Sec. III, we will consider the momentum equation for the beam, which will determine the current sources in the field equations. In Sec. IV, we will reduce the dispersion relation governing our system and demonstrate that the cold beam (2) couples the longitudinal and transverse modes. This effect results in an enhanced spatial growth in the amplifier, as will be demonstrated in Sec. IV, where we will present numerical examples and compare our results with the results of Hirshfield *et al.*[2] and those predicted for free electron lasers, operating in a comparable regime.

II. FIELD EQUATIONS

Consider an electromagnetic wave propagating along a relativistic cold electron beam, gyrating in a uniform magnetic field $\mathbf{B} = \mathbf{B}_0\hat{\mathbf{e}}_z$. Adopting a one-dimensional model, we can describe the electromagnetic fields $\mathbf{E}(z,t)$ and $\mathbf{B}(z,t)$ by the system of Maxwell equations:

$$c\mathbf{e}_z \times \frac{\partial \mathbf{B}_\perp}{\partial z} = \frac{\partial \mathbf{E}_\perp}{\partial t} - 4\pi e N \mathbf{V}_\perp\,, \tag{3}$$

$$-c\mathbf{e}_z \times \frac{\partial \mathbf{E}_\perp}{\partial z} = \frac{\partial \mathbf{B}_\perp}{\partial t}\,, \tag{4}$$

$$\frac{\partial \mathbf{E}_z}{\partial z} = -4\pi e N\,, \tag{5}$$

$$B_z = 0\,. \tag{6}$$

Here $\mathbf{V}(z,t)$ is the velocity of the electrons and N is the electron density, satisfying the continuity equation

 0021-8979/82/064011-05$02.40

$$\frac{\partial N}{\partial t}+\frac{\partial}{\partial z}(NV_z)=0\,. \tag{7}$$

The subscript $\perp$ in Eqs. (3) and (4) describes components of the electromagnetic field transverse to the z axis.

We are considering a stationary amplifier problem, namely, introduce an electromagnetic perturbation of frequency ω at $z=0$ and solve for the electromagnetic field in the device as a function of z. Consistent with this problem we write

$$\mathbf{E}(z,t)=\mathrm{Re}\left(\frac{mc^2}{e}\,\mathbf{a}(z)e^{i\omega(z/c-t)}\right), \tag{8}$$

$$\mathbf{B}(z,t)=\mathrm{Re}\left(\frac{mc^2}{e}\,\mathbf{b}(z)e^{i\omega(z/c-t)}\right), \tag{9}$$

$$\mathbf{V}(z,t)=\mathbf{V}_0(z)+\mathrm{Re}(\mathbf{v}(z)e^{i\omega(z/c-t)}), \tag{10}$$

$$N(z,t)=N_0+\mathrm{Re}(n(z)e^{i\omega(z/c-t)}), \tag{11}$$

where $N_0=\text{const}$ and $\mathbf{V}_0(z)$ are the density and the velocity field characterizing the beam when the electromagnetic wave is absent. Note that in Eqs. (8) and (9) we are considering only rightward propagating waves, which is consistent with the amplifier problem considered in this paper. Equations (3) and (4) can be now combined and yield on linearization

$$\frac{d^2\mathbf{a}_\perp}{dz^2}+2i\frac{\omega}{c}\frac{d\mathbf{a}_\perp}{dz}=i\frac{\omega}{c^4}(\omega_p^2\mathbf{v}_\perp+\mathbf{V}_{0\perp}n)\,, \tag{12}$$

where $\omega_p^2=4\pi e^2N_0/m$. Similarly Eq. (5) reduces to

$$\left(i\frac{\omega}{c}+\frac{d}{dz}\right)a_z=-\frac{n}{c^2}, \tag{13}$$

and the linearized continuity Eq. (7) becomes

$$\frac{1}{c}\left[i\omega\left(\frac{V_{0z}}{c}-1\right)+V_{0z}\frac{d}{dz}\right]n=-\omega_p^2\left(i\frac{\omega}{c}+\frac{d}{dz}\right)v_z\,. \tag{14}$$

Assume now that the various natural frequencies characterizing the electron beam (such as ω_p and $\Omega=e\mathbf{B}_0/mc\gamma$) are much less than ω. Then we expect the spatial variation of $\mathbf{a}$, $\mathbf{b}$, $\mathbf{v}$, and n to be on a scale slow compared to the fast oscillatory part $e^{i\omega z/c}$ in Eqs. (8)–(11). Namely, in order of magnitude, for $x=a$, da/dz, v, n:

$$\left|\frac{d\ln x}{dz}\right|\ll\frac{\omega}{c}\,. \tag{15}$$

With this assumption we can rewrite Eqs. (12)–(14) in the following approximate form:

$$\frac{d\mathbf{a}_\perp}{dz}=\frac{1}{2c^3}(\omega_p^2\mathbf{v}_\perp+\mathbf{V}_{0\perp}n)\,, \tag{16}$$

$$a_z=i\frac{n}{\omega c}\,, \tag{17}$$

$$\frac{1}{c}\left[i\omega\left(\frac{V_{0z}}{c}-1\right)+V_{0z}\frac{d}{dz}\right]n=-i\frac{\omega_p^2\omega}{c}v_z\,. \tag{18}$$

III. MOMENTUM EQUATION

Consider now the momentum equation

$$\left(\frac{\partial}{\partial t}+V_z\frac{\partial}{\partial z}\right)(\gamma\mathbf{V})=-\frac{e}{m}\left(\frac{\mathbf{V}}{c}\times[\mathbf{B}+\mathbf{B}(z,t)]+\mathbf{E}(z,t)\right). \tag{19}$$

In the absence of the electromagnetic fields, this equation describes a gyrating electron beam with

$$\mathbf{V}_0=-w[\hat{\mathbf{e}}_x\cos(k_0z+\phi)+\hat{\mathbf{e}}_y\sin(k_0z+\phi)]+u\hat{\mathbf{e}}_z\,, \tag{20}$$

where $u,w=\text{Const}$; $k_0=e\mathbf{B}_0/mc\gamma u=\Omega/u$ and ϕ defining the velocity of the beam at $z=0$. With no loss of generality let us assume that $\phi=0$ and define a rotating coordinate system with the base vectors

$$\hat{\mathbf{e}}_1=-\hat{\mathbf{e}}_x\sin k_0z+\hat{\mathbf{e}}_y\cos k_0z\,, \tag{21}$$

$$\hat{\mathbf{e}}_2=-\hat{\mathbf{e}}_x\cos k_0z-\hat{\mathbf{e}}_y\sin k_0z\,, \tag{22}$$

$$\hat{\mathbf{e}}_3=\hat{\mathbf{e}}_z\,. \tag{23}$$

Then $\mathbf{V}_0=w\hat{\mathbf{e}}_2+u\hat{\mathbf{e}}_3$ and the linearized momentum equation for perturbed velocities, in components along $\hat{\mathbf{e}}_i(i=1,2,3)$, becomes

$$\frac{1}{c}\left[i\omega\left(\frac{u}{c}-1\right)+u\frac{d}{dz}\right]v_1=k_0w\left(\frac{u\Gamma}{c^2\gamma_0}+\frac{v_3}{c}\right)+\frac{1}{\gamma_0}\left(\frac{u}{c}b_2-a_1\right), \tag{24}$$

$$\frac{1}{c}\left[i\omega\left(\frac{u}{c}-1\right)+u\frac{d}{dz}\right]v_2=-w\frac{\Gamma'}{c^2\gamma_0}-\frac{1}{\gamma_0}\left(\frac{u}{c}b_1+a_2\right), \tag{25}$$

$$\frac{1}{c}\left[i\omega\left(\frac{u}{c}-1\right)+u\frac{d}{dz}\right]v_3=u\frac{\Gamma'}{c^2\gamma_0}+\frac{1}{\gamma_0}\left(\frac{w}{c}b_1-a_3\right), \tag{26}$$

where similar to Eqs. (8)–(11) we defined

$$\gamma=\gamma_0+\mathrm{Re}(\Gamma(z)e^{i\omega(z/c-t)}), \tag{27}$$

and

$$\Gamma'=\frac{1}{c}\left[i\omega\left(\frac{u}{c}-1\right)+u\frac{d}{dz}\right]\Gamma\,. \tag{28}$$

The energy conservation equation

$$\frac{d\gamma}{dt}=-\frac{e}{mc^2}(V_1E_1+V_2E_2+V_3E_3), \tag{29}$$

can be employed, to get on linearization

$$\Gamma'=-\frac{w}{c}a_2-\frac{u}{c}a_3\,. \tag{30}$$

Finally, in the new coordinates, the field and density Eqs. (16)–(18) become

$$\frac{da_1}{dz}-k_0a_2=\frac{\omega_p^2v_1}{2c^3}\,, \tag{31}$$

$$\frac{da_2}{dz}+k_0a_1=\frac{1}{2c^3}(\omega_p^2v_2+wn)\,, \tag{32}$$

$$a_3=i\frac{n}{\omega c}\,, \tag{33}$$

$$\frac{1}{c}\left[i\omega\left(\frac{u}{c}-1\right)+u\frac{d}{dz}\right]n=-i\frac{\omega_p^2}{c}v_3\,. \tag{34}$$

Equations (24)–(26), (30), and (31)–(34) comprise a system of first-order, linear, ordinary differential equations, describing our system completely for any given set of initial conditions at $z=0$. Note that due to the choice of the base vectors $\hat{\mathbf{e}}_i(i=1,2,3)$ we have a system of equations with constant coefficients, which allows us to seek the solution in

the form $\psi(z)=\psi_k \exp(ikz)$, where ψ stands for $v_i, a_i, b_i (i=1,2,3)$, Γ and n. Then Eqs. (24)–(26) become

$$i\Delta v_{1k} = \frac{wk_0}{c} v_{3k} + \frac{wuk_0}{c^2\gamma_0}\Gamma_k + \frac{1}{\gamma_0}\left(\frac{u}{c} b_{2k} - a_{1k}\right), \tag{35}$$

$$i\Delta v_{2k} = -i\Delta\Gamma_k \frac{w}{c\gamma_0} - \frac{1}{\gamma_0}\left(\frac{u}{c} b_{1k} + a_{2k}\right), \tag{36}$$

$$i\Delta v_{3k} = -i\Delta\Gamma_k \frac{u}{c\gamma_0} + \frac{1}{\gamma_0}\left(\frac{w}{c} b_{1k} - a_{3k}\right), \tag{37}$$

where

$$\Delta = \frac{\omega}{c}\left(\frac{u}{c} - 1\right) + k\frac{u}{c}. \tag{38}$$

Similarly Eq. (30) reduces to

$$i\Delta\Gamma_k = -\frac{w}{c} a_{2k} - \frac{u}{c} a_{3k}, \tag{39}$$

and the field and density Eqs. (31)–(34) give

$$ika_{1k} - k_0 a_{2k} = \frac{\omega_p^2}{2c^3} v_{1k}, \tag{40}$$

$$ika_{2k} + k_0 a_{1k} = \frac{1}{2c^3}(\omega_p^2 v_{2k} + w n_k), \tag{41}$$

$$a_{3k} = i\frac{n_k}{\omega c}, \tag{42}$$

$$\Delta n_k = -\frac{\omega_p^2 \omega}{c} v_{3k}. \tag{43}$$

Expressions for b_{1k} and b_{2k} in Eqs. (35)–(37) can be found from Eq. (4):

$$b_{1k} = -a_{2k} + \frac{ic}{\omega}(ika_{2k} + k_0 a_{1k}), \tag{44}$$

$$b_{2k} = a_{1k} - \frac{ic}{\omega}(ika_{1k} - k_0 a_{2k}). \tag{45}$$

On using Eqs. (40) and (41) on the left-hand sides of Eqs. (44) and (45), substituting the resulting expressions and Γ_k from Eq. (39) into the momentum Eqs. (35)–(37) and expressing a_{3k} through v_{3k} via Eqs. (42) and (43) we get

$$i\left(\Delta + \frac{\omega_p^2 u}{2\gamma_0\omega c^2}\right) v_{1k} = \left(\frac{u}{c} - 1\right)\frac{a_{1k}}{\gamma_0} + \frac{iw^2 uk_0}{\Delta c^3\gamma_0} a_{2k} + \frac{wk_0}{c}\left[1 + \frac{\omega_p^2 u^2}{\Delta^2 c^4 \gamma_0}\right] v_{3k}, \tag{46}$$

$$i\left(\Delta + \frac{\omega_p^2 u}{2\gamma_0\omega c^2}\right) v_{2k} = \left(\frac{w^2}{c^2} + \frac{u}{c} - 1\right)\frac{a_{2k}}{\gamma_0} - \frac{i\omega_p^2 uw}{2\gamma_0 c^4 \Delta} v_{3k}, \tag{47}$$

$$(\Delta^2 - \zeta^2) v_{3k} = i\frac{\Delta w(1-u/c)}{c}\frac{a_{2k}}{\gamma_0} + \frac{\omega_p^2 w\Delta}{2\gamma_0\omega c^2} v_{2k}, \tag{48}$$

where

$$\zeta = \left[\frac{\omega_p^2}{c^2\gamma_0}\left(1 - \frac{u^2}{c^2} - \frac{w^2}{c^2}\right)\right]^{1/2}, \tag{49}$$

is the plasma longitudinal response frequency. Assume now that

$$\frac{\omega_p^2 u}{2\gamma_0\omega c^2|\Delta|} \ll 1. \tag{50}$$

An *a posteriori* check of this assumption has shown that it is satisfied for all the numerical examples considered in this paper. Inequality (50) and additional assumptions of $w/c \lesssim 1/\gamma_0$ and $1 - u/c \ll 1$, which are consistent with our treatment of a high-frequency device, allow us to write the solutions of Eqs. (46)–(48) for $v_{ik} (i=1,2,3)$ in the following approximate form:

$$v_{1k} = \frac{w^2 k_0 a_{2k}}{c^2\Delta^2\gamma_0}\left[1 + \frac{\omega_p^2}{\gamma_0 c^2}\frac{[1-(u/c)][1-(w^2/2c^2)]}{\Delta^2 - \zeta^2}\right] + i\left(1 - \frac{u}{c}\right)\frac{a_{1k}}{\Delta\gamma_0}, \tag{51}$$

$$v_{2k} = \frac{ia_{2k}}{\Delta\gamma_0}\left[1 - \frac{u}{c} - \frac{w^2}{c^2} - \frac{\omega_p^2 uw^2[1-(u/c)]}{2c^4\gamma_0(\Delta^2 - \zeta^2)}\right], \tag{52}$$

$$v_{3k} = \frac{i\Delta w[1-(u/c)]a_{2k}}{c(\Delta^2 - \zeta^2)\gamma_0}. \tag{53}$$

IV. STABILITY ANALYSIS AND NUMERICAL EXAMPLES

On substituting Eqs. (51)–(53) into the field equations (40) and (41), we can write the latter as

$$\epsilon_{11} a_{1k} + \epsilon_{12} a_{2k} = 0, \qquad \epsilon_{21} a_{1k} + \epsilon_{22} a_{2k} = 0, \tag{54}$$

where the dielectric tensor is

$$\epsilon_{11} = ik - \frac{i\omega_p^2(1-u/c)}{2c^2\gamma_0\Delta}, \tag{55}$$

$$\epsilon_{12} = -k_0 - \frac{\omega_p^2 w^2 k_0}{2\gamma_0 c^4 \Delta^2}\left[1 + \frac{\omega_p^2(1-u/c)}{\gamma_0 c^2(\Delta^2 - \zeta^2)}\right], \tag{56}$$

$$\epsilon_{21} = k_0, \tag{57}$$

$$\epsilon_{22} = ik - \frac{i\omega_p^2}{2c^2\gamma_0\Delta}\left[1 - \frac{u}{c} - \frac{w^2}{c^2} - \frac{\omega w^2\Delta(1-u/c)}{c^3(\Delta^2 - \zeta^2)}\right]. \tag{58}$$

Existence of a nontrivial solution of Eq. (54) for a_{1k}, a_{2k} requires

$$D = \epsilon_{11}\epsilon_{22} - \epsilon_{12}\epsilon_{21} = 0, \tag{59}$$

which is the dispersion relation governing our system.

When the beam density goes to zero, the dielectric tensor becomes $\epsilon_{11} = \epsilon_{22} = ik$, $\epsilon_{21} = -\epsilon_{12} = k_0$. The dispersion relation in this case yields $k = \pm k_0$, which, of course, is the vacuum solution. This suggests, that for $\omega_p^2 \neq 0$, but small enough, we can treat the terms proportional to ω_p^2 in the expressions for ϵ_{ij}, as small perturbations and seek solutions for k in the form $k = \pm k_0 + x$, where $|x| \ll k_0$. We will use this perturbative approach in the rest of the paper.

First let $k = -k_0 + x$. Then if $\omega/c \simeq 2k_0\gamma^2$, Δ is the order of k_0 and therefore $\Delta^2 - \zeta^2 \simeq k_0^2$, so that the resonance denominators in Eqs. (56) and (58) are relatively large. The solution for x in this case is real, the mode is stable and does not contribute to the possible amplification in our system. Consider now the case $k = k_0 + x$. The values of Δ in this case will be of the order of x, if again $\omega/c \simeq 2k_0\gamma^2$, and the resonance denominator $\Delta^2 - \zeta^2$ in Eqs. (56) and (58) may

become very small. The dispersion relation now has the following approximate form:

$$(\beta - \Delta)(\Delta^2 - \zeta^2) + \frac{1}{4}\xi^2\zeta^2\mu = 0, \tag{60}$$

where

$$\beta = \frac{\omega}{c}\left(\frac{u}{c} - 1\right) + k_0\frac{u}{c}, \tag{61}$$

$$\beta' = \beta + k_0\left(1 - \frac{u}{c}\right), \tag{62}$$

$$\mu = \beta' - k_0\frac{\zeta^2}{\Delta^2}, \tag{63}$$

and $\xi = \omega\gamma_0/c$.

The dispersion relation (60) has some features similar to the case of a conventional free electron laser. The similarity is expressed in the fact that as in the free electron lasers Eq. (60) describes the coupling between the electromagnetic ($\Delta \simeq \beta$) and beam ($\Delta \simeq \pm\zeta$) modes and $\xi\zeta$ can be viewed as the parameter characterizing the strength of the coupling. Moreover, Eq. (60) reduces to the dispersion relation for the free electron laser[3] if we set $\mu = -2k_0$. Note, that for $\Delta \ll \beta$ and ζ^2 small enough, Eq. (60) predicts a solution at $\Delta \simeq \zeta$. Then $\mu \simeq -k_0$ and we can expect in this regime to have a solution of (60) for Δ similar to the solution we have in a free electron laser with the same values of k_0, γ_0, and the beam density twice lower than in our device. Together with these similarities, the apparent difference from the case of a free electron laser is in a more complicated form of μ which leads in our case to the higher-order dispersion relation and, as will be shown below, to coexistence of more than one unstable modes.

We now present some numerical examples. Figure 1 shows the calculated growth rates of the two unstable

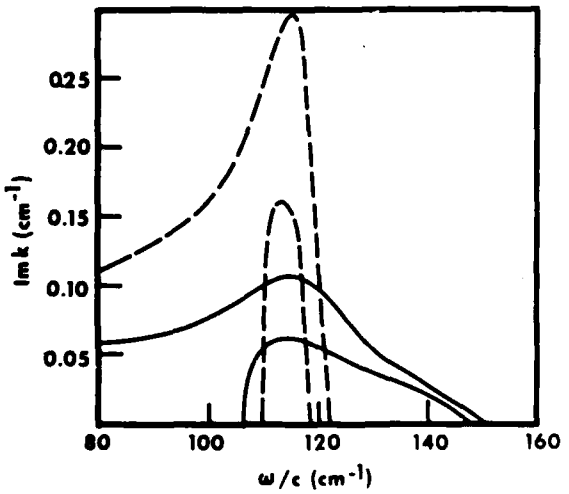

FIG. 1. Spatial growth rates Imk vs normalized frequency ω/c. The parameters are $\omega_p^2/c^2 = 2$ cm^{-2} and $k_0 = 3$ cm^{-1}, $\gamma_0 = 5$ (solid lines) and $k_0 = 18.75$ cm^{-1}, $\gamma_0 = 2$ (dashed lines). For each set of parameters, two unstable modes are present in the system.

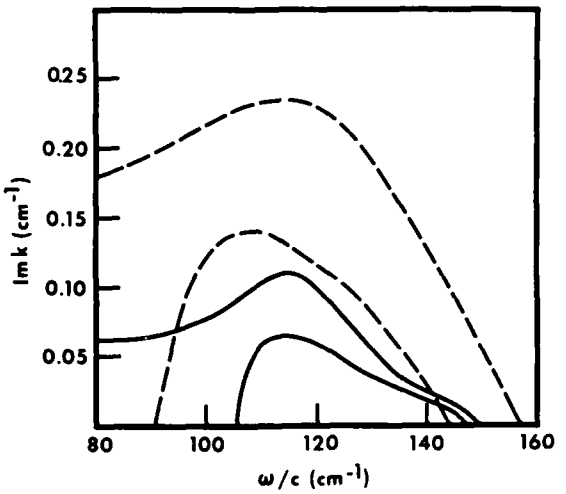

FIG. 2. Spatial growth rates Imk vs normalized frequency ω/c. The parameters are $\gamma_0 = 5$, $k_0 = 3$ cm^{-1}, and $\omega_p^2/c^2 = 2$ cm^{-2} (solid lines) and $\omega_p^2/c^2 = 20$ cm^{-2} (dashed lines).

modes, which are present in the system, for fixed density of the beam and two different combinations of the strength of the axial magnetic field and the beam energy. The combinations were chosen so that $k_0\gamma^2$ in both cases remains the same. In addition we used $\omega/c = 0.1$ in both regimes. The comparison with the recent calculations for Raman free electron lasers,[3] shows that for the case of higher energy of the beam ($\gamma_0 = 5$) the maximum growth rate in our system is about 30% lower than in the free electron laser with the same values of γ_0, w, and ω_p^2. If we use an approximate formula $Imk = w\omega_p/c^2(2\gamma_0)^{1/2}$ derived in Ref. 2 for the beam (1), we find that for $\gamma_0 = 5$ the gain in our system is ~40% higher. For the second set of parameters, with lower beam energy ($\gamma_0 = 2$), the maximum growth rate in our system becomes considerably higher than that predicted in Ref. 2 in this case ($Imk \simeq 0.1$ cm^{-1}). In Fig. 2 we present the cases of two different beam densities, and fixed values of k_0 and γ_0. Significant enhancement of the growth rate is evident with an increase of the beam density. For the higher density case ($\omega_p^2/c^2 = 20$ cm^{-2}) the maximum growth rate is ~0.23 cm^{-1} as compared to ~0.13 cm^{-1} for the beam (1) in this case.

In summary, we have considered an amplifier based on the fully cold, guided, relativistic electron beam. It has been demonstrated that such a system may be superior to the device considered in Ref. 2. In the submillimeter regime the growth rates of the unstable modes in our system are comparable to those found in conventional free electron lasers. The use of only uniform guide magnetic fields allows one to explore electron beams with larger radial dimensions, as compared to those used in free electron lasers, where the best operation is obtained close to the axis of a magnetostatic scatterer. With all the aforementioned advantages, it is still necessary to find the best experimental methods of achieving the suggested configuration of the beam. The effects of a thermal spread in the beam on the growth rates in the sys-

tem, as well as nonlinear saturation effects also must be considered to provide better understanding of more realistic experimental situations.

ACKNOWLEDGMENTS

The authors would like to thank Professor I. B. Bernstein and Professor F. Dothan for their helpful comments and suggestions in the preparation of this paper. The authors also acknowledge the support in part by the U. S. Office of Naval Research and by the U. S.-Israel Binational Science Foundation.

[1]For a review of past work see P. Sprangle, R. A. Smith, and V. L. Granatstein, "Free Electron Lasers and Stimulated Scattering from Relativistic Electron Beams" in *Infrared and Millimeter Waves*, Vol. 1, edited by K. J. Button (Academic, New York, 1979), p. 279.

[2]J. L. Hirshfield, K. R. Chu, and S. Kainer, Appl. Phys. Lett. **33**, 847 (1978).

[3]L. Friedland and A. Fruchtman, Phys. Rev. A **25**, 2693 (1982).

Amplification on relativistic electron beams in combined helical and axial magnetic fields

L. Friedland* and A. Fruchtman
Center for Plasma Physics, Racah Institute of Physics, Hebrew University of Jerusalem, Jerusalem, Israel
(Received 9 July 1981)

A free-electron laser with the guide magnetic field operating as an amplifier is analyzed. A simple dispersion relation, similar in form with or without the guide field, is derived. The study of the solutions of the dispersion relation indicates that the guide allows us to (a) enhance the spatial instability in the amplifier, and (b) significantly extend the frequency range of the instability to lower and higher frequencies. This improved operation of the amplifier with the guide field may be achieved at lower values of the pump helical magnetic field. An expression for the power gain in the amplifier as a function of its length is derived and applied in numerical examples to demonstrate the effects of the guide field.

I. INTRODUCTION

Free-electron lasers, in which the energy of a relativistic electron beam is transferred into high-frequency coherent radiation, have been studied extensively in recent years.[1] One can schematically divide free-electron-laser experiments into two groups. The first is characterized by low beam densities ($I \sim 1$ A) and high relativistic factors γ for electrons ($\gamma > 20$).[2,3] In these devices collective plasma effects are usually unimportant and the single-particle theory is used to describe the interaction. The second group of experiments, for example,[4–6] uses intense electron beams ($I > 1$ kA) with relatively low energies ($\gamma < 10$). In such lasers the collective interaction plays the major role. An important feature of the latter group of experiments is the presence of a strong axial guide magnetic field, primarily designed to collimate the high current electron beam in the interaction region. An analysis of the effects of the presence of the guide field was recently carried out.[7–9] The single-particle theory of such lasers[8] showed that the addition of the guide field may provide a significant increase of the small signal gain due to a resonance effect between the frequency of the scattered electromagnetic wave and the natural response frequency of the steady-state electron orbits in the combined pump and guide fields. In addition, the cold fluid, fully collective theory of the laser[9] predicted an extension of the frequency range of the spatial instability.

In this paper we continue the study of the free-electron laser with a guide magnetic field and consider a conventional amplifier problem. In contrast to Ref. 9, where only the mode stability analysis was carried out, our aim will be to actually find the spatial development of the electromagnetic wave along the amplifier. We shall employ a number of physical approximations which will result in a much simpler dispersion relation than that developed in Ref. 9. The problem is thereby significantly simplified and leads to a clearer understanding of the device.

The work proceeds as follows. In Secs. II and III a system of transport equations for the amplitude of the electromagnetic wave in the amplifier is derived. Section IV deals with current sources in the transport equations by considering the momentum equation for the electrons described by the cold fluid model. A simple dispersion relation is derived in Sec. V and there its solutions are analyzed both analytically and numerically. In Sec. VI formulas for the z dependence of the amplitude of the electromagnetic wave in the amplifier are obtained. We shall simplify these formulas in several limiting cases in this section and present numerical examples. Finally, conclusions are listed and discussed in Sec. VII.

II. FIELD EQUATIONS

Consider a cold relativistic electron beam propagating along the z axis of combined helical pump and axial guide magnetic fields described by

$$\vec{\mathscr{B}}(z) = \mathscr{B}_{\perp 0}(\vec{e}_x \cos k_0 z + \vec{e}_y \sin k_0 z) + \mathscr{B}_{\parallel 0}\vec{e}_z , \quad (1)$$

where $\mathscr{B}_{\perp 0}$ and $\mathscr{B}_{\parallel 0}$ are constants. The helical part of $\mathscr{B}$ represents the field on the axis of a magnetic wiggler, commonly used in free-electron lasers and $k_0=2\pi/\lambda$, where λ is the pitch of the wiggler.

In addition to the electron beam we introduce an electromagnetic wave propagating in the same direction as the electron beam. Our aim is to solve the conventional amplifier, namely, to find the electromagnetic field at a point $z>0$ in the system if this field is known at $z=0$.

We assume that the system is infinite and homogeneous in the direction perpendicular to the guide field. Then the electromagnetic fields $\vec{E}(z,t)$, $\vec{B}(z,t)$ are described by

$$c\vec{e}_z\times\frac{\partial\vec{B}_\perp}{\partial z}=\frac{\partial\vec{E}_\perp}{\partial t}-4\pi eN\vec{V}_\perp\,, \tag{2}$$

$$-c\vec{e}_z\times\frac{\partial\vec{E}_\perp}{\partial z}=\frac{\partial\vec{B}_\perp}{\partial t}\,, \tag{3}$$

$$\frac{\partial E_z}{\partial z}=-4\pi eN\,, \tag{4}$$

$$B_z=0\,, \tag{5}$$

where the cold fluid description of the electron beam is used and $N(z,t)$ and $\vec{V}(z,t)$ are, respectively, the electron density and the velocity field. They satisfy the continuity equation

$$\frac{\partial N}{\partial t}+\frac{\partial}{\partial z}(NV_z)=0\,. \tag{6}$$

The subscript $\perp$ in (2) and (3) describes the components of the corresponding fields which are perpendicular to the z axis. Since a stationary problem is considered here, we Fourier decompose in time various time-dependent quantities and seek solutions for $\vec{E}$ and $\vec{B}$ in the form

$$\vec{E}(z,t)=\mathrm{Re}\left[\frac{mc^2}{e}\hat{E}(z)e^{-i\omega t}\right],\qquad \vec{B}(z,t)=\mathrm{Re}\left[\frac{mc^2}{e}\hat{B}(z)e^{-i\omega t}\right]. \tag{7}$$

In addition, we assume that the electromagnetic field is weak enough so that it only slightly perturbs the beam and one can write

$$N(z,t)=N_0+\mathrm{Re}\left[\frac{m}{4\pi e^2}\hat{M}(z)e^{-i\omega t}\right], \tag{8}$$

$$\vec{V}(z,t)=\vec{V}_0(z)+\mathrm{Re}[\hat{V}(z)e^{-i\omega t}]\,, \tag{9}$$

where $N_0=\text{const}$ and $\vec{V}_0(z)$ are the density and the velocity field characterizing the beam without the presence of the electromagnetic wave and $\hat{M}$ and $\hat{V}$ are small perturbations. Equations (2) and (3) are then combined and yield on linearization

$$\frac{d^2\hat{E}_\perp(z)}{dz^2}+\frac{\omega^2}{c^2}\hat{E}_\perp(z)=i\frac{\omega}{c^4}[\omega_p^2\hat{V}_\perp(z)+\vec{V}_{0\perp}\hat{M}(z)]\,, \tag{10}$$

where $\omega_p^2=4\pi e^2N_0/m$. The first term on the right-hand side of the wave equation (10) represents transverse currents induced by the electromagnetic wave, while the second term describes the axial bunching of the electron density due to the ponderomotive forces of the wiggler magnetostatic field and the magnetic component of the wave. It is this bunching term which causes the *free-electron-laser instability*[1] and is the largest part of the source in the wave equation. The reason for the importance of the axial bunching is the strong coupling between the transverse electromagnetic wave and the axial motion of the electrons which travel with the velocities close to the phase velocity of the wave. We shall demonstrate this effect later. Nonetheless, for simplicity, already at this early stage, we neglect the first term in the source in (10) and rewrite the wave equation as

$$\frac{d^2\hat{E}_\perp(z)}{dz^2}+\frac{\omega^2}{c^2}\hat{E}_\perp(z)=i\frac{\omega}{c^4}\vec{V}_{0\perp}\hat{M}(z)=\vec{F}(z)\,. \tag{11}$$

The general solution of (11) is

$$\begin{aligned}\hat{E}_\perp(z)&=\hat{E}_\perp(0)\cos\frac{\omega}{c}z+\frac{\hat{E}'_\perp(0)}{\omega/c}\sin\frac{\omega}{c}z+\frac{c}{\omega}\int_0^z d\xi\,\vec{F}(\xi)\sin\frac{\omega}{c}(z-\xi)\\&=\tfrac{1}{2}\hat{E}_\perp(0)(e^{i(\omega/c)z}+e^{-i(\omega/c)z})-\frac{i\hat{E}'_\perp(0)}{2\omega/c}(e^{i(\omega/c)z}-e^{-i(\omega/c)z})\\&\quad-\frac{ic}{2\omega}\int_0^z d\xi\,\vec{F}(\xi)e^{i(\omega/c)(z-\xi)}-e^{-i(\omega/c)(z-\xi)})\,.\end{aligned} \tag{12}$$

Thus, the full wave solution for the perpendicular component of the electric field becomes

$$\frac{e\vec{E}_\perp(z,t)}{mc^2}=\frac{1}{2}\mathrm{Re}\left\{e^{i[(\omega/c)z-\omega t]}\left[\hat{E}_\perp(0)-\frac{i\hat{E}'_\perp(0)}{\omega/c}-\frac{ic}{\omega}\left[\int_0^z d\xi\,\vec{F}(\xi)e^{-i(\omega/c)\xi}-e^{-2i(\omega/c)z}\int_0^z d\xi\,\vec{F}(\xi)e^{i(\omega/c)\xi}\right]\right]\right.$$
$$\left.+e^{-i[(\omega/c)z+\omega t]}\left[\hat{E}_\perp(0)+i\frac{\hat{E}'_\perp(0)}{\omega/c}\right]\right\}. \tag{13}$$

In order to further simplify the problem we now make the following assumptions. Firstly, consistent with the amplifier conditions, we neglect in (13) the term proportional to

$$\exp[-i(\omega z/c+\omega t)]$$

which represents a constant amplitude wave propagating in the negative z direction. Namely, we set

$$\hat{E}_\perp(0)+i\frac{\hat{E}'_\perp(0)}{\omega/c}=0\,. \tag{14}$$

Secondly, we assume that the frequency ω of the amplified electromagnetic wave is much larger than any other characteristic frequency of the system, such as the plasma frequency ω_p, the effective undulation frequency ck_0 of the wiggler, or the natural response frequency $c\mu$ of the electrons[7] (see also Sec. III). This assumption is common to many treatments of free-electron lasers, where one is usually interested in frequencies ω of the order of $2\gamma^2k_0c$ with appreciable values of the relativistic factor

$$\gamma=[1-(v/c)^2]^{-1/2}\,.$$

Exploring this disparity in frequencies we assume that

$$\hat{E}(z)=\vec{a}(z)e^{i(\omega/c)z}\,,$$
$$\hat{B}(z)=\vec{b}(z)e^{i(\omega/c)z}\,, \tag{15}$$

with amplitude $\vec{a}$ and $\vec{b}$ varying on the scale much slower than that described by the exponential factors in (15), namely, in orders of magnitude

$$\frac{d\ln a}{dz},\ \frac{d\ln b}{dz}\ll\frac{\omega}{c}\,. \tag{16}$$

Accordingly, one can also write $\hat{V}$ and $\hat{M}$ and therefore $\hat{F}$ in the form

$$\hat{V}(z)=c\vec{v}(z)e^{i(\omega/c)z}\,,$$
$$\hat{M}(z)=n(z)e^{i(\omega/c)z}\,, \tag{17}$$
$$\vec{F}(z)=\vec{f}(z)e^{i(\omega/c)z}=i\frac{\omega}{c}\frac{\vec{V}_{0\perp}}{c}\frac{n(z)}{c^2}e^{i(\omega/c)z}\,,$$

where $\vec{v}$, n, and $\vec{f}$ satisfy inequalities similar to (16). Then, on using (14)–(17) in Eq. (13), one gets

$$\vec{a}_\perp(z)=\vec{a}_\perp(0)-\frac{i}{2\omega/c}\left[\int_0^z d\xi f(\xi)-e^{-2i(\omega/c)z}\int_0^z d\xi\,f(\xi)e^{2i(\omega/c)\xi}\right]. \tag{18}$$

Differentiation of this equation yields

$$\frac{d\vec{a}_\perp}{dz}=e^{-2i(\omega/c)z}\int_0^z d\xi\,\vec{f}(\xi)e^{2i(\omega/c)\xi}\,. \tag{19}$$

Finally the equation for the z component of $\vec{a}$ is obtained from (4):

$$\left[i\frac{\omega}{c}+\frac{d}{dz}\right]a_z=-\frac{n(z)}{c^2}\,. \tag{20}$$

III. LAPLACE TRANSFORMATION OF THE FIELD EQUATIONS

In order to solve the field equations (19) and (20) we have to specify the unperturbed velocity $\vec{V}_0$ of the electrons in the beam. We will use here the results of a recent study[7] of the unperturbed orbits in free-electron lasers with the guide magnetic field. There it was demonstrated that simple helical trajectories, having the same pitch as the wiggler magnetic field and described by

$$\vec{V}_0=-w(\vec{e}_x\cos k_0z+\vec{e}_y\sin k_0z)+u\vec{e}_z\,, \tag{21}$$

are allowed in magnetic field configuration (1). In Eq. (21),

$$u=\text{const}\,,$$
$$w=\frac{u\Omega_\perp/\gamma}{k_0u-\Omega_\parallel/\gamma}=\text{const}\,, \tag{22}$$

where $\Omega_{\perp,\parallel}=e\mathscr{B}_{\perp,\parallel}/mc$. There exists the possibility of several different solutions (22) for u and w (and therefore several different orbits) for a given set of the values of $\Omega_\perp$, $\Omega_\parallel$, k_0, and γ. As an example, Fig. 1 shows the axial velocity u/c versus

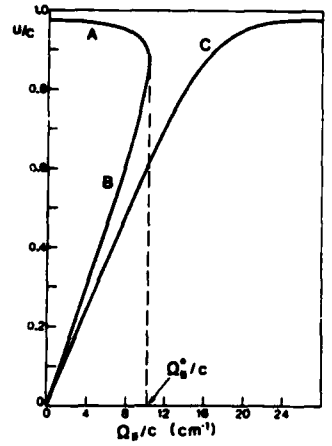

FIG. 1. Steady-state normalized axial velocity u/c vs normalized axial magnetic field $\Omega_{\parallel}/c$.

$\Omega_{\parallel}/c$ for the case $k_0=3$ cm^{-1}, $\gamma=5$, and $\Omega_1/\gamma c=0.3$ cm^{-1}. It can be seen in the figure that for $\Omega_{\parallel}>\Omega_{\parallel}^*$ only one solution (branch c) exists. But when $\Omega_{\parallel}<\Omega_{\parallel}^*$ two additional branches (A and B) are allowed. It was shown in Ref. 7 that only branches A and C are stable, against perturbations, while branch B is unstable and therefore cannot be used in applications.

We now proceed to the solution of Eqs. (19) and (20) for the fields. First, we use a more natural coordinate system in which the components of the magnetic field (1) and of the unperturbed electron velocity (21) are constants. For this purpose let

$$\begin{aligned}\vec{e}_1&=-\vec{e}_x\sin k_0z+\vec{e}_y\cos k_0z\ ,\\ \vec{e}_2&=-\vec{e}_x\cos k_0z-\vec{e}_y\sin k_0z\ ,\\ \vec{e}_3&=\vec{e}_z\ .\end{aligned}\tag{23}$$

Then

$$\vec{\mathscr{B}}(z)=-\mathscr{B}_{\perp 0}\vec{e}_2+\mathscr{B}_{\parallel 0}\vec{e}_3\ ,\tag{24}$$

$$\vec{V}_0(z)=w\vec{e}_2+u\vec{e}_3\ ,\tag{25}$$

and, on writing

$$\vec{a}=a_1\vec{e}_1+a_2\vec{e}_2+a_3\vec{e}_3\ ,$$

Eqs. (19) and (20) become

$$\frac{da_1}{dz}-k_0a_2=e^{-2i(\omega/c)z}\vec{e}_1\cdot\left[\int_0^z\vec{f}(\xi)e^{2i(\omega/c)\xi}d\xi\right],\tag{26}$$

$$\frac{da_2}{dz}+k_0a_1=e^{-2i(\omega/c)z}\vec{e}_2\cdot\left[\int_0^z\vec{f}(\xi)e^{2i(\omega/c)\xi}d\xi\right],\tag{27}$$

$$\left[i\frac{\omega}{c}+\frac{d}{dz}\right]a_3=-\frac{n}{c^2}\ .\tag{28}$$

This system of equations can be solved by means of a Laplace transformation. Namely, if one defines

$$a_{ik}=\int_0^{\infty}dz\,a_i(z)e^{-ikz},\quad n_k=\int_0^{\infty}dz\,n(z)e^{-ikz}\ ,\tag{29}$$

where Imk is negative enough to ensure convergence, then (26)–(28) transforms into

$$ika_{1k}-k_0a_{2k}=a_1(0)+\frac{k_0}{k_0^2-[k+2(\omega/c)]^2}\frac{i\omega wn_k}{c^4}\ ,\tag{30}$$

$$ika_{2k}+k_0a_{1k}=a_2(0)-\frac{[k+2(\omega/c)]}{k_0^2-[k+2(\omega/c)]^2}\frac{\omega wn_k}{c^4}\ ,\tag{31}$$

$$i\left[\frac{\omega}{c}+k\right]a_{3k}=-\frac{n_k}{c^2}\ .\tag{32}$$

According to (15), $kc/\omega, k_0c/\omega\ll 1$, and therefore we can write the field equations in the following approximate form:

$$ika_{1k}-k_0a_{2k}=a_1(0)\ ,\tag{33}$$

$$ika_{2k}+k_0a_{1k}=\frac{1}{2}\frac{wn_k}{c^3}+a_2(0)\ ,\tag{34}$$

$$a_{3k}=i\frac{n_k}{\omega c}\ .\tag{35}$$

Equations (33)–(35) must be supplemented by the equation for the electron density perturbation n_k. This is obtained by taking the Laplace transformation of the linearized continuity equation (6):

$$\begin{aligned}n_k&=-\omega_p^2\frac{\omega+ck}{\omega(u/c-1)+ku}v_{3k}\\ &\simeq-\omega_p^2\frac{\omega}{\omega(u/c-1)+ku}v_{3k}\ .\end{aligned}\tag{36}$$

It is the factor

$$\omega/[\omega(1-u/c)-ku]\gg 1\ ,$$

which makes the bunching in the electron beam density so important and justifies the transition from Eq. (10) to Eq. (11).

IV. MOMENTUM EQUATION

In addition to Eq. (36) for the density one has to use the momentum equation

$$\left[\frac{\partial}{\partial t}+V_z\frac{\partial}{\partial z}\right](\gamma\vec{V})=-\frac{e}{m}\left[\frac{\vec{V}}{c}\times[\vec{\mathcal{B}}(z)+\vec{B}(z,t)]+\vec{E}(z,t)\right] \tag{37}$$

in order to find v_{3k} in (36) and thus completely define the system of Eqs. (33)–(35). The components of (37) in the natural coordinate system (23) are

$$\left[\frac{\partial}{\partial t}+V_3\frac{\partial}{\partial z}\right]V_1=V_2\left[k_0V_3-\frac{\Omega_{||}}{\gamma}\right]-\frac{\Omega_\perp}{\gamma}V_3-V_1\frac{\left[\frac{\partial}{\partial t}+V_3\frac{\partial}{\partial z}\right]\gamma}{\gamma}+\frac{e}{m\gamma}\left[\frac{V_3}{c}B_2-E_1\right], \tag{38}$$

$$\left[\frac{\partial}{\partial t}+V_3\frac{\partial}{\partial z}\right]V_2=-V_1\left[k_0V_3-\frac{\Omega_{||}}{\gamma}\right]-V_2\frac{\left[\frac{\partial}{\partial t}+V_3\frac{\partial}{\partial z}\right]\gamma'}{\gamma}-\frac{e}{m\gamma}\left[\frac{V_3}{c}B_1+E_2\right], \tag{39}$$

$$\left[\frac{\partial}{\partial t}+V_3\frac{\partial}{\partial z}\right]V_3=\frac{\Omega_\perp}{\gamma}V_1-V_3\frac{\left[\frac{\partial}{\partial t}+V_3\frac{\partial}{\partial z}\right]\gamma}{\gamma}-\frac{e}{m\gamma}\left[\frac{V_1}{c}B_2-\frac{V_2}{c}B_1+E_3\right]. \tag{40}$$

Here, energy conservation yields

$$\left[\frac{\partial}{\partial t}+V_3\frac{\partial}{\partial z}\right]\gamma=-\frac{e}{mc^2}(V_1E_1+V_2E_2+V_3E_3)\,. \tag{41}$$

Linearization of (41) gives

$$\Gamma'\equiv\left[i\omega\left[\frac{u}{c}-1\right]+u\frac{d}{dz}\right]\Gamma=-wa_2-ua_3\,, \tag{42}$$

where, similar to (7) and (15), we defined

$$\gamma=\gamma_0+\mathrm{Re}[\Gamma(z)e^{-i[\omega t-(\omega/c)kz]}]\,, \tag{43}$$

where γ_0 is the unperturbed relativistic factor and to orders of magnitude $d(\ln\Gamma)/dz<<\omega/c$. Linearizing Eqs. (38)–(40) and taking the Laplace transformation we get

$$i\Delta v_{1k}=av_{2k}+bv_{3k}+g\frac{\Gamma_k}{\gamma_0}+\frac{1}{\gamma_0}\left[\frac{u}{c}b_{2k}-a_{1k}\right], \tag{44}$$

$$i\Delta v_{2k}=-av_{1k}-i\Delta\frac{w}{c}\frac{\Gamma_k}{\gamma_0}-\frac{1}{\gamma_0}\left[\frac{u}{c}b_{1k}+a_{2k}\right], \tag{45}$$

$$i\Delta v_{3k}=dv_{1k}-i\Delta\frac{u}{c}\frac{\Gamma_k}{\gamma_0}+\frac{1}{\gamma_0}\left[\frac{w}{c}b_{1k}-a_{3k}\right], \tag{46}$$

where

$$\Delta=\frac{\omega}{c}\left[\frac{u}{c}-1\right]+k\frac{u}{c}$$

and

$$a=k_0u/c-\Omega_{||}/c\gamma_0=\Omega_\perp u/c\gamma_0w\,, \tag{47}$$

$$b=k_0w/c-\Omega_\perp/c\gamma_0=\Omega_{||}w/c\gamma_0u\,, \tag{48}$$

$$d=\Omega_\perp/c\gamma_0\,, \tag{49}$$

$$g=wa/c+ub/c\,. \tag{50}$$

In order to eliminate b_{1k} and b_{2k} from (44)–(46) we use Eq. (3), which reduces to

$$b_{1k}=-a_{2k}+\frac{ic}{\omega}[ika_{2k}+k_0a_{1k}-a_2(0)]\,, \tag{51}$$

$$b_{2k}=a_{1k}-\frac{ic}{\omega}[ika_{1k}-k_0a_{2k}-a_1(0)]\,. \tag{52}$$

Further simplification is possible by using (33), (34), and (36):

$$b_{1k}=-a_{2k}+\frac{iw}{2\omega}\frac{n_k}{c^2}=-a_{2k}-i\frac{\omega_p^2}{2c^3}\frac{w}{\Delta}v_{3k}\,, \tag{53}$$

$$b_{2k}=a_{1k}\,. \tag{54}$$

Finally the substitution of (53), (54), and (35) in (44)–(46) gives

$$i\Delta v_{1k}=av_{2k}+bv_{3k}+g\frac{\Gamma_k}{\gamma_0}+\left[\frac{u}{c}-1\right]\frac{a_{1k}}{\gamma_0}\,, \tag{55}$$

$$i\Delta v_{2k}=-av_{1k}-i\Delta\frac{w}{c}\frac{\Gamma_k}{\gamma_0}+\left[\frac{u}{c}-1\right]\frac{a_{2k}}{\gamma_0}+i\frac{\omega_p^2}{2c^4}\frac{uw}{\gamma_0}\frac{1}{\Delta}v_{3k}\,, \tag{56}$$

$$i\Delta v_{3k}=dv_{1k}-i\Delta\frac{u}{c}\frac{\Gamma_k}{\gamma_0}-\frac{w}{c}\frac{a_{2k}}{\gamma_0}+i\frac{\omega_p^2}{c^2\gamma_0}\left[1-\frac{w^2}{2c^2}\right]\frac{1}{\Delta}v_{3k}\,. \tag{57}$$

Equations (55)–(57) for v_{ik} $(i=1,2,3)$ are now easily solved. First, we multiply Eq. (57) by $i\Delta$ and eliminate $i\Delta u_{2k}$ and $i\Delta u_{3k}$ in the resulting equation and finally, on using Eqs. (56) and (57), we find

$$(\mu^2-\Delta^2)v_{1k}=i\Delta\left[\frac{u}{c}-1\right]\frac{a_{1k}}{\gamma_0}-S\frac{a_{2k}}{\gamma_0}+i\frac{\omega_p^2}{c^2\gamma_0}T\frac{v_{3k}}{\Delta}\,, \tag{58}$$

where

$$\mu^2=a^2-bd\,, \tag{59}$$

and

$$S=a-\left[a\frac{u}{c}-b\frac{w}{c}\right]=a-\frac{w\mu^2}{cd}\,,$$

$$T=b+\frac{w}{2c}\left[a\frac{u}{c}-b\frac{w}{c}\right]=b+\frac{w^2\mu^2}{2c^2d}\,. \tag{60}$$

The frequency μ is the natural response frequency to external perturbations.[8] It also defines the stability of the orbits in the absence of the electromagnetic field.[7] In the limit of zero axial field, $\mu=k_0u$, namely, μ is in this case the undulation frequency of the electron beam in the wiggler. The addition of the guide field allows us to parametrically change the value of μ, and, for example, to significantly decrease it. Then, as was demonstrated recently,[8] the response of the system to perturbing electromagnetic waves becomes very strong, with a consequent increase in the gain of the amplifier. This effect of increased response at lower values of μ on stable branches A and C (see Fig. 1) is clearly seen in solution (58) for v_{1k}.

Substitution of v_{1k} from (58) into (57) results in

$$v_{3k}=\frac{iR\Delta}{\Delta^2-\eta^2}\frac{a_{2k}}{\gamma_0}-\frac{d[1-(u/c)]\Delta^2}{(\mu^2-\Delta^2)(\Delta^2-\eta^2)}\frac{a_{1k}}{\gamma_0}\,, \tag{61}$$

where

$$R=\frac{dS}{\mu^2-\Delta^2}+\frac{w}{c}\left[1-\frac{u}{c}\right]\,, \tag{62}$$

and

$$\eta^2=\frac{\omega_p^2}{c^2\gamma_0}\left[\frac{dT}{\mu^2-\Delta^2}+1-\frac{u^2}{c^2}-\frac{w^2}{2c^2}\right]\,. \tag{63}$$

V. DISPERSION RELATION

Substitution of (61) into (34) allows us to write the field equations (33) and (34) in the form

$$\epsilon_{11}a_{1k}+\epsilon_{12}a_{2k}=a_1(0)\,, \tag{64}$$

$$\epsilon_{21}a_{1k}+\epsilon_{22}a_{2k}=a_2(0)\,, \tag{65}$$

where

$$\epsilon_{11}=ik\,, \tag{66}$$

$$\epsilon_{12}=-k_0\,, \tag{67}$$

$$\epsilon_{21}=k_0-\frac{\omega_p^2\omega w}{2c^4\gamma_0}\frac{d[1-(u/c)]\Delta}{(\mu^2-\Delta^2)(\Delta^2-\eta^2)}\,, \tag{68}$$

$$\epsilon_{22}=ik+i\frac{\omega_p^2\omega w}{2c^4\gamma_0}\frac{R}{(\Delta^2-\eta^2)}\,. \tag{69}$$

Note that the resonances of $\Delta^2=\mu^2$ and $\Delta^2=\eta^2$ appear in the present theory very naturally, in contrast to the previous results,[9] where these physical effects were hidden by algebraic complexities of the reduced dielectric tensor.

Solutions of Eqs. (64) and (65) can be written

$$a_{1k}=\frac{a_1(0)\epsilon_{22}-a_2(0)\epsilon_{12}}{D}\,, \tag{70}$$

$$a_{2k}=\frac{a_2(0)\epsilon_{11}-a_1(0)\epsilon_{21}}{D}\,, \tag{71}$$

where

$$D=\epsilon_{11}\epsilon_{22}-\epsilon_{12}\epsilon_{21}$$

$$=-k^2+k_0^2-\frac{\omega_p^2\omega W}{2c^4\gamma_0}\frac{1}{(\Delta^2-\eta^2)}\left[kR+\frac{k_0 d[1-(u/c)]\Delta}{\mu^2-\Delta^2}\right]. \quad (72)$$

In order to find the z dependence of the electric field of the wave we take the inverse Laplace transformation of (70) and (71). As a preparation to this goal (which will be accomplished in Sec. VI) we shall in this section study the dispersion relation

$$D(\omega,k)=0\,, \quad (73)$$

which defines the poles of the right-hand sides of (70) and (71). We restrict ourselves to the case where the term in (72) proportional to ω_p^2 is much less than k_0^2. Then the zeros of (73) can be found by using perturbation analysis. To the lowest order, namely, for $\omega_p^2=0$, there are two roots $k=\pm k_0$. To the next order we seek solutions of the form $k=\pm k_0+x$, with $|x|<<k_0$.

First consider solutions of the form $k=-k_0+x$. Assume also that we are interested in frequencies ω which satisfy

$$\left|\omega\left[\frac{u}{c}-1\right]+k_0 u\right|<<k_0 u \quad (74)$$

or

$$\omega\simeq\frac{k_0 u}{1-u/c}=\left[1+\frac{u}{c}\right]\gamma_z^2 k_0 u=\omega_0\,, \quad (75)$$

that is, in frequencies which are close to the doubly Doppler upshifted frequency ω_0, characteristic of free electron lasers. In this case

$$\Delta=\frac{\omega}{c}\left[\frac{u}{c}-1\right]-k_0\frac{u}{c}+x\frac{u}{c}\simeq-2k_0 u/c\,,$$

and therefore if $\mu^2<4(k_0u/c)^2$ (this condition exists on branch A in Fig. 1, where $\mu<k_0u$ as well as on branch C for $\Omega_{||}/\gamma_0<3k_0u$ then (73) yields

$$x_1=\frac{\omega_p^2}{16c^2\gamma_0}\frac{w\omega}{k_0^2u^2}\left[\frac{d\{S-2[1-(u/c)]k_0(u/c)\}}{\mu^2-4k_0^2u^2/c^2}+\frac{w}{c}\left[1-\frac{u}{c}\right]\right]. \quad (76)$$

The solution is real and no instability exists for this mode. Moreover, the resonance condition $\mu^2=4k_0^2u^2$ in (76) cannot be easily achieved, so that the values of x_1 are usually so small that they hardly affect the vacuum mode at $k=-k_0$.

Now let $k=k_0+x$. Assuming again the existence of (74), we then have

$$\Delta=\beta+xu/c<<k_0u/c\,, \quad (77)$$

where

$$\beta=\frac{\omega}{c}\left[\frac{u}{c}-1\right]+k_0\frac{u}{c} \quad (78)$$

is the mismatch frequency, characterizing the difference between ω and ω_0 [see (75)]. Thus, in this case,

$$D\simeq-2k_0x-\frac{\omega_p^2 w\omega}{2c^4\gamma_0}\frac{k_0R}{\Delta^2-\eta^2}\,, \quad (79)$$

where we neglected the second term in the large parentheses in Eq. (72), which is proportional to Δ. The dispersion relation then becomes

$$(\Delta-\beta)(\Delta^2-\eta^2)+\frac{\omega_p^2}{4\gamma_0}\frac{uw\omega}{c^5}R=0\,. \quad (80)$$

This dispersion relation can be easily analyzed for the case

$$\mu^2>>\Delta^2\,. \quad (81)$$

Only this case will be considered in this paper. Note that the inequality (81) still allows us to use values of μ^2 significantly lower than $(k_0u)^2$ and thus explore the possibility of an enlarged electron response to perturbations.[8] Consistent with (81) we have

$$\eta^2=\frac{\omega_p^2}{c^2\gamma_0}\left[1-\frac{u^2}{c^2}+\frac{bd}{\mu^2}\right]=\frac{\omega_p^2}{c^2\gamma_0}\left[\frac{1}{\gamma_z^2}+\frac{bd}{\mu^2}\right] \quad (82)$$

and

$$R=\frac{ds}{\mu^2}+\frac{w}{c}\left[1-\frac{u}{c}\right]=\frac{w}{u}\left[\frac{1}{\gamma_z^2}+\frac{bd}{\mu^2}\right]. \quad (83)$$

Finally the dispersion relation (80) becomes

$$(\Delta-\beta)(\Delta^2-\eta^2)+\alpha^2\eta^2=0 \quad (84)$$

where

$$\alpha^2=\frac{\omega w^2}{4c^3}\,. \quad (85)$$

Note, that the form of Eq. (84) is exactly the same as the well-known and studied cubic dispersion relation for the case without the guide field. In the latter case $b=\Omega_{\parallel}w/\gamma_0 u=0$ and

$$\eta_0^2=\frac{\omega_p^2}{c^2\gamma_0}\frac{1}{\gamma_z^2}\ . \tag{86}$$

Properties of the roots of (84) in this case are well understood. For example, when $\eta<<k_0<<\omega$, two roots of (84) are complex in the interval[10]

$$-\alpha^2\lesssim\beta\lesssim\left[\frac{27\alpha^2\eta_0^2}{4}\right]^{1/3}\ . \tag{87}$$

At $\beta=0$ the unstable roots of (84) have a maximum imaginary part and the three roots are approximately

$$x_2=-(\alpha^2\eta_0^2)^{1/3},\quad x_{3,4}=(\alpha^2\eta_0^2)^{1/3}\left[\frac{\sqrt{3}}{2}\pm\frac{i}{2}\right]\ . \tag{88}$$

The presence of the guide magnetic field adds several new effects. Here the behavior of the solutions of the dispersion relation depends on the branch of the steady-state orbits (branches A and C in Fig. 1). In order to demonstrate the effect of the guide field we shall make the comparison suggested in Refs. 8 and 9, between two free-electron lasers identical except that one has an axial guide field, while the second does not. In the first laser the pump magnetic field is *reduced* so that

$$\frac{w}{u}=\frac{\Omega_{\perp}/\gamma_0}{k_0u-\Omega_{\parallel}\gamma_0} \tag{89}$$

is the same in both lasers. If without the guide field $w/c=\xi/\gamma_0$ then the latter condition defines the value of the pump field for a given value of the axial field

$$\Omega_{\perp}=\frac{c\xi}{u}(k_0u-\Omega_{\parallel}/\gamma_0)\ . \tag{90}$$

In our comparison the guide field affects only the parameter η^2 in (93). Thus, if $\eta^2>0$, the use of different values of the field is equivalent to the use of different beam densities. This means that for $\eta^2>0$ the general properties of the solutions of (84) for k [(87) and (88), for example] remain the same as in the case without the guide field. This effect is demonstrated in Fig. 2, where the imaginary part of the solution of (84) for k is shown as a function of ω/c for various values of the guide field in a sample case $\gamma_0=5$, $k_0=3\ \mathrm{cm}^{-1}$, $\xi=0.5$, $\omega_p^2/c^2=2\ \mathrm{cm}^{-2}$ (this set of parameters is characteristic to the Naval Research Laboratory VEBA accelerator conditions). It can be seen in the figure that the parametric behavior of Imk on different branches (A or C) is different. On branch A, $bd>0$ (since $\Omega_{\parallel}/\gamma_0<k_0u$) and therefore η^2 on this branch is always larger than η_0^2 [Eq. (86)]. When μ^2 decreases, η^2 increases and so does Imk. A similar effect of an increased response was also found in the single-particle theory.[8] Consistent with (87) the upper frequency bound of the instability remains fixed in Fig. 2 and the lower frequency bound decreases with an increase of η^2. In contrast, on branch C, $bd<0$ ($\Omega_{\parallel}/\gamma_0>k_0u$) and therefore η^2 decreases as $\Omega_{\parallel}/\gamma_0$ approaches k_0u, until η^2 vanishes at $\Omega_{\parallel}/\gamma_0=1.25k_0u$. At this point the coupling between the modes in (84) disappears and so does the instability. In order to understand this effect let us again consider Eq. (57) for v_{3k} which, as we already know, defines the bunching in the electron density, responsible for the free-electron-laser instability. The first three terms in this equation are important to the discussion that follows. The parts of these terms proportional to a_{2k} describe (a) the effect of the ponderomotive force on the electrons due to the pump field, (b) the relativistic effect of the change of v_3 due to the force a_2 in the perpendicular direction, and (c) the ponderomotive force of the electromagnetic wave. It can be checked that these three factors lead to the appearance of the quantity

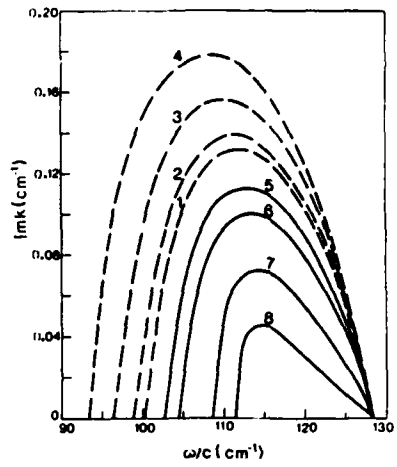

FIG. 2. Spatial growth rates Imk vs normalized frequency ω/c on branch A (dashed lines) and C (solid lines) for various values of $r=\Omega_{\parallel}/k_0u\gamma_0$: Curves 1, $r=0$; 2, $r=0.5$; 3, $r=0.8$; 4, $r=0.9$; 5, $r=2.0$; 6, $r=1.5$; 7, $r=1.3$; 8, $r=1.26$. In these calculations $\gamma_0=5$, $k_0=3\ \mathrm{cm}^{-1}$, $\xi=0.5$, and $\omega_p^2/c^2=2.0\ \mathrm{cm}^{-2}$. Note that in all the cases in the figure $\eta^2>0$.

$1/\gamma_z^2+bd/\mu^2$ in the expression (82) for η^2. On branch C the ponderomotive forces act in opposite directions. This leads to a competition and to the possibility that η^2 vanishes. By simple algebra, we find that this happens when

$$\frac{\Omega_{||0}}{\gamma_0}=k_0u(1+\xi^2) \tag{91}$$

or in our sample case when $\Omega_{||0}/\gamma_0=1.25k_0u$. This is consistent with the results in Fig. 2. At this point $\eta^2=0$ on branch C.

A new and important effect appears if one further decreases $\Omega_{||}/\gamma_0$ on branch C, thus forcing η^2 to become negative. The formulas for the roots of a cubic then indicate that the region of β where (84) has complex roots is now defined by

$$\beta\gtrsim\left[\frac{27\alpha^2\eta^2}{4}\right]^{1/3}, \tag{92}$$

$$\beta\lesssim-\alpha^2, \tag{93}$$

which is the region on the β axis complementary to the interval defined in (87). Thus the possibility of getting negative values of η^2 on branch C allows one to extend the range of the instability to both lower and higher frequencies. This effect for our sample case is demonstrated in Fig. 3, where Imk on branch C is plotted versus ω/c for several values of $\Omega_{||}<\Omega_{||0}$. Note that in both regions (92) and (93) Imk approaches approximately the same value for large enough values of β. This property of the solution can be seen directly from the dispersion relation (84) which at large β is approximately

$$-\beta(\Delta^2-\eta^2)+\alpha^2\eta^2=0\,.$$

The solutions

$$\Delta=\beta+ku=\pm\left[\eta^2\left[1+\frac{\alpha^2}{\beta}\right]\right]^{1/2}$$

become purely imaginary for β large enough when $\eta^2<0$ and Imk approaches $\pm(|\eta^2|)^{1/2}$.

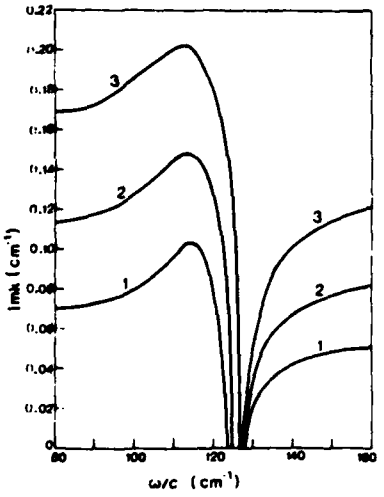

FIG. 3. Spatial growth rates Imk vs ω/c on branch C in the sample case ($\gamma_0=5$, $k_0=3$ cm^{-1}, $\xi=0.5$, $\omega_p^2/c^2=2$ cm^{-2}) in the regime $\Omega_{||}<\Omega_{||0}(\eta^2<0)$. Each curve corresponds to different value of $r=\Omega_{||}/k_0u\gamma_0$: Curves 1, $r=1.2$; 2, 1.15; 3, $r=1.1$.

VI. INVERSION OF LAPLACE TRANSFORMATION

The z dependence of the amplitude of the transverse electric field of the wave in the amplifier can be found on applying the inverse Laplace transformation to Eqs. (70) and (71). We write the resulting expressions in the form

$$a_1(z)=-[a_2(0)+ia_1(0)]A_1(z)+a_1(0)C_1(z)\,, \tag{94}$$

$$a_2(z)=i[a_2(0)+ia_1(0)]A_2(z)+a_2(0)C_2(z)\,, \tag{95}$$

where

$$A_1(z)=\frac{1}{2\pi}\int dk\frac{\epsilon_{12}}{D}e^{ikz}\,,$$
$$A_2(z)=\frac{1}{2\pi}\int dk\frac{\epsilon_{21}}{D}e^{ikz}\,, \tag{96}$$

and

$$C_1(z)=\frac{1}{2\pi}\int dk\frac{\epsilon_{22}+i\epsilon_{12}}{D}e^{ikz}\,,$$
$$C_2(z)=\frac{1}{2\pi}\int dk\frac{\epsilon_{11}-i\epsilon_{21}}{D}e^{ikz}\,, \tag{97}$$

and the integration in (96) and (97) is carried out in the upper half of the complex plane (Im$k>0$) and the path of the integration is taken to be above all possible poles of corresponding integrands. We will concentrate now on evaluation of the integrals A_1, A_2, C_1, and C_2 in terms of the residues of the integrands.

The poles of the integrands in (96) and (97) are defined by the roots of the dispersion relation $D=0$. It was shown in Sec. V that four such roots are of interest. One of these roots $k_1=-k_0+x_1$ is located near the point $-k_0$. The remaining three roots $k_i=k_0+x_i$ ($i=2,3,4$) are all in the

neighborhood of the point k_0, so that they are well separated from k_1. Consider first the residues associated with the roots $k_{2,3,4}$. In this case in the neighborhood of these roots we write $k=k_0+x$, with $|x|<<k_0$ and thus [see (66)–(69), (82), and (85)]

$$\epsilon_{11}=ik_0+ix\ , \tag{98}$$

$$\epsilon_{12}=-k_0\ , \tag{99}$$

$$\epsilon_{21}\simeq k_0\ , \tag{100}$$

$$\epsilon_{22}=ik_0+ix+i\frac{2\alpha^2\eta^2 c}{u(\Delta^2-\eta^2)}\ . \tag{101}$$

Here, we have neglected additional term in ϵ_{21} [see (68)] as we also have done in the derivation of the dispersion relation (84). The determinant D then becomes [see Eq. (84)]:

$$D=-\frac{2k_0c}{u(\Delta^2-\eta^2)}[(\Delta-\beta)(\Delta^2-\eta^2)+\alpha^2\eta^2]$$
$$=-\frac{2k_0c}{u(\Delta^2-\eta^2)}(\Delta-\Delta_2)(\Delta-\Delta_3)(\Delta-\Delta_4)\ , \tag{102}$$

where

$$\Delta_i=\beta+x_iu/c\quad(i=2,3,4)$$

are the roots of the cubic (84). Thus

$$\frac{\epsilon_{12}}{D}=-\frac{\epsilon_{21}}{D}=\frac{u(\Delta^2-\eta^2)}{2c(\Delta-\Delta_2)(\Delta-\Delta_3)(\Delta-\Delta_4)}\ , \tag{103}$$

$$\frac{\epsilon_{22}+i\epsilon_{12}}{D}=-\frac{ixu(\Delta^2-\eta^2)+2i\alpha^2\eta^2c}{2ck_0(\Delta-\Delta_2)(\Delta-\Delta_3)(\Delta-\Delta_4)}\ , \tag{104}$$

$$\frac{\epsilon_{11}-i\epsilon_{21}}{D}=-\frac{ixu(\Delta^2-\eta^2)}{2ck_0(\Delta-\Delta_2)(\Delta-\Delta_3)(\Delta-\Delta_4)}\ . \tag{105}$$

On employing the equality

$$x_iu(\Delta_i^2-\eta^2)=-\alpha^2\eta^2c\ (i=2,3,4)$$

we now find the integrals associated with the modes k_2,k_3,k_4:

$$A_1^{(2,3,4)}(z)=-A_2^{(2,3,4)}(z)$$
$$=-\frac{i}{2}\alpha^2\eta^2c\left[\frac{e^{ix_2z}}{x_2u(\Delta_2-\Delta_3)(\Delta_2-\Delta_4)}+\frac{e^{ix_3z}}{x_3u(\Delta_3-\Delta_2)(\Delta_3-\Delta_4)}+\frac{e^{ix_4z}}{x_4u(\Delta_4-\Delta_2)(\Delta_4-\Delta_3)}\right]e^{ik_0z}\ , \tag{106}$$

$$C_1^{(2,3,4)}(z)=-C_2^{(2,3,4)}(z)=+\frac{\alpha^2\eta^2}{2k_0}\left[\frac{e^{ix_2z}}{(\Delta_2-\Delta_3)(\Delta_2-\Delta_4)}+\frac{e^{ix_3z}}{(\Delta_3-\Delta_2)(\Delta_3-\Delta_4)}+\frac{e^{ix_4z}}{(\Delta_4-\Delta_2)(\Delta_4-\Delta_3)}\right]e^{ik_0z}\ . \tag{107}$$

Since $|x_i|<<k_0$, the contribution the integrals C_1 and C_2 make in Eqs. (94) and (95) can be neglected and therefore the part of the solution for $a_1(z)$ and $a_2(z)$ associated with the modes k_2, k_3, and k_4 can be written

$$a_1^{(2,3,4)}(z)=-ia_2^{(2,3,4)}(z)=-\frac{a_1(0)-ia_2(0)}{2}\alpha^2\eta^2\left[\frac{e^{ix_2z}}{P_2(P_2-P_3)(P_2-P_4)}+\frac{e^{ix_3z}}{P_3(P_3-P_2)(P_3-P_4)}\right.$$
$$\left.+\frac{e^{ix_4z}}{P_4(P_4-P_2)(P_4-P_3)}\right]e^{ik_0z}\ , \tag{108}$$

where $P_i=x_iu/c$.

In order to find the contribution of the remaining mode $k_1=-k_0+x_1$ one can use the initial conditions, rather than find the integrals (96) and (97) directly. Namely, on writing

$$a_1(z)=Q_1e^{-ik_1z}+a_1^{(2,3,4)}(z)\ , \tag{109}$$
$$a_2(z)=Q_2e^{-ik_1z}+a_2^{(2,3,4)}(z)\ ,$$

we find

$$Q_1=a_1(0)-a_1^{(2,3,4)}(0)=a_1(0)+\frac{a_1(0)-ia_2(0)}{2}\alpha^2\eta^2H\ ,$$
$$Q_2=a_2(0)+\frac{a_2(0)+ia_1(0)}{2}\alpha^2\eta^2H\ , \tag{110}$$

where

$$H=\frac{1}{P_2(P_2-P_3)(P_2-P_4)}+\frac{1}{P_3(P_3-P_2)(P_3-P_4)}+\frac{1}{P_4(P_4-P_2)(P_4-P_3)}=\frac{1}{P_2P_3P_4}\ . \tag{111}$$

On the other hand from (102),

$$P_2P_3P_4=(\Delta_2-\beta)(\Delta_3-\beta)(\Delta_4-\beta)=-\alpha^2\eta^2\ , \tag{112}$$

and therefore

$$Q_1=iQ_2=\frac{a_1(0)+ia_2(0)}{2}\ . \tag{113}$$

Thus, finally, the full solutions for the amplitudes are

$$a_1(z)=-ia_2(z)=\tfrac{1}{2}[a_1(0)+ia_2(0)]e^{-i(k_0-x_1)z}$$
$$-\tfrac{1}{2}[a_1(0)-ia_2(0)]\alpha^2\eta^2\left[\frac{e^{ix_2z}}{P_2(P_2-P_3)(P_2-P_4)}+\frac{e^{ix_2z}}{P_3(P_3-P_2)(P_3-P_4)}\right.$$
$$\left.+\frac{e^{ix_3z}}{P_4(P_4-P_2)(P_4-P_3)}\right]e^{ik_0z}\ . \tag{114}$$

Assume now that initially

$$a_1(0)+ia_2(0)=0\ , \tag{115}$$

namely, no electromagnetic energy is stored in the k_1 mode. Then, on using (111) and (112) we write (114) as

$$a_1(z)=-ia_2(z)=a_1(0)\left[1+\alpha^2\eta^2\left[\frac{1-e^{ix_2z}}{P_2(P_2-P_3)(P_2-P_4)}+\frac{1-e^{ix_3z}}{P_3(P_3-P_2)(P_3-P_4)}\right.\right.$$
$$\left.\left.+\frac{1-e^{ix_4z}}{P_4(P_4-P_2)(P_4-P_3)}\right]\right]e^{ik_0z}\ . \tag{116}$$

In several limiting cases this expression can be simplified and reduced to already familiar results.

(a) In the first example let $|x_iz|<<1$. In this case we expand the exponentials in (116) in powers of x_iz, by using

$$\frac{P_2^n}{(P_2-P_3)(P_2-P_4)}+\frac{P_3^n}{(P_3-P_2)(P_3-P_4)}+\frac{P_4^n}{(P_4-P_2)(P_4-P_3)}=\begin{cases}0, & n=0\\ 0, & n=1\\ 1, & n=2\end{cases} \tag{117}$$

we obtain the approximation

$$a_1(z)=-ia_2(z)=a_1(0)\left[1+i\frac{c^3\alpha^2\eta^2z^3}{6u^3}\right]e^{ik_0z}\ . \tag{118}$$

A similar result was obtained in Ref. 10 for the case without the guide field. In contrast to Ref. 10, however, we did not assume conditions of maximum spatial growth in the deriviation of (118).

(b) In the second example we consider the case when one of the roots of (84), say root Δ_2, is close to β (namely, $|\Delta_2-\beta|<<|\beta|$) and the two remaining roots satisfy $|\Delta_3|, |\Delta_4|<<\beta$. These conditions are

fulfilled when

$$\frac{\beta^2}{|\eta^2|} >> \max\left[1, \left|\frac{\alpha^2}{\beta}\right|\right] \tag{119}$$

and then

$$P_2 = x_2 u/c = \Delta_2 - \beta = -\frac{\alpha^2\eta^2}{\beta^2}\ , \tag{120}$$

$$P_{3,4} = x_{3,4} u/c = \Delta_{3,4} - \beta = -\beta \pm \left[\eta^2\left[1+\frac{\alpha^2}{\beta}\right]\right]^{1/2}\ . \tag{121}$$

Thus, in (116),

$$P_2(P_2-P_3)(P_2-P_4) \simeq -\alpha^2\eta^2\ , \tag{122}$$

$$P_3(P_3-P_2)(P_3-P_4) \simeq 2\beta^2\Delta_3\ , \tag{123}$$

$$P_4(P_4-P_2)(P_4-P_3) \simeq -2\beta^2\Delta_3\ . \tag{124}$$

Thus, for $|\beta z| \gtrsim 1$, we rewrite Eq. (116) in the approximate form

$$a_1(z) = -ia_2(z) \simeq a_1(0)\left[1+i\frac{\alpha^2\eta^2}{\beta^2\Delta_3}\sin\frac{c\Delta_3 z}{u_3}e^{-ic\beta z/u}\right]e^{ik_0 z}$$

$$\simeq a_1(0)\left[1+i\frac{c\alpha^2\eta^2 z}{\beta^2 u}e^{-ic\beta z/u}\right]e^{ik_0 z}\ . \tag{125}$$

Therefore, on defining the power gain as

$$G(z) = \frac{|a_1(z)|^2+|a_2(z)|^2}{|a_1(0)|^2+|a_2(0)|^2} - 1 = \frac{a_1(z)a_1^*(z)}{a_1(0)a_1^*(0)} - 1 \tag{126}$$

we find from (125) that

$$G(z) \simeq 2\frac{c\alpha^2\eta^2 z}{\beta^2 u}\sin(c\beta z/u) = 2\frac{c^3\alpha^2\eta^2}{u^3}z^3\frac{\sin(c\beta z/u)}{(c\beta z/u)^2}\ . \tag{127}$$

The same formula for the gain was derived in the single particle, small gain theory.[8] Thus the single-particle theory corresponds to the region in parameter space defined by inequality (119), which was used in reducing Eq. (127).

We finally present a numerical example of the application of Eq. (116) in our sample case. Figure 4 shows the frequency dependence of the power gain at 25 wiggler periods for three values of $r = \Omega_{||}/k_0 u\gamma_0 = 0.8$ (branch A), 1.1 and 2.0 (branch C). It follows from (91) that for $r = 0.8$ and 2, $\eta^2 > 0$, while for $r = 1.1$, $\eta^2 < 0$. It can be seen in the figure that the frequency dependence of G for positive and negative values of η^2 is completely different which reflects different type of dependence of $\mathrm{Im}k$ on ω (see Figs. 2 and 3). If for $\eta^2 > 0$ we see a relatively narrow frequency range for significant gain, then for $\eta^2 < 0$ this range is greatly extended. In Fig. 5 we present the z dependence of the gain in the amplifier on branch C in our sample case. The values of $r = \Omega_{||}/k_0 u\gamma_0 = 1.1$ at $\omega/c = 145\ \mathrm{cm}^{-1}$ (curve 1 in the figure) and $r = 2.0$ at $\omega/c = 105$, 112, and 125 cm^{-1} (curves 2a, 2b, and 2c) were again used in the calculations. The oscillations in G at short distances are due to the spatial interference of the modes in the amplifier. It is seen that only at relatively large distances does the spatial instability take over and the growth of the gain becomes exponential.

VII. CONCLUSIONS

We have the following conclusions.

(1) The free-electron-laser amplifier with a guide magnetic field was analyzed, using the cold fluid description of the electron beam.

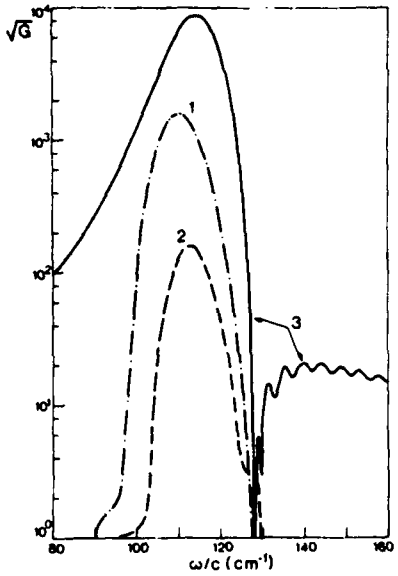

FIG. 4. Frequency dependence of the power gain in the amplifier at the distance of 25 wiggler periods in the sample case. Different curves correspond to different values $r=\Omega_{||}/k_0 u\gamma_0$: Curves 1, $r=0.8$ (branch A); 2, $r=2.0$ (branch C, $\eta^2>0$); 3, $r=1.1$ (branch C, $\eta^2<0$).

(2) It was shown that in a large region of parameters space, similar to the case without the guide field, the amplified electromagnetic wave splits into four modes propagating in the direction of the electron beam. Three of the modes are coupled and one of them may be spatially unstable. The competition between these three modes defines various regimes of operation of the amplifier.

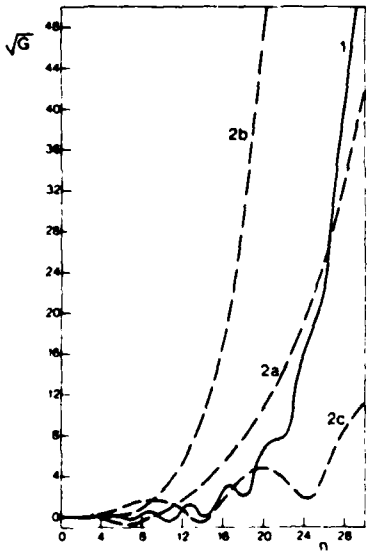

FIG. 5. Power gain in the amplifier vs the length of the interaction region measured in numbers of wiggler periods for the parameters of the sample case: Curves 1, $\Omega_{||}/\gamma_0=1\ 1k_0u$, $\omega/c=145\ \text{cm}^{-1}$; 2, $\Omega_{||}/\gamma_0=2k_0u$, a, $\omega/c=105\ \text{cm}^{-1}$, b, $\omega/c=112\ \text{cm}^{-1}$, c, $\omega/c=125\ \text{cm}^{-1}$.

(3) A simple dispersion relation for the coupled modes was derived and analyzed. The form of the dispersion relation is similar to the well-known cubic dispersion relation for the case without the guide field, which makes the mode stability analysis easier.

(4) The mode analysis gives the basis for the construction of the actual electromagnetic fields along the interaction region in the amplifier. Various limiting cases were considered and agreed with the results of existing theories. The power gain versus the length of the interaction region was found numerically in a sample case. The calculations demonstrated the effect of spatial interference of the modes at shorter interaction lengths and transition to exponentially growing gain at distances when the spatial instability becomes important.

(5) The main effects due to the presence of the guide field can be summarized as follows:

(i) Two types of helical orbits of the electrons can be used in the amplifier with the guide field (branches A and C in Fig. 1) for given values of γ_0, k_0, and $\Omega_\perp$.

(ii) On branch A the response of the electrons to electromagnetic perturbation and therefore also the spatial instability can be enhanced if the natural response frequency (see Sec. IV) of the electrons becomes small. This effect is equivalent to the increase of the density of the electron beam.

(iii) On branch C there exists an axial field $\Omega_{||0}$ [see Eq. (91)] for which the coupling between the modes disappears as well as the spatial instability. This effect is the result of the competition between the ponderomotive forces on the electron due to the pump and electromagnetic waves. For $\Omega_{||}>\Omega_{||0}$ the parametric behavior of the modes is similar to that on branch A. If $\Omega_{||}<\Omega_{||0}$, however, the frequency range of the instability extends significantly to both lower and higher frequencies in contrast to branch A (and branch C for $\Omega_{||}>\Omega_{||0}$) where this range is relatively small and usually has an upper limit close to $\omega_0=2k_0\gamma_0^2 c$.

(iv) The effects described in (i)–(iii) can be achieved for given helical orbits in the presence of the guide field at much lower values of the pump field.

ACKNOWLEDGMENTS

The authors would like to thank Professor F. Dothan and Dr. H. Mitchell for their helpful comments and suggestions in the preparation of this paper. This research was supported in part by the U. S. Office of Naval Research, and by the U. S.-Israel Binational Science Foundation.

---

*Also at Yale University, New Haven, Connecticut 06520.

[1]For a review of past works see P. Sprangle, R. A. Smith, and V. L. Granatstein, in *Infrared and Millimeter Waves*, edited by K. Button (Academic, New York, 1979), Vol. 1.

[2]L. R. Elias, W. M. Fairbank, J. M. J. Madey, H. A. Schwettman, and T. I. Smith, Phys. Rev. Lett. 36, 717 (1976).

[3]D. A. G. Deacon, L. R. Elias, J. M. J. Madey, G. J. Ramian, H. A. Schwettman, and T. I. Smith, Phys. Rev. Lett. 38, 892 (1977).

[4]V. L. Granatstein, S. P. Schlesinger, M. Herndon, R. K. Parker, and J. A. Pasour, Appl. Phys. Lett. 30, 384 (1977).

[5]D. B. McDermott, T. C. Marshall, S. P. Schlesinger, R. K. Parker, and V. L. Granatstein, Phys. Rev. Lett. 41, 1368 (1978).

[6]R. M. Gilgenbach, T. C. Marshall, and S. P. Schlesinger, Phys. Fluids 22, 971 (1978).

[7]L. Friedland, Phys. Fluids 23, 2376 (1980).

[8]L. Friedland and J. L. Hirshfield, Phys. Rev. Lett. 44, 1456 (1980).

[9]I. B. Bernstein and L. Friedland, Phys. Rev. A 23, 816 (1981).

[10]I. B. Bernstein and J. L. Hirshfield, Phys. Rev. A 20, 1661 (1979).

PHYSICAL REVIEW A VOLUME 26, NUMBER 5 NOVEMBER 1982

Nonlinear theory of the free-electron laser with an axial magnetic field

Lazar Friedland and Ira B. Bernstein
Department of Applied Physics, Yale University, New Haven, Connecticut 06520
(Received 17 December 1981)

A nonlinear, one-dimensional formulation of the free-electron laser with an axial magnetic field is presented. The problem is formulated in the cold-fluid approximation for the electron beam, and is reduced to a system of the first-order, nonlinear, coupled, ordinary differential equations. Nonlinear effects due to the departure of the electrons in the beam from the conventional helical orbits are considered and illustrated in numerical examples. The formalism also allows the study of the initial phase of saturation in the laser. In the presence of the axial magnetic field the saturation is shown to be mainly due to the development of undesirable large radial excursion of the electron trajectories.

I. INTRODUCTION

Free-electron lasers operating in the Raman regime are believed to be promising sources of intense submillimeter coherent radiation. This prediction was tested in experiments at the Navy Research Laboratory (NRL) and Columbia University,[1-4] and recently with improved electron beam quality at NRL.[5,6] The Raman free-electron lasers operate with relatively low electron energies (relativistic $\gamma < 10$) and high beam currents ($I > 1$ kA). These experimental conditions, especially the high beam currents, necessarily require the presence of an axial guide magnetic field, in addition to the magnetic wiggler, conventionally used in free-electron laser experiments. As was demonstrated in recent theoretical studies by Friedland *et al.*,[7-10] the simple addition of the guide field results in many nontrivial consequences. For example, in the presence of the guide field electron trajectories may become very complex, and, only for certain combinations of injection conditions on the electron beam, the electrons will move on simple helical orbits.[7] Moreover, even on the helical orbits, in combined guide and wiggler magnetic fields, the beam response to perturbations is characterized by an additional response frequency, which may be varied without changing the helical orbit itself. It was shown in the single-particle theory of the laser[8] that the resonance between this natural response frequency and the frequency of a driving electromagnetic wave can be exploited to provide higher gain in the system. These predictions were confirmed by the self-consistent collective theories[9,10] which also demonstrated the presence of additional effects. For example, under certain conditions, the frequency range of the free-electron laser instability may be substantially extended to both lower and higher frequencies. The effect was explained in Ref. 10 by the presence of an unstable beam mode in the system.

All this complex behavior, induced by the presence of the guide field in the system, has been studied in Refs. 7-10 on the basis of linearized theories. The linearization procedure itself was based on two assumptions. First of all it was assumed that the perturbing electromagnetic fields were so weak that all the induced nonlinear effects were small and could be neglected. Second, the assumption was made that the unperturbed electron beam propagated on one of the helical orbits [branches A or C (Refs. 8-10)] and the linearized perturbation analysis was performed around these steady-state trajectories. Both these assumptions impose serious limitations on the theory. Indeed, the linear theories predicted the possibility of very high gains, so that the nonlinear electromagnetic effect might become important and lead to saturation after the radiation traversed a relatively short distance. Moreover, as was already mentioned, the helical orbits, in the presence of the guide magnetic field, are exceptions rather than the rule. In case of a departure of the beam from the helical orbits, the electron dynamics becomes intrinsically nonlinear, which may play an important role in realistic systems even when the radiation fields are weak.

In this paper we present a nonlinear theory of the free-electron laser with the guide field and consider both aforementioned nonlinear effects. A nonlinear theory for the laser without the guide field was

given by Sprangle *et al.*[11,12] Their approach was primarily designed to study saturation effects due to particle trapping in the ponderomotive potential of the wave and the wiggler field. The trapping occurs on a scale length comparable to the wavelength of the electromagnetic wave. The number of test particles, separated initially by distances short compared to the period of the wave, were necessary to model the saturation effects. Here we present a more simple approach based on the cold-fluid model of the electron beam. The method requires one to follow only one test particle along the laser. Although the trapping effect, in principle, cannot be described by our formalism, its use is very convenient in describing all the effects occurring on the scale length long compared to the wavelength. We will show that in the presence of the guide field, both the departure from the helical orbits and the initial saturation phase belong to this class of slowly varying effects, and thus can be treated within the cold-fluid approximation.

The scope of the paper is as follows. In Sec. II we derive a reduced system of equations for the amplitude of the radiation field. In Sec. III we consider the momentum equation defining the sources in the field equations. A complete set of first-order, coupled, nonlinear ordinary differential equations governing our system will be presented at the end of Sec. III. This set of equations, in Sec. IV, will form a basis for the discussion of possible nonlinear effects in the system, which will be illustrated by numerical examples.

II. FIELD EQUATIONS

Consider a one-dimensional model of a free-electron laser, where the electromagnetic field is described by the Maxwell equations

$$c\vec{e}_z\times\frac{\partial\vec{B}_\perp}{\partial z}=\frac{\partial\vec{E}_\perp}{\partial t}-4\pi e(N\vec{V}_\perp-\langle N\vec{V}_\perp\rangle_{av}) , \tag{1}$$

$$-c\vec{e}_z\times\frac{\partial\vec{E}_\perp}{\partial z}=\frac{\partial\vec{B}_\perp}{\partial t} , \tag{2}$$

$$\frac{\partial E_z}{\partial t}=4\pi e(NV_z-\langle NV_z\rangle_{av}) , \tag{3}$$

$$\frac{\partial E_z}{\partial t}=0 , \tag{4}$$

$$\frac{\partial E_z}{\partial z}=-4\pi e(N-\langle N\rangle_{av}) , \tag{5}$$

$$\frac{\partial B_z}{\partial z}=0 . \tag{6}$$

Here the electron beam propagates in the z direction and is described in the cold-fluid approximation. The electron beam density N and velocity $\vec{V}$, and the electromagnetic fields $\vec{E}$ and $\vec{B}$, in Eqs. (1)–(6) are assumed to depend only on z and time, and the subscript $\perp$ describes directions perpendicular to the z axis. Moreover, we are interested in solutions of (1)–(6) periodic in time with period $2\pi/\omega$ and consequently subtract off the time-averaged parts

$$\langle N\vec{V}\rangle_{av}=\frac{\omega}{2\pi}\int_0^{2\pi/\omega}N\vec{V}\,dt ,$$
$$\langle N\rangle_{av}=\frac{\omega}{2\pi}\int_0^{2\pi/\omega}N\,dt , \tag{7}$$

of the sources in Eqs. (1), (3), and (5).

The periodicity condition allows one to expand the electromagnetic fields in the Fourier series

$$\vec{E}(z,t)=\frac{1}{2}\sum_{\substack{n=-\infty\\ n\neq 0}}^{+\infty}\vec{E}_n(z)e^{-in\omega t}$$
$$=\sum_{n=1}^{\infty}\mathrm{Re}[\vec{E}_n(z)e^{-in\omega t}] ,$$
$$\vec{B}(z,t)=\sum_{n=1}^{\infty}\mathrm{Re}[\vec{B}_n(z)e^{-in\omega t}] . \tag{8}$$

We assume now that only the $n=1$ component in (8) is excited, which is the usual case in free-electron lasers operating in the linear regime. The coupling to higher harmonics is a second-order nonlinear effect, as can be seen from Eqs. (1) and (3), and we will neglect this effect in the present work. Thus we write

$$\vec{E}(z,t)=\mathrm{Re}[\vec{E}_1(z)e^{-i\omega t}] ,$$
$$\vec{B}(z,t)=\mathrm{Re}[\vec{B}_1(z)e^{-i\omega t}] , \tag{9}$$

and accordingly

$$N(z,t)=N_0(z)+\mathrm{Re}[N_1(z)e^{-i\omega t}] ,$$
$$\vec{V}(z,t)=\vec{V}_0(z)+\mathrm{Re}[\vec{V}_1(z)e^{-i\omega t}] . \tag{10}$$

We also assume here that ω is much larger than various characteristic frequencies of the electron beam (such as the plasma frequency ω_p, the undulation frequency, the natural response frequency,[8] etc.). Then we can separate "fast" spatial oscillations in (9) and (10) from the slow ones which are imposed by the presence of the electron beam. Namely, we write

$$\vec{E}_1(z)=\frac{mc^2}{e}\vec{a}(z)e^{i(\omega/c)z},$$
$$\vec{B}_1(z)=\frac{mc^2}{e}\vec{b}(z)e^{i(\omega/c)z},$$
$$N_1(z)=\frac{m}{4\pi e^2}\nu^2(z)e^{i(\omega/c)z}, \tag{11}$$
$$\vec{V}_1(z)=\vec{v}(z)e^{i(\omega/c)z},$$

where in order of magnitude for $X=a,b,\nu^2,v$,

$$\left|\frac{d\ln X}{dz}\right|\ll\frac{\omega}{c}. \tag{12}$$

Note that at this point we have excluded from the analysis all waves with wave vectors in the direction opposite to the direction of propagation of the electron beam. These backward waves can only arise from noise and their amplitudes are assumed to be negligible in comparison with the main amplified signal which propagates in the direction of the beam. Although in some cases the backward waves are absolutely unstable[13] they are characterized in such cases by long wavelengths and therefore can be easily suppressed by appropriate construction of the amplifier cavity.[13]

We now proceed to the derivation of the approximate equations, describing the slowly varying amplitudes of the electromagnetic fields. First, we combine (1) and (2) to give the wave equation

$$\frac{\partial^2\vec{E}_\perp}{\partial z^2}-\frac{1}{c^2}\frac{\partial^2\vec{E}_\perp}{\partial t^2}=-\frac{4\pi e}{c^2}\frac{\partial}{\partial t}(N\vec{V}_\perp). \tag{13}$$

Substituting (9) and (10) into (13), applying definitions (11), and neglecting the higher-frequency harmonics, we get

$$\frac{d^2\vec{a}_\perp}{dz^2}+2i\frac{\omega}{c}\frac{d\vec{a}_\perp}{dz}=i\frac{\omega}{c^4}(\omega_p^2\vec{v}_\perp+\vec{V}_{0\perp}\nu^2). \tag{14}$$

Finally, exploiting the assumption of the weakness of the z dependence of $d\vec{a}_\perp/dz$, we neglect the second-order derivative in Eq. (14) and rewrite it in the approximate form

$$\frac{d\vec{a}_\perp}{dz}=\frac{1}{2c^3}(\omega_p^2\vec{v}_\perp+\vec{V}_{0\perp}\nu^2). \tag{15}$$

In the notation of (11), Eq. (5) becomes

$$\frac{da_z}{dz}+i\frac{\omega}{c}a_z=-\frac{\nu^2}{c^2} \tag{16}$$

and (3) can be written as

$$-i\frac{\omega}{c}a_z-\frac{1}{c^3}(\omega_p^2v_z+V_{0z}\nu^2)=0. \tag{17}$$

On expressing ν^2 via (17), and substituting it into (16) we have

$$\left[-i\frac{\omega}{c}\left(1-\frac{V_{0z}}{c}\right)+\frac{V_{0z}}{c}\frac{d}{dz}\right]a_z=\frac{\omega_p^2}{c^2}\frac{v_z}{c}. \tag{18}$$

Note that in (18)

$$\frac{\omega}{c}\left(1-\frac{V_{0z}}{c}\right)\simeq\frac{\omega}{c}\frac{1}{2\gamma_z^2},$$

where γ_z is the relativistic factor associated with the axial velocity of the electron beam. Therefore for $\omega/c\simeq 2\gamma_z^2k_0$, which is characteristic of free-electron lasers with a pitch $\lambda=2\pi/k_0$, we have

$$\frac{\omega}{c}\left(1-\frac{V_{0z}}{c}\right)\simeq k_0$$

and thus (18) indeed describes variation of $a_z(z)$ on a scale long compared with the fast oscillations of the electromagnetic field.

Equation (17) can be also used to eliminate ν^2 from Eq. (15), which then becomes

$$\frac{d\vec{a}_\perp}{dz}=\frac{1}{2c^3}\left[\omega_p^2\vec{v}_\perp-\frac{\vec{V}_{0\perp}}{V_{0z}}(\omega_p^2v_z+i\omega c^2a_z)\right]. \tag{19}$$

The form of the operator in the square brackets in Eq. (18) suggests the use of an independent variable other than z, namely, we introduce variable τ via

$$\frac{dz}{d\tau}=V_{0z}(z). \tag{20}$$

Then for any quantity of the form

$$\tilde{X}(z,\tau)=X(z)e^{i(\omega/c)(z-c\tau)} \tag{21}$$

we have

$$\frac{1}{c}\frac{d\tilde{X}}{d\tau}=\frac{1}{c}\left[\frac{\partial}{\partial\tau}+V_{0z}\frac{\partial}{\partial z}\right]\tilde{X}$$
$$=e^{i(\omega/c)(z-c\tau)}\left[-i\frac{\omega}{c}\left(1-\frac{V_{0z}}{c}\right)+\frac{V_{0z}}{c}\frac{d}{dz}\right]X. \tag{22}$$

Therefore (18) can be rewritten as

$$\frac{1}{c}\frac{d\tilde{a}_z}{d\tau}=\frac{\omega_p^2}{c^3}\tilde{v}_z. \tag{23}$$

In addition to simplifying the notation, τ has an im-

portant physical interpretation: It measures the time along the trajectory were the electron to move with velocity $V_{0z}(z)$. As we will show in the next section, convective derivatives similar to $d/d\tau$ in Eq. (23) appear naturally in the momentum equation for the electron beam. Thus, in the following we will adopt τ as the independent variable in the problem. Consistent with this approach we also rewrite Eq. (19) in the form

$$\frac{1}{c}\frac{d\tilde{\vec{a}}_\perp}{d\tau}=-i\frac{\omega}{c}\left[1-\frac{V_{0z}}{c}\right]\tilde{\vec{a}}_\perp + \frac{1}{2c^4}[\omega_p^2 V_{0z}\tilde{\vec{v}}_\perp-\vec{V}_{0\perp}(\omega_p^2\tilde{v}_z+i\omega c^2\tilde{a}_z)] . \tag{24}$$

Equations (23) and (24) are the desired equations for the electromagnetic field.

III. MOMENTUM EQUATION

Consider the momentum equation describing the electron beam

$$\left[\frac{\partial}{\partial t}+V_z\frac{\partial}{\partial z}\right](\gamma\vec{V})=-\frac{e}{m}\left[\vec{E}+\frac{\vec{V}}{c}\times(\vec{B}+\vec{\mathscr{B}})\right], \tag{25}$$

where the static magnetic field is given by

$$\vec{\mathscr{B}}(z)=-\hat{e}_\perp(z)\mathscr{B}_\perp+\hat{e}_z\mathscr{B}_z \tag{26}$$

with the vector

$$\hat{e}_\perp(z)=-(\hat{e}_x\cos k_0 z+\hat{e}_y\sin k_0 z) \tag{27}$$

representing the direction of the helical field on the axis of a magnetic wiggler commonly used in theories of free-electron lasers. Substituting (9) and (10) into (25), using definitions (11), and retaining only the first-time harmonic in the resulting equation, we have

$$\gamma_0\dot{\vec{v}}+\vec{V}_0\dot{g}+v_z\frac{d}{dz}(\gamma_0\vec{V}_0)+V_{0z}\left[g\frac{d\vec{V}_0}{dz}+\vec{v}\frac{d\gamma_0}{dz}\right]+\frac{i}{2}\frac{\omega}{c}v_z^*\vec{v}g=-c^2\left[\vec{a}+\frac{\vec{V}_0}{c}\times\vec{b}\right]-\vec{v}\times\vec{\Omega} . \tag{28}$$

Here we defined $\Omega=e\vec{\mathscr{B}}/mc$,

$$\gamma=\gamma_0+\mathrm{Re}[g(z)e^{i(\omega/c)(z-ct)}] \tag{29}$$

and $(\cdots)^{\cdot}=[-i\omega(1-V_{0z}/c)+V_{0z}d/dz](\cdots)$. In the last term on the left-hand side of Eq. (28), which is the only nonlinear term of the third order, in view of (12), we have neglected $d\vec{v}/dz$ and dg/dz compared with $i(\omega/c)\vec{v}$ and $i(\omega/c)g$, respectively. An equation for the quantity $\dot{g}$ in (28) is obtained from the energy balance

$$mc^2\left[\frac{\partial}{\partial t}+V_z\frac{\partial}{\partial z}\right]\gamma=-e\vec{V}\cdot\vec{E} \tag{30}$$

which yields

$$\dot{g}=-v_z\frac{d\gamma_0}{dz}-\vec{V}_0\cdot\vec{a} . \tag{31}$$

Also, it follows from (2), that

$$\vec{b}_\perp=-i\frac{c}{\omega}\hat{e}_z\times\left[i\frac{\omega}{c}\vec{a}_\perp+\frac{d\vec{a}_\perp}{dz}\right] . \tag{32}$$

Then in (28)

$$\left[\vec{a}+\frac{\vec{V}_0}{c}\times\vec{b}\right]=\frac{ic}{\omega}\dot{\vec{a}}_\perp+\hat{e}_z\left[\frac{\vec{V}_{0\perp}}{c}\cdot\left[\vec{a}_\perp-i\frac{c}{\omega}\frac{d\vec{a}_\perp}{dz}\right]+a_z\right]\simeq\frac{ic}{\omega}\dot{\vec{a}}_\perp+\hat{e}_z\left[\frac{\vec{V}_{0\perp}}{c}\cdot\vec{a}_\perp+a_z\right] . \tag{33}$$

The appearance of the dotted quantities in Eqs. (28), (31), and (33) suggests that one change from the variable z in these equations to the time τ along the steady (time-independent) component of the electron motion in the z direction [see the definition in Eq. (20)]. Then, on using notation (21), observing that $\dot{\tilde{X}}\exp[i(\omega/c)(z-ct)]=d\tilde{X}/d\tau$ and $V_{0z}dX/dz=dX/d\tau$, and substituting (33) into (28) we get

$$\gamma_0\frac{d\vec{v}'}{d\tau}=-\vec{V}_0\frac{dg}{d\tau}-\vec{v}'\times\vec{\Omega}-\frac{ic^3}{\omega}\frac{d\tilde{\vec{a}}_\perp}{d\tau}-c^2\hat{e}_z\left[\frac{\vec{V}_{01}}{c}\cdot\tilde{\vec{a}}+\tilde{a}_z\right]$$

$$-\frac{\tilde{v}_z}{V_{0z}}\frac{d}{d\tau}(\gamma_0\vec{V}_0)-\tilde{g}\frac{d\vec{V}_0}{d\tau}-\vec{v}'\frac{d\gamma_0}{d\tau}+\frac{i\omega}{2c}\tilde{v}_z^*\vec{v}'\tilde{g}\,, \tag{34}$$

where $\vec{v}'$ has components $\tilde{v}_x$, $\tilde{v}_y$, and $\tilde{v}_z$, etc., and where according to (31)

$$\frac{d\tilde{g}}{d\tau}=-\frac{\tilde{v}_z}{V_{0z}}\frac{d\gamma_0}{d\tau}-\vec{V}_0\cdot\tilde{\vec{a}}\,. \tag{35}$$

Because of the form of the helical part of the magnetostatic field $\vec{\mathcal{B}}$ it is convenient in the following to introduce a rotating coordinate system defined by the base vectors

$$\hat{e}_1=-\hat{e}_x\sin k_0z+\hat{e}_y\cos k_0z,\quad \hat{e}_2=\hat{e}_\perp\,,$$

$$\hat{e}_3=\hat{e}_z\,. \tag{36}$$

Then, finally, components in Eqs. (23), (24), (34), and (35) become

$$\frac{d\tilde{a}_1}{d\tau}=k_0V_{03}\tilde{a}_2-i\omega\left[1-\frac{V_{03}}{c}\right]\tilde{a}_1+\frac{1}{2c^3}[\omega_p^2V_{03}\tilde{\gamma}_1-V_{01}(\omega_p^2\tilde{v}_3+i\omega c^2\tilde{a}_3)]\,, \tag{37}$$

$$\frac{d\tilde{a}_2}{d\tau}=-k_0V_{03}\tilde{a}_1-i\omega\left[1-\frac{V_{03}}{c}\right]\tilde{a}_2+\frac{1}{2c^3}[\omega_p^2V_{02}\tilde{v}_2-V_{02}(\omega_p^2\tilde{v}_3+i\omega c^2\tilde{a}_3)]\,, \tag{38}$$

$$\frac{d\tilde{a}_3}{d\tau}=\frac{\omega_p^2}{c^2}\tilde{v}_3\,, \tag{39}$$

$$\gamma_0\frac{d\tilde{v}_1}{d\tau}=\gamma_0k_0V_{03}\tilde{v}_2-V_{01}\frac{d\tilde{g}}{d\tau}-\Omega_\perp\tilde{v}_3-\Omega_{||}\tilde{v}_2-\frac{ic^3}{\omega}\left[\frac{d\tilde{a}_1}{d\tau}-k_0V_{03}\tilde{a}_2\right]-\frac{\tilde{v}_3}{V_{03}}\left[\frac{d}{d\tau}(\gamma_0V_{01})-\gamma_0k_0V_{02}V_{03}\right]$$

$$-\tilde{g}\left[\frac{dV_{01}}{d\tau}-k_0V_{02}V_{03}\right]-\tilde{v}_1\frac{d\gamma_0}{d\tau}+\frac{i\omega}{2c}\tilde{v}_3^*\tilde{v}_1\tilde{g}\,, \tag{40}$$

$$\gamma_0\frac{d\tilde{v}_2}{d\tau}=-\gamma_0k_0V_{03}\tilde{v}_1-V_{02}\frac{d\tilde{g}}{d\tau}+\Omega_{||}\tilde{v}_1-\frac{ic^3}{\omega}\left[\frac{d\tilde{a}_2}{d\tau}+k_0V_{03}\tilde{a}_1\right]-\frac{\tilde{v}_3}{V_{03}}\left[\frac{d}{d\tau}(\gamma_0V_{02})+\gamma_0k_0V_{01}V_{03}\right]$$

$$-\tilde{g}\left[\frac{dV_{02}}{d\tau}+k_0V_{01}V_{03}\right]-\tilde{v}_2\frac{d\gamma_0}{d\tau}+\frac{i\omega}{2c}\tilde{v}_3^*\tilde{v}_2\tilde{g}\,, \tag{41}$$

$$\gamma_0\frac{d\tilde{v}_3}{d\tau}=(c-V_{03})\left[\frac{d\tilde{g}}{d\tau}-c\tilde{a}_3\right]+\frac{c\tilde{v}_3}{V_{03}}\frac{d}{d\tau}\left[\gamma_0\left[1-\frac{V_{03}}{c}\right]\right]+\Omega_\perp\tilde{v}_1-\tilde{v}_3\frac{d\gamma_0}{d\tau}-\tilde{g}\frac{dV_{03}}{d\tau}+\frac{i\omega}{2c}\tilde{v}_3^*\tilde{v}_3\tilde{g}\,, \tag{42}$$

$$\frac{d\tilde{g}}{d\tau}=V_{01}\tilde{a}_1-V_{02}\tilde{a}_2-V_{03}\tilde{a}_3-\frac{\tilde{v}_3}{V_{03}}\frac{d\gamma_0}{d\tau}\,. \tag{43}$$

Equations (32)–(43) describe the nonlinear evolution of the time-dependent parts of various quantities characterizing the free-electron laser. These equations are combined here into a system of first-order, nonlinear, coupled differential equations, which can be solved numerically with an appropriate set of initial conditions. In order to do so, we still have to complete this system by the equations for the steady (time-independent) parts of various quantities ($\omega_p,\gamma_0,\vec{V}_0$). One such equation is ob-

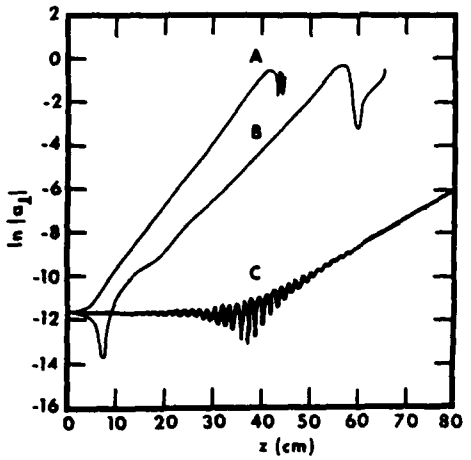

FIG. 1. Dependence of the absolute value of the perpendicular component of the electric field on z. A: $r=0.868$ (branch A) $\omega/c=75$ cm^{-1}. B: $r=1.077$ (branch C), $\omega/c=75$ cm^{-1}. C: $r=1.077$, $\omega/c=130$ cm^{-1}. In all the examples $\omega_p^2/c^2=0.5$ cm^{-2}, $\gamma_0=3$, $k_0=6$ cm^{-1}, and $\xi=0.5$.

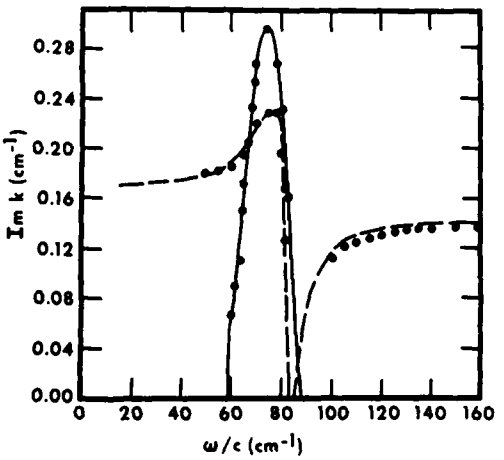

FIG. 2. Spatial growth rates (Imk) vs ω/c in the linear regimes in the sample case. Solid and dashed lines are the results of the linear theory (Ref. 9) for $r=0.868$ and $r=1.077$, respectively. The dots are the results of the present calculations.

tained from the continuity equation

$$\frac{\partial N}{\partial t}+\frac{\partial}{\partial z}(NV_z)=0\,, \tag{44}$$

the time-independent part of which is

$$\frac{d}{dz}(\omega_p^2 V_{0z}+\langle \nu^2 v_z\rangle_+)=0\,, \tag{45}$$

or, on using (17)

$$\omega_p^2 V_{03}=(\omega_p^2 V_{03})\,|_{\tau=0} + \frac{1}{V_{03}}(\omega_p^2\langle \tilde{v}_3\tilde{v}_3\rangle_+ +\omega c^2\langle \tilde{a}_3\tilde{v}_3\rangle_-)\,, \tag{46}$$

where we have used the notations

$$\langle \alpha\beta\rangle_+=\tfrac{1}{2}\,\mathrm{Re}(\alpha^*\beta)\,,\qquad \langle \alpha\beta\rangle_-=\tfrac{1}{2}\,\mathrm{Im}(\alpha^*\beta)\,. \tag{47}$$

Similarly to (45) the steady part of (30) gives

$$\frac{d\gamma_0}{d\tau}\simeq\frac{\omega}{c}\langle \tilde{v}_3\tilde{g}\rangle_- -\langle \tilde{v}_1\tilde{a}_1\rangle_+ -\langle \tilde{v}_2\tilde{a}_2\rangle_+ -\langle \tilde{v}_2\tilde{a}_3\rangle_+\,. \tag{48}$$

And, finally, an equation for $\vec{V}_0$ is obtained by considering the steady part of the momentum equation (25), which can be written in components as

$$\frac{dV_{01}}{d\tau}=V_{02}\left[k_0 V_{03}-\frac{\Omega_{\parallel}}{\gamma_0}\right]-\frac{\Omega_\perp}{\gamma_0}V_{03}+\frac{\Delta_1}{\gamma_0}\,, \tag{49}$$

$$\frac{dV_{02}}{d\tau}=-V_{01}\left[k_0 V_{03}-\frac{\Omega_{\parallel}}{\gamma_0}\right]+\frac{\Delta_2}{\gamma_0}\,, \tag{50}$$

$$\frac{dV_{03}}{d\tau}=V_{01}\frac{\Omega_\perp}{\gamma_0}+\frac{\Delta_3}{\gamma_0}\,, \tag{51}$$

where

$$\Delta_1\simeq -V_{01}\frac{d\gamma_0}{d\tau}+\frac{\omega}{c}(\gamma_0\langle \tilde{v}_3\tilde{v}_1\rangle_- +V_{01}\langle \tilde{v}_3\tilde{g}\rangle_-)+k_0(V_{02}\langle \tilde{v}_3\tilde{g}\rangle_+ +V_{03}\langle \tilde{v}_2\tilde{g}\rangle_+ +\gamma_0\langle \tilde{v}_2\tilde{v}_3\rangle_+)+c\langle \tilde{v}_3\tilde{a}_1\rangle_+\,, \tag{52}$$

$$\Delta_2\simeq -V_{02}\frac{d\gamma_0}{d\tau}+\frac{\omega}{c}(\gamma_0\langle \tilde{v}_3\tilde{v}_2\rangle_- +V_{02}\langle \tilde{v}_3\tilde{g}\rangle_-)-k_0(V_{01}\langle \tilde{v}_3\tilde{g}\rangle_+ +V_{03}\langle \tilde{v}_1\tilde{g}\rangle_+ +\gamma_0\langle \tilde{v}_3\tilde{v}_1\rangle_+)+c\langle \tilde{v}_3\tilde{a}_2\rangle_+\,, \tag{53}$$

$$\Delta_3\simeq -V_{03}\frac{d\gamma_0}{d\tau}-\frac{\omega}{c}\langle \tilde{v}_3\tilde{g}\rangle_- -c(\langle \tilde{v}_1\tilde{a}_1\rangle_+ +\langle \tilde{v}_2\tilde{a}_2\rangle_+)\,. \tag{54}$$

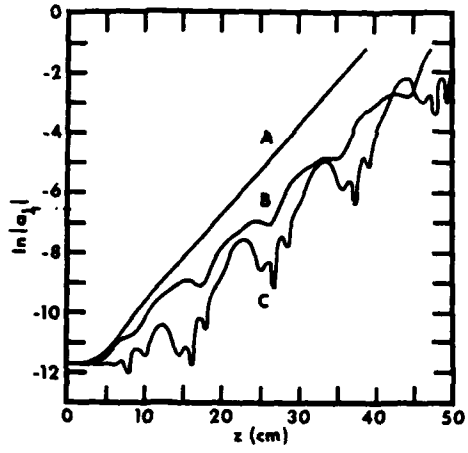

FIG. 3. Effects of the departure from the steady-state trajectories on the gain in the amplifier in the sample case. All the curves correspond to initial value of $r=0.868$ and $\omega/c=75\ \mathrm{cm}^{-1}$. *A*: $\psi=0$. *B*: $\psi=0.1$. *C*: $\psi=0.3$.

IV. NUMERICAL EXAMPLES

In the following numerical applications we will consider the case where $k_0=6\ \mathrm{cm}^{-1}$ and initially the beam is characterized by $\gamma_0=3$ and $\omega_p^2/c^2=0.5\ \mathrm{cm}^{-2}$. This sample case has been studied in the recent linear theory of the laser,[9] and therefore provides a convenient example of our nonlinear formulation.

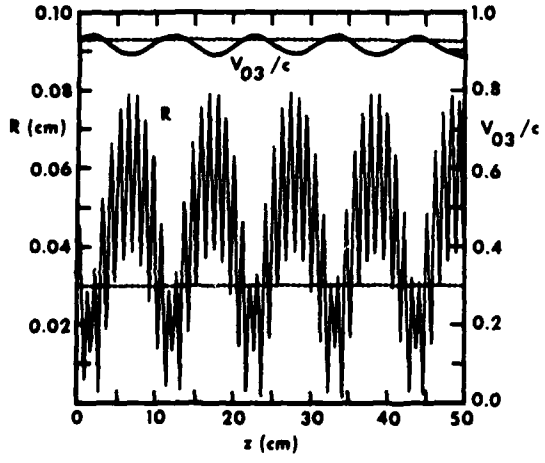

FIG. 4. Axial, time-independent component of the velocity V_{03} and electron displacement R vs z in the sample case. Initially (at $z=0$) in the figure $r=0.868$ and $\omega/c=75\ \mathrm{cm}^{-1}$. The dashed lines represent the case $\psi=0$ (steady-state trajectories) and the solid lines correspond to $\psi=0.3$.

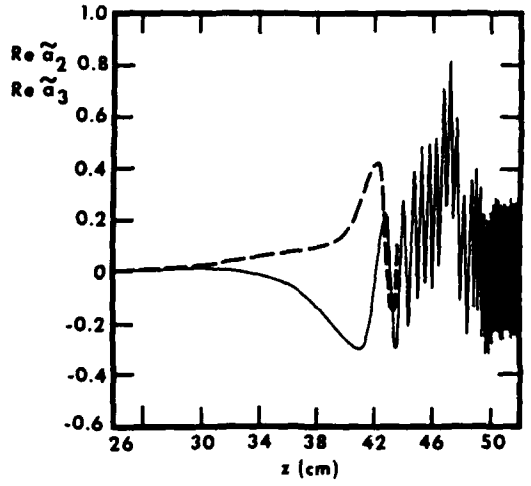

FIG. 5. z dependence of real parts of $\tilde{a}_2$ (the solid line) and $\tilde{a}_3$ (the dashed line) in the saturation phase. The parameters are $\omega/c=75\ \mathrm{cm}^{-1}$, $\psi=0$, $r=0.868$.

As a first application we will assume that as in Ref. 9 the electron beam enters the interaction region on one of the two possible "steady-state" helical orbits (branches *A* and *C* of Ref. 9). These two regimes are characterized in the linear theory by different ranges of parameter $r=\Omega_{\|}/\gamma_0 k_0 V_{03}$ (on branch *A*, $r<1$, while on branch *C*, $r>1$). In these calculations we will change r by varying $\Omega_{\|}$. We will simultaneously adjust $\Omega_{\perp}$ so that in all the examples, initially at $\tau=0$, we will have $V_{0\perp}/c=\xi/\gamma_0$ with $\xi=0.5$. In Fig. 1 we present some typical results of the nonlinear calculations of the evolution of the absolute value of the perpendicular component of the electric field $|\tilde{\mathbf{a}}_{\perp}|$ along the amplifier. The cases $r=0.868$ (branch *A*) with $\omega/c=75\ \mathrm{cm}^{-1}$ and $r=1.077$ (branch *C*) with $\omega/c=75\ \mathrm{cm}^{-1}$, $130\ \mathrm{cm}^{-1}$ are shown. It can be seen in the figure that the evolution of the electromagnetic signal in the device passes through the qualitatively different stages. At short distances the interference of the linear modes in the system leads to a nontrivial occasionally oscillatory dependence of $|\tilde{a}_{\perp}|$ on z. At longer distances the electromagnetic gain in the amplifier is linear and the corresponding slopes of the curves in Fig. 1 are determined by the maximum spatial growth rate (Imk) in the system as described in the linear theory. Finally, when the intensity of the wave becomes large enough, the nonlinear effects start playing a major role and the wave enters the saturation stage. We will discuss the saturation effects in our system later in this section and now proceed with a more detailed comparison with the results of the linear theory. Figure 2

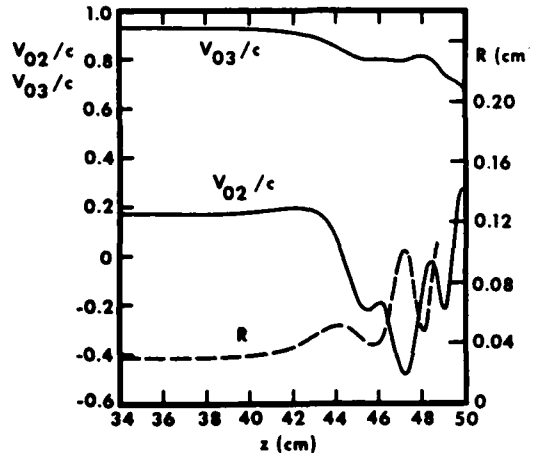

FIG. 6. Time-independent components V_{02}, V_{03}, and radial displacement R vs z in the saturation phase in the amplifier. The curves correspond to the case $\omega/c=75$ cm^{-1}, $\psi=0$, $r=0.868$.

presents such a comparison. The frequency dependence of the linear spatial growth rates on branches A ($r=0.868$) and C ($r=1.077$), shown in this figure has been obtained from the results similar to those shown in Fig. 1. An excellent agreement with the linear theory[9] is obvious.

Next we proceed to the study of nonlinear effects. First consider the effects due to the departure of the beam from the steady-state branches A and C. This situation is likely to occur in experiments as a result of an inaccurate alignment of the direction of injection of the beam into the amplifier. In Fig. 3 we demonstrate the effects on the gain of the departure from the helical orbits. We present the case of $\omega/c=75$ cm^{-1}, for which the gain on branches A and C is maximum, and assume that at $\tau=0$, $V_{01}=\psi/\gamma_0$ (on the helical trajectories $\psi=0$) and $V_{02}=(\xi^2-\psi^2)^{1/2}/\gamma_0$, so that as before $|\mathbf{V}_{01}||_{\tau=0}=\xi/\gamma_0$. The three curves in the figure correspond to $r|_{\tau=0}=0.868$ and $\psi=0,0.1,0.3$. Note that even for $\psi=0.3$ the reduction of the gain is not very significant, although the z dependence of the gain becomes more complex. Note also that in the examples in Fig. 3 the intensity of the radiation field is relatively weak and the nonlinear dependence of the gain is a result of the nonlinear dynamics of the beam in combined helical pump and axial guide magnetic fields. We demonstrate this nonlinear behavior in Fig. 4, where the time-averaged axial velocity V_{03} and radial displacement R of a typical electron trajectory are shown as functions of z in the cases $\psi=0$ (the dashed lines) and $\psi=0.3$ (solid lines). For $\psi=0.3$ we see the development of oscillations in V_{03} with the natural response frequency[7] and period of ~ 12 cm. The same frequency is present in the dependence on z of the radical displacement, where we also see additional rapid oscillations with the period of the helical field (~ 1 cm). Note that with an increase of ψ the radial displacements of the trajectories increase, which may lead to the violation of the conventional assumption in the theory that the beam is close to the axis of the magnetic wiggler. Increased radial excursions of the beam require inclusion of the radial component of the magnetic field of the wiggler and may result in additional destruction of the gain.

Finally, we discuss nonlinear saturation effects due to the radiation field itself. In the following example we assume that the beam initially is on branch A with $r=0.868$. The z dependence of the real parts of a_2 and a_3 for this case in the saturation phase, is shown in Fig. 5. The reason for the saturation in its initial stage becomes clear from Fig. 6, where the z dependence of V_{03}, V_{02}, and R is shown at saturation distances. We see in this figure that the saturation occurs mainly due to the destruction of the electron trajectory. The beam slows down, thus violating necessary conditions for the instability. In addition the radial excursions of the trajectories increase significantly.

It can be seen in Fig. 5 that at the late phase of the saturation, the amplitude of the electromagnetic field starts oscillating with increasing frequency as z increases. When the wavelength of these oscillations becomes comparable to the wavelength of the wave (~ 0.08 cm in the example in Fig. 5), inequality (12) is violated and our formulation becomes invalid for larger values of z. In Fig. 5 this happens at $z\sim 49$ cm. At this stage, new nonlinear effects occurring on a scale comparable with the wavelength of the electromagnetic wave may take place. One such effect is the trapping of the electrons in a strong ponderomotive potential. Our method cannot describe such effects and a more complicated approach, similar to that used in Refs. 11 and 12 must be applied at this stage. Nevertheless, the present theory is still valid at the onset of the saturation and describes its initial phase.

ACKNOWLEDGMENTS

This work was supported in part by the Office of Naval Research and by the National Science Foundation. The authors are also grateful to Mr. A. Fruchtman for his assistance in the numerical part of the work.

[1]T. C. Marshall, S.Talmage, and P. Efthimion, Appl. Phys. Lett. 31, 320 (1977).
[2]V. L. Granatstein, S. P. Schlesinger, M. Herndon, R. K. Parker, and J. A. Pasour, Appl. Phys. Lett. 30, 384 (1977).
[3]D. B. McDermott, T. C. Marshall, S. P. Schlesinger, R. K. Parker, and V. L. Granatstein, Phys. Rev. Lett. 41, 1368 (1978).
[4]R. M. Gilgenbach, T. C. Marshall, and S. P. Schlesinger, Phys. Fluids 22, 971 (1978).
[5]R. H. Jackson, R. K. Parker, and S. H. Gold, Bull. Am. Phys. Soc. 25, 947 (1980).
[6]S. H. Gold, P. H. Jackson, R. K. Parker, H. P. Freund, V. L. Granatstein, P. C. Efthimion, M. Herndon, and A. K. Kinkead, in *Physics of Quantum Electronics*, Vol. 9, edited by S. F. Jacobs, H. S. Piloff, M. Sargent, M. O. Scully, and R. Spitzer (Addison-Wesley, Reading, Mass., 1982), p. 741.
[7]L. Friedland, Phys. Fluids 23, 2376 (1980).
[8]L. Friedland and J. L. Hirshfield, Phys. Rev. Lett. 44, 1456 (1980).
[9]L. Friedland and I. B. Bernstein, Phys. Rev. A 23, 816 (1981).
[10]L. Friedland and A. Fruchtman, Phys. Rev. A 25, 2693 (1982).
[11]P. Sprangle, Cha-Mei Tang, and W. M. Manheimer, Phys. Rev. Lett. 43, 1932 (1979).
[12]P. Sprangle, Cha-Mei Tang, and W. M. Manheimer, Phys. Rev. A 21, 302 (1980).
[13]P. C. Liewer, A. T. Lin, and J. M. Dawson, Phys. Rev. A 23, 1251 (1981).

Wiggler-free free electron waveguide laser in a uniform axial magnetic field: Single particle treatment

A. Fruchtman
Center for Plasma Physics, Racah Institute of Physics, Hebrew University of Jerusalem, Jerusalem, Israel

(Received 10 January 1983; accepted for publication 5 May 1983)

A wiggler-free free electron laser operating in a waveguide is analyzed by using a single particle treatment. The use of either a TE or a TM mode is shown to enhance the gain for a resonant frequency much higher than the cyclotron frequency. It is demonstrated that a source of a submillimeter radiation, based on this analysis, may have output power comparable to that of a wiggler-type free electron laser.

PACS numbers: 41.70. + t, 52.25.Ps, 42.55. − f, 41.80.Dd

I. INTRODUCTION

Considerable effort has been made in recent years to develop sources of coherent radiation, using relativistic electron beams moving along helical trajectories. The radiation wavelength in these so-called "free electron lasers" (FELS) is the Doppler-shifted pitch of the electron motion $\lambda \simeq \lambda_0/2\gamma^2$ where λ_0 is the electron pitch, $\gamma = [1 - (v/c)^2]^{-1/2}$ is the relativistic factor, and v is the velocity of the beam. One class of such devices is the wiggler-type free electron laser,[1] where a periodic magnetic structure forces the electrons into helical motion. Most of the experimental and theoretical research up to now has been aimed at this type of FEL.

Recently interest arose in a second class of FEL, the "wiggler-free free electron lasers." Here the electrons move on helical orbits in a simple uniform magnetic field (which is different from the longitudinally[2] or transversally[3] modulated axial magnetic field). In contrast to the gyrotron,[4] the frequency here is the Doppler up-shifted cyclotron frequency. Chu and Hirshfield[5] treated the collective interaction and showed the existence of an unstable growing mode. They also compared in detail the two bunching mechanisms. Later it was demonstrated that gain enhancement can be achieved by a careful choice of the electron momentum distribution function.[6]

The various gain mechanisms were clearly explained using a single-particle approach.[7,8] Ride and Colson[7] showed that two sources of bunching exist as a result of the electron-wave interaction. One source of bunching is the ponderomotive force due to the product of the perpendicular component of the electron equilibrium velocity and the magnetic vector of the electromagnetic wave. The second source of bunching is the modulation of the cyclotron frequency due to the relativistic change of the electron mass. Each one of the sources causes gain proportional to L^3 (L is the length of the amplifier), but acting simultaneously they nearly cancel each other. There remains a lower order gain proportional to L^2.

In all these previous papers the wave was assumed to propagate parallel to the direction of the uniform magnetic field. In a realizable device there must be a waveguide within which the radiation propagates. Ott and Manheimer published a collective theory for a thin slab beam in a parallel plate waveguide.[9] The difference between bunching mechanisms for TE and TM modes which we describe below using a single-particle model are not easily identified in their treatment. Moreover for practical devices the applicability of the thin beam model may be limited. The main role of this paper is to study the influence of the waveguide modes on the interaction within the framework of a single-particle approach. The two aforementioned sources of bunching which cancel that part of the gain proportional to L^3 will be shown here not to do so when, as in the case of waveguide modes, propagation is not exactly parallel to the magnetic field. There is a residual term proportional to L^3, similar to the case of a wiggler-type free electron laser. Thus the use of waveguide modes may enhance the gain. This enhanced gain mechanism can be exploited for the design of a practical device for submillimeter wave generation or amplification within the constraints of a single-particle interaction. A practical example, similar to that in Ref. 9, will be described based on the present analysis.

Electron beam sources of radiation for the submillimeter portion of the spectrum usually employ high current densities, where collective effects play an important role. The present single-particle calculation, by describing clearly the physical picture, may be used as an important first step for a self-consistent collective description in future work.

II. THE EQUATIONS OF MOTION

A relativistic electron beam is guided by a uniform magnetic field along a waveguide within which an electromagnetic wave propagates in the same direction. The gain is found by calculating the energy loss of the electrons as they pass through the structure. In doing it, two assumptions are used. The first is that the intensity of the radiation is big enough (or the electron density low enough), so that the wave amplitude remains constant. Secondly we assume that the intensity of the radiation relative to the magnetostatic field is small enough to allow the use of a perturbation method to solve the electron equations of motion. The uniform magnetic field is

$$\mathbf{B}_0 = B_0 \mathbf{e}_z. \tag{1}$$

For simplicity we choose a waveguide made of two infinite plane parallel plates with distance a between them. The wave is assumed to be coherent and is either a TE or a TM mode. Its components are[10]

 0021-8979/83/084289-06$02.40

$$\left.\begin{aligned} E_y' &= -(A'\omega'/k_\perp c)\cos(k_\perp x)\cos(\beta z-\omega' t),\\ B_x' &= (A'\beta/k_\perp)\cos(k_\perp x)\cos(\beta z-\omega' t),\\ B_z' &= A'\sin(k_\perp x)\sin(\beta z-\omega' t),\end{aligned}\right\}\ \text{TE mode},$$

$$\left.\begin{aligned} E_z' &= A'\sin(k_\perp x)\sin(\beta z-\omega' t),\\ E_x' &= (\beta/k_\perp)A'\cos(k_\perp x)\cos(\beta z-\omega' t),\\ B_y' &= (\omega'/k_\perp c)A'\cos(k_\perp x)\cos(\beta z-\omega' t).\end{aligned}\right\}\ \text{TM mode}. \tag{2}$$

ω' is the wave frequency, x is the coordinate perpendicular to the plates, and β and $k_\perp$ are the components of the wave vector related by

$$(\omega'/c)^2 = k_\perp^2 + \beta^2. \tag{3}$$

$k_\perp$ will have discrete values

$$k_\perp = (n\pi/a) \quad n = 1,2\ldots. \tag{4}$$

The equation of motion of the electron is

$$\frac{d}{dt}(\gamma\mathbf{v}) = -\frac{e}{mc}\mathbf{v}\times(\mathbf{B}_0+\mathbf{B}') - \frac{e}{m}\mathbf{E}'. \tag{5}$$

e and m are the electron charge and mass, respectively. The equation of motion is easily solved by using a rotating system of coordinates which is better suited to this problem, because of the helical nature of the electron orbit. A similar system of coordinates was used previously in dealing with the wiggler-type FEL problem.[11,12] For an electron, whose perpendicular velocity in the entrance makes an angle ψ_0 with the negative x axis, we define

$$\begin{aligned} \mathbf{e}_1(z,\psi_0) &= -\mathbf{e}_x\sin(k_0 z+\psi_0) + \mathbf{e}_y\cos(k_0 z+\psi_0),\\ \mathbf{e}_2(z,\psi_0) &= -\mathbf{e}_x\cos(k_0 z+\psi_0) - \mathbf{e}_y\sin(k_0 z+\psi_0),\\ \mathbf{e}_3(z,\psi_0) &= \mathbf{e}_z. \end{aligned} \tag{6}$$

k_0 is chosen later. Let us use the following notations:

$$\begin{aligned} &\mathbf{u} = \mathbf{v}/c, \quad \tau' = tc, \quad \mathbf{E} = e\mathbf{E}'/mc^2,\\ &\mathbf{B} = e\mathbf{B}'/mc^2, \quad \omega = \omega'/c, \quad A = eA'/mc^2,\\ &\Omega = eB_0/mc^2. \end{aligned} \tag{7}$$

With these notations Eq. (5) becomes

$$\begin{aligned} \dot{u}_1 &= u_2(k_0u_3 - \Omega/\gamma) - \frac{u_1}{\gamma}\dot{\gamma} + \frac{1}{\gamma}(u_3B_2 - u_2B_3 - E_1),\\ \dot{u}_2 &= -u_1(k_0u_3 - \Omega/\gamma) - \frac{u_2}{\gamma}\dot{\gamma} - \frac{1}{\gamma}(u_3B_1 - u_1B_3 + E_2),\\ \dot{u}_3 &= -\frac{u_3}{\gamma}\dot{\gamma} - \frac{1}{\gamma}(u_1B_2 - u_2B_1 + E_3), \end{aligned} \tag{8}$$

where

$$\begin{aligned} &E_3 = 0, \quad \text{TE mode},\\ &B_3 = 0, \quad \text{TM mode}, \end{aligned} \tag{9}$$

and the dot represents differentiation with respect to τ'. Conservation of energy dictates that the energy change of the electrons equals the work done by the wave fields:

$$\dot{\gamma} = -\mathbf{u}\cdot\mathbf{E}. \tag{10}$$

The components of the wave in the rotating system of coordinates are

$$\left.\begin{aligned} E_1 &= -(A\omega/2k_\perp)\cos(k_\perp x)\cos[(\beta+k_0)z-\omega(\tau+\tau_0)+\psi_0],\\ E_2 &= (A\omega/2k_\perp)\cos(k_\perp x)\sin[(\beta+k_0)z-\omega(\tau+\tau_0)+\psi_0],\\ B_1 &= -(\beta/\omega)E_2, \quad B_2 = (\beta/\omega)E_1,\\ B_3 &= A\sin(k_\perp x)\sin[\beta z-\omega(\tau+\tau_0)],\end{aligned}\right\}\ \text{TE mode},$$

$$\left.\begin{aligned} E_1 &= -(A\beta/2k_\perp)\cos(k_\perp x)\sin[(\beta+k_0)z-\omega(\tau+\tau_0)+\psi_0],\\ E_2 &= -(A\beta/2k_\perp)\cos(k_\perp x)\cos[(\beta+k_0)z-\omega(\tau+\tau_0)+\psi_0],\\ B_1 &= -(\omega/\beta)E_2, \quad B_2 = (\omega/\beta)E_1,\\ E_3 &= A\sin(k_\perp x)\sin[\beta z-\omega(\tau+\tau_0)].\end{aligned}\right\}\ \text{TM mode}. \tag{11}$$

Terms which oscillate with high frequency were omitted keeping only terms which might be resonant. τ_0 is the time the electron is at $z=0$, and τ is the time which has passed since then.

The equations of motion (8) are solved perturbatively. First we find the steady-state electron orbit in the absence of the wave. Then its perturbed velocity and position are calculated when the EM fields are taken along the steady-state orbits. The energy transfer is found only in the second order.

To zero order there are no wave fields:

$$\mathbf{E} = \mathbf{B} = 0, \quad \gamma = \gamma_0. \tag{12}$$

The equations of motion are

$$\begin{aligned} \dot{u}_{10} &= u_{20}(k_0u_{30} - \Omega/\gamma_0),\\ \dot{u}_{20} &= u_{10}(k_0u_{30} - \Omega/\gamma_0),\\ \dot{u}_{30} &= 0. \end{aligned} \tag{13}$$

The third of these equations yields $u_3 = u_{30} = \text{const}$. The definition of our rotating system of coordinates is completed by setting $k_0 = \Omega/\gamma_0 u_{30}$, in which case u_{10} and u_{20} are constant too. We are still free to choose u_{10} and u_{20}, with ψ_0 determining the initial velocity of each electron. For our convenience, u_{10} is set equal to 0, in which case for each

electron $u_2 = u_{20}$ and $\mathbf{e}_2$ is always in the direction of the perpendicular velocity. This means that $\mathbf{e}_i$ can be different for different electrons. The electrons are assumed to enter the waveguide with the same velocity components parallel and perpendicular to the magnetic field. The solution of Eq. (13) is therefore

$$u_{10} = 0, \quad u_{20} = \text{const}, \quad u_{30} = \text{const},$$
$$\gamma_0 = (1 - u_{20}^2 - u_{30}^2)^{-1/2}. \tag{14}$$

The x and z coordinates of the electron position are to zero order

$$z_0(\tau) = u_{30}\tau,$$
$$x_0 = (\tau) = x_e - r_0 \sin(k_0 u_{30}\tau + \psi_0), \tag{15}$$
$$r_0 = u_{20}/k_0 u_{30}.$$

r_0 is the Larmor radius. From now on assume

$$k_\perp r_0 \ll 1. \tag{16}$$

Due to Eq. (16) we approximate the amplitude of the wave in the first-order equations of motion

$$\cos(k_\perp x_0) = \cos\rho_e,$$
$$\sin(k_\perp x_0) = \sin\rho_e, \tag{17}$$
$$\rho_e = k_\perp x_e,$$

and exclude the excitation of higher cyclotron harmonics. The fields along the steady-state trajectories are

$$E_{10} = -(E_0/2)\sin(\nu\tau + \xi),$$
$$E_{20} = -(E_0/2)\cos(\nu\tau + \xi), \tag{18}$$

where

$$\left.\begin{aligned} E_0 &= A\,(\omega/k_\perp)\cos\psi_e, \\ \xi &= -\omega\tau_0 + \psi_0 + \pi/2, \end{aligned}\right\} \text{ TE mode,}$$
$$\left.\begin{aligned} E_0 &= A\,(\omega/k_\perp)\cos\psi_e, \\ \xi &= -\omega\tau_0 + \psi_0. \end{aligned}\right\} \text{ TM mode.} \tag{19}$$

The "resonance parameter" ν is

$$\nu = (\beta + k_0)u_{30} - \omega. \tag{20}$$

The interaction between the electrons and the wave fields is strongest when the resonance condition is fulfilled, namely when $\nu \simeq 0$. In order that the resonant frequency will be high we require that $\beta \gg k_\perp$ and that $u_{30} \gg u_{20}$.
Then

$$\omega \simeq \frac{k_0}{1 - u_{30}} \simeq 2k_0\gamma_0^2. \tag{21}$$

B_{30} or E_{30} were omitted because they oscillate with high frequency. We linearize the electron velocity and energy.

$$u_1 = w_1(\tau,\tau_0),$$
$$u_2 = u_{20} + w_2(\tau,\tau_0),$$
$$u_3 = u_{30} + w_3(\tau,\tau_0), \tag{22}$$
$$\gamma = \gamma_0 + \Gamma(\tau,\tau_0).$$

Next we write the equations of motion for these perturbed quantities

$$\dot{w}_1 = k_0 u_{20} w_3 + k_0 u_{20} u_{30}\frac{\Gamma}{\gamma_0} + \frac{E_{10}}{\gamma_0}(g u_{30} - 1),$$
$$\dot{w}_2 = -\frac{u_{20}}{\gamma_0}\dot{\Gamma} + \frac{E_{20}}{\gamma_0}(g u_{30} - 1), \tag{23}$$
$$\dot{w}_3 = -\frac{u_{30}}{\gamma_0}\dot{\Gamma} + \frac{B_{10}}{\gamma_{10}}u_{20},$$

where

$$g = \beta/\omega, \quad \text{TE mode},$$
$$g = \omega/\beta, \quad \text{TM mode}. \tag{24}$$

The third of Eqs. (23) shows that the longitudinal velocity is perturbed by two forces. The first term on the right-hand side of this equation gives rise to the cyclotron maser instability. Its origin lies in the relativistic change of mass of the electrons. The second term represents the ponderomotive force of the magnetic component of the wave on the perpendicular velocity of the electron. This force drives the Weibel-type instability. A detailed comparison of these two bunching mechanisms was given by Chu and Hirshfield[5] and also by Ride and Colson.[7] To first order the energy Eq. (10) is

$$\dot{\Gamma}_1 = -u_{20}E_{20}. \tag{25}$$

The solutions of Eq. (23) using Eq. (25) are

$$\dot{w}_1 = \left(\frac{E_0}{2\gamma_0}\right)\left(\frac{S_1}{\nu^2}\right)[\cos\xi - \cos(\nu\tau + \xi) - \nu\tau\sin\xi\,] + \left(\frac{E_0}{2\gamma_0}\right)(1 - g u_{30})\tau\sin\xi,$$
$$\dot{w}_2 = \left(\frac{E_0}{2\gamma_0}\right)\left(\frac{S_2}{\nu}\right)[\sin(\nu\tau + \xi) - \sin\xi\,],$$
$$\dot{w}_3 = \left(\frac{E_0}{2\gamma_0}\right)\left(\frac{S_3}{\nu}\right)[\sin(\nu\tau + \xi) - \sin\xi\,], \tag{26}$$
$$S_1 = \nu(1 - g u_{30}) + k_0 u_{20}^2 g,$$
$$S_2 = 1 - g u_{30} - u_{20}^2,$$
$$S_3 = u_{20}(g - u_{30}).$$

III. THE ENERGY GAIN

We solved the equations of motion to first order. This enables us to calculate the net energy loss of the electrons to second order, which is the lowest order where it does not vanish. To second order Eq. (10) is

$$\dot{\Gamma} = -w_1 E_{10} - w_2 E_{20} - u_{20}E_{21} - w_3 E_{30} - u_{30}E_{31}. \tag{27}$$

For the TM mode $E_{30} = E_{31} = 0$. The net energy transfer is found by averaging on τ_0, the time of entrance ($\langle ... \rangle$ denotes this averaging). It is in fact averaging on ξ, which means that the distribution of ψ_0 is irrelevant. This distribution has an influence on higher cyclotron harmonics; it also can be important when collective effects become dominant.[6]

Thus

$$\langle -w_1E_{10}\rangle = \left(\frac{E_0^2}{8\gamma_0}\right)\left[\left(\frac{S_1}{\nu^2}\right)(\sin\nu\tau - \nu\tau\cos\nu\tau) + (1-gu_{30})\tau\cos\nu\tau\right],$$

$$\langle -w_2E_{20}\rangle = \left(\frac{E_0^2}{8\gamma_0}\right)\left(\frac{S_2}{\nu}\right)\sin\nu\tau. \tag{28}$$

The resonant term in E_{21} is due to modulations in axial position Δz.

$$\Delta z = \int_0^\tau w_3 d\tau = \left(\frac{E_0}{2\gamma_0}\right)\left(\frac{S_3}{\nu^2}\right)[-\nu\tau\sin\xi - \cos(\nu\tau+\xi) + \cos\xi\,]. \tag{29}$$

Using again the fact that the wave is only a perturbation on the steady-state orbit, E_{21} is

$$E_{21} = \left(\frac{E_0}{2}\right)(\beta + k_0)\Delta z\sin(\nu\tau+\xi), \tag{30}$$

and the energy transfer is

$$\langle -u_{20}E_{21}\rangle = \left(\frac{E_0^2}{8\gamma_0}\right)\left(\frac{u_{20}S_3}{\nu^2}\right)\times(k_0+\beta)(\nu\tau\cos\nu\tau - \sin\nu\tau). \tag{31}$$

Adding the terms in Eqs. (28) and (31) we obtain the contribution to total energy transfer from the perpendicular part of the radiation

$$\langle\dot{\Gamma}_{2_\perp}\rangle = \frac{1}{\nu}\left(\frac{E_0^2}{8\gamma_0}\right)[2(1-gu_{30})\sin\nu\tau - u_{20}^2\nu\tau\cos\nu\tau] + \frac{1}{\nu^2}\left(\frac{E_0^2}{8\gamma_0}\right)u_{20}^2(\omega-\beta g)(\sin\nu\tau - \nu\tau\cos\nu\tau). \tag{32}$$

The last expression is different for the two modes

$$\omega - \beta g = k_\perp^2/\omega, \quad \text{TE mode},$$
$$\omega - \beta g = 0, \quad \text{TM mode}. \tag{33}$$

For the TE mode there remains the term proportional to $1/\nu^2$, whilst it vanishes for the TM mode. This residual term proportional to $1/\nu^2$ is the major contribution to the gain. Thus the gain for the TE mode is

$$\langle\dot{\Gamma}_2\rangle_{TE} = \left(\frac{E_0^2}{8\gamma_0}\right)u_{20}^2\frac{k_\perp^2}{\omega}\left(\frac{\sin\nu\tau - \nu\tau\cos\nu\tau}{2}\right). \tag{34}$$

When the wave propagates parallel to the magnetic field $k_\perp = 0$ and the gain is the first term in Eq. (32) only, and is proportional to $1/\nu$ instead of to $1/\nu^2$. This result, when $k_\perp$ is 0, agrees with Ride and Colson's result.[7] Thus the use of a TE mode may indeed enhance the gain.

It is interesting to note that in the opposite case, namely when $\beta = 0$ and $k_\perp = \omega$, our result for the TE mode gain agrees with the gain in the gyrotron.[7] In fact, being near cutoff the magnetic component of the wave is in the z direction only, and the ponderomotive force, which is one of the two bunching sources, vanishes. The second bunching source exists alone; this is the cyclotron maser bunching mechanism. This case does interest us since $\beta = 0$ gives no Doppler up-shift.

Let us now complete our study of the gain of the TM mode. Until now the gain for the TM case due to the work done on the electrons by the perpendicular fields is low and proportional to $1/\nu$ only. But for this mode there is still the work done by the axial electric field of the wave.

The work done on the electrons by the axial field is composed of two terms. The first term is $-w_3E_{30}$ and its average vanishes since E_{30} oscillates with high frequency. The second term is $u_{30}E_{31}$. E_{31} contains resonant terms. The perturbation on the axial field due to the perturbed trajectory is, after linearization

$$E_{31} = A(\cos\rho_e)(k_\perp\Delta x)\sin[(\beta u_{30}-\omega)\tau - \omega\tau_0]. \tag{35}$$

High frequency terms were omitted. Only terms linear in Δx or Δz were kept.

Using the rotating coordinate system Δx is

$$\Delta x = -\Delta x_1\sin(k_0u_{30}\tau + \psi_0) - \left(\frac{u_{20}}{u_{30}}\Delta x_3 + \Delta x_2\right)\cos(k_0u_{30}\tau + \psi_0). \tag{36}$$

Equations (35) and (36) yield for E_{31}

$$E_{31} = \frac{A}{2}(\cos\rho_e)k_\perp[\Delta x_1\cos(\nu\tau+\xi) - \left(\frac{u_{20}}{u_{30}}\Delta x_3 + \Delta x_2\right)\sin(\nu\tau+\xi)]. \tag{37}$$

The next step is to calculate the Δx_1 and Δx_2. Using the identities

$$\dot{\mathbf{e}}_1 = k_0u_3\mathbf{e}_2, \quad \dot{\mathbf{e}}_2 = -k_0u_3\mathbf{e}_1, \tag{38}$$

we obtain the equations

$$\Delta\dot{x}_1 = w_1 + k_0u_{30}\Delta x_2,$$
$$\Delta\dot{x}_2 = w_2 - k_0u_{30}\Delta x_1 - \frac{u_{20}}{u_{30}}w_3. \tag{39}$$

The solutions of these equations (keeping resonant terms only) are

$$\Delta x_1 = \left(\frac{E_0}{2\gamma_0}\right)\frac{(1-gu_{30})}{k_0u_{30}}\left[\frac{\sin(\nu\tau+\xi)-\sin\xi}{\nu}\right],$$
$$\Delta x_2 = \left(\frac{E_0}{2\gamma_0}\right)\left(\frac{1}{k_0u_{30}}\right)\times\left\{S_1\left[\frac{\cos(\nu\tau+\xi)-\cos\xi+\nu\tau\sin\xi}{\nu^2}\right] - (1-gu_{30})\tau\sin\xi\right\}. \tag{40}$$

Therefore the work done by the axial field is

$$\langle -u_{30}E_{31}\rangle = \left(\frac{E_0^2}{8\gamma_0}\right)\left(\frac{k_\perp^2}{\beta}\right)\times\left[u_{20}^2\left(\frac{\nu\tau\cos\nu\tau - \sin\nu\tau}{\nu^2}\right) - \frac{(1-gu_{30})}{k_0u_{30}}\frac{\sin\nu\tau}{\nu}\right]. \tag{41}$$

The main contribution to the gain comes from the term proportional to $1/\nu^2$. Thus the gain for the TM mode is

$$\langle\dot{\Gamma}_2\rangle_{TM} = \left(\frac{E_0^2}{8\gamma_0}\right)u_{20}^2\frac{k_\perp^2}{\beta}\left(\frac{\nu\tau\cos\nu\tau - \sin\nu\tau}{\nu^2}\right). \tag{42}$$

The gain for both the TE and the TM mode may be written in a similar form

AD-A134 270 WAVE-PARTICLE INTERACTIONS ON RELATIVISTIC ELECTRON BEAMS(U) YALE UNIV NEW HAVEN CONN I B BERNSTEIN ET AL. 20 OCT 83 N00014-79-C-0588 2/2

UNCLASSIFIED F/G 20/5 NL

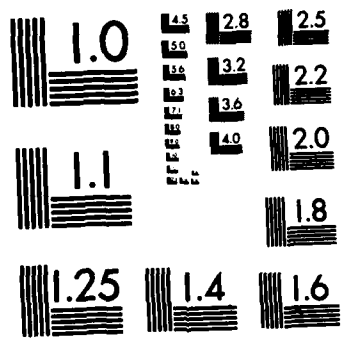

$$\langle \dot{\Gamma} \rangle = \left(\frac{E_0^2}{8\gamma_0} \right) u_{20}^2 \frac{k_\perp^2}{P} \left(\frac{\nu\tau \cos \nu\tau - \sin \nu\tau}{\nu^2} \right), \quad (43)$$

$P = -\omega$, TE mode,

$P = \beta$, TM mode.

The total energy loss of an electron along the amplifier is obtained by integrating $\langle \dot{\Gamma} \rangle$

$$\langle \Delta\gamma \rangle = \int_0^\tau \langle \dot{\Gamma} \rangle d\tau. \quad (44)$$

The energy gain of the wave is the energy loss of all the electrons divided by the energy of the fields at $z = 0$ across the plates

$$G(\tau) = -\frac{\langle \Delta\gamma \rangle_T mc^2 N_0}{W_{n_0}}, \quad (45)$$

where n_0 and W_{n_0} are the electron and the initial wave energy densities, respectively. $\langle \Delta\gamma \rangle_T$ is the sum of energy changes across the plates. The electron beam is assumed to fill uniformly the gap between the plates.

Thus

$$\langle \Delta\gamma \rangle_T = \int_{x'}^{x'+a} \langle \Delta\gamma \rangle dx_e,$$

$$W_{n_0} = \frac{(mc^2)^2 A^2}{e^2 16\pi} a \left(\frac{\omega}{k_\perp} \right)^2. \quad (46)$$

Writing $L = u_{30}\tau$ where L is the length of the amplifier, the gain along the amplifier is

$$G(L) = \frac{1}{8} \frac{\omega_p^2}{c^2} \frac{k_\perp^2}{\gamma_0 \omega} \frac{u_{20}^2}{u_{30}^3} L^3 F'(\theta), \quad \text{TE mode},$$

$$G(L) = -\frac{1}{8} \frac{\omega_p^2}{c^2} \frac{\beta k_\perp^2}{\gamma_0 \omega^2} \frac{u_{20}^2}{u_{30}^3} L^3 F'(\theta), \quad \text{TM mode}, \quad (47)$$

where $F'(\theta)$ is the line-shape function

$$F(\theta) = \left(\frac{\sin\theta}{\theta} \right)^2,$$

$$\theta = \frac{\nu\tau}{2}. \quad (48)$$

The gain for the TE mode is higher by the factor (ω/β) than for the TM mode. In our case, far from cutoff $\beta \simeq \omega$, the gain in both cases is about the same. The form of the gain (47) is very similar to the form of gain obtained for the wiggler-type FEL.[13] As a matter of fact we can write a general expression for the gain in these devices.

$$G = \left(\frac{\omega_p^2}{8c^2\gamma_0} \right) \eta u_{20}^2 L^3 F'(\theta),$$

$$\eta_{\text{WFEL}} = k_0,$$

$$\eta_{TE} = k_\perp^2/\omega u_{30}^3,$$

$$\eta_{TM} = k_\perp^2/\omega^2 u_{30}^3. \quad (49)$$

WFEL denotes wiggler-type FEL.

The gain in the proposed wiggler-free FEL is decreased relative to the wiggler-type by the factor

$$\frac{G_{\text{TE}}}{G_{\text{WFEL}}} = \frac{k_\perp^2}{\omega k_0 u_{30}^3} = \frac{k_0}{\omega u_{20}^2 u_{30}} (k_\perp r_0)^2. \quad (50)$$

Since $k_0/\omega u_{20}^2 \gtrsim 1$ and $(k_\perp r_0)^2 \ll 1$ this last ratio is smaller than 1. The gain here, even though enhanced relative to the case without waveguide, is still small relative to the case where one uses the wiggler. Yet the advantages gained by the simplicity of the magnetic configuration and the possible use of large interaction volume could outweigh the somewhat smaller gain in many situations.

IV. DISCUSSION

Here we sketch a possible practical device based on the ideas described hitherto.

A magnetron injection gun emits an electron beam into a hollow coaxial cylindrical waveguide. The inner and outer radii are 10 and 13 cm, respectively. Since the gap 3 cm is small relative to each radius our analysis of the two infinite plane parallel plates may be applied here. The electron beam fills the waveguide uniformly [in contrast to the case in Eq. (9)]. A radiation of wavelength 785 μm is launched into the waveguide. The fourth mode has $k_\perp = 4.2\ \text{cm}^{-1}$. The electrons are injected with $\gamma_0 = 5$ (energy of 2 MeV). They enter with perpendicular velocity $u_{20} = 0.1$. We apply a uniform magnetic field of 16.5 kG which yields $k_0 = 2\ \text{cm}^{-1}$. Following Eq. (21) the above wavelength is resonant. $k_\perp r_0$ is 0.2 and obeys the condition (16). For a gain of 10% the required current density is 6 A cm^2 or a total current of about 1.2 kA. Other modes are not excited for $L \simeq 100$ cm since $\Delta\nu L = \Delta\beta L$, $\beta\Delta\beta = k_\perp \Delta k_\perp$, and $\Delta k_\perp = \pi/a$ yield $\Delta\nu L = (k_\perp/\beta)(\pi/a)L > \pi$. In order to satisfy the resonance condition for gain, $\Delta\nu L$ should be less than 2π, where $\Delta\nu$ is due to the spread in energy and angle in the initial electron beam. From the definition of ν [Eq. (20)] it follows that $\Delta\alpha/\alpha (tg\alpha \equiv u_{20}/u_{30})$ should be less than λ/Lu_{20}^2, and $\Delta\gamma/\gamma$ less than $1/N (= 2\pi/k_0 L)$.

We now compare the proposed device to a wiggler-type FEL. Imagine that the electrons in the wiggler-type FEL move on similar helical orbits. By Eq. (49) the current density needed is 0.6 A/cm^2 only. On the other hand when $k_0 = 2\ \text{cm}^{-1}$ the pitch of the wiggler is 3.1 cm. Considering that the desired wiggler-field is only at a radius of less than 0.3 cm,[14] the volume of interaction has a cross section of 0.3 cm^2. In our device it is much bigger, about 200 cm^2 so that its power output would undoubtedly be larger. In addition, the current required to create the wiggler-field (320 G) is about 15 kA. In view of these facts the advantage of the wiggler-type FEL on the proposed device is not clear.

In summary, we have demonstrated the possibility of operation of a novel source of submillimeter radiation. It is built simply from a waveguide immersed in an intense uniform magnetic field in which a relativistic electron beam interacts with one of its modes. By amplifying the Doppler-shifted electron cyclotron frequency, it becomes, in terms of its gain and its simplicity, a viable source of submillimeter radiation.

ACKNOWLEDGMENTS

Stimulating discussions with L. Friedland are acknowledged, as are the many helpful comments and the critical reading of this manuscript by J. L. Hirshfield. This work was

supported by the Israel-U.S. Binational Science Foundation and the Office of Naval Research.

[1]For a review of past work see *Physics of Quantum Electronics*, Vol. 5 (1978), Vol. 7 (1980), Vols. 8 and 9 (1982) (Addison-Wesley, Reading, Mass.); IEEE J. Quantum Electron. Special Issue on Free-Electron Lasers, QE-17 (1981).
[2]R. C. Davidson and W. A. McMullin, Phys. Rev. A 26, 1997 (1982).
[3]A. Grossman, T. C. Marshall, and S. P.Schlesinger, Phys. Fluids 26, 337 (1983).
[4]For a review of past work see J. L. Hirshfield, "Gyrotrons," in *Infrared and Millimeter Waves*, edited by K. J. Button (Academic, New York, 1979).
[5]K. R. Chu and J. L. Hirshfield, Phys. Fluids 21, 461 (1978).
[6]A. Fruchtman and L. Friedland, J. Appl. Phys. 53, 4011 (1982).
[7]S. K. Ride and W. B. Colson, Appl. Phys. 20, 41 (1979).
[8]Y. Gell, J. R. Torstensson, H. Wilhelmsson, and B. Levush, Appl. Phys. B 27, 15 (1982).
[9]E. Ott and W. M. Manheimer, IEEE Trans. Plasma Sci. PS-3, 1 (1975).
[10]S. Ramo, J. R. Whinnery, and T. Van Duzer, *Fields and Waves in Communication Electronics* (Wiley, New York, 1967), p. 385.
[11]I. B. Bernstein and J. L. Hirshfield, Phys. Rev. A 20, 1661 (1979).
[12]L. Friedland and J. L. Hirshfield, Phys. Rev. Lett. 44, 1456 (1980).
[13]W. B. Colson, *Physics of Quantum Electronics* (Addison-Wesley, Reading, Mass., 1977), Vol. 5.
[14]On the stringent requirements of the wiggler field during operation see P. Diament, Phys. Rev. A 23, 2537 (1981).

Theory of a Nonwiggler Collective Free Electron Laser in Uniform Magnetic Field

A. FRUCHTMAN AND L. FRIEDLAND

Abstract—A nonwiggler free electron laser, operating in uniform guide magnetic field, is analyzed. The amplifier problem is solved self-consistently on the basis of the kinetic theory. It is shown that the asymmetry in the azimuthal distribution of the electrons' momentum leads to a coupling between the transverse and the space-charge modes. This, in turn, enhances the gain in the amplifier. In the case of a cold beam, with the electrons gyrating coherently, the spatial growth in the collective nonwiggler free electron laser (FEL) is comparable to that found in conventional free electron lasers operating in similar regimes.

I. INTRODUCTION

CONVENTIONAL free electron lasers (FEL's) explore the idea of backscattering of a low-frequency pump wave by relativistic electron beams. The pump wave forces the beam to oscillate coherently, resulting in possible stimulated emission at a wavelength shorter by roughly a factor $\alpha\gamma^2$ (γ being the relativistic factor of the beam) than the wavelength λ_0 of the pump wave [1]. For $\gamma^2 >> 1$ the coefficient α is 4 or 2, depending on whether the pump is a regular electromagnetic wave or a magnetostatic spatially periodic field. The latter is typically produced on the axis of a magnetic wiggler (a bifilar helical current winding with equal and opposite currents in each helix).

Since the first successful operation of FEL at Stanford University [2], wigglers became an integral part in most FEL experiments. Nonetheless, both theory [3], [4] and experiments [5] showed that special care should be taken in constructing wigglers and in choosing radial dimensions and entrance conditions of the beam in order to observe coherent helical electron orbits in the laser. Together with this it was appreciated recently that spatially coherent undulation of the beam, and therefore also Doppler upshifted stimulated emission, can be caused not only by a wiggler but also by the natural gyration of the electron beam in a uniform guide magnetic field. In fact, in a cold beam, the electrons move on coherent helical orbits with the pitch $\lambda_0 = 2\pi\gamma u/\Omega$

Manuscript received June 11, 1982; revised October 12, 1982. This work was supported in part by the U.S. Office of Naval Research and by the U.S Israel Binational Science Foundation.

The authors are with the Center for Plasma Physics, Racah Institute of Physics, Hebrew University of Jerusalem, Jerusalem, Israel.

0018-9197/83/0300-0327$01.00

where Ω is the nonrelativistic cyclotron frequency, characterizing the guide field, and u is the velocity of the electrons in the direction of the guide field. Thus, amplification in the system is expected at a wavelength $\lambda = \lambda_0/2\gamma^2 = \pi u/\gamma\Omega$. Single particle calculations of small and large signal gains in such a nonwiggler FEL [6], [7] confirmed the attractive possibility of replacing the wigglers by a uniform guide field, which was, as a matter of fact, almost always present in conventional FEL experiments. However, the encouraging predictions of the single particle theories could not be applied to the collective regime of operation, when intense electron beams ($I > 1$ kA) with relatively low energies ($\gamma < 10$) were used. The collective interaction, usually termed "stimulated Raman scattering," had to be treated by a self-consistent theory.

Ott and Manheimer published a theory for a thin slab beam in a waveguide [8]. The first study of a nonwiggler FEL operating in the collective regime in free space was given by Hirshfield *et al.* [9], who showed the existence of a spatially unstable mode at the Doppler upshifted cyclotron frequency. They considered a randomly gyrophased electron beam, in which the momentum distribution function of the electrons was

$$f(p_\perp, p_z, \phi) = f(p_\perp, p_z). \tag{1}$$

Here $p_\perp$ and p_z are the momentum components, perpendicular and parallel to the direction of the guide field, and ϕ is the azimuthal angle ($t_g \phi = p_y/p_x$). It was also shown in [9] that the longitudinal and transverse modes of the system are decoupled and only the azimuthal bunching mechanism drives a cyclotron maser type instability. In this respect, the device, considered in [9] and based on randomly gyrophased beams, differs significantly from the conventional FEL's, where the axial density bunching is primarily responsible for the spatial instability.

We now show that the mode decoupling described in [9] is the result of the random gyrophase distribution of the electrons in the beam. We write the distribution function in the form

$$f(p, z, t) = \tilde{f}(p, z, t)\, \tilde{N}(z, t) \tag{2}$$

where

$$\int \tilde{f}(p, z, t)\, d^3p = 1. \tag{3}$$

Let $\tilde{f} = \tilde{f}_0 + \tilde{f}_1$ and $\tilde{N} = \tilde{N}_0 + \tilde{N}_1$ where $\tilde{f}_0$ and $\tilde{N}_0$ are the values of $\tilde{f}$ and $\tilde{N}$ when there are no perturbing electromagnetic fields. Then the linearized perturbed transverse electron current, which is the source in the Maxwell equations for the transverse fields, is written as

$$J_\perp = e\tilde{N}_0 \langle v_{\perp 1} \rangle + e \langle v_{\perp 0} \rangle \tilde{N}_1 \tag{4}$$

where

$$\langle v_{\perp 1} \rangle = \int v_\perp \tilde{f}_1\, d^3p, \quad \langle v_{\perp 0} \rangle = \int v_\perp \tilde{f}_0\, d^3p \tag{5}$$

and the subscript $\perp$ denotes components transverse to the guide field. In the case of the random gyrophase distribution (1), $\langle v_{\perp 0} \rangle$ vanishes and, as a result, only the transverse velocity perturbation $\langle v_{\perp 1} \rangle$ contributes to $J_\perp$. If, however, the momentum distribution has an azimuthal asymmetry, then $\langle v_{\perp 0} \rangle \neq 0$ and the density modulation $\tilde{N}_1$ (or the axial density bunching) can also drive transverse modes of the system.

An example of a nonwiggler FEL with an azimuthally asymmetric electron beam was recently studied in [10]. The beam was assumed to be cold, and the momentum distribution at the entrance into the device was taken to be

$$f(p_\perp, p_z, \phi) = \frac{N_0}{2\pi p_\perp} \delta(p_\perp - p_{\perp 0})\, \delta(p_z - p_{z0})\, \delta(\phi - \phi_0). \tag{6}$$

We will use the term "helical beam" to describe such a beam configuration. It was demonstrated in [10] that in a laser the helical beam provides enhanced spatial gain compared to that found with a randomly gyrophased electron beam. The origin of the gain enhancement is the aforementioned increased role of the axial bunching in driving the instability.

This paper presents a kinetic theory of nonwiggler FEL's in a uniform guide magnetic field. We consider an arbitrary ϕ dependence of the electron momentum distribution function and, in contrast to the cold fluid model of [10], we base the theory on a Maxwell-Vlasov description. The scope of the paper is as follows. In Section II the Maxwell equations are reduced to a simple set of first order ordinary differential equations for the electric component of the electromagnetic field in the system. The current and density sources for the field equations are found in Section III. In Section IV we apply the Laplace transformation to the field equations and derive the dispersion relation governing the stability of our system. Finally, in Section V the dispersion relation is studied numerically for several configurations of the electron beam. In the same section we also solve the field equations directly and find the actual gain in a finite length nonwiggler FEL amplifier.

II. Field Equations

Consider an electromagnetic wave propagating along a relativistic electron beam, gyrating in a uniform magnetic field $\mathcal{B} = \mathcal{B}_0 \hat{e}_z$. Assuming a one-dimensional model, we can describe the electromagnetic fields $E(z, t)$ and $B(z, t)$ by the system of Maxwell equations

$$c\hat{e}_z \times \frac{\partial B_\perp}{\partial z} = \frac{\partial E_\perp}{\partial t} + 4\pi J_\perp \tag{7}$$

$$-c\hat{e}_z \times \frac{\partial E_\perp}{\partial z} = \frac{\partial B_\perp}{\partial t} \tag{8}$$

$$\frac{\partial E_z}{\partial z} = -4\pi eN \tag{9}$$

$$B_z = 0 \tag{10}$$

where $J_\perp$ and N are the self-consistent transverse current and electron density perturbations caused by the presence of the electromagnetic wave.

We restrict our analysis to the stationary amplifier problem, namely, we introduce an electromagnetic perturbation of frequency ω at $z = 0$ and solve for the electromagnetic fields at given $z > 0$. Respectively, we write

$$E(z, t) = \mathrm{Re}\left[\frac{mc^2}{e}\, a(z)\, \Phi\right] \tag{11}$$

$$B(z,t) = \mathrm{Re}\left[\frac{mc^2}{e}\, b(z)\,\Phi\right] \tag{12}$$

$$J_\perp(z,t) = \mathrm{Re}\left[\frac{m}{4\pi e^2}\, j_\perp(z)\,\Phi\right] \tag{13}$$

$$N(z,t) = \mathrm{Re}\left[\frac{m}{4\pi e^2}\, n(z)\,\Phi\right] \tag{14}$$

where

$$\Phi = \exp\left[i\,\frac{\omega}{c}\,(z - ct)\right]. \tag{15}$$

Note that consistent with the amplifier problem we left in (11)-(14) only waves propagating in the positive z-direction, which is also the direction of propagation of the electron beam. Equations (7) and (8) can be combined and yield on linearization

$$\frac{d^2 a_\perp}{dz^2} + 2i\,\frac{\omega}{c}\,\frac{da_\perp}{dz} = i\,\frac{\omega}{c^4}\, j_\perp. \tag{16}$$

Similarly, (9) becomes

$$\left(i\,\frac{\omega}{c} + \frac{d}{dz}\right) a_z = -\,\frac{n}{c^2}. \tag{17}$$

Assume now that various frequencies characteristic to the electron beam (such as the plasma frequency ω_p and the cyclotron frequency $\Omega = e\mathcal{B}_0/mc$) are much less than ω. Then we expect $j_\perp$, n, a, and b to vary on the scale much longer than ω/c, or more precisely in order of magnitude for $X = j_\perp, n, a, b$

$$\left|\frac{d \ln X}{dz}\right| \ll \frac{\omega}{c}. \tag{18}$$

This disparity in scales allows us to simplify (16) and (17) significantly and rewrite them in the following approximate form:

$$\frac{da_\perp}{dz} = \frac{j_\perp}{2c^2} \tag{19}$$

$$a_z = \frac{in}{\omega c}. \tag{20}$$

These are the desired field equations, describing the electromagnetic wave propagating along the amplifier.

III. Perturbed Current and Electron Density

At this stage we adopt the kinetic description of the electron beam, introduce the electron momentum distribution function $f(p, z, t)$, and employ the Vlasov equation

$$\frac{\partial f}{\partial t} + v_z\,\frac{\partial f}{\partial z} - e\left[E + \frac{v}{c} \times (B + \mathcal{B})\right] \cdot \frac{\partial f}{\partial p} = 0. \tag{21}$$

Choosing the cylindrical coordinate system $(\hat{e}_\perp, \hat{e}_z, \hat{e}_\phi)$ in the p-space and writing $f = f_0(p_z, p_\perp, \phi, z) + f_1(p_z, p_\perp, \phi, z, t)$ where f_1 is the perturbed part of the distribution caused by the electromagnetic wave we get in the zero order

$$\frac{\partial f_0}{\partial z} + \chi\,\frac{\partial f_0}{\partial \phi} = 0 \tag{22}$$

with

$$\chi = \frac{\Omega}{\gamma v_z}. \tag{23}$$

If initially (at $z = 0$) we have

$$f_0(p_z, p_\perp, \phi, 0) = \frac{m}{4\pi e^2}\, G(p_z, p_\perp, \phi) \tag{24}$$

then (22) yields

$$f_0(p_z, p_\perp, \phi, z) = \frac{m}{4\pi e^2}\, G(p_z, p_\perp, \phi - \chi z). \tag{25}$$

Consider now the first-order linearized Vlasov equation

$$\frac{\partial f_1}{\partial t} + v_z\,\frac{\partial f_1}{\partial z} - \frac{e}{c}\,(v \times \mathcal{B}) \cdot \frac{\partial f_1}{\partial p} = e\left(E + \frac{v \times B}{c}\right) \cdot \frac{\partial f_0}{\partial p}. \tag{26}$$

Similarly to (11)-(14) let

$$f_1 = \mathrm{Re}\left[\frac{m}{4\pi e^2}\, \Psi(p_z, p_\perp, \phi, z)\,\Phi\right]. \tag{27}$$

Then (26) becomes

$$\left[-i\omega\left(1 - \frac{v_z}{c}\right) + v_z\left(\frac{\partial}{\partial z} + \chi\,\frac{\partial}{\partial \phi}\right)\right]\Psi = 4\pi e^2 c^2 \left(a + \frac{v \times b}{c}\right) \cdot \frac{\partial f_0}{\partial p}. \tag{28}$$

Expressing b through a from (8), it can be shown that in (28) we can approximate

$$a + \frac{v \times b}{c} = \frac{i}{\omega}\left[-i\omega\left(1 - \frac{v_z}{c}\right) + v_z\,\frac{\partial}{\partial z}\right] a_\perp + \left(\frac{v_\perp}{c} \cdot a + a_z\right)\hat{e}_z. \tag{29}$$

It is convenient now to introduce the following orthonormal set of base vectors

$$\hat{e}_+ = \frac{1}{\sqrt{2}}\,(\hat{e}_y - i\hat{e}_x)$$

$$\hat{e}_- = \frac{1}{\sqrt{2}}\,(\hat{e}_y + i\hat{e}_x) \tag{30}$$

Then, on writing $a_\perp = a_+\hat{e}_+ + a_-\hat{e}_-$, substituting (29) into (28), using (25) and expanding

$$\Psi = \sum_{n=-\infty}^{+\infty} A_n e^{in\phi} \tag{31}$$

$$f_0 = \frac{m}{4\pi e^2} \sum_{n=-\infty}^{+\infty} C_n e^{in\phi}, \qquad G = \sum_{n=-\infty}^{+\infty} G_n e^{in\phi}. \tag{32}$$

Note that the coefficients A_0 and $A_{\pm 1}$ are the only ones necessary to know in order to find the perturbed current and density in the field equations (19) and (20). Indeed,

$$n = \iiint \Psi p_\perp\, dp_\perp\, dp_z\, d\phi = 2\pi \iint A_0 p_\perp\, dp_\perp\, dp_z \tag{33}$$

and

$$j_\perp = \iiint v_\perp \Psi p_\perp \, dp_\perp \, dp_z \, d\phi = \hat{e}_+ j_+ + \hat{e}_- j_- \tag{34}$$

where

$$j_z = \pm\sqrt{2}\pi i \iint v_\perp A_{z1} p_\perp \, dp_\perp \, dp_z. \tag{35}$$

On Solving (29) for A_0 and A_{z1}, substituting the solutions into (33) and (35), and integrating in the resulting equations by parts in order to eliminate the derivatives of the coefficients C_n with respect to $p_\perp$ and p_z, we finally get

$$n = 2\pi mc^2 \iint dp_\perp \, dp_z \left(\int_0^z dz' \, e^{-\alpha_0 \Delta z} \left\{ a_z C_0 \frac{v_\perp}{v_z^2} \left(1 - \frac{v_z^2}{c^2}\right) \left(1 + \frac{i\omega \Delta z}{v_z}\right) + \frac{i v_\perp^2}{\sqrt{2} c v_z^2} (a_- C_{+1} - a_+ C_{-1}) \right.\right.$$
$$\left.\left. \cdot \left[1 + \frac{i\omega \Delta z}{v_z}\left(1 - \frac{v_z^2}{c^2}\right)\right] - \frac{\Omega \Delta z v_\perp^2}{2c^2 \gamma v_z^2} (a_- C_{+1} + a_+ C_{-1}) \right\} \right) \tag{36}$$

$$j_z = \pm\sqrt{2}\pi i m c^2 \iint dp_\perp \, dp_z \left(\frac{v_\perp}{\sqrt{2}\omega} \left[\mp 2 a_z C_0 - \frac{v_\perp^2}{c^2} (a_- C_0^2 - a_+ C_{-2}^0) \right] + \int_0^z dz' \, e^{-\alpha_z \Delta z} \left\{ a_z C_{z1} \frac{v_\perp^2}{v_z^2} \right.\right.$$
$$\cdot \left[1 + \frac{i\Delta z}{v_z}\left(\omega\left\{1 - \frac{v_z^2}{c^2}\right\} \mp \frac{\Omega}{\gamma}\right)\right] + \frac{i v_\perp^3}{\sqrt{2} c v_z^2} \left[(a_- C_0^2 - a_+ C_{-2}^0) \left(1 + \frac{v_z^2}{c^2} + \frac{i\Delta z}{v_z}\left\{\omega\left(1 - \frac{v_z^2}{c^2}\right) \mp \frac{\Omega}{\gamma}\right\}\right) \right.$$
$$\left.\left.\left. - (a_- C_0^2 + a_+ C_{-2}^0) \frac{\Omega v_z}{\omega \gamma c} \left\{1 - \frac{i\Delta z \omega}{v_z}\right\} \right] + \frac{\sqrt{2} i \Omega v_\perp}{\gamma \omega v_z} a_z C_0 \right\} \right) + K_z \tag{37}$$

where $\Delta z = z - z'$ and the constants K_z are chosen so that $j_z|_{z=0} = 0$, and

$$\alpha_0 = -\frac{i\omega}{v_z}\left(1 - \frac{v_z}{c}\right) \tag{38}$$

and

$$\alpha_z = \alpha_0 \pm i\chi. \tag{39}$$

According to (25) and (32)

$$C_n = G_n e^{-in\chi z}. \tag{40}$$

Note that the last expression for C_n, after being substituted into (36) and (37), allows one to express n and j_z through the distribution function of the electrons at $z = 0$. At this point, we restrict our analysis to distribution functions of the form

$$G(p_z, p_\perp, \phi) = \frac{\omega_p^2}{2\pi p_\perp} \delta(p_z - p_{z0}) \, \delta(p_\perp - p_{\perp 0}) \, g(\phi). \tag{41}$$

In this case

$$C_n = \frac{\omega_p^2}{2\pi p_\perp} \delta(p_z - p_{z0}) \, \delta(p_\perp - p_{\perp 0}) \, g_n e^{-in\chi z} \tag{42}$$

where $g_n = [\int_0^{2\pi} g \exp(-in\phi) \, d\phi]/2\pi$. Thus, after performing the integration with respect to $p_\perp$ and p_z in (36) and (37), we get

$$n = R_0 + \int_0^z dz' \, \Delta z e^{-\alpha_0^0 \Delta z} S_0(z') + \int_0^z dz' \, e^{-\alpha_0^0 \Delta z} Q_0(z') \tag{43}$$

$$j_z' = R_z + \int_0^z dz' \, \Delta z e^{-\alpha_0^0 \Delta z} S_z(z') + \int_0^z dz' \, e^{-\alpha_0^0 \Delta z} Q_z(z') \tag{44}$$

where $j_z' = j_z e^{\mp i\chi_0 z}$, $\chi_0 = \Omega/\gamma_0 v_{z0}$, $\alpha_0^0 = -i(\omega/v_{z0})(1 - v_{z0}/c)$, $1/\gamma_0^2 = 1 - v_{z0}^2/c^2 - v_{\perp 0}^2/c^2$, and if we define $a_z' = a_z e^{\mp i\chi_0 z}$, then

$$R_0 = 0 \tag{45}$$

$$S_0 = \frac{i\omega\omega_p^2 c^2}{v_{z0}^3 \gamma_0} \left\{ \left(1 - \frac{v_{z0}^2}{c^2}\right) \left[a_z g_0 + \frac{i v_{\perp 0}}{\sqrt{2} c} (a_-' g_{+1} - a_+' g_{-1}) \right] + \frac{i\Omega v_{z0} v_{\perp 0}}{\sqrt{2}\omega\gamma_0 c^2} (a_-' g_{+1} + a_+' g_{-1}) \right\} \tag{46}$$

$$Q_0 = \frac{c^2 \omega_p^2}{\gamma_0 v_{z0}^2} \left[a_z g_0 \left(1 - \frac{v_{z0}^2}{c^2}\right) + \frac{i v_{\perp 0}}{\sqrt{2} c} (a_-' g_{+1} - a_+' g_{-1}) \right] \tag{47}$$

$$R_z = \frac{ic^2 \omega_p^2}{\gamma_0 \omega} \left[-a_z' g_0 \mp \frac{v_{\perp 0}^2}{2c^2} (a_-' g_0^2 - a_+' g_{-2}^0) \right] + K_z e^{\pm i\chi_0 z} \tag{48}$$

$$S_z = \pm \frac{ic^2 v_{\perp 0} \omega_p^2}{\sqrt{2}\gamma_0 v_{z0}^3} \left\{ i a_z g_{z1} \left[\omega \left(1 - \frac{v_{z0}^2}{c^2}\right) \mp \frac{\Omega}{\gamma_0} \right] - \frac{v_{\perp 0}}{\sqrt{2} c} (a_-' g_0^2 - a_+' g_{-2}^0) \left[\omega \left(1 - \frac{v_{z0}^2}{c^2}\right) \mp \frac{\Omega}{\gamma_0} \right] - \frac{v_{\perp 0} \Omega v_{z0}}{\sqrt{2} c^2 \omega \gamma_0} (a_-' g_0^2 + a_+' g_{-2}^0) \right\} \tag{49}$$

$$Q_z = \frac{ic^2 \omega_p^2}{\sqrt{2}\gamma_0} \left\{ \pm \frac{v_{\perp 0}}{v_{z0}^2} \left[a_z g_{z1} + \frac{i v_{\perp 0}}{\sqrt{2} c} \left(1 + \frac{v_{z0}^2}{c^2}\right) (a_-' g_0^2 - a_+' g_{-2}^0) - \frac{i v_{\perp 0} \Omega v_{z0}}{\sqrt{2} c^2 \omega \gamma_0} (a_-' g_0^2 + a_+' g_{-2}^0) \right] \pm \frac{i\sqrt{2}\Omega}{\gamma_0 \omega v_{z0}} g_0 a_z' \right\}. \tag{50}$$

Finally, we substitute (43) and (44) into the field equations (19) and (20) and we get the following complete set of integro-differential equations describing the evolution of the electromagnetic wave along the amplifier.

$$\frac{da'_\pm}{dz} \mp i\chi_0 a'_\pm = \frac{1}{2c^3} \cdot \left\{R_\pm + \int_0^z dz'\, e^{-\alpha_0^0 \Delta z}[\Delta z S_\pm(z') + Q(z')]\right\} \tag{51}$$

$$a_z = \frac{i}{c\omega}\left\{\int_0^z dz'\, e^{-\alpha_0^0 \Delta z}[\Delta z S_0(z') + Q_0(z')]\right\}. \tag{52}$$

IV. Analysis of the Field Equations

Equations (51) and (52) comprise a set of linear integro-differential equations with all integrals in the form of convolutions. Thus, we can solve this system by means of the Laplace transformation. Namely, if we define for $\xi = \xi(z)$

$$\xi_k = \int_0^\infty e^{-ikz}\xi(z)\,dz \tag{53}$$

where Im k is assumed to be negative enough to assure convergence, we can apply transformation (53) to the field equations and get

$$i(k \mp \chi_0)a'_{\pm k} = \frac{1}{2c^3}\left[R_{\pm k} + \frac{S_{\pm k}}{(\alpha_0^0 + ik)^2} + \frac{Q_{\pm k}}{(\alpha_0^0 + ik)}\right] + a'_\pm(0) \tag{54}$$

$$a_{zk} = \frac{i}{c\omega}\left[\frac{S_{0k}}{(\alpha_0^0 + ik)^2} + \frac{Q_{0k}}{(\alpha_0^0 + ik)}\right]. \tag{55}$$

On using the expressions for the transforms S_{0k}, Q_{0k}, $R_{\pm k}$, $S_{\pm k}$, and $Q_{\pm k}$, we can rewrite (54) and (55) in the following vector form.

$$\begin{pmatrix} \epsilon_{++} & \epsilon_{+-} & \epsilon_{+z} \\ \epsilon_{-+} & \epsilon_{--} & \epsilon_{-z} \\ \epsilon_{z+} & \epsilon_{z-} & \epsilon_{zz} \end{pmatrix}\begin{pmatrix} a'_{+k} \\ a'_{-k} \\ a_{zk} \end{pmatrix} = \begin{pmatrix} a'_+(0) \\ a'_-(0) \\ 0 \end{pmatrix} \tag{56}$$

where the dielectric tensor $\underline{\epsilon}$ is given by

$$\epsilon_{\pm\pm} = i\left[k \mp \chi_0 + \frac{\omega_p^2 g_0}{2c\omega\gamma_0}\left(1 \mp \frac{\Omega}{\gamma_0\Delta} - Z_\pm\right)\right] \tag{57}$$

$$\epsilon_{\pm z} = -\frac{i\omega_p^2 v_{\perp 0}^2 g_{\pm 2}}{2c^2\gamma_0\Delta^2}\left[k \mp \chi_0\left(1 - \frac{v_{z0}}{c}\right)\right] \tag{58}$$

$$\epsilon_{\substack{z+ \\ z-}} = \mp \frac{v_{\perp 0}\omega_p^2 g_{\pm 1}}{2\sqrt{2}c\gamma_0\Delta^2}\left[\frac{\omega}{c}\left(1 - \frac{v_{z0}}{c}\right) + k \mp \chi_0\right] \tag{59}$$

$$\epsilon_{\substack{0+ \\ 0-}} = \pm \frac{iv_{\perp 0}\omega_p^2 g_{\pm 1}}{\sqrt{2}c\gamma_0\Delta^2}\left[\left(1 - \frac{v_{z0}}{c} + \frac{ck}{\omega}\right) \mp \frac{\chi_0 v_{z0}}{\omega}\right] \tag{60}$$

$$\epsilon_{zz} = 1 - \frac{\omega_p^2}{\omega\gamma_0\Delta^2}\left(1 - \frac{v_{z0}^2}{c^2}\right)(\omega + ck) \tag{61}$$

and

$$\Delta = -\omega\left(1 - \frac{v_{z0}}{c}\right) + kv_{z0} \tag{62}$$

$$Z_\pm = -\frac{v_{\perp 0}^2\omega}{c\Delta^2}(k \mp \chi_0). \tag{63}$$

The dispersion relation is now defined via Det $\underline{\epsilon} = 0$. The knowledge of the roots $k = k(\omega)$ of this dispersion relation allows one, in principle, to apply the inverse Laplace transformation to the solution a_k of (56) and thus find the actual z-dependence of the amplitude of the wave along the amplifier. Nevertheless, because of the complexity of the dielectric tensor $\underline{\epsilon}$, the inversion of the transforms in our case is a rather complicated algebraic procedure. Usually in such situations one restricts the study to the search of the roots of the dispersion relation only, which allows one to find the asymptotic z-dependence of spatially unstable modes. We use this approach in the next section and find roots of the dispersion relation for several configurations of electron beams. In addition, in order to avoid complexity of taking the inverse Laplace transformation, but nevertheless willing to find the z-dependence of the fields, we solve the field equations directly in the next section. With this purpose in mind, we transform here the field equations (51) and (52) into a system of first order ordinary differential equations.

Define

$$I_1^\alpha = \int_0^z dz'\, e^{-\alpha_0^0 \Delta z} S_\alpha(z') \tag{64}$$

$$I_2^\alpha = \int_0^z dz'\, e^{-\alpha_0^0 \Delta z}[Q_\alpha(z') - z' S_\alpha(z')] \tag{65}$$

where α is +, - or 0. Then (51) and (52) can be rewritten as

$$\frac{da'_\pm}{dz} \mp i\chi_0 a'_\pm = \frac{1}{2c^3}(R_\pm + zI_1^\pm + I_2^\pm) \tag{66}$$

$$a_z = \frac{i}{c\omega}(zI_1^0 + I_2^0), \tag{67}$$

and, differentiating (64) and (65),

$$\frac{dI_1^\alpha}{dz} = -\alpha_0^0 I_1^\alpha + S_\alpha \tag{68}$$

$$\frac{dI_2^\alpha}{dz} = -\alpha_0^0 I_2^\alpha + Q_\alpha - zS_\alpha. \tag{69}$$

Equations (66)-(69) comprise a complete set of first order differential equations, which can be solved numerically with an appropriate set of initial conditions.

V. Stability Analysis and Direct Solution of the Field Equations

In this section we apply the theory to the following three electron momentum distribution functions.

1) A randomly gyrophased electron beam, characterized by $g(\phi) = 1$, so that $g_0 = 1$ and $g_n = 0$ $(n = \pm 1, \pm 2, \cdots)$.

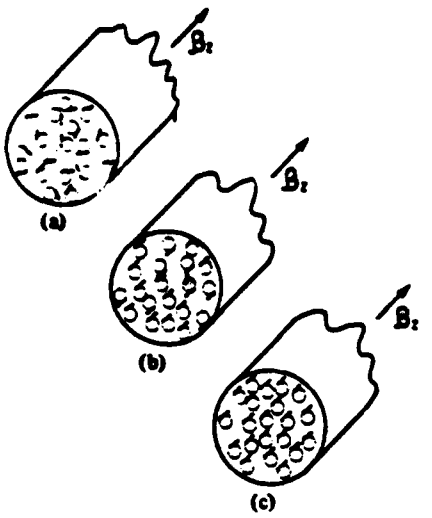

Fig. 1. Schematic of transverse cross sections of various beam configurations. (a) Randomly gyrophased beam, (b) double helical beam, (c) helical beam. The arrows show the directions of the transverse velocities of individual electrons in the beam.

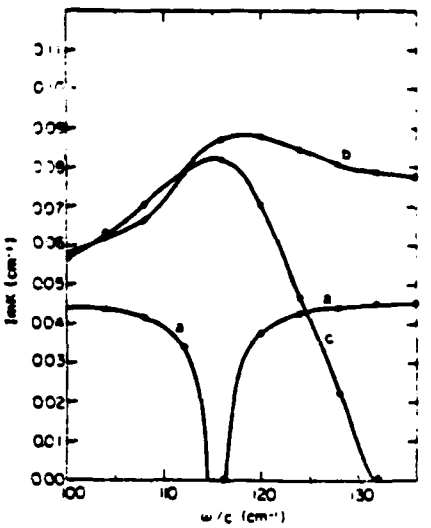

Fig. 2. Spatial growth rates Im k versus normalized frequency ω/c. The parameters are $\omega_p^2/c^2 = 2$ cm^{-2}, $\chi_0 = 3$ cm^{-1}, $\gamma_0 = 5$, and $v_{\perp 0}/c = 0.1$. (a) Randomly gyrophased beam, (b) double helical beam, (c) helical beam.

2) A double helical beam with $g(\phi) = \pi[\delta(\phi - 0) + \delta(\phi - \pi)]$. In this case $g_{2m} = 1$ and $g_{2m+1} = 0$ $(m = 0, \pm 1, \pm 2, \cdots)$.

3) A helical beam, described by $g(\phi) = 2\pi\delta(\phi - 0)$ and $g_n = 1$ $(n = 0, \pm 1, \pm 2, \cdots)$. These three types of the electron beam are illustrated schematically in Fig. 1.

In the case of an azimuthally symmetric electron beam [case 1)] all the off-diagonal elements of the dielectric tensor $\underline{\underline{\epsilon}}$ vanish and the dispersion relation simply becomes $\epsilon_{++}\epsilon_{--}\epsilon_{zz} = 0$. In this case the three possibilities ϵ_{++}, ϵ_{--}, and $\epsilon_{zz} = 0$ correspond respectively to the right-hand transverse wave, the left-hand transverse wave, and the relativistic longitudinal space-charge wave. The equation $\epsilon_{++} = 0$ is identical to the dispersion relation derived in [9] for the case $\omega/c \gg \chi_0$. As was shown in [9], $\epsilon_{++} = 0$ yields for Δ small enough and large ω a pair of complex roots for k, one of which has a negative imaginary part

$$\text{Im } k \simeq -\frac{\omega_p}{\sqrt{2}\gamma_0}\frac{v_{\perp 0}}{cv_{z0}} \tag{70}$$

and therefore describes a spatially unstable mode in the amplifier.

We now consider cases 2) and 3). In case 2) the dispersion relation is given by

$$(\epsilon_{++}\epsilon_{--} - \epsilon_{+-}\epsilon_{-+})\epsilon_{zz} = 0. \tag{71}$$

We see that the left-hand and right-hand modes are coupled. Nevertheless, as in case 1) the space-charge mode is still uncoupled. The reason for this is that both distributions 1) and 2) are azimuthally symmetric and, therefore, the average unperturbed transverse velocity in the beam $\langle v_{\perp 0}\rangle$ is zero (see Section I).

In contrast to cases 1) and 2), the distribution function of the electrons in case 3) is azimuthally asymmetric, and as a result all the off-diagonal elements of the dielectric tensor are nonzero. In this case the space-charge mode couples to the transverse modes. Because of the complexity of the dispersion relation in cases 2) and 3), their analytic study becomes difficult. We therefore find the roots numerically for the sample case: $\omega_p^2/c^2 = 2$ cm^{-1}, $\chi_0 = 3$ cm^{-1}, $\gamma_0 = 5$, and $v_{\perp 0}/c = 0.1$. This set of parameters is typical of a collective type Raman free electron laser. In Fig. 2 we compare the computed growth rates for the three distribution functions 1), 2), and 3). The solid lines represent the solutions of the dispersion relation for the sample case, and the dots were found by solving the field equations directly for large values of z, where the exponentially growing modes with the largest growth rates are dominant. We see from the figure that in case 1) (the randomly phased electron beam) the maximum growth rate is 0.044 cm^{-1} in agreement with (70). For the double helical beam [case 2)] the growth rate at maximum is 0.087 cm^{-1}. The growth rates found for the helical beam [case 3)] agree well with the results of the cold fluid theory [10] and for both cases 2) and 3) are comparable in magnitude with the growth rates one has in conventional FEL's operating in similar regimes [11]. Thus, we see in Fig. 2 that the coupling between the transverse modes in case 2) enhances the gain. In case 3) the enhancement effect comes from the coupling to the space-charge modes, which enables the axial density bunching to drive the instability.

The improved operation of the amplifier in the cases of the helical and double-helical beams is demonstrated in Fig. 3, where the actual z-dependence of the gain along the amplifier is shown for aforementioned three distributions in the sample case. These results were obtained by solving the field equations (66)-(69) directly. We see in the figure that the exponential growth for distribution 1) becomes dominant only after the beam passes 60-100 cm along the device, while in the cases of the helical and double-helical beams the growth is exponential already at ~30 cm and its actual value quickly becomes very high.

These results should motivate attempts to generate helical beams for a practical nonwiggler FEL. One way is to shoot

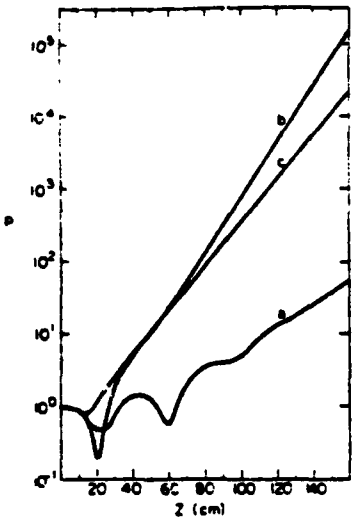

Fig. 3. The square root of the relative power gain $P = |a(z)|/|a(0)|$ versus the interaction distance in the sample case for $\omega/c = 120\ cm^{-1}$. (a) Randomly gyrophased beam, (b) double helical beam, (c) helical beam.

the beam at an angle to the magnetic field. Perhaps more promising is to pass the beam through a magnetic "kicker" which will give all the electrons the same perpendicular momentum component.

In conclusion,

1) We have presented a kinetic theory of nonwiggler FEL operating in strong uniform guide magnetic fields. The amplifier problem is reduced to a solution of a system of first order ordinary differential equations for the electric component of the electromagnetic field.

2) Our numerical examples demonstrate the potential of operating a nonwiggler FEL in the collective regime, where the spatial growth rates can be comparable to those in the convential FEL's.

3) The form of the azimuthal distribution of the momentum of the electrons in the beam in the nonwiggler FEL is extremely important and influences the growth rates in both their magnitude and form. The asymmetry in the azimuthal distribution results in higher gains in the system due to the coupling of the transverse and space-charge modes.

Acknowledgment

The authors would like to thank Prof. J. L. Hirshfield, Prof. P. Avivi, and Dr. H. Mitchell for their helpful comments and suggestions in the preparation of this paper.

References

[1] For a review of past work see P. Sprangle, R. A. Smith, and V. L. Granatstein, "Free electron lasers and stimulated scattering from relativistic electron beams," in *Infrared and Millimeter Waves*, vol. 1, K. J. Button, Ed. New York: Academic, 1979, p. 279.

[2] L. R. Elias, W. M. Fairbank, J.M.J. Madey, H. A. Schewettman and T. I. Smith, "Observation of stimulated emission of radiation by relativistic electrons in a spatially periodic transverse magnetic field," *Phys. Rev. Lett.*, vol. 36, pp. 717-720, 1976.

[3] L. Friedland, "Electron beam dynamics in combined guide and pump magnetic fields for free electron laser applications," *Phys. Fluids*, vol. 23, pp. 2376-2382, 1980.

[4] P. Diament, "Electron orbits and stability in realizable and unrealizable wigglers of free electron lasers," *Phys. Rev. A*, vol. 23, pp. 2537-2552, 1981.

[5] P. Avivi, F. Dothan, A. Fruchtman, A. Ljudmirsky, and J. L. Hirshfield, "Orbit stability in free electron lasers," *Int. J. Infrared Millimeter Waves*, vol. 2, no. 5, pp. 1071-1080, 1981.

[6] S. K. Ride and W. B. Colson, "A free-electron laser in a uniform magnetic field," *Appl. Phys.*, vol. 20, pp. 41-50, 1979.

[7] Y. Gell, J. R. Torstensson, H. Wilhelmsson, and B. Levush, "On a free-electron-laser in a uniform magnetic field: A solution for arbitrary strong electromagnetic radiation field," *Appl. Phys.*, vol B27, pp. 15-18, 1982.

[8] E. Ott and W. M. Manheimer, "Theory of microwave emission by velocity-space instabilities of an intense relativistic electron beam," *IEEE Trans. Plasma Sci.*, vol. PS-3, pp. 1-5, 1975.

[9] J. L. Hirshfield, K. R. Chu, and S. Kainer, "Frequency up-shift for cyclotron-wave instability on a relativistic electron beam," *Appl. Phys. Lett.*, vol. 33, pp. 847-848, 1978.

[10] A. Fruchtman and L. Friedland, "Amplification of frequency upshifted radiation by cold relativistic guided electron beams," *J. Appl. Phys.*, vol. 53, pp. 4011-4015, 1982.

[11] I. B. Bernstein and L. Friedland, "Theory of free electron laser in combined helical pump and axial guide field," *Phys. Rev. A*, vol. 23, pp. 816-823, 1981.

A. Fruchtman, photograph and biography not available at the time of publication.

L. Friedland, photograph and biography not available at the time of publication.

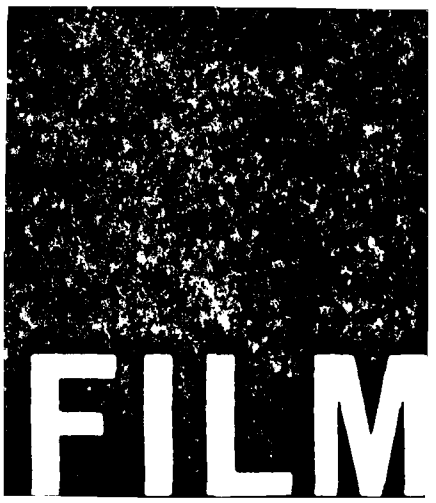
FILM